

# **Solid Oxide Catalysts for Making Dimethyl Carbonate**

**Thesis Submitted to AcSIR  
for the Award of the Degree of  
Doctor of Philosophy  
in  
Chemical Sciences**



**By  
Unnikrishnan P  
(AcSIR Roll No.: 10CC11J26073)**

**Under the Guidance of  
Dr. D. Srinivas**

**CSIR- National Chemical Laboratory  
Pune- 411008, India**

**December 2015**



# सीएसआयआर-राष्ट्रीय रासायनिक प्रयोगशाला

(वैज्ञानिक तथा औद्योगिक अनुसंधान परिषद)

डॉ. होमी भाभा मार्ग, पुणे - 411 008. भारत



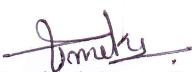
## CSIR-NATIONAL CHEMICAL LABORATORY


(Council of Scientific & Industrial Research)

Dr. Homi Bhabha Road, Pune - 411008. India

### Certificate

This is to certify that the work incorporated in this Ph.D. thesis entitled "***Solid Oxide Catalysts for Making Dimethyl Carbonate***" submitted by ***Mr. Unnikrishnan P*** to Academy of Scientific and Innovative Research (AcSIR) in fulfillment of the requirements for the award of the Degree of ***Doctor of Philosophy***, embodies original research work under my supervision. I further certify that this work has not been submitted to any other University or Institution in part or full for the award of any degree or diploma. Research material obtained from other sources has been duly acknowledged in the thesis. Any text, illustration, table etc., used in the thesis from other sources, have been duly cited and acknowledged.


  
Unnikrishnan P  
(Research Student)

  
Dr. D. Srinivas  
(Research Guide)

Date: 16-12-2015

Place: Pune

Communication  
Channels

  
NCL Level DID : 2590  
NCL Board No. : +91-20-25902000  
EPABX : +91-20-25893300  
: +91-20-25893400

FAX

Director's Office : +91-20-25902601  
COA's Office : +91-20-25902660  
COS&P's Office : +91-20-25902664

WEBSITE

[www.ncl-india.org](http://www.ncl-india.org)

## DECLARATION

I hereby declare that the work described in the thesis entitled “*Solid Oxide Catalysts for Making Dimethyl Carbonate*” submitted for the degree of *Doctor of Philosophy in Chemical Sciences* to the Academy of Scientific and Innovative Research (AcSIR), New Delhi, has been carried out by me at the Catalysis and Inorganic Chemistry Division, CSIR-National Chemical Laboratory, Pune-411008, India under the supervision of *Dr. D. Srinivas*. I further declare that the material obtained from other sources has been duly acknowledged in this thesis. The work is original and has not been submitted in part or full by me for any other degree or diploma to this or any other university.

Date: 16-12-2015

Place: Pune



**Mr. Unnikrishnan P**

Research Scholar



***Dedicated to my parents***

***The reason of what I become today.....***

## **Acknowledgements**

*First and foremost I want to thank my research guide Dr. D. Srinivas for his constant inspiration, contributions of time and ideas for making my Ph.D. experience in a proper perspective. The joy and enthusiasm he has for his research was contagious and motivational for me, even during tough times in the Ph.D. pursuit. I take this opportunity to express my intense reverence towards him for guiding me in a right direction throughout the course of this work.*

*I thank Dr. Vijaya Mohanan Pillai, Director and Dr. Sourav Pal (Ex-Director), CSIR-NCL, Pune for giving me the opportunity to work in this institute and exploit all the infrastructural facilities needed for my research work.*

*I thank the Council of Scientific and Industrial Research, New Delhi for the research fellowship.*

*I am grateful to Dr. A. P. Singh (Ex-head), Catalysis Division, for letting me to access all the divisional facilities for the research work.*

*I am lucky enough to have critical suggestions and timely help from Dr. C.V.V. Satyanarayana, Dr. Anil Kumar, and Dr. A.A. Kelkar. Their interest, positive approach and stable support have always been a source of encouragement to me.*

*I sincerely thank Dr. P.R. Rajamohanam and all other scientific staff in Central NMR facility for help in catalyst and product characterization. I also express my gratitude to Dr. R. Nandini Devi, Dr. S.B Umbarkar, Dr. C.S. Gopinath, Dr. P. Dhepe, Dr. C. V. Rode, Dr. R. Banerjee, Ms. Violet Samuel, Dr. S. P. Mirajkar, Dr. Tejas, Dr. (Mrs.) S. S. Deshpande, Mr. R. K. Jha, and Centre for Material Characterization Division for help in catalyst characterization. I also thank Dr. P.N. Joshi, Dr. V.V. Bokade and Dr. Niphadkar for their creative discussions, Many thanks to Mr. P. K. Purushothaman, Mr. Madhu and Mr. Milind for their help and cooperation in official matters during these years.*

*Many thanks to my labmates, Dr. Jithendra, Dr. Anuj, Dr. Bhogesh, Dr. Mehejabeen, Dr. Joby, Devadutta, Sagar, Poonam and Anthony for their patience, friendship, humour, arguments, understanding, discussions and of course, for enduring my eloquence.*

*I miss if did not thank many people who accompanied and accommodated me. Thanks to Sabarish, Vishal, Chithra, Ravindra, Vikram, Sreenavya, Sarath, Dr. Thushara, Dr. Raja Ambal, Devaraji, Lenin, Rakesh, Rajeesh, Vineesh, Sumesh, Dr. Ajay, Sharada, Dr. Prakash, Atul, Shiva, Dr. Eldho, Dr. Rajesh, Dr. Deepa, Dr. Bihag, Prajitha, Manu, Manjunath, Sunil, Vysakh and rest all other Kerala community .*

*Thanks to all of my BSc. and MSc. teachers especially Dr. M.S. Latha for their encouragement and good wishes.*

*So much love and thanks to my parents, my sisters and their family and Kavya for their continuing understanding and sacrifice in support of my education. Their support, prayer and love encouraged me to look optimistically into the future even in my stressful times.*

**Unnikrishnan P**

## Abbreviations

$^{27}\text{Al}$	Aluminium (atomic weight = 27)
BET	Brunauer, Emmet and Teller
BJH	Barret-Joyner-Halenda
BuAc	Butylacetate
CCS	Carbon dioxide capture and storage
CCU	Carbon dioxide capture and utilization
2-CP	2-Cyanopyridine
DMC	Dimethyl carbonate
DMP	2,2- Dimethoxypropane
DMS	Dimethyl sulphate
$E_a$	Activation energy
EDX	Energy dispersive X-ray analysis
EC	Ethylene carbonate
EG	Ethylene glycol
EO	Ethylene oxide
GC	Gas chromatography
GC-MS	Gas chromatography mass spectrometry
Gt	Giga ton
GWP	Global warming potential
$^1\text{H}$	Proton
HRTEM	High-resolution transmission electron microscopy
HTs	Hydrotalcites
ICP-OES	Inductively coupled plasma-optical emission spectroscopy
ILs	Ionic liquids
LHSV	Liquid hourly space velocity
MAS	Magic-angle spinning
MC	Methyl carbamate
MEK	Methyl ethyl ketone
MeI	Methyl iodide
MEK	Methyl ethyl ketone
MIBK	Methyl isobutyl ketone
MIR	Maximum incremental reactivity

mmol/g	mmol of product formed per gram weight of catalyst
2-MP	2-Methyl picolinate
MPa	Mega pascal
MTBE	Methyl tertiarybutyl ether
NMR	Nuclear magnetic resonance spectroscopy
<sup>31</sup> P	Phosphorous (atomic weight = 31)
2-PA	2-Picolinamide
PC	Propylene carbonate
PG	Propylene glycol
PM	Particulate matter
PO	Propylene oxide
ppm	Parts per million
PROX	Preferential oxidation
PVP	Polyvinylpyridine
SEM	Scanning electron microscopy
SOFC	Solid oxide fuel cell
TBAI	Tetrabutyl ammonium iodide
TG	Thermogravimetry
TMM	Trimethoxy methane
TOF	Turnover frequency
TON	Turnover number
TPD	Temperature-programmed desorption
VOCs	Volatile organic chemicals
WGS	Water-gas shift reaction
XRD	X-ray diffraction
	Chemical shift

## Table of Contents

<b>Chapter -1: General Introduction</b>	<b>1</b>
1.1. Introduction	2
1.2. General properties and advantages of DMC	2
1.3. Applications of DMC	3
1.3.1. Methylation and methoxycarbonylation agent	4
1.3.2. Solvent	5
1.3.3. Fuel additive	6
1.3.4. Polycarbonate synthesis	6
1.4. Conventional methods for making DMC	7
1.4.1. Phosgenation of methanol	7
1.4.2. Oxycarbonylation of methanol	7
1.5. CO <sub>2</sub> utilisation in DMC synthesis	9
1.5.1. Carbon dioxide - a sustainable chemical feed stock	9
1.5.2. Indirect utilization via transesterification	13
1.5.2.1. Urea methanolysis	13
1.5.2.2. Transesterification of cyclic carbonate	14
1.5.3. Direct utilization	18
1.5.3.1. One-pot synthesis of DMC from CO <sub>2</sub> , oxiranes and methanol	18
1.5.3.2. Direct synthesis of DMC from methanol and CO <sub>2</sub>	18
1.6. Solid oxide catalyst for DMC synthesis	23
1.6.1. Hydrotalcites and their derivatives	24
1.6.2. Sodium titanate nanotubes	25
1.6.3. Zirconium phenyl phosphonate phosphite	26
1.6.4. Cerium oxide	27
1.7. Scope and objective of the work	28
1.8. Organization of thesis	28
1.9. References	31
<b>Chapter -2: Experimental Methods and Characterisation Techniques</b>	<b>39</b>
2.1. Introduction	40
2.2. Catalyst preparation	40
2.2.1. Hydrotalcites-derived mixed oxides	40
2.2.2. Sodium titanate nanotubes	41



2.2.3.	Calcined zirconium phenyl phosphonate phosphite	41
2.2.3.1.	Synthesis of ZrPP-HF-C	41
2.2.3.2.	Synthesis of ZrPP-1-C	42
2.2.3.3.	Synthesis of ZrPP-2-C and ZrPP-3-C	42
2.2.3.4.	Zirconium pyrophosphate	42
2.2.4.	CeO <sub>2</sub> of different morphology	42
2.2.4.1.	Spindles	42
2.2.4.2.	Cubes	43
2.2.4.3.	Rods	43
2.2.4.4.	No-definite morphology	43
2.3.	Catalyst characterisation techniques	43
2.3.1.	X-ray powder diffraction	43
2.3.2.	N <sub>2</sub> - physisorption	44
2.3.3.	Inductively coupled plasma-optical emission spectroscopy	46
2.3.4.	Fourier transform infrared spectroscopy	47
2.3.5.	FT-Raman spectroscopy	47
2.3.6.	MAS NMR	48
2.3.7.	Scanning Electron microscopy / Energy dispersive X-ray analysis	48
2.3.8.	Transmission electron microscopy	49
2.3.9.	Thermogravimetric analysis	50
2.3.10.	Temperature-programmed desorption	50
2.3.11.	Titration method for ion-exchange capacity measurement	51
2.4.	Reaction procedure	51
2.4.1.	Transesterification of cyclic carbonate with methanol	51
2.4.1.1.	Hydrotalcites- derived solid oxides	51
2.4.1.2.	NaTNT	52
2.4.2.	Direct conversion of CO <sub>2</sub> into DMC	52
2.4.2.1.	ZrPP	52
2.4.2.2.	CeO <sub>2</sub>	53
2.5.	Product analysis	53
2.5.1.	Transesterification of cyclic carbonate	53
2.5.1.1.	Gas chromatography	53
2.5.1.2.	<sup>1</sup> H-NMR spectroscopy	54

2.5.2.	Direct conversion of CO <sub>2</sub> to DMC	55
2.6.	Conclusions	56
2.7.	References	56

---

**Chapter-3: Transesterification of Ethylene and Propylene Carbonates over Mixed Oxide Catalysts** 59

---

3.1.	Introduction	60
3.2.	Experimental	62
3.2.1.	Catalyst preparation	62
3.2.2.	Characterization techniques	62
3.2.3.	Reaction procedure	62
3.3.	Results and discussions	63
3.3.1.	Catalyst characterization	63
3.3.1.1.	XRD	63
3.3.1.2.	ICP-OES	66
3.3.1.3.	Surface area analysis	66
3.3.1.4.	FTIR	66
3.3.1.5.	<sup>27</sup> Al MAS NMR	68
3.3.1.5.	CO <sub>2</sub> -TPD	69
3.3.2.	Catalytic activity - transesterification of propylene carbonate	70
3.3.2.1.	Effect of rare-earth elements	71
3.3.2.2.	Effect of calcination temperature	73
3.3.2.3.	Effect of reaction parameters	74
3.3.2.4.	Catalyst recyclability	74
3.3.3.	Catalytic activity - transesterification of ethylene carbonate	78
3.3.3.1.	Effect of rare-earth elements	78
3.3.3.2.	Effect of reaction parameters	80
3.3.3.3.	Catalyst recyclability	80
3.4.	EC/PC transesterification with HT-X La-C: kinetic parameters and perspectives	84
3.5.	Conclusions	86
3.6.	References	87

---

**Chapter-4: Transesterification of Ethylene and Propylene Carbonates over NaTNT Catalyst** 90

---

4.1.	Introduction	91
------	--------------	----

4.2.	Experimental	92
4.2.1.	Catalyst synthesis	92
4.2.2.	Characterization techniques	92
4.2.3.	Reaction procedure	93
4.3.	Results and discussions	93
4.3.1.	Catalyst characterization	93
4.3.1.1.	Microscopic analysis	93
4.3.1.2.	XRD	94
4.3.1.4.	FTIR	95
4.3.1.4.	N <sub>2</sub> - Physisorption	96
4.3.1.5.	CO <sub>2</sub> -TPD	97
4.3.2.	Catalytic activity	98
4.3.2.1.	Transesterification of ethylene carbonate	98
4.3.2.2.	Transesterification of propylene carbonate	102
4.4.	Conclusions	102
4.5.	References	103
<b>Chapter-5: Direct Synthesis of Dimethyl Carbonate from CO<sub>2</sub> and Methanol over ZrPP Catalysts</b>		<b>104</b>
5.1.	Introduction	105
5.2.	Experimental	106
5.2.1.	Materials and catalyst preparation	106
5.2.2.	Characterization techniques	106
5.2.3.	Reaction procedure	107
5.3.	Results and discussions	107
5.3.1.	Catalyst characterization	107
5.3.1.1.	XRD	107
5.3.1.2.	FTIR	108
5.3.1.3.	<sup>31</sup> P MAS NMR	109
5.3.1.4.	Thermogravimetric analysis	110
5.3.1.5.	N <sub>2</sub> -Physisorption analysis	112
5.3.1.6.	Acidity-basicity measurement	113
5.3.2.	Catalytic activity	114
5.3.2.1.	Effect of reaction parameters	116

5.3.2.2.	Effect of CO <sub>2</sub> pressure	118
5.3.2.3.	Effect of dehydrating agent and solvents	118
5.3.2.4.	Catalyst recyclability	120
5.3.2.5.	Tentative reaction mechanism	122
5.4.	Conclusions	122
5.5.	References	123
<b>Chapter-6: Direct Synthesis of DMC from CO<sub>2</sub> and Methanol over CeO<sub>2</sub> Catalysts</b>		<b>125</b>
6.1.	Introduction	126
6.2.	Experimental	127
6.2.1.	Catalyst preparation	127
6.2.2.	Characterization techniques	127
6.2.3.	Reaction procedure	128
6.3.	Results and discussions	129
6.3.1.	Catalyst characterization	129
6.3.1.1.	XRD	129
6.3.1.2.	HRTEM	129
6.3.1.3.	Raman spectroscopy	131
6.3.1.4.	Surface area analysis	131
6.3.1.5.	Acid and base properties	133
6.3.2.	Catalytic activity	133
6.3.2.1.	Effect of reaction parameters	136
6.3.2.2.	Structure-activity correlations	136
6.3.2.3.	Tentative reaction mechanism	138
6.4.	Conclusions	139
6.5.	References	139
<b>Chapter-7: Summary and Conclusions</b>		<b>141</b>
<b>List of Publications and Patents</b>		<b>146</b>

## List of Figures

Fig. No.	Figure Caption	Page No.
1.1.	DMC consumption in various countries	2
1.2.	Applications of DMC	4
1.3.	CO <sub>2</sub> emission from different industries	10
1.4.	Processes for CO <sub>2</sub> mitigation	11
1.5.	CO <sub>2</sub> utilization into fuels and chemicals	12
1.6.	CO <sub>2</sub> utilization in DMC synthesis	13
1.7.	Pictorial representation of HTs	25
1.8.	Schematic representation of sodium titanate nanotube formation	26
1.9.	Tentative structures of ZrPP	26
1.10.	Crystal structure of CeO <sub>2</sub>	27
2.1.	<sup>1</sup> H-NMR spectrum of PC transesterification product	54
3.1.	Powder XRD patterns of “neat” and lanthanum incorporated HTs: (a) as-synthesized and (b) calcined samples	64
3.2.	Powder XRD of (a) as-synthesized and (b) calcined 8 mol% rare-earth ion incorporated HTs	65
3.3.	FTIR spectra of as-synthesized and calcined HTs	68
3.4.	<sup>27</sup> Al MASNMR spectra of (a) HT-as-syn, (b) HT-8 La, (c) HT-8 La-C and (d) spent HT-8 La-C	69
3.5.	CO <sub>2</sub> -TPD profiles of calcined HT and lanthanum modified HT catalysts	70
3.6.	Correlation between catalytic activity and density of basic sites on HT La-C catalysts	72
3.7.	Time profile of the <sup>1</sup> H NMR spectra of the reaction mixture of transesterification of PC with methanol	73
3.8.	Influence of reaction parameters on transesterification of PC with methanol over HT-8 La-C	75
3.9.	Catalyst recyclability studies	76
3.10.	Fresh and spent HT-8 La catalysts: (a) XRD and (b) FT-IR	77
3.11.	Correlation between catalytic activity and density of basic sites on HT La-C catalysts	80
3.12.	Catalytic performance of HT-10 La-C in transesterification of	81

	ethylene carbonate (EC) with methanol: (a) Effect of reaction time, (b) Effect reaction temperature, (c) Effect of catalyst amount.	
3.13.	Catalyst recyclability test	82
3.14.	(a) XRD and (b) FTIR spectra of fresh and spent HT-10 La-C catalyst	82
4.1.	SEM image of NaTNT	94
4.2.	HRTEM images of NaTNT	94
4.3.	XRD patterns of (a) TiO <sub>2</sub> and (b) NaTNT	95
4.4.	FT-IR spectra of (a) anatase TiO <sub>2</sub> and (b) NaTNT	96
4.5.	N <sub>2</sub> -adsorption/desorption isotherms and pore size distribution (inset) of NaTNT	97
4.6.	CO <sub>2</sub> -TPD profile of NaTNT	98
4.7.	Influence of the amount of catalyst on transesterification of EC	99
4.8.	Effect of reaction time on DMC yield	99
4.9.	Catalyst recyclability test	100
4.10.	(a) XRD and (b) FTIR of fresh and spent catalysts (after 4 <sup>th</sup> recycle) of NaTNT	101
5.1.	Powder XRD of (a) uncalcined and (b) calcined zirconium phenyl phosphonate phosphite catalysts and ZrP <sub>2</sub> O <sub>7</sub>	107
5.2.	FTIR spectra of calcined ZrPP catalysts and ZrP <sub>2</sub> O <sub>7</sub>	108
5.3.	<sup>31</sup> P MASNMR spectra of uncalcined (ZrPP-1, ZrPP-HF) and calcined (ZrPP-HF-C) zirconium phenylphosphonate phosphites.	109
5.4.	Thermogravimetric plots of (a) ZrPP-1, (b) ZrPP-2, (c) ZrPP-3, (d) ZrPP-HF	110
5.5.	Thermogravimetric plot of ZrPP-HF-C	112
5.6.	N <sub>2</sub> adsorption/desorption isotherms of calcined zirconium phenyl phosphonate phosphite	112
5.7.	NH <sub>3</sub> -TPD profiles of (a) ZrPP-HF-C, (b) ZrPP-1-C, (c) ZrPP-2-C, (d) ZrPP-3-C	113
5.8.	CO <sub>2</sub> -TPD profiles of (a) ZrPP-HF-C, (b) ZrPP-1-C, (c) ZrPP-2-C and (d) ZrPP-3-C	114
5.9.	Correlation of DMC yield with acidity and basicity of calcined ZrPP catalysts	116
5.10.	Influence of (a) reaction time and (b) reaction temperature on the	117

	DMC yield	
5.11.	Effect of CO <sub>2</sub> pressure on DMC synthesis in the absence of solvent using ZrPP-HF-C catalyst	118
5.12.	Catalyst recyclability test	120
5.13.	(a) XRD and (b) FTIR of spent ZrPP-HF-C catalyst	121
5.14.	Tentative reaction mechanism for direct DMC synthesis over ZrPP-HF-C	122
6.1.	XRD patterns of ceria with different morphology.	129
6.2.	HRTEM images of ceria samples: (a & b) Ce - C, (c & d) Ce - R and (e & f) Ce - S	130
6.3.	TEM image of Ce-N	130
6.4.	FT-Raman spectra of ceria samples of different morphology	131
6.5.	NH <sub>3</sub> -TPD (top) and CO <sub>2</sub> -TPD (bottom) profiles of Ce - C (a & e), Ce - R (b & f), Ce - S (c & g) and Ce - N (d & h)	134
6.6.	Influence of (a) reaction temperature and (b) reaction time on DMC yield over Ce - S catalyst	136
6.7.	Correlation between catalytic activity (methanol conversion and DMC yield) with acid / base sites of medium strength of ceria catalysts	137
6.8	Proposed mechanism for DMC synthesis from methanol and CO <sub>2</sub> over ceria catalysts	138

---

## List of Schemes

<b>Scheme. No.</b>	<b>Scheme Caption</b>	<b>Page No.</b>
1.1.	Methylation and methoxycarbonylation by DMC	4
1.2.	Bisphenol-A polycarbonate synthesis using DMC	6
1.3.	DMC synthesis via transesterification of cyclic carbonate	14
1.4.	One-pot synthesis of DMC from epoxides (EO/PO), CO <sub>2</sub> and methanol	18
1.5.	DMC synthesis from CO <sub>2</sub> and methanol	19
3.1.	Transesterification of EC/PC with methanol	61
4.1.	Benign route for DMC synthesis	92
6.1.	Direct synthesis of DMC from CO <sub>2</sub> and methanol in presence of 2-CP	127

## List of Tables

<b>Table No.</b>	<b>Table Caption</b>	<b>Page No.</b>
1.1.	Comparison of properties of DMC with other reagents and solvents	3
1.2.	Activity of homogeneous base catalysts for EC/PC transesterification	15
1.3.	Activity comparison of solid catalysts for EC/PC transesterification with methanol	17
1.4.	Thermodynamic data of substances involved in the direct synthesis of DMC from CO <sub>2</sub> and methanol	19
1.5.	Solid catalyst system for direct synthesis of DMC from CO <sub>2</sub> and methanol	22
3.1.	Elemental composition, structure, and textural properties of HTs	67
3.2.	Catalytic activity data of rare-earth modified HTs for transesterification of PC and methanol	71
3.3.	Effect of calcination temperature of HT-8 La on the transesterification activity	74
3.4.	Comparative catalytic activities of different solid catalysts for transesterification of PC with methanol	78
3.5.	Catalytic activity for transesterification of EC with methanol	79



---

3.6.	Comparison of activity of different catalysts for transesterification of ethylene carbonate (EC) with methanol	83
3.7.	Catalytic activity as a function of reaction time for transesterification of cyclic carbonate with methanol over HT-8 La-C and HT-10 La-C	85
3.8.	Kinetic parameters for transesterification of EC/PC with methanol over HT-8 La-C and HT-10 La-C	86
4.1.	Physicochemical properties of NaTNT	97
4.2.	Kinetic parameters for transesterification of EC with methanol using NaTNT	100
4.3.	Catalytic activity of NaTNT for transesterification of propylene carbonate with methanol	102
5.1.	Structural and textural properties of ZrPP based catalysts	111
5.2.	Physicochemical and catalytic properties of calcined ZrPP	115
5.3.	Catalytic activity data of ZrPP-HF-C	119
6.1.	Textural, acid-base and catalytic properties of ceria samples	132
6.2.	Catalytic activity data of ceria for direct synthesis of DMC	135
7.1.	Comparative catalytic activity of solid oxide in transesterification of EC/PC with methanol	144
7.2.	Direct synthesis of DMC from CO <sub>2</sub> and methanol	145

---

**Chapter - 1**  
**General Introduction**

## 1.1. Introduction

The chemical industry is determined to improve the conventional unsafe processes which accumulate greenhouse gases, solid particulate matter and toxic compounds in the atmosphere with well acknowledged green and sustainable alternative ones. Organic carbonates synthesis is one of such processes undergoing this transformation. Organic carbonates have been recognized as green and sustainable substitutes to many insecure chemicals. The green aspect of organic carbonates is attributed to their low toxicity, high degradability and excellent physicochemical properties. On the other hand, the sustainable aspect is related to its synthesis from greenhouse gas carbon dioxide [1]. Organic carbonates are divided into two classes: (a) linear carbonates (e.g., dimethyl carbonate and diethyl carbonate) and cyclic carbonates (e.g., ethylene carbonate, propylene carbonate, butylene carbonate and glycerol carbonate). Dimethyl carbonate (DMC) is the simplest organic carbonate among these. DMC finds various applications such as fuel additive, pharmaceutical, electrolyte in Li-ion batteries and as a solvent and reagent in organic reactions [1-4]. The current global production of DMC is around 330 kt/year of which captive consumption is 240 kt/year and merchant capacity is 90 kt/year. Fig. 1.1 shows the world DMC consumption in 2013 where India occupies the third position [3].

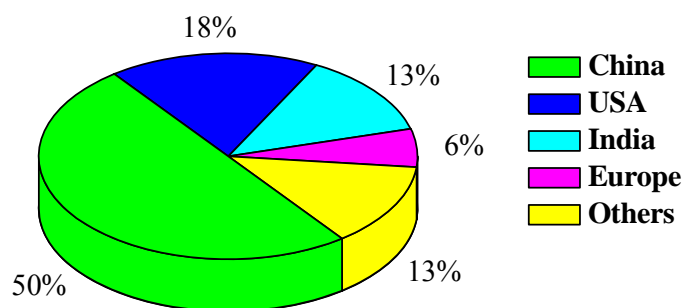


**Fig. 1.1.** DMC consumption in various countries [3].

## 1.2. General properties and advantages of DMC

DMC has been exempted from the list of volatile organic chemicals (VOCs). It is a flammable liquid (boiling point = 90 °C) with an odor similar to methanol (MeOH). DMC is safe to handle as it does not impart any kind of poisonous effect either by inhalation or by contact. These inherent properties of DMC along with its low water solubility, relatively high flash point and low maximum incremental reactivity (MIR) values make it an excellent substitute

to conventional organic solvents such as acetone, ethyl acetate and tert.-butyl acetate (t-BuAc) (Table 1.1). As a chemical synthon, DMC has desirable physicochemical properties as compared to phosgene, dimethyl sulfate (DMS) and methyl iodide (MeI) (Table 1.1).

**Table 1.1.** Comparison of properties of DMC with those of other reagents and solvents

Solvent properties	DMC	Acetone	Ethyl acetate	t-BuAc
Solubility in water (g/100 ml)	13.9	Complete	8.9	0.8
Evaporation rate (n-BuAC = 1)	3.2 - 3.4	7.7	6.2	2.8
Flash point (°C)	17	-20	-3.3	16.7
MIR value (per gram)	0.06	0.36	0.63	0.18
Toxicological properties	DMC	Phosgene	DMS	MeI
Oral acute toxicity (rats; LD 50 in g/kg)	13.8	-	0.44	0.076
Acute dermal toxicity (rabbit; LD 50 in g/kg)	> 5	-	-	-
Acute toxicity per contact (cavy; LD 50 in g/kg )	> 2.5	-	-	0.11
Acute toxicity/inhalation (rats; LC 50 in g/l)	0.14 (4 h)	0.016 (0.75 h)	0.0015 (4 h)	1.3 (4 h)
Mutagenic effect	Negative	-	Carcinogen	Carcinogen
Product classification	Non-toxic	Poisonous gas	Corrosive/poison	Noxious gas
Biodegradability (OECD 301C)	> 90% (28 days)	Rapid hydrolysis	Rapid hydrolysis	-

### 1.3. Applications of DMC

The distinctive chemical properties of DMC make it versatile in various applications such as reagent in methylation, carbonylation and methoxycarbonylation reactions, fuel additive, solvent and adhesive etc. Some of them are briefly discussed below.

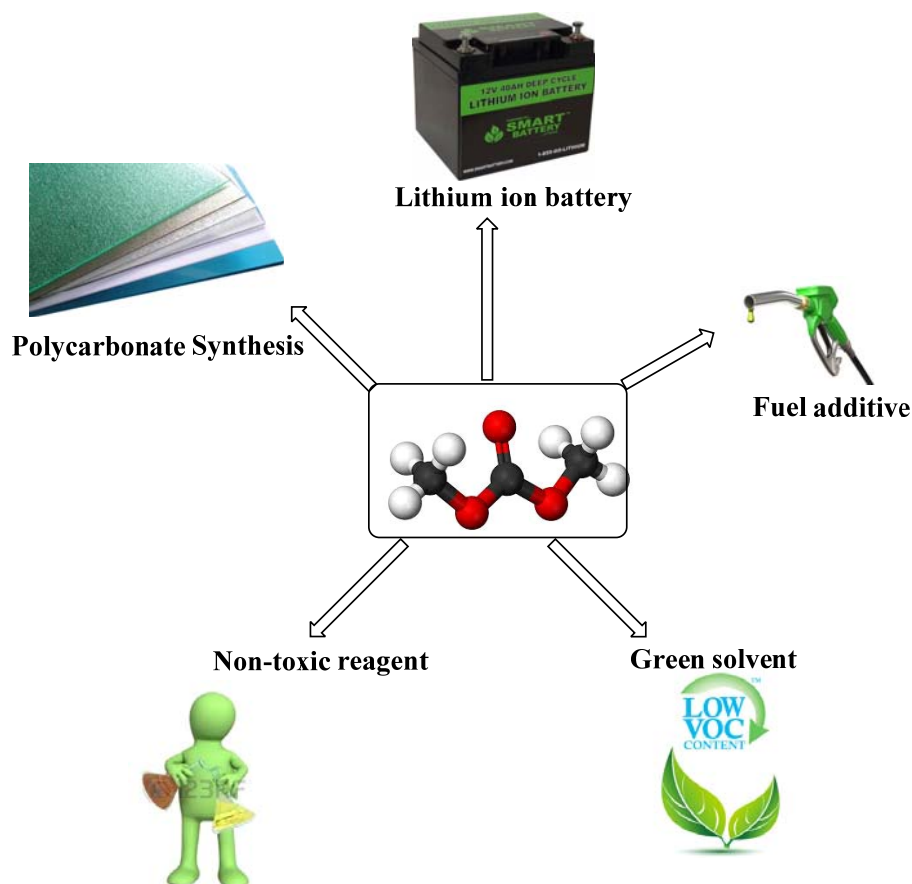
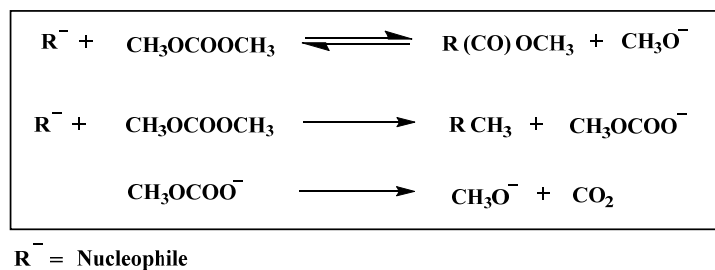


Fig. 1.2. Applications of DMC

### 1.3.1. Methylation and methoxycarbonylation agent

DMC is an environmentally benign reagent replacing toxic and hazardous methyl halides ( $\text{CH}_3\text{X}$ ,  $\text{X} = \text{I}, \text{Br}$  and  $\text{Cl}$ ), DMS and phosgene ( $\text{COCl}_2$ ) in methylation reactions and stoichiometric quantities of bases in methoxycarbonylation reactions. These conventional reagents generate stoichiometric amounts of inorganic salts whereas DMC produces only methanol and  $\text{CO}_2$  as byproducts (Scheme 1.1) [5].



Scheme 1.1. Methylation and methoxycarbonylation with DMC.

Chemically, DMC is an ambident electrophile with three active centers; two methyl groups and one carbonyl carbon [6,7]. At lower temperatures it acts as a methoxy carbonylating agent (substitute for phosgene) and at high temperatures as a methylating agent. Methoxy carbonylation of primary or secondary amines with DMC produces carbamate, which can be converted to commercially attractive isocyanate through decomposition [7]. DMC is used in methylation reactions at C, N, O and S centers in place of alkyl halides, DMS, etc. [4]. Selective methylation of arylacetonitriles, aryloxyacetates and methylarylacetates at  $\alpha$ -position selectively to monomethyl derivative has been successfully achieved with DMC [8,9]. On the other hand, O-methylation of phenols produces arylalkylethers (anisoles), which are widely used in the synthesis of dyes, agrochemicals and antioxidants for oils, greases and plastics [10]. Methylation with DMC is a benign method for N-methylation of indole in high yields [11,12]. Methylation of aliphatic and aromatic thiols using DMC has also been reported [7]. Furthermore, DMC reacts with silica at 277-327 °C to form tetramethoxysilane, a simple and convenient approach for the depolymerization of silica [13].

### **1.3.2. Solvent**

DMC is a cost-effective oxygenated solvent with excellent solubility properties compared to methylethylketone (MEK), methylisobutylketone (MIBK), ethylacetate, butylacetate and glycol ethers. It is also competitive to acetone, toluene and ethanol. Its use in coating, cleaning and adhesive resins is promising due to strong solvation effects and economic aspects [14]. DMC is partially soluble in water which permits water to be highly effective in preventing DMC based fires. The harmful and carcinogenic solvents such as dichloromethane, acetone, etc., can be replaced with DMC in organic chemical synthesis. DMC was found to be a successful solvent in biaryls synthesis [15]. It is also a highly efficient solvent in regio- and stereo-controlled ring opening of 3-membered heterocyclics at ambient conditions [16]. DMC was used as both reagent and solvent in the synthesis of N-carboxymethyl pyrrolidine from 4-amino-1-butanol [17]. DMC acts a non-aqueous electrolyte component in lithium-ion rechargeable batteries [18,19]. The electrolytes for such batteries are generally prepared by dissolving a lithium salt in an organic solvent most likely propylene or ethylene carbonates. Although these cyclic carbonates allow good dissolution of lithium salts, their strong viscosity limit the efficiency of lithium electrochemical cycle. Adding DMC into such electrolytes appreciably improves the

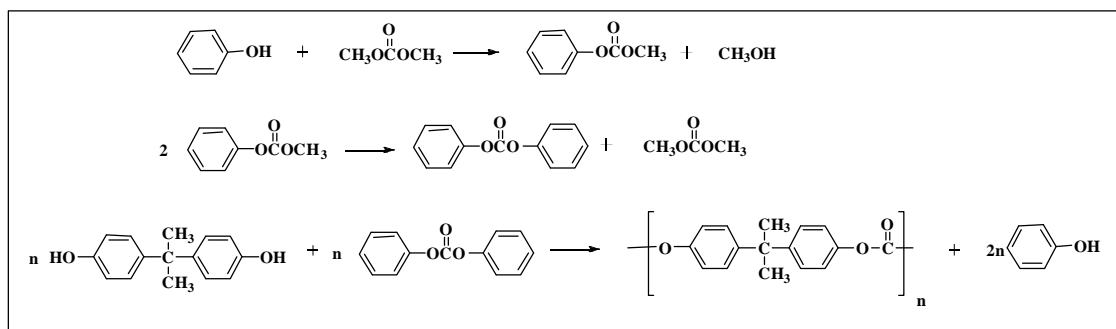
conductivity (strong solvation force towards lithium ions) and reduces the viscosity. As a result the electrolyte resistance reduces which in turn improves the efficiency [14].

### 1.3.3. Fuel additive

A good quality fuel additive is characterized by its solubility in gasoline/diesel, suitable boiling point and excellent combustion/emission properties. In this regard, DMC is a promising fuel additive. Its high oxygen content (53.3 wt%) and blending properties provide efficient combustion as compared to less oxygen content (18.2 wt%) and conventionally used methyl tertiary butyl ether (MTBE) [20-22]. In 1943, Standard Oil Development Co. has reported an octane number of 116 for gazoles containing 3-5 vol% of DMC [23]. Union Oil Co. reported a 10-30% reduction in soot particle release for gazole containing 5 wt% DMC [24,25]. DMC blended diesel shows longer ignition delay, shorter combustion duration, low particulate matter (PM) emission and increased thermal efficiency to that without DMC [26].

### 1.3.4. Polycarbonate synthesis

Bisphenol-A based aromatic polycarbonates are well-known engineering thermoplastics. Conventionally bisphenol-A polycarbonate is prepared by condensation polymerization of bisphenol-A and phosgene. An alternating way avoiding the use of hazardous phosgene has been reported. In this method, DMC is transesterified with phenol to produce diphenyl carbonate which is subsequently transesterified with bisphenol-A to produce the polycarbonate (Scheme 1.2). EniChem [27] and Asahi Kasei [28] have been commercialized this eco-friendly route for polycarbonate synthesis.

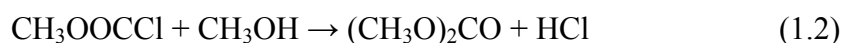
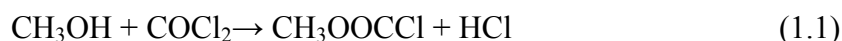


**Scheme 1.2.** Bisphenol-A polycarbonate synthesis using DMC

## 1.4. Conventional methods of making DMC

### 1.4.1. Phosgenation of methanol

Methanol phosgenation is the traditional method used for DMC production. It was widely used in industries (Bayer and Société Nationale des Poudres et Explosifs, SNPE France) during 1940-1980 [14]. The reaction scheme for DMC synthesis by phosgene is shown in Eqs. (1.1) & (1.2). It involves the formation of methyl chloroformate intermediate in the first-step followed by its methanolysis in second-step to give DMC with the formation of corrosive HCl as byproduct.



A DMC yield of 82% and 85% with respect to methanol and phosgene is reachable through this method at 0 °C in anhydrous solvents such as toluene or dichloromethane. The second-step of this reaction is slow. However, the presence of an acid trapper (pyridine) or an inorganic base (NaOH) can shift the equilibrium towards DMC formation [29,30]. Although the method is advantageous in view of DMC yield, it has some serious issues such as handling of toxic/explosive phosgene and the need to neutralize HCl. These drawbacks increased the economics of the process which in turn directed the research to economic and eco-friendly reaction pathways [29,30].

### 1.4.2. Oxycarbonylation of methanol

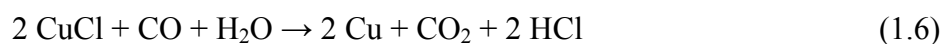
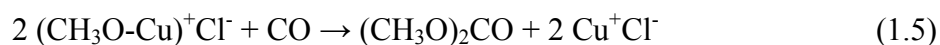
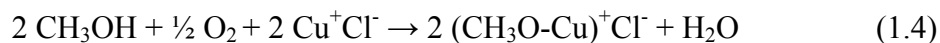
In 1980s, catalytic oxidative carbonylation of methanol (Eq. (1.3)) started to familiarize as an alternate route to methanol phosgenation. It is an economic route in terms of operating conditions and reaction thermodynamics ( $\Delta_r G_{298\text{K}} = -250.8 \text{ kJ}\cdot\text{mol}^{-1}$ ,  $\Delta_r H_{298\text{K}} = -311.9 \text{ kJ}\cdot\text{mol}^{-1}$ ) [31].



Depending on the physical state of methanol, the process is categorized into two types: liquid-phase and gaseous-phase. In 1983, Enichem industrialized this process in a slurry mode using CuCl as the catalyst (Eqs. (1.4) and (1.5)) [32-34]. A DMC yield of 30-40% was attainable through the process which also involves recycling of methanol back to the reactor and CO<sub>2</sub> (byproduct) for CO synthesis. At a total pressure of 2.4 MPa and a reaction temperature of 130 °C, the turn over frequency (TOF) of the catalyst was 130 g DMC/l<sub>cat</sub>/h. Although the process is competent compared to methanol phosgenation, it has several limitations such as



separation of DMC-H<sub>2</sub>O mixtures, corrosion problems and high operating pressures. Additionally, oxygen posed as a limiting reactant due to its explosive risk (> 4 mol% of O<sub>2</sub> at CO rich regions).

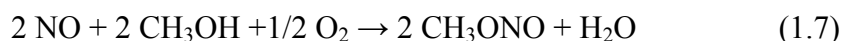


The catalytic activity strongly depends upon the Cl/Cu ratio. The selectivity to DMC is maximum when this ratio is unity. However, maintaining the ratio at unity is a difficult challenge due leaching of Cl in presence of H<sub>2</sub>O (Eq. 1.6). An active approach to maintain the ratio steady is the co-feeding of HCl but its presence can divert the selectivity of the reaction towards formation of CH<sub>3</sub>Cl and CH<sub>3</sub>OCH<sub>3</sub> [35].

An incessant effort was continued to design catalyst systems with excellent efficiency and low chlorine content. To enhance the catalytic activity, homogeneous catalysts have been tested in presence of base additives and ionic liquids as promoters [36-38]. Immobilizing homogeneous catalysts (CuCl or CuCl<sub>2</sub>) on polymer supports and mesoporous materials have also been tested to tackle the separation issues [39,40]. But all these efforts were insufficient to address the existing limitations in a satisfactory level. Thus, the research focus was then moved slowly into the gas-phase process. By the end of 1980, Dow Chemical Company has established the gas-phase process in an industrial level using CuCl supported on activated carbon [41]. Catalyst improvement studies showed [Cu(OCH<sub>3</sub>)(pyridine)Cl]<sub>2</sub> supported on activated carbon as the efficient catalyst for this reaction [41,42]. According to Dow Chemicals, activity studies with other inorganic supports such as MgO, ZnO, SiO<sub>2</sub>, TiO<sub>2</sub>, and Al<sub>2</sub>O<sub>3</sub> were not encouraging as the oxide ions and hydroxyl groups on the supports destabilized the active species more than the activated carbon [43]. A bimetallic catalyst system composed of PdCl<sub>2</sub>-CuCl<sub>2</sub> on activated carbon in presence of alkaline promoter (DMC yield > 28% at 150 °C and 0.64 MPa total pressure) [44] and chlorine-free Cu-zeolite (Cu-MOR, Cu-ZSM5, Cu-Y and Cu-SAPO-37) catalysts (DMC yield = 0.2-2.5% at 130-170 °C and 0.4-1 MPa total pressure) have also been reported for the direct oxidative reaction [45,46].

To avoid the safety issues in the direct oxidative carbonylation process, UBE developed a two step indirect process for DMC synthesis in the gas-phase through methyl nitrite

carbonylation (Eqs. 1.7 and 1.8). The reaction is performed in presence of PdCl<sub>2</sub> supported on activated charcoal. UBE has commercialized the process with a production capacity of 6000 t/year [14]. In this process, the first step involves the formation of methylnitrite (CH<sub>3</sub>ONO) from NO, CH<sub>3</sub>OH and O<sub>2</sub> in the liquid-phase performed in reactor-1 (Eq. 1.7). Water produced in this step is efficiently removed to produce DMC in anhydrous media. The second step consists of the vapor phase reaction of CH<sub>3</sub>ONO and CO in presence of the catalyst in a fixed-bed reactor (Eq. 1.8). The catalyst showed a space time yield of ~ 200 to 600 kg DMC/m<sup>3</sup>cata/h (at 80-150 °C and 0.2-0.5 MPa pressure) [47]. Although the method is able to avoid catalyst deactivation due to water, it deviates from green chemistry principles precisely by the use of toxicological and ecotoxicological gas NO.



## 1.5. CO<sub>2</sub> utilization in DMC synthesis

### 1.5.1. Carbon dioxide - a sustainable chemical feedstock

Carbon dioxide is the dominant greenhouse gas present in atmosphere. Industrialization and other anthropogenic activities accelerate its accumulation in atmosphere. CO<sub>2</sub> is regarded as the major cause for global warming and its after effects in terms climate change. At present, on an average 36 Gt of CO<sub>2</sub> is emitted per year globally by combustion of fossil fuels [48]. During the last decade, the average annual increase of CO<sub>2</sub> in the atmosphere was 2.1 ppm per year [49]. Today, CO<sub>2</sub> concentration in atmosphere is 50 ppm higher than the safety limit of 350 ppm. The main sources and their contribution to CO<sub>2</sub> emission are shown Fig. 1.3 [50]. The major portion of CO<sub>2</sub> emission is shared by cement, oil refinery, iron and steel industries.

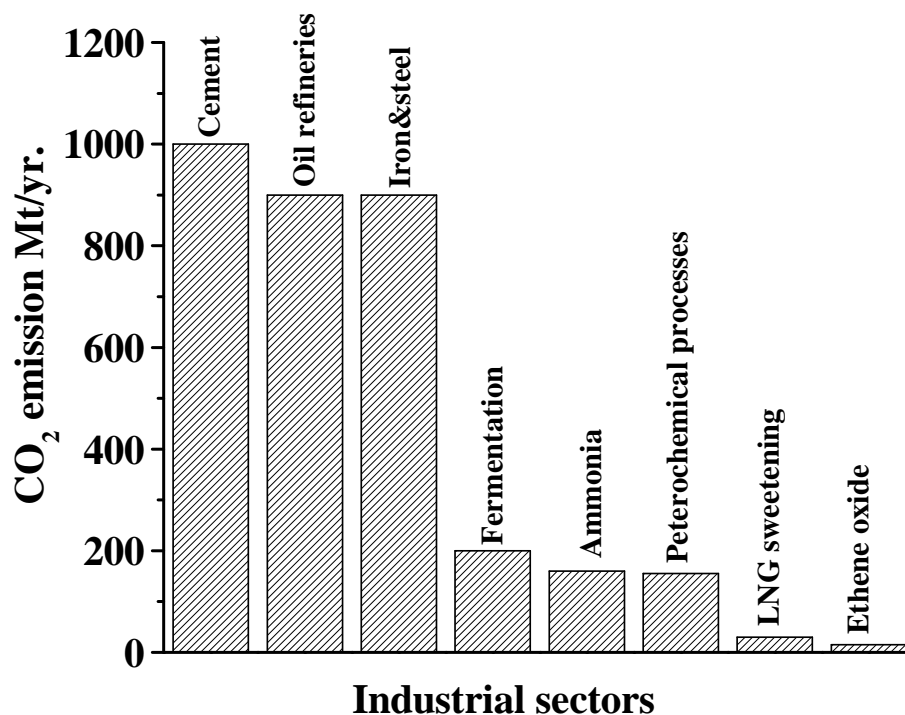


**Fig. 1.3.** CO<sub>2</sub> emission from different industries [50]

Carbon dioxide capture and storage (CCS) and carbon dioxide capture and utilization (CCU) are the major options available for CO<sub>2</sub> mitigation (Fig. 1.4). In CCS, CO<sub>2</sub> is captured from post-conversion, pre-conversion and oxy-fuel combustion of carbon sources, which is then compressed and transferred to appropriate places for long term storage. CCS has several technical and economical issues such as the ambiguity in the rate of CO<sub>2</sub> leakage, transportation and injection cost before its organization into large scale [51]. On the other hand, CCU is more promising since the method is aimed to convert waste CO<sub>2</sub> into valuable products such as fuels and chemicals hence can make a positive contribution in reducing global warming [52,53].

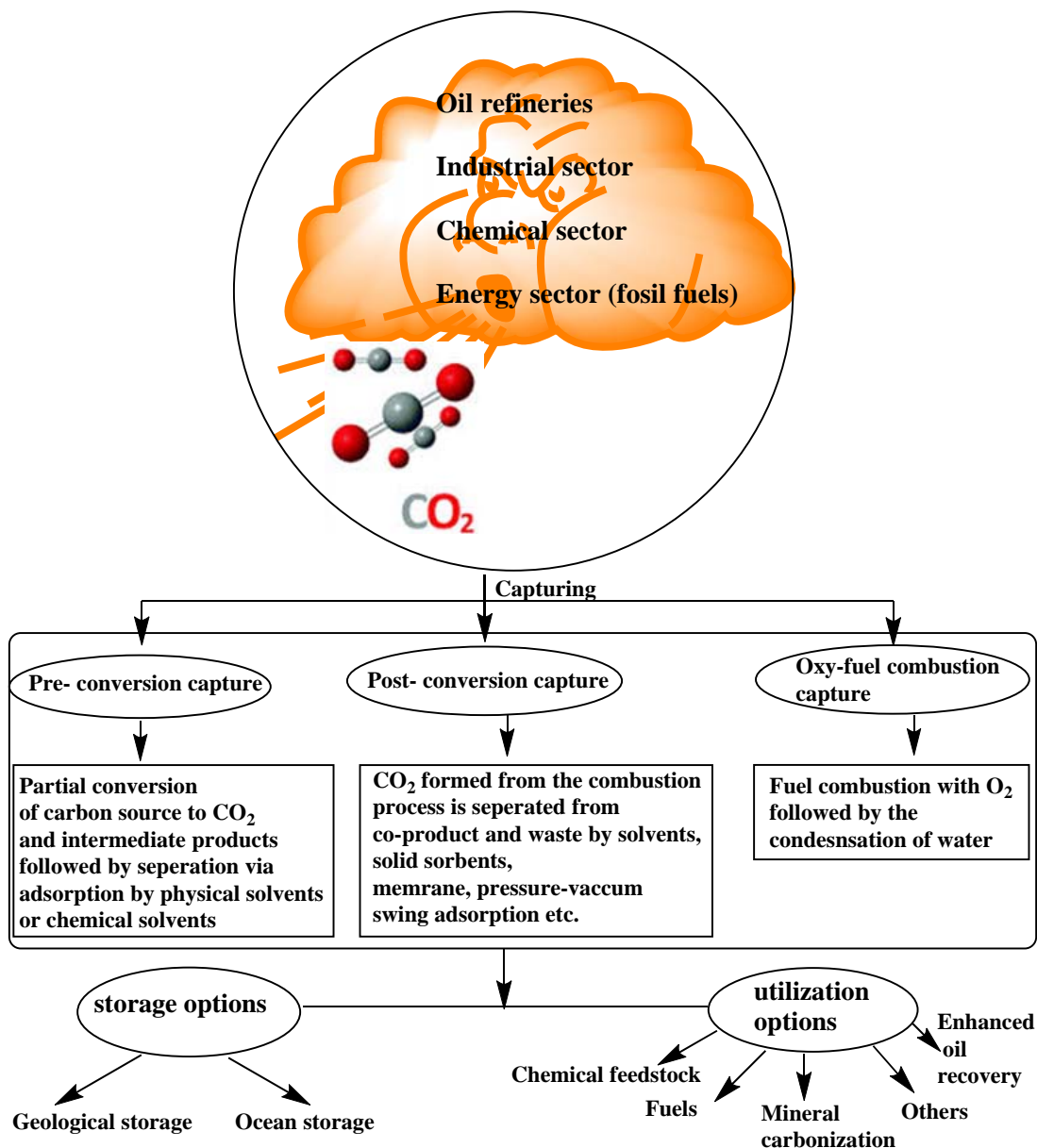


**Fig.1.4.** Processes for CO<sub>2</sub> mitigation [54]

In contrast to traditional non-renewable petrochemical feedstock, CO<sub>2</sub> is abundant, inexpensive, less toxic and technically renewable. Chemically, CO<sub>2</sub> is thermodynamically stable and kinetically inert. Thermodynamic unfavorability can be overcome by reacting CO<sub>2</sub> with energy rich molecules such as epoxides, amines, unsaturated compounds, etc., and the kinetic barrier can be overcome by activation of CO<sub>2</sub> by using catalysts and photochemical and electrochemical pathways. Only a handful of commercial processes that use CO<sub>2</sub> as a C1 building block exists. They include: urea synthesis (CO<sub>2</sub> consumption: 120 Mt/year),

manufacture of salicylic and para-hydroxybenzoic acids (CO<sub>2</sub> consumption: 30,000 tons/year), cyclic and polycarbonates synthesis (ca., 1.5 Mt/year) and synthesis of methanol (CO<sub>2</sub> consumption: 2 Mt/year) [55,56]. Based on statistics, only a small fraction of CO<sub>2</sub> produced by anthropogenic activities is recycled in chemical industries (< 1%). At present, little number of reactions and processes utilizing CO<sub>2</sub> are on investigation (Fig. 1.5).

Methodologies for CO<sub>2</sub> conversion into valuable chemicals can be categorized into two: (a) reductive transformation and (b) non-reductive transformation. CO<sub>2</sub> transformation to methanol, formate and methane falls under the former category and CO<sub>2</sub> to organic carbonate, carbamate, urea, carboxylates, polyurethanes and polycarbonates belongs to the later category. Reductive transformation is an energy intensive process than non-reductive process. Among the chemicals synthesized by non-reductive pathway, organic carbonates are getting more scientific interest due to their biodegradability, low-toxicity, non-corrosiveness to use as a monomer in the synthesis of polycarbonate and polyurethane resins, as electrolytes in lithium ion battery, as alkylating and carbonylating agent, as solvents and as fuel additives. Among several organic carbonates, the lowest homologue, DMC is getting more commercial interests due to its desirable physicochemical properties (Table 1.1) [57].

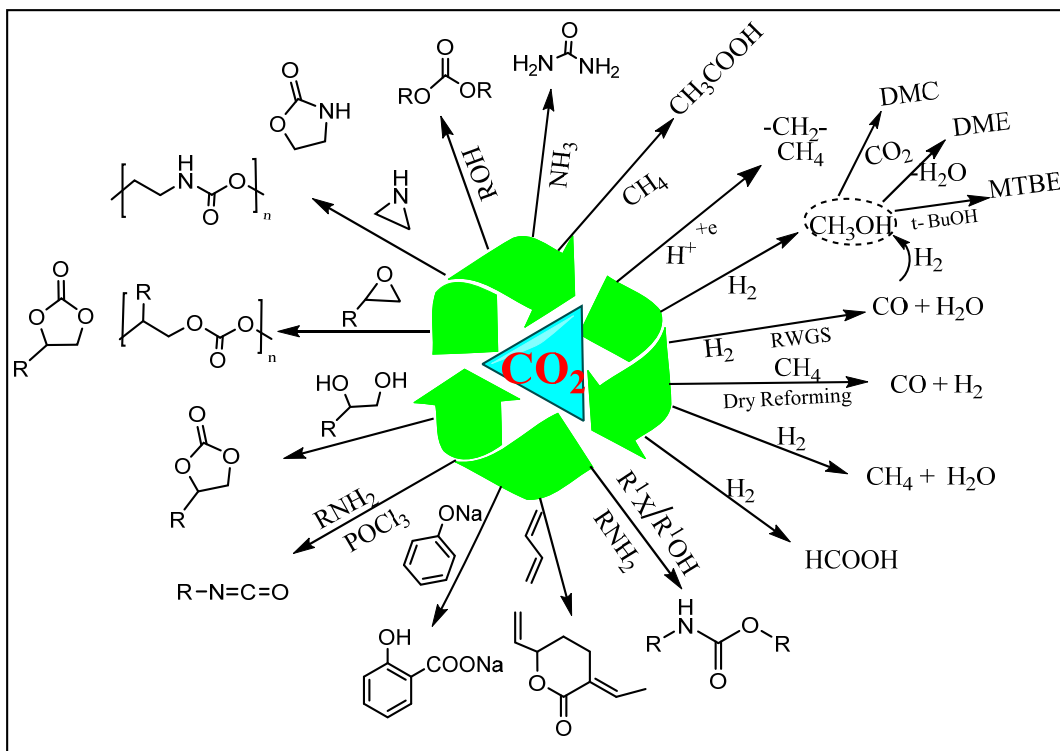


Fig. 1.5. CO<sub>2</sub> utilization into fuels and chemicals [53].

As compared to conventional/industrial DMC synthesis processes, use of CO<sub>2</sub> in its synthesis reduces the global warming potential (GWP) by 4.3 times and ozone layer depletion by 13 times [54]. Direct and indirect schemes involving CO<sub>2</sub> in DMC synthesis have been designed (Fig. 1.6). Direct use of CO<sub>2</sub> is the benign way to synthesize DMC. It also incorporates great opportunities for technology development.

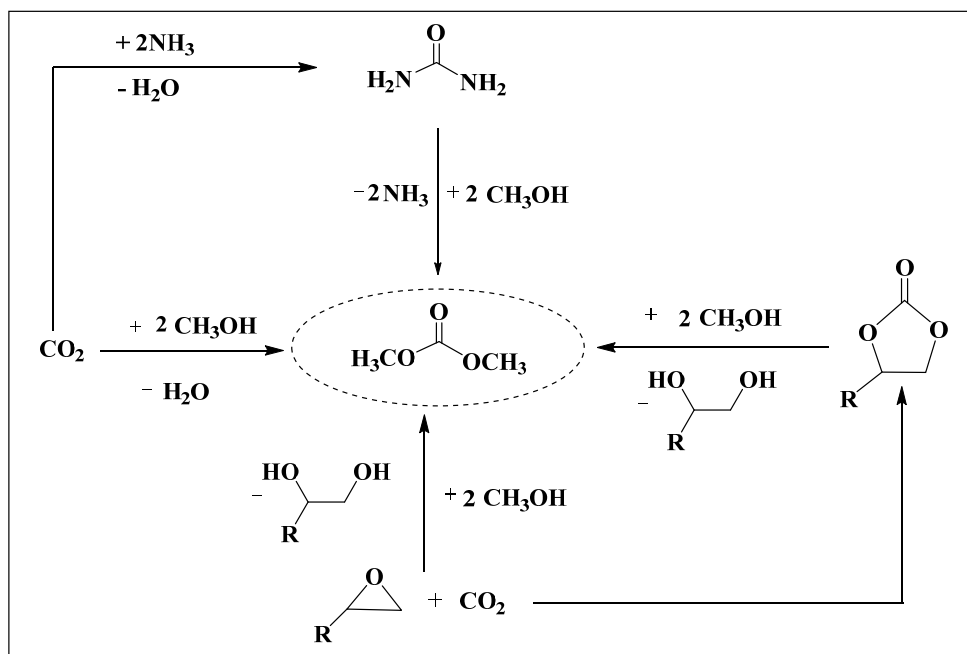


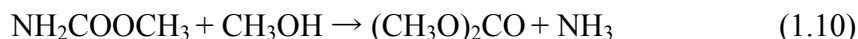
Fig. 1.6. CO<sub>2</sub> utilization in DMC synthesis.

## 1.5.2. Indirect utilization via transesterification

### 1.5.2.1. Urea methanolysis

Transesterification of urea with methanol produces DMC as the main product and ammonia as the byproduct (Eqs. 1.9 and 1.10). It is a two step reaction in which first step is the formation of methyl carbamate (MC, Eq. 1.9). MC formation is fast and highly selective due to fast decomposition of urea into ammonia and isocyanic acid (HNCO). Isocyanic acid reacts very fast with methanol to produce MC. In the second step, the MC intermediate reacts with one mole of methanol to generate DMC (Eq. 1.10) and is the rate determining step. Thermodynamically the reaction is non-spontaneous therefore two temperature regimes are used, first step ( $\Delta_r G_{298K} = -16.02$  kJ/mol) is carried at  $\sim 100$  °C and the second step ( $\Delta_r G_{298K} = 3.4$  kJ/mol) is carried out at 180-190 °C [31]. The reaction can also be carried out from the second step alone using MC as

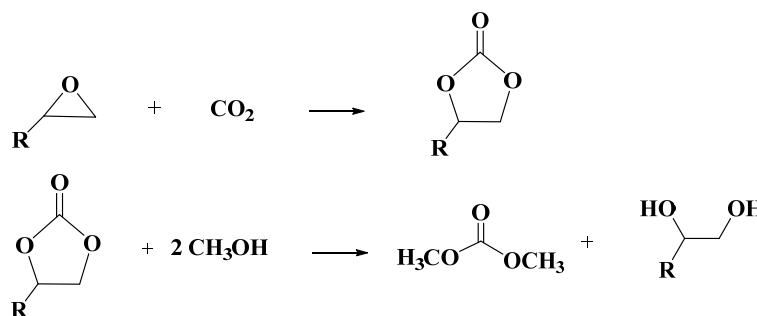
the raw material [31,58]. The main advantage of this method is the abundance and low cost of reactants. Moreover,  $\text{NH}_3$  formed can be recycled to produce urea.



A number of basic catalysts such as organotin catalyst [59], ZnO based catalysts [60-62], different metal oxides such as CaO, MgO,  $\text{ZrO}_2$ , PdO,  $\text{La}_2\text{O}_3$ , etc., [61,63] and supported metal oxide catalysts [64] were scrutinized for the reaction. The highest yield of DMC was reported using ZnO-CeO<sub>2</sub>-La<sub>2</sub>O<sub>3</sub> mixed oxides (50 mol% at 170 °C, 4 h) [65]. The process has been elevated to pilot plant scale and aimed at a production of thousands of tons of DMC per annum [66,67].

### 1.5.2.2. Transesterification of cyclic carbonate

Transesterification of cyclic carbonates with methanol also produces DMC as the main product and glycol as the byproduct. Like urea transesterification, it is also a two step process. In the first step, epoxides like ethylene oxide (EO) and propylene oxide (PO) are reacted with  $\text{CO}_2$  to produce ethylene carbonate (EC) and propylene carbonate (PC), respectively. In the second step, ester exchange reaction of EC and PC with methanol occurs to produce DMC (Scheme 1.3). These two steps are generally carried out independently.



**Scheme 1.3.** DMC synthesis via transesterification of cyclic carbonate

Transesterification of EC and PC produces ethylene glycol and propylene glycol, respectively, which are considered as chemicals of commercial importance especially in polyester industry. Cyclic carbonates (EC/PC) can be made in high yields with absolute selectivity at moderate reaction conditions using several catalysts. Srivastava et al. [68-70] reported several modified silica-based heterogeneous systems for this reaction. Three different types of epoxides (PO, epichlorohydrin and styrene oxide) were used. Among the different solid

catalysts reported so far, organo-functionalized metallocsilicate catalyst, Ti(Al)-SBA-15-grafted adenine were found to be the best (80- 90mol% yields, 120 °C, 0.69 MPa CO<sub>2</sub>, 6 h) [53]. Between EO and PO, the former has difficulties in handling due to explosion limits. But EC transesterification was found to be much easier than PC transesterification because of its low steric hindrance and low diffusional limitations. Special attention was given to improve the yield of DMC via PC transesterification.

Both homogeneous and heterogeneous acidic/basic catalysts were attempted for EC/PC transesterification with methanol. A nucleophilic substitution mechanism is followed in homogeneous basic catalysts and the activity depends on the strength of nucleophilicity of the catalyst (Table 1.2). Alkali metals [71], strong nitrogen bases and verkade super bases (porazaphosphotrane) are highly active in the transesterification of EC/PC with methanol [72]. Zhao et al. [73] reported a quaternary ammonium salt functionalized chitosan based catalyst for the transesterification of PC. The catalyst yielded 54 mol% DMC at 71 mol% PC conversion. Jagtap et al. [74] reported a recyclable polyvinylpyridine (PVP) catalyst for the transesterification of EC and methanol. Distillation of the reaction mixture enabled the separation of the catalyst due to its high boiling point. After 3 recycles the DMC yield was 75 mol%, 7 mol% less than the initial yield.

**Table 1.2.** Activity of homogeneous base catalysts for EC/PC transesterification with methanol

Catalyst	EC/PC:MeOH (molar ratio)	T (°C)	t (h)	P (MPa)	DMC yield (%)	Ref.
LiOH	EC:MeOH (1:4)	25	1	0.34	61.5	[71]
NaOH	EC:MeOH (1:4)	25	1	0.34	55.1	[71]
K <sub>2</sub> CO <sub>3</sub>	EC:MeOH (1:4)	25	1	0.34	55.2	[71]
1-Ethyl 3-methyl imidazolium chloride	EC:MeOH (1:8)	140	6	1.38	76.2	[89]
[C <sub>4</sub> DABCO]OH	EC:MeOH (1:10)	70	4	-	50.0	[90]
Poly(4-vinylpyridine)	PC:MeOH (1:8)	140	4	0.1	82.0	[74]
LiOMe	PC:MeOH(1:4.1)	120	-	-	78.0	[72]
NaOMe	PC:MeOH(1:4.1)	120	-	-	77.0	[72]
Tetrabutyl ammonium chloride	PC: MeOH (1:8)	140	6	2.07	47.6	[91]



The unique properties of ionic liquids (ILs) were also exploited in the transesterification. Dharman et al. [75] reported the use of different ILs (1-alkyl-3-methyl imidazolium and tetraalkyl ammonium salts) in the transesterification of EC under microwave irradiation. A DMC yield of 81.7 mol% with 95.8% selectivity was obtainable by using tetrabutylammonium iodide (TBAI) at 100 W microwave powers for 15 min. Abimanyu et al. [76] studied the activities of MgO–CeO<sub>2</sub> mixed oxides modified by different ionic liquids (1-alkyl-3-methyl imidazolium hexafluorophosphates, 1-butyl-3-methyl imidazolium trifluoromethanesulphonate and 1-butyl-3-methyl imidazolium tetrafluoroborate) in the transesterification of EC. Catalytic activity was increased by the involvement of ILs and was identified due to the enhancement of strength and quantity of surface basicity of the catalyst. The catalyst prepared with 1-butyl-3-methylimidazolium tetrafluoroborate ([Bmim][BF<sub>4</sub>]) showed the best activity (DMC yield = 56.6 mol% with 87% selectivity at 150 °C, liquid hourly space velocity (LHSV) = 3 h<sup>-1</sup>). Wang et al. [77] investigated the role of cations (1-butyl-3-methylimidazolium, 1-octyl-3-methylimidazolium and tetrabutylammonium)/anions (Cl<sup>-</sup>, Br<sup>-</sup>, BF<sub>4</sub><sup>-</sup>, PF<sub>6</sub><sup>-</sup>, bis(trifluoromethylsulfonyl)imide) of 1-alkyl-3-methylimidazolium and quaternary ammonium salt based ILs in the transesterification of EC, nevertheless they were unsatisfactory due to low DMC selectivity and high yield of unwanted 2-hydroxyethyl methyl carbonate. At the same time, carboxylic functionalized imidazolium salt showed the high DMC yield (82 mol%) with 99% selectivity. Additionally, silica-supported ILs (BMImBr-AS and QCl-MS41) were also reported for this reaction as efficient recyclable catalysts [78, 79].

Although homogeneous inorganic bases and ILs efficiently catalyzed the reaction, their separation and reuse is a big concern. In this context, solid base catalysts were attempted for the reaction (Table 1.3). Watanabe et al. [80] reported the use of Mg-Al hydrotalcites in EC transesterification. The catalyst was able to yield only 35 mol% DMC at 70 °C in 6 h in a batch reaction. Feng et al [81] used amino functionalized MCM-41 as solid base catalyst in the transesterification of EC in a fixed bed glass reactor to yield a DMC yield of 44 mol%. Sankar et al. [82] reported a DMC yield of 80 mol% in the transesterification of EC at ambient conditions over a sodium tungstate catalyst in a batch process. The group continued the study over CaO-ZnO based catalysts with varying Ca/Ca+Zn ratios and reported a DMC yield of 84 mol% both in batch and continuous reactions [83]. Wang et al [84] reported a DMC yield of 54 mol% in EC transesterification over binary zinc-yttrium oxides (Table 1.3).

**Table 1.3.** Activity comparison of solid catalysts for transesterification of EC/PC with methanol

Catalyst	EC/PC:MeOH (molar ratio)	T (°C)	t (h)	P (MPa)	DMC yield (%)	Ref.
K-TS-I	EC:MeOH (1:4)	65	3	-	64.0	[85]
MgO	EC:MeOH (1:4)	150	4	-	60.0	[92]
Smectite-Mg-Na	EC:MeOH (1:8)	150	4	-	78.0	[93]
Smectite-Mg-Na-K	EC:MeOH (1:8)	150	4	-	88.0	[93]
Na <sub>2</sub> WO <sub>4</sub> .2H <sub>2</sub> O	EC:MeOH (1:10)	RT	5	-	80.0	[82]
Amberlyst A-21	EC:MeOH (1:8)	120	14	-	85.0	[94]
MgO-CeO <sub>2</sub>	EC:MeOH (1:8)	150	-	0.2	64.0	[95]
Mg-Al HT-C (Mg/Al=3)	EC:MeOH (1:4)	70	6	0.1	35.0	[96]
Na-Dawsonite-C	EC:MeOH (1:4)	70	6	0.1	65.0	[96]
CaO-ZnO(Ca/Ca+Zn =0.4)	EC:MeOH (1:10)	27	4	-	83.0	[83]
ZnO- Y <sub>2</sub> O <sub>3</sub> (3:1)	EC:MeOH (1:8)	65	1	-	54.0	[84]
Na-ZSM5	EC:MeOH (1:8)	70	-	-	80.0	[97]
THA-MS41	EC:MeOH (1:8)	180	4	1.17	76.3	[98]
Meso graphitic carbon nitride	EC:MeOH (1:10)	160	-	0.6	81.3	[99]
CaO	PC:MeOH (1:4)	10	2	-	48	[100]
Fe-Zn Double metal cyanide	PC:MeOH (1:10)	170	8	-	86.6	[87]
Au/CeO <sub>2</sub>	PC:MeOH (1:10)	140	6	-	35	[101]
Egg shell	PC:MeOH (1:10)	25	2	0.1	79	[102]
Mg-La oxide	PC:MeOH (1:10)	150	2	-	55.9	[103]

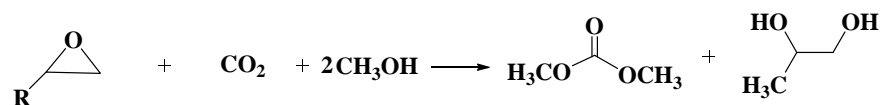
Potassium exchanged TS-1 was reported as a catalyst by Tatsumi et al. [85] in the transesterification of EC. The catalyst produced 64 mol% of DMC at 65 °C in a 3 h reaction. Wang et al. [86] reported the transesterification of PC with methanol in a continuous distillation reactor over CaO-ZrO<sub>2</sub> catalyst (PC conversion = 95 mol% at 150 °C and 0.5 MPa pressure). The catalyst was found to be stable in activity on a 250 h run. Srivastava et al. [87] reported the use of a Fe<sup>2+</sup>-Zn<sup>2+</sup> double-metal cyanide catalyst in the transesterification of PC. The catalyst was found to be the most active and selective than the reported catalysts. At a PC conversion of

100 mol%, a selectivity of >99% and an isolated DMC yield of 86 mol% was achieved. Asahi Kasei Corp. (Japan) and Chi Mei Corp. (Taiwan) have commercialized the EC transesterification process in 2002 [88].

### 1.5.3. Direct utilization

#### 1.5.3.1. One-pot synthesis of DMC from CO<sub>2</sub>, oxiranes and methanol

In order to eliminate the disadvantages of two step transesterification process (i.e., separation of intermediate EC/PC and subsequent transesterification with methanol) a one-pot synthesis route was investigated (Scheme 1.4).



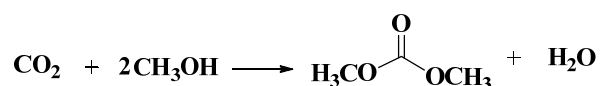
**Scheme 1.4.** One-pot synthesis of DMC from epoxides (EO/PO), CO<sub>2</sub> and methanol

Bhanage et al. [92] studied MgO as a catalyst for the one-pot synthesis of DMC from EO/PO, CO<sub>2</sub> and methanol. The catalyst gave 96.1 mol% of EO and 99.2 mol% of PO conversions with a DMC selectivity of 28.0 and 13.6%, respectively. Structure-activity correlations concluded that strong and moderately strong basic sites to be essential in cyclic carbonate formation, and moderately strong basic sites for transesterification. Cui et al. [104] reported the reaction in supercritical CO<sub>2</sub> using a combination of KI and K<sub>2</sub>CO<sub>3</sub>. Reaction temperature and CO<sub>2</sub> pressure found to have a major role on the reaction rate and DMC selectivity. Formation rate of DMC decreased with increase in pressure and increased with increase in temperature [105]. Supporting KI and K<sub>2</sub>CO<sub>3</sub> on ZnO increased the activity and facilitated easy separation [106]. A number of other catalyst systems such as Re(CO)<sub>5</sub>Cl/K<sub>2</sub>CO<sub>3</sub> [107], KOH/4A molecular sieve [108], n-Bu<sub>4</sub>NBr / n-Bu<sub>3</sub>N [109], [bmim]/BF<sub>4</sub> [110], Mg containing Smectite [111] and inorganic base/phosphonium halide functionalized polyethylene glycol [112] has also been reported for the one-pot synthesis of DMC. Although this method is advantageous in terms of low energy consumption and cost, it is limited because of low DMC selectivity (< 40%).

#### 1.5.3.2. Direct synthesis of DMC from methanol and CO<sub>2</sub>

Direct synthesis of DMC from CO<sub>2</sub> and methanol (Scheme 1.5) is the simplest and eco-friendly approach than all the greener alternative routes existing for DMC production. However,

due to thermodynamic and equilibrium limitations and kinetic barrier, its implementation in commercial level is difficult.



**Scheme 1.5.** DMC synthesis from CO<sub>2</sub> and methanol

Thermodynamic parameters of various substances involved in the direct synthesis of DMC are given in Table 1.4. Enthalpy ( $\Delta_r H^\circ_{298}$ ) and Gibbs free energy ( $\Delta_r G^\circ_{298}$ ) of the reaction at 25 °C are calculated with the assistance of enthalpy of formation ( $\Delta_f H^\circ$ ) and free energy of formation ( $\Delta_f G^\circ$ ) values [113].

**Table 1.4.** Thermodynamic data of substances involved in the direct synthesis of DMC from CO<sub>2</sub> and methanol [113]

Substance	$\Delta_f H^\circ$ (kJ/mol)	$\Delta_f G^\circ$ (kJ/mol)	$C_p$ (0–127 °C, kJ/mol/K)
DMC(l)	-613.78	-464.23	0.1095
H <sub>2</sub> O (l)	-285.83	-237.14	0.0753
CO <sub>2</sub> (g)	-393.51	-394.38	0.0371
CH <sub>3</sub> OH (l)	-239.10	-166.60	0.0816

$$\Delta_r H^\circ_{298} = -27.90 \text{ kJ/mol} \quad (1.11)$$

$$\Delta_r G^\circ_{298} = 26.21 \text{ kJ/mol} \quad (1.12)$$

Positive  $\Delta_r G^\circ$  and negative  $\Delta_r H^\circ$  values indicate the non-spontaneous and exothermic nature of the reaction, respectively. Assuming  $C_p$  being independent of temperature, heat of reaction at different temperatures can be calculated with the help of Kirchoff law as,

$$\Delta H_r^\circ = \Delta_r H^\circ_{(298\text{K})} + \Delta C_p (T-298) = -23.29 - 0.0155T \quad (1.13)$$

$\Delta_r G^\circ$  at different temperatures can be calculated from Gibbs-Helmholtz equation as,

$$d\left(\frac{\Delta_r G^\circ}{T}\right) = \left[\frac{23.29 + 0.155 T}{T^2}\right] dT \quad (1.14)$$

On integration and rearrangement, Eq. 1.14 transforms to Eq. 1.15.

$$\Delta_r G_T^\circ = \left[\frac{T \Delta_r G^\circ_{(298\text{K})}}{298}\right] - 23.29 T \left[\left(\frac{1}{T}\right) - \left(\frac{1}{298}\right)\right] + 0.0155 T \ln\left(\frac{T}{298}\right) \quad (1.15)$$

According to Eqs. 1.13 and 1.15, as the temperature increases  $\Delta H_r^\theta$  becomes more negative and  $\Delta_r G_T^\theta$  becomes more positive. Therefore, lower temperatures are preferable for DMC synthesis [113].

The  $\Delta_r G_P^\theta$  in terms of pressure, at constant temperature, can be calculated as follows.

$$dG = VdP - SdT \quad (1.16)$$

$$d\Delta_r G = \Delta V dp = (V_l - V_g) dP \quad (1.17)$$

when  $V_g \gg V_l$

$$d\Delta_r G = \Delta V dp = -V_g dP = -(RT/P)dP \quad (1.18)$$

$$\Delta_r G_P^\theta = \Delta_r G^\theta - RT \ln(P/P^\theta) \quad (1.19)$$

Based on Eq. 1.19, an enormous pressure ( $\geq 2.41 \times 10^4$  MPa at  $T = 80$  °C) is required to run the reaction ( $\Delta_r G_P^\theta$  becomes  $\leq 0$ ) [113].

A wide range of homogeneous and heterogeneous catalysts were studied for this synthesis route. Fang et al. [114] were the first to use inorganic bases (alkali metal hydroxides, carbonates and alkoxides) as catalysts and  $\text{CH}_3\text{I}$  as promoter in the synthesis DMC from  $\text{CO}_2$  and MeOH.  $\text{K}_2\text{CO}_3$  was found to be the best catalyst among them (DMC yield = 12.4 mol%-based on methanol at 100 °C and 200 mmol of  $\text{CO}_2$ ). Bhanage et al. [115] investigated the reaction mechanism and confirmed that  $\text{CH}_3\text{I}$  participated in the reaction as a reactant than as a promoter. Organotin alkoxides for instance dibutyltin dimethoxide showed 1.5 mol% DMC yield under an operating condition of 20 MPa  $\text{CO}_2$ , 150 °C and 15 h. The catalyst was deactivated by the presence of byproduct water [116]. Choi et al. [117] used molecular sieve 3A and 2,2-dimethoxypropane (DMP) as dehydrating agent to improve the DMC yield up to 28 mol% (30 MPa  $\text{CO}_2$ , 180 °C and 24 h). Although organotin alkoxy compounds showed good activity, they were unstable and are regarded as mammalian toxic reagents [31]. The same group developed a Ti analogue of organotin compounds and reported a maximum DMC yield of 41 mol% in presence of polyether type ligands (decyl-18-crown-6) under the same reaction conditions [118]. Nickel acetate showed good productivity (DMC yield = 3 mol%) even in the presence of water at moderate reaction conditions of 10 MPa of  $\text{CO}_2$  and 32 °C [119]. Alkaline metal free organic catalyst (1,8-Diazabicyclo[5.4.0.]undec-7-ene) with  $\text{CH}_2\text{Br}_2$  as solvent and hydrophobic ionic

liquid ([BMIF]PF<sub>6</sub>) as promoter showed good catalytic activity of 48 mol% DMC yield at 70 °C, 18 h and 1 MPa of CO<sub>2</sub> [120].

Catalytic activities of several heterogeneous catalysts are presented in Table 1.5. Among them, ceria, zirconia and tin-based systems were identified as the most effective due to their acid-base properties. Tomishige et al. [121,122] have reported a set of ZrO<sub>2</sub> catalysts prepared by the calcination of zirconium hydroxide at different temperatures. A maximum DMC yield of 1 mol% at 5 MPa CO<sub>2</sub> and 160 °C for 16 h was reachable on the catalyst calcined at 400 °C. Acidic and basic sites present on ZrO<sub>2</sub> surface are responsible for DMC formation. In the proposed reaction pathway, basic sites activate methanol and CO<sub>2</sub> and acidic sites assist the formation of methyl group from the methanol. Later, this mechanism was confirmed by Jung et al. [123] by in situ Fourier transform infrared (FTIR) and Raman spectroscopic techniques. The same group also studied the performance of monoclinic and triclinic ZrO<sub>2</sub> and identified monoclinic ZrO<sub>2</sub> to be superior in catalytic activity due to its high quantity and strength of basic sites. Jiang et al. [124] improved the quantity and strength of acid sites of ZrO<sub>2</sub> by post acid modification with H<sub>3</sub>PW<sub>12</sub>O<sub>40</sub> and reached a DMC yield upto 4.3 mol% (Table 1.5, entry no. 3). Unfortunately, the strong acid sites reduced the selectivity by favoring the byproduct formation (dehydration of methanol to dimethyl ether). An appropriate strength of acidity and basicity is essential for high DMC yield in MeOH + CO<sub>2</sub> reaction. Yoshida et al [125] reported CeO<sub>2</sub> as an effective catalyst for the activation of CO<sub>2</sub> and methanol in direct synthesis of DMC (Table 1.5, entry no. 4). Tomishige et al. [126] noticed an enhancement in catalytic activity in the case of a CeO<sub>2</sub>/ZrO<sub>2</sub> solid solution. A DMC yield of 1.7 mol% was obtained over CeO<sub>2</sub>/ZrO<sub>2</sub> with the composition of Ce/(Ce + Zr) at 20% (Table 1.5, entry no. 2 ). Other composite oxides like Ga<sub>2</sub>O<sub>3</sub>/Ce<sub>x</sub>Zr<sub>1-x</sub>O<sub>2</sub> and H<sub>3</sub>PW<sub>12</sub>O<sub>40</sub> modified CeO<sub>2</sub> and Ce<sub>x</sub>Ti<sub>1-x</sub>O<sub>2</sub> were also found to be highly active than pure CeO<sub>2</sub> and ZrO<sub>2</sub>. The enhancement in DMC yield was attributed to the increase in amount of acidic-basic sites, synergetic effect and catalyst stability [127, 128]. Tkatchenko et al. [129] demonstrated an improvement in DMC yield (> 4 mol% of DMC/Zr & Sn) with ZrO<sub>2</sub> and SnO<sub>2</sub> supported on SiO<sub>2</sub>. Very recently, the effect of morphology of CeO<sub>2</sub> crystallites on DMC yield was also investigated. CeO<sub>2</sub> with spindle morphology showed higher DMC yield (0.43 mol%) than rods (0.28 mol%), cubes (0.19 mol%) and polyhedral morphology (0.038 mol%) [130]. All these studies concluded that both acidic and basic sites are essential for the

reaction. Without a dehydration system the yields were very low. The maximum DMC yield obtained was 5.0 mol% (ie. 10 mmol/g<sub>cat</sub>) (Table 1.5, entry no. 5).

**Table 1.5.** Solid catalyst systems for direct synthesis of DMC from CO<sub>2</sub> and methanol

No.	Catalyst	T (°C)	t (h)	P <sub>CO2</sub> (Mpa)	Water trapper	DMC yield (mol %)	Ref
1	ZrO <sub>2</sub>	160	16	5	-	1	[122]
2	CeO <sub>2</sub> - ZrO <sub>2</sub>	110	16	21	-	1.7	[126]
3	H <sub>3</sub> PW <sub>12</sub> O <sub>40</sub> /ZrO <sub>2</sub>	100	3.5	1	-	4.3	[124]
4	CeO <sub>2</sub>	130	4	6	-	0.7	[125]
5	H <sub>3</sub> PW <sub>12</sub> O <sub>40</sub> /Ce <sub>0.1</sub> Ti <sub>0.9</sub> O <sub>2</sub>	170	12	5	-	5.0	[127]
6	Al <sub>2</sub> O <sub>3</sub> /CeO <sub>2</sub>	135	5	5	-	2.1	[135]
7	Rh/ZSM5	120	n.a	0.1	-	0.2	[136]
8	SnO <sub>2</sub>	150	100	20	-	1.6	[137]
9	Sn-SBA-CH <sub>3</sub>	150	70	20	-	0.75	[138]
10	Cu-Ni/graphite oxide	105	3	1.2	-	9.1	[131c]
11	Cu-Fe /SiO <sub>2</sub>	120	-	1.2	-	4.6	[131e]
12	CeO <sub>2</sub> -ZrO <sub>2</sub>	110	140	6	2,2Dimethoxypropane	7.2	[139]
13	CeO <sub>2</sub>	150	48	0.5	Acetonitrile	8.9	[140]
14	ZrO <sub>2</sub> -KCl-MgO	150	8	5	Butylene oxide	7.2	[141]
15	Ce <sub>0.5</sub> Zr <sub>0.5</sub> O <sub>2</sub>	100	34	12	1,1,1Trimethoxy methane	10	[142]
16	CeO <sub>2</sub>	150	86	1	Benzonitrile	47	[143]
17 <sup>a</sup>	Hydrotalcite	130	n.a	n.a	Silica lyogel (gas phase reaction)	16	[144]
18	CeO <sub>2</sub>	120	12	5	2-cyanopyridine (2-CP)	94	[134]

<sup>a</sup>CH<sub>3</sub>OH/CO<sub>2</sub> = 1/25 and residence time of 0.047 ml/min.

In addition to these discussed catalyst systems, several other heterogeneous catalysts such as Cu-Ni and Cu-Fe bimetallic catalysts on different supports (DMC yield in the range of 3.7 to

9.1 mol% at 100-120 °C and 1.2 MPa of CO<sub>2</sub>) [131], Mo-Cu-Fe/SiO<sub>2</sub> (6.1 mol% of DMC at 120 °C and 0.6 MPa of CO<sub>2</sub>) [132] and copper modified (Ni,V,O) photocatalyst (4.0 mol% of DMC at 120 °C and 1.2 MPa of CO<sub>2</sub>) [133] were also investigated in the gas phase reaction system. Gas phase reaction system is a dehydrating system, which is expected to constitute a water free reaction system by purging with inert gas [57]. In order to avoid the equilibrium limitations of DMC yield, removal of water with different chemicals and materials were also extensively studied. The dehydrating agents used in the reaction are classified into two types. They are: (a) non-reactive dehydrating systems and (b) reactive dehydrating agents. Non-reactive dehydration systems include membrane separation (polyimide-silica hybrid membrane and NaA-type tubular ceramic membrane) and inorganic adsorbents (molecular sieve 3A and silica lyogel). They can improve the DMC yield up to 16% [57]. Reactive dehydrating agents, such as butylene oxide, acetals (2,2-dimethoxy propane (DMP)), orthoesters (trimethoxymethane (TMM)), aliphatic and aromatic nitriles (acetonitrile, benzonitrile and 2-cyanopyridine), etc., react with water and give corresponding products such as butylene glycol, ketone, esters and amides [57]. Highest DMC yield, 94 mol% (138.2 mmol/g<sub>cat</sub>) was achieved by using CeO<sub>2</sub> as catalyst and stoichiometric quantity of 2-cyanopridine as a dehydrating agent (Table 1.5, entry no. 18) [134]. Reactive dehydrating agents especially nitriles are more promising when considering the DMC yield. Non-reactive dehydrating systems like molecular sieve are attractive in view of eco-friendliness. Design of novel and competent catalysts along with in situ water removal techniques represent a major challenge. At this stage, the process is far from commercialization. Development of a stable catalyst with high productivity with economically favorable dehydration technology needs a serious and systematic scientific research.

### 1.6. Solid oxide catalyst for DMC synthesis

Solid catalysts are the major representatives of industrial chemical research. In 2013, the global demand of heterogeneous (solid) catalysts was more than 4,900 kt. This amount was around 80% of the global market share. The solid catalyst technology is spread over various sectors which include chemical manufacturing, petroleum refining, pharmaceuticals, polymer synthesis, renewable fuel and transportation fuel production and several others. Chemicals manufacturing is the major consumer of solid catalysts. It demands 1800 kt i.e., about 40% of the total demand. It is expected to grow rapidly in coming years, especially in Asia Pacific and Latin America. Environmental catalysis, petroleum refineries and polymer industry are the other major



consumers of catalysts [145]. The new approaches in catalyst design and application always make great impact on global catalyst market. Solid oxide catalysts are attractive in a commercial perspective because of the ease of preparation and excellent/tunable physicochemical properties. It is widely accepted that tuning the structure, morphology, composition, surface properties and crystallographic phases for particular chemical reactions of oxide catalysts is a fascinating area of research. Multi-component oxides and mixed metal oxides are used widely as catalysts in academia and industry than simple oxides. Mixed metal oxides are the oxides which contain two or more metal cations in a defined stoichiometry. Catalytic activity of such material is always better than the physical mixing of individual oxides. It is quite difficult to say the exact active site on those catalysts, because of the chemical and structural complexity. The arrangement of one metal ion depends on the nature and chemical environment of the other, which ultimately influences the catalytic activity [146].

### 1.6.1. Hydrotalcites and their derivatives

Hydrotalcites (HTs) are layered double hydroxides with general formula:  $[M^{2+}_{(1-x)}M^{3+}_x(OH)_2]^{x+}(A^{n-}_{x/n})_x \cdot yH_2O$ , where  $M^{2+}$  and  $M^{3+}$  are di- and trivalent metal ions and  $A^{n-}$  are interlayer anions (Fig. 1.7). HTs are structural analogues of brucite structure. In the brucite structure,  $Mg(OH)_6^{4-}$  octahedron unit forms an infinite sheet by sharing the edges, which is then stacked over one another through H-bonding interactions. To form HTs, a part of bivalent metal ions in the brucite structure is isomorphically substituted with trivalent metal ions resulting in an excess positive charge in the layers. This extra positive charge is balanced by anions such as  $CO_3^{2-}$ ,  $NO_3^-$ ,  $F^-$  and  $Cl^-$  present in the interlayer (anionic clay). Water of crystallization is also present in the interlayer galleries. These anions and water molecules are loosely bound and capable of moving over the layers through bond breaking and making phenomenon. The interlayer distance of HT structure depends on the number, size, orientation and strength of bond between anions and hydroxyl groups [147]. HTs can be used as an additive in polymers and as a precursor for magnetic materials. The main advantage of HTs as catalysts is their tunable acid-base properties. They have been used as effective catalysts in base-catalyzed organic reactions such as hydrogenation, polymerization, steam reforming and transesterification, and in medicine as antacid, antipeptin and stabilizer [147-149].

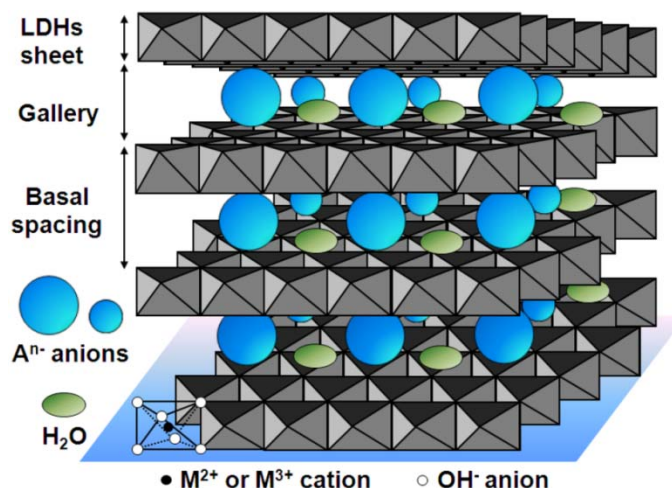


**Fig. 1.7.** Pictorial representation of HTs [150]

Calcination of HTs above 400 °C results in dehydration, dehydroxylation and decarbonylation to form homogeneous mixed metal oxides. Mixed oxides derived from HTs possess high surface area, basic properties and a homogeneous mixture of oxides with small crystallite size and high thermal stability to be used as catalysts [147]. They are relatively cheap, do not contain toxic metals and present enhanced stability both at high temperatures and in aqueous solutions [149].

### 1.6.2. Sodium titanate nanotube

Titanium dioxide (TiO<sub>2</sub>) is a well-known transition metal oxide which is non-toxic, eco-friendly and corrosion resistant for material applications. It has also been used in a number of chemical transformations as catalyst. The catalytic activity of these materials depends on their surface area which can be increased by reducing their crystallite size. Nano-range geometries such as nanotubes and nanorods allow modifying their physical, chemical and electronic properties with increase in surface area. Kasuga et al. [151] reported a novel method to synthesize mesoporous sodium titanate nanotubes in a non-templated, hydrothermal approach. In their procedure, TiO<sub>2</sub> was treated with a highly concentrated NaOH solution (> 6 M) followed by aging at a given temperature (100 - 180 °C) for a specified time (20 - 170 h) (Fig. 1.8). The product obtained was identified to be hydrous sodium trititanate with chemical formula Na<sub>2</sub>Ti<sub>3</sub>O<sub>7</sub>.nH<sub>2</sub>O. Sodium is essential for stabilizing the nanotubular structure. They are promising catalysts and catalyst supports in heterogeneous catalytic reactions (hydrogenation,

transesterification, oxidation, etc) due to excellent textural properties, high sodium content and good ion exchange ability [152-154].

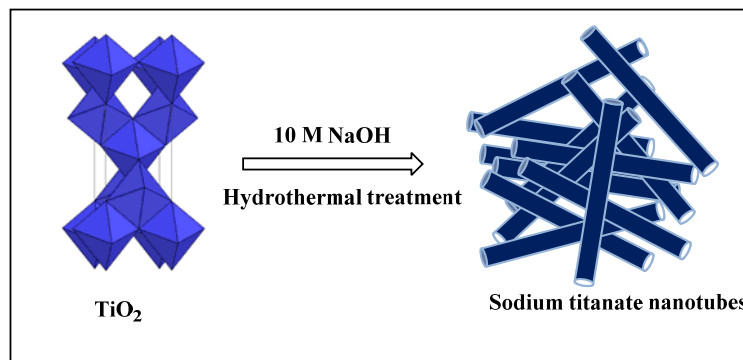


**Fig. 1.8.** Schematic representation sodiumtitanate nanotube formation.

### 1.6.3. Zirconium phenyl phosphonate phosphite

Zirconium phosphonates are layered materials with molecular formula  $Zr(O_3PR)_2$ . In the structure, the planes of  $Zr^{4+}$  ions are linked through oxygen atoms of phosphonate groups. The R groups (organic compounds, H and OH) are oriented alternatively above and below in a bilayer fashion in the interlayer region [155]. Structural analogues of zirconium phosphonates permit materials with unique surface characteristics.

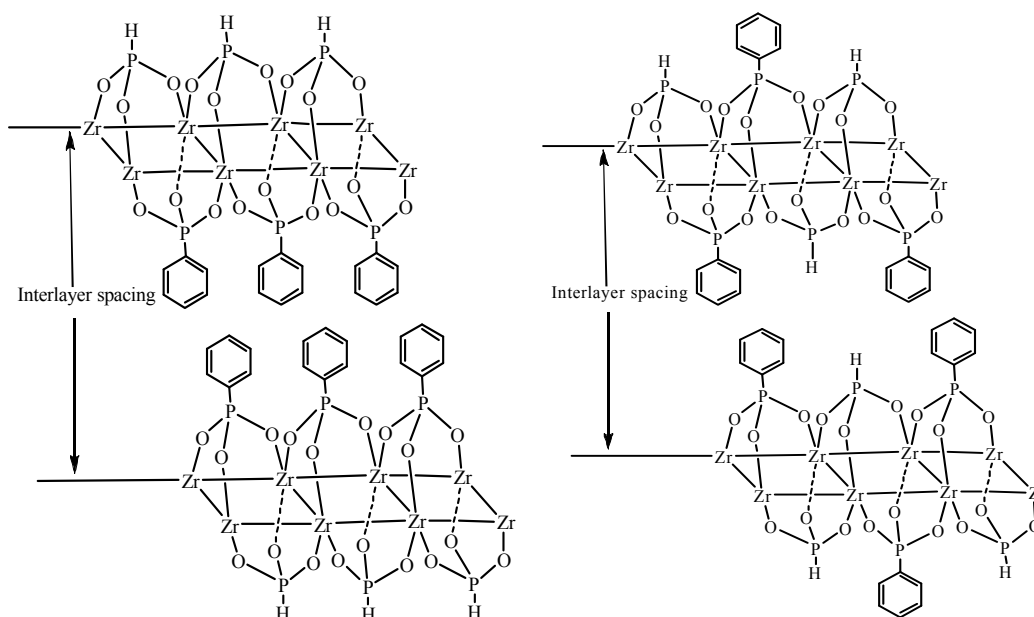


**Fig. 1.9.** Tentative structures of ZrPP

Zirconium phenyl phosphonate phosphite (ZrPP) (Fig. 1.9) is a structural derivative of  $\text{Zr}(\text{O}_3\text{PR})_2$  with molecular formula  $\text{Zr}(\text{C}_6\text{H}_5\text{PO}_3)_{2-x}(\text{HPO}_3)_x$ , where  $x$  varies between 0.8 and 1.7 according to phenyl phosphonic acid to phosphorous acid molar ratio, preparation method, etc. [156]. They are prepared by two methods: (a) slow decomposition of  $\text{ZrF}_6^{2-}$  in presence of a mixture of organic phosphonic acid and phosphorous acid and (b) rapid precipitation of zirconium salt with phosphorous acid and phosphonic acid mixture. Former method allows the formation of highly staged and crystalline material in which the organic and inorganic groups are separated in the adjacent layers where as the later method results in the formation of an amorphous material with each phosphonate group positioned opposite to phosphite group [157].

#### 1.6.4. Cerium oxide

Ceria ( $\text{CeO}_2$ ) is the most abundant rare-earth oxide present in earth's crust. It is a well-known material in the field of heterogeneous catalysis especially in pollution abatement, steam and dry reforming of hydrocarbons and oxygenates, CO oxidation and preferential CO oxidation in presence of  $\text{H}_2$  (PROX), water–gas shift (WGS) reaction and several organic reactions [158]. Apart from these applications, ceria is also used as a cathode, anode and electrolyte material in solid oxide fuel cells (SOFCs) and in biomedical applications (neuroprotective activity, retinopathy, cancer therapy, biosensors, etc.) [159,160]. A distinctive combination of high oxide ion diffusivity, high oxygen storage/release capacity and redox properties make it more versatile in different fields.  $\text{CeO}_2$  crystallizes in highly stable fcc cubic fluorite structure (Fig. 1.10).  $\text{CeO}_2$  can be precipitated by using different precipitating agents such as alkaline solutions, ammonia and urea in the presence and/or absence of templates to tailor its shape and fine tune its properties (defect concentration and density of oxygen vacancies) [161].

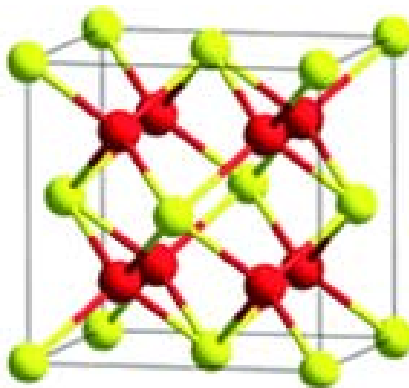


**Fig. 1.10.** Crystal structure of  $\text{CeO}_2$  (●O, ●Ce) [162]

### 1.7. Scope and objective of the work

DMC synthesis has attained a great interest in recent times due to its potential as a reagent in the synthesis of commercially important chemicals and as a fuel additive. Due to its unique properties and eco-friendly nature, DMC is able to find wide range of applications in various sectors of chemical industry. Several studies show that DMC has low toxicity, better evaporation rate and high biodegradability compared to other alternatives. Synthesis of DMC through oxidative carbonylation of methanol and other conventionally used industrial methods need to be replaced with eco-friendly green routes. Its synthesis via direct or indirect conversion of cheap, non-toxic, non-flammable and abundant  $C_1$ -feedstock,  $CO_2$  is attractive because of its significant role in mitigating global warming and climate change issues. Design of stable and efficient catalyst systems to activate and convert  $CO_2$  into DMC at a commercial level is highly desirable. Transesterification of cyclic carbonate with methanol is one of the viable routes for producing DMC. However, the hitherto known catalyst systems are energy intensive and less productive. Design of stable, highly active, solid base catalyst is crucial for this route. On the other hand, direct synthesis of DMC from  $CO_2$  and methanol is important. This method is more challenging due to its equilibrium limitation and non-spontaneous nature. In order to overcome these limitations, development of a highly efficient catalyst with suitable dehydrating system is indispensable.

The present work deals the use of solid base and solid acid-base bi-functional oxide catalysts for making DMC through transesterification of cyclic ethylene and propylene carbonates with methanol and direct methanolysis of  $CO_2$ . Catalytic activities of four sets of solid oxide catalysts: HT-derived mixed oxides and sodium titanate nanotubes (solid base catalysts for transesterification of cyclic carbonate) and calcined zirconium phenyl phosphonate phosphite and  $CeO_2$  of different morphology (solid acid-base bi-functional catalysts for  $CO_2$  + methanol reaction in the presence of different dehydrating agents) for DMC synthesis were explored. The influence of reaction parameters on catalytic activity was probed. One of the objectives of this study is to find out the governing factors influencing catalytic activity of said solid catalysts through structure-activity correlations.

### 1.8. Organization of thesis

The thesis is divided into seven chapters. A short narration of the contents of each chapter is given below.

**Chapter 1** presents a general introduction to properties, advantages and applications of DMC. It describes the conventional and green synthetic routes for making DMC. It reports different solid oxide catalyst systems employed for the direct and indirect conversion of CO<sub>2</sub> into DMC. Finally the objectives and scope of the work are presented.

**Chapter 2** illustrates the synthesis methodology of different solid catalysts used in this study. It also presents the various physicochemical characterization technique used in this work. A brief description of reaction procedures and product analysis is also provided. The various solid oxide catalysts investigated in the present work are:

- 1) Hydrotalcite (HT)-derived mixed oxide (for transesterification of cyclic ethylene and propylene carbonates (EC/PC) with methanol),
- 2) Sodium titante nanotubes (NaTNT) (for transesterification of EC/PC with methanol),
- 3) Calcined zirconium phenyl phosphonate phosphite (ZrPP-C) (for direct synthesis of DMC from carbon dioxide (CO<sub>2</sub>) and methanol), and
- 4) Ceria (CeO<sub>2</sub>) of different morphologies (for direct synthesis of DMC from CO<sub>2</sub> and methanol).

**Chapter 3** presents DMC synthesis through transesterification of cyclic carbonate with methanol over La-Mg-Al mixed oxides. Mg-Al HT modified with rare-earth elements (La<sup>3+</sup>, Ce<sup>3+</sup>, Y<sup>3+</sup>, Pr<sup>3+</sup> and Sm<sup>3+</sup>) and different mol% of La were prepared by a co-precipitation method. Calcination of these precursors yielded ternary lanthanum-magnesium-aluminum oxides. Among the catalysts, La (10 mol%) modified HT showed the highest activity (DMC yield = 95 mol% and 58 mol% (from EC and PC, respectively)) at moderate reaction conditions (80 °C and 4 h for EC + MeOH and 150 °C and 2 h for PC + MeOH). The influence of reaction parameters and calcination temperature on catalytic activity was also investigated. Kinetic parameters were determined for EC as well as for PC transesterifications. This catalyst was found to be reusable without loss in activity in at least four cycling experiments. The basicity of the catalyst plays a crucial role in its catalytic activity.

**Chapter 4** discusses the application of NaTNT catalyst in the transesterification of EC/PC. The catalytic activity of Na<sub>2</sub>Ti<sub>3</sub>O<sub>7</sub> nanotubes obtained by alkaline hydrothermal treatment was investigated for the cyclic carbonate transesterification at ambient reaction conditions. The influence of reaction time and catalyst amount on the DMC yield was studied. They are highly active yielding 90% of DMC from EC at room temperature and 66% of DMC

from PC at 100 °C. Kinetic study has been carried out at three different reaction temperatures and at varying reaction times, which revealed that the activation energy required for this catalyst is lower than other known catalysts. It was found that basicity with high surface accessibility to reactants is the principal factor that drives this reaction efficiently.

**Chapter 5** discusses the direct synthesis of DMC from CO<sub>2</sub> and methanol over calcined zirconium phenyl phosphonate phosphite (ZrPP-C) catalysts. ZrPP of different composition and crystalline nature were prepared by changing the synthesis procedure (phosphorous acid/phenylphosphonic acid molar ratio, use of HF and calcination temperature). Controlled calcination of ZrPP resulted in the formation of zirconium pyrophosphate like structure with bi-functional sites. This hydrophobic, acid-base bi-functional catalyst was highly active in DMC synthesis from CO<sub>2</sub> and methanol yielding 8.03 mmol/g of DMC at 170 °C for 12 h. The activity was further improved up to 26.06 mmol/g of DMC by using dimethyl formamide (DMF) (10 ml) and 3A-molecular sieves (0.5 g) as solvent and water scavenger, respectively. The role of acid-base sites, hydrophobicity and other structural- textural properties on catalytic activity and stability were established by methodical characterization and structural-activity correlations.

**Chapter 6** presents the factors influencing catalytic activity of CeO<sub>2</sub> on the direct synthesis of DMC in presence of stoichiometric quantities of 2-cyanopyridine as the reactive dehydrating agent. CeO<sub>2</sub> of varying morphology (cubes, rods, spindles and no definite shape) was used as a catalyst. CeO<sub>2</sub> with spindle morphology (Ce-S) was found to be superior in catalytic activity. The influence of reaction parameters and calcination temperature on DMC yield of spindle catalyst was also investigated. Defect site concentration and medium type acid/base site ratio of CeO<sub>2</sub> markedly influenced its catalytic activity/selectivity. The highest catalytic activity of Ce-S was attributed to its spindle morphology having a right balance of medium acid-base sites and defect centres.

**Chapter 7** furnishes an overall summary and conclusion of the thesis work.

By and large, this thesis contributes towards developing an eco-friendly, sustainable catalytic process for making DMC through transesterification of cyclic carbonate with methanol, and direct synthesis from CO<sub>2</sub> and methanol. Factors influencing the catalytic performance of solid oxide catalysts for these reactions were investigated.

## 1.9. References

- [1] B.A.V. Santos, V.M.T.M. Silva, J.M. Loureiro, A.E. Rodrigues, *ChemBioEng Rev.* 1 (2014) 214-229.
- [2] E. Leino, P. Maki-Arvela, V. Etta, D.Y. Murzin, T. Salmi, J.-P. Mikkola, *Appl. Catal. A: Gen.* 383 (2010) 1-13.
- [3] L.R. Rudnick (Ed.), *Synthetics, Mineral Oils, and Bio-Based Lubricants: Chemistry and Technology*, CRC Press, Taylor and Francis group, US, (2013).
- [4] Y. Ono, *Appl. Catal. A: Gen.* 155 (1997) 133-166.
- [5] P. Tundo, M. Selva, *Acc. Chem. Res.* 35 (2002) 706-716.
- [6] P. Tundo, L. Rossi, A. Lorris, *J. Org. Chem.* 70 (2005) 2219-2224.
- [7] F. Aricò, P. Tundo, *Russ. Chem. Rev.* 79 (2010) 479-489.
- [8] M. Selva, C.A. Marques, P. Tundo, *J. Chem. Soc. Perkin Trans. 1* (1994) 1323-1328.
- [9] A. Bomben, M. Selva, P. Tundo, *J. Chem. Res. (S)* (1997) 448-449.
- [10] S.T. Gadge, A. Mishra, A.L. Gajengi, N.V. Shahi, B.M. Bhanage, *RSC Adv.* 4 (2014) 50271-50276.
- [11] X. Jiang, A. Tiwari, M. Thompson, Z. Chen, T.P. Cleary, T.B.K. Lee, *Org. Process Res. Dev.* 5 (2001) 604-608.
- [12] S.T. Gadge, A. Mishra, A.L. Gajengi, N.V. Shahi, B.M. Bhanage, *RSC Adv.* 4 (2014) 50271-50276.
- [13] Y. Ono, M. Akiyama, E. Suzuki, *Chem. Mater.* 5 (1993) 442-447.
- [14] N. Keller, G. Rebmann, V. Keller, *J. Mol. Catal. A: Chem.* 317 (2010) 1-18.
- [15] K. Inamoto, C. Hasegawa, K. Hiroya, Y. Kondo, T. Osako, Y. Uozumi, T. Doi, *Chem. Commun.* 48 (2012) 2912- 2914.
- [16] G. Righi, P. Bovicelli, M. Barontinic, I. Tirota, *Green Chem.* 14 (2012) 495-502.
- [17] F. Aricò, U. Toniolo, P. Tundo, *Green Chem.* 14 (2012) 58-61.
- [18] M. Berhil, N. Lebrun, A. Tranchant, R. Messina, *J. Power Sources* 55 (1995) 205-210.
- [19] R. Naejus, R. Coudert, P. Willmann, D. Lemordant *Electrochimica Acta* 43 (1998) 275-284.
- [20] D. Fabbri, V. Bevoni, M. Notary, F. Rivetti, *Fuel* 86 (2007) 690-697.
- [21] Z. Ilham, S. Saka, *Bioresour. Technol.* 100 (2009) 1793-1796.
- [22] Z. Ilham, S. Saka, *Bioresour. Technol.* 101 (2010) 2735-2740.



- [23] P.J. Gaylor, US Patent 2,331,336 (1943).
- [24] D.M. Kane, R.Y. Iwamoto US Patent 4,904,279 (1990).
- [25] D.M. Dillon, R.Y. Iwamoto US Patent 4,891,049 (1990).
- [26] G.D. Zhang, H. Liu, X.X. Xia, W.G. Zhang, J.H. Fang, Proc. Inst. Mech. Eng. Part D 219 (2005) 7897-7903.
- [27] [https://www.eni.com/en\\_IT//Diphenylcarbonate-fl-lug09.pdf](https://www.eni.com/en_IT//Diphenylcarbonate-fl-lug09.pdf)
- [28] S. Faukoka, I. Fukawa, M. Tojo, K. Oonishi, H. Hachiya, M. Aminaka, K. Hasegawa, K. Komiya, Catal. Surv. Asia 14 (2010) 146-163.
- [29] M. Arresta, M. Galatola, J. Clean. Prod. 7 (1999) 181-193.
- [30] A.-A.G. Shaikh, S. Sivaram, Chem. Rev. 96 (1996) 951-976.
- [31] S. Huang, B. Yan, S. Wang, X. Ma, Chem. Soc. Rev. 44 (2015) 3079-3116.
- [32] U. Romano, R. Tesei, G. Cipriani, L. Micucci, US Patent 4,218,391 (1980).
- [33] U. Romano, F. Rivetti, N. Di Muzio, US Patent 4,318,862 (1982).
- [34] A.K. Bhattacharya, J.T. Nolan, US Patent 4,636,576 (1987).
- [35] F. Rivetti, U. Romano, EP 534,545 (1992).
- [36] W. Mo, H. Liu, H. Xiong, M. Li, G. Li, Appl. Catal. A:Gen. 333 (2007) 172-176.
- [37] V. Raab, M. Merz, J. Sundermeyer, J. Mol. Catal. A: Chem. 175 (2001) 51-63.
- [38] M. Stricker, T. Linder, B. Oelkers, J. Sundermeyer, Green Chem. 12 (2010) 1589-1598.
- [39] H. Wang, B. Wang, C.-L. Liu, W.-S. Dong, Microporous Mesoporous Mater. 134 (2010) 51-57.
- [40] Y. Cao, J.-C. Hu, P. Yang, W.-L. Dai and K.-N. Fan. Chem. Commun. (2003) 908-909.
- [41] G.L. Curnutt, US Patent 4625044A (1986).
- [42] G.L. Curnutt, US Patent 5004827A (1991).
- [43] G. L. Curnutt, D.L. Harley, Plenum Publishing Co. New York. (1988) 215-228.
- [44] Z. Zhang, X.B. Ma, J. Zhang, F. He, S.P. Wang, J. Mol. Catal. A: Chem. 227 (2005) 141-146.
- [45] Y.H. Zhang, D.N. Briggs, E. de Smit, A.T. Bell, J. Catal. 251 (2007) 443-452.
- [46] T.H.D. Thi, M. Bartoszik, M. Schneider, D.L. Hoang, U. Bentrup, A. Martin, Appl. Catal. B: Env. 121 (2012) 115-122.
- [47] T. Matsuzaki, A. Nakamura, Catal. Surv. Jap. 1 (1997) 77-88.
- [48] GlobalCarbonBudget.org

- [49] [http://scrippsco2.ucsd.edu/data/atmospheric\\_co2.html](http://scrippsco2.ucsd.edu/data/atmospheric_co2.html).
- [50] M. Arresta, A. Dibenedetto, A. Angelini, J. CO<sub>2</sub> Utiliz. 3-4 (2013) 65-73.
- [51] M. Peters, B. Köhler, W. Kuckshinrichs, W. Leitner, P. Markewitz, T.E. Müller, ChemSusChem 4 (2011) 1216-1240.
- [52] T. Sakakura, J. -C. Choi, H. Yasuda, Chem. Rev. 107 (2007) 2365-2387.
- [53] P. Unnikrishnan, D. Srinivas in: Industrial Catalysis and Separations: Innovations for Process Intensification, K.V. Raghavan and B. M. Reddy (Eds.), Apple Academic Press Inc., NJ, USA, (2015).
- [54] R.M. Cue' llar-Franca, A. Azapagic, J. CO<sub>2</sub> Utiliz. 9 (2015) 82-102.
- [55] T.E. Müller, W. Leitner, P. Markewitz, W. Kuckshinrichs, in: Carbon Capture Storage and Use, W. Kuckshinrichs, J. Hake (Eds.), Springer, Switzerland, 2015.
- [56] M.P-. Fortes, A.B-. Dumitriu, E. Tzimas, Eng. Proc. 63 (2014) 7968-7975.
- [57] M. Honda, M. Tamura, Y. Nakagawa, K. Tomishige, Catal. Sci. Technol. 4 (2014) 2830-2845.
- [58] D. Wang, X. Zhang, J. Ma, H. Yu, J. Shen, W. Wei, Catal. Sci. Technol. DOI. 10.1039/C5CY01712B (2016).
- [59] H. Lin, B. Yang, J. Sun, X. Wang, D. Wang, Chem. Eng. J. 103 (2004) 21-27.
- [60] C. Wu, X. Zhao, Y. Wang, Catal. Comm. 6 (2005) 694-698.
- [61] M. Wang, N. Zhao, W. Wei, Y. Sun, Ind. Eng. Chem. Res. 44 (2005) 7596-7599.
- [62] M. Wang, H. Wang, N. Zhao, W. Wei, Y. Sun, Ind. Eng. Chem. Res. 46 (2007) 2683-2687.
- [63] M. Wang, H. Wang, N. Zhao, W. Wei, Y. Sun, Catal. Comm. 7 (2006) 6-10.
- [64] C. Zhang, B. Lu, X. Wang, J. Zhao, Q. Cai. Catal. Sci. Technol. 2 (2012) 305-309.
- [65] W. Joe, H.J. Lee, U.G. Hong, Y.S. Ahn, C.J. Song, B.J. Kwon, I.K. Song, J. Ind. Eng. Chem. Res. 18 (2012) 1730-1735.
- [66] W. Wei, Y.H. Sun, M.H. Wang, N. Zhao, J.H. Yang, X.Z. Wang, Chin. Pat. 02155479. X (2002).
- [67] W. Wei, Y.H. Sun, N. Zhao, B.Y. Sun, B.S. Zhang, Y.J. Chen, Chin. Pat. 200410012504.1 (2004).
- [68] R. Srivastava, D. Srinivas, P. Ratnasamy, Catal. Lett. 89 (2003) 81-85.
- [69] R.Srivastava, D. Srinivas, P. Ratnasamy, Catal. Lett. 91 (2003) 133-137.

- [70] R.Srivastava, D. Srinivas, P. Ratnasamy, J. Catal. 233 (2005) 1-15.
- [71] M.S. Han, B.G. Lee, B.S. Ahn, K.Y. Park, S.I. Hong, React. Kinet. Lett. 73 (2001) 33-38.
- [72] D.B.G. Williams, M.S. Sibiya, P.S. Heerden, M. Kirk, R. Harris, J. Mol. Cat. A: Chem. 304 (2009) 147-152.
- [73] Y. Zhao, L.N. He, Y.Y. Zhuang, J.Q. Wang, Chin. Chem. Lett. 19 (2008) 286-290.
- [74] S.R. Jagtap, M.D. Bhor, B.M. Bhange, Catal. Comm. 9 (2008) 1928-1931.
- [75] M.M. Dharman, H.Y. Ju, H.L. Shim, M.K. Lee, J. Mol. Catal. A: chem. 303 (2009) 96-101.
- [76] H. Abimanyu, B.S. Ahn, C.S. Kim, K.S. Yoo, Ind. Eng. Chem. Res. 46 (2007) 7936-7941.
- [77] J.-Q. Wang, J. Sun, W.-G. Cheng, C.-Y. Shi, K. Dong, X.-P. Zhang, S.-J. Zhang, Catal. Sci. Technol. 2 (2012) 600-605.
- [78] D.-W. Kim, C.-W. Kim, J.-C. Koh, D.-W. Park, J. Ind. Eng. Chem. 16 (2010) 474-478.
- [79] D.-W. Kim, D.-O. Lim, D.-H. Cho, J.-C. Koh, D.-W. Park, Catal. Today 164 (2011) 556-560.
- [80] Y. Watanabe, T. Tatsumi, Microporous Mesoporous Mater. 22 (1998) 399-407.
- [81] X.J. Feng, X.B. Lu, R. He, Appl. Catal. A: Gen. 272 (2004) 347-352.
- [82] M. Sankar, C. Madhavan Nair, K.V.G.K. Murty, P. Manikandan, Appl. Catal. A: Gen. 312 (2006) 108-114.
- [83] M. Sankar, S. Satav, P. Manikandan, ChemSusChem 3 (2010) 575-578.
- [84] L. Wang, Y. Wang, S. Liu, L. Lu, X. Ma, Y. Deng, Catal. Commun. 16 (2011) 45-49.
- [85] T. Tatsumi, Y. Watanabe, K.A. Koyano, Chem. Commun. (1996) 2281-2282.
- [86] H. Wang, M. Wang, N. Zhao, W. Wei, Y. Sun. Catal. Lett. 105 (2005) 253-257.
- [87] R. Srivastava, D. Srinivas, P. Ratnasamy, J. Catal. 241 (2006) 34-44.
- [88] S. Fukuoka, M. Tojo, H. Hachiya, M. Aminaka, K. Hasegawa, Polymer J. 39 (2007) 91-114.
- [89] H.Y. Ju, M.D. Manju, D.W. Park, Y. Choi, S.W. Park, React. Kinet. Catal. Lett. 90 (2007) 3-9.
- [90] Z.Z. Yang, L.N. He, X.Y. Dou, S. Chanfreau, Tetrahedron Lett. 51 (2010) 2931-2934.
- [91] E.S. Jeong, K.H. Kim, D.W. Park, S.W. Park, J.W. Lee, React. Kinet. Catal. Lett. 86

- (2005) 241-248.
- [92] B.M. Bhanage, S. Fujita, Y. Ikushima, M. Arai, *Appl. Catal. A: Gen.* 219 (2001) 259-266.
- [93] B.M. Bhanage, S. Fujita, Y. He, Y. Ikushima, M. Shirai, K. Torri, M. Arai, *Catal. Lett.* 83 (2002) 137-141.
- [94] S. Dhuri, V.V. Mahajani, *J. Chem. Technol. Biotechnol.* 81 (2006) 62-69.
- [95] H. Abhimanyu, C.S. Kim, B.S. Ahn, K.S. Yoo, *Catal. Lett.* 118 (2007) 30-35.
- [96] G. Stoica, S. Abello, J. Perez-Ramerez, *ChemSusChem* 2 (2009) 301-304.
- [97] Z.Z. Yang, X.Y. Dou, F. Wu, L.N. He, *Can. J. Chem.* 89 (2011) 544-548.
- [98] D.W. Kim, D.O. Lim, D.H. Cho, J.C. Kho, D.W. Park, *Catal. Today* 164 (2011) 556-560.
- [99] J. Xu, K.-Z. Long, T. Chen, B. Xue, Y.-X. Li, Y. Cao, *Catal. Sci. Technol.* 3 (2013) 3192-3199.
- [100] T. Wei, M. H. Wang, W. Wei, Y.H. Sun, B. Zhong, *Fuel Process. Technol.* 83 (2003) 175-182.
- [101] R. Juarez, A. Corma, H. Garcia, *Green Chem.* 11 (2009) 949-951.
- [102] Y. Gao, C.L. Xu, *Catal. Today*, 190 (2012) 107-111.
- [103] C. Murugan, H.C. Bajaj, *Ind. J. Chem., Sect. A.* 52 (2013) 459-466.
- [104] H. Cui, T. Wang, F. Wang, C. Gu, P. Wang, Y. Dai, *Ind. Eng. Chem. Res.* 42 (2003) 3865-3870.
- [105] H. Cui, T. Wang, F. Wang, C. Gu, P. Wang, Y. Dai, *Ind. Eng. Chem. Res.* 43 (2004) 7732-7739.
- [106] Y. Chang, T. Jiang, B. Han, Z. Liu, W. Wu, L. Gao, J. Li, H. Gao, G. Zhao, J. Huang. *Appl. Catal. A: Gen.* 263 (2004) 179-186.
- [107] J. Jiang, R. Hua, *Chem. Res. Chin. Univ.* 23 (2007) 374-402.
- [108] Y. Li, X. Zhao, Y. Wang, *Appl. Catal. A: Gen.* 279 (2005) 205-208.
- [109] J. Tian, J. Wang, J. Chen, J. Fan, F. Cai, L. He, *Appl. Catal. A: Gen.* 301 (2006) 215-221.
- [110] X. Chen, C.Hu, J. Su, T. Yu, Z. Gao, *Chin. J. Catal.* 27 (2006) 485-488.
- [111] B.M. Bhanage, S. Fujita, Y. Ikushima, K. Torii, M. Arai, *Green. Chem.* 5 (2003) 71-75.
- [112] J. Tian, C. Miao, J. Wang, F. Cai, Y. Du, Y. Zhao, L. He, *Green. Chem.* 9 (2007) 566-571.
- [113] Q. Cai, B. Lu, L. Guo, Y. Shan, *Catal. Commun.* 10 (2009) 605-609.

- [114] S. Fang, K. Fujimoto, *Appl. Catal. A: Gen.* 142 (1996) L1-L3.
- [115] S. Fujita, B.M. Bhanage, Y. Ikushima, M. Arai, *Green. Chem.* 3 (2001) 87-91.
- [116] D. Ballivet-Tkatchenko, S. Chambrey, R. Keiski, R. Ligabue, L. Plasseraud, P. Richard, H. Turunen, *Catal. Today* 115 (2006) 80-87.
- [117] J.C. Choi, L. He, H. Yasuda, T. Sakakura, *Green Chem.* 4 (2002) 230-234.
- [118] K. Kohno, J. C. Choi, Y. Ohshima, H. Yasuda, T. Sakakura, *ChemSusChem* 1 (2008) 186-188.
- [119] T. Zhao, Y. Han, Y. Sun, *Fuel Process. Technol.* 62 (2000) 187-194.
- [120] Y.N. Lim, C. Lee, H.Y. Jang, *Eur. J. Org. Chem.* 2014 (2014) 1823-1826.
- [121] K. Tomishige, T. Sakaihorii, Y. Ikeda, K. Fujimoto, *Catal. Lett.* 58 (1999) 225-229.
- [122] K. Tomishige, Y. Ikeda, T. Sakaihorii, K. Fujimoto, *J. Catal.* 192 (2000) 355-362.
- [123] (a) K.T. Jung, A.T. Bell, *J. Catal.* 204 (2001) 339-347; (b) S.B. Xie, A.T. Bell, *Catal. Lett.* 70 (2000) 137-143.
- [124] C.J. Jiang, Y.H. Guo, C.G. Wang, C.W. Hu, Y. Wu, E.B. Wang, *Appl. Catal. A: Gen.* 256 (2003) 203-212.
- [125] Y. Yoshida, Y. Arai, S. Kado, K. Kunimori, K. Tomishige, *Catal. Today* 115 (2006) 95-101.
- [126] K. Tomishige, Y. Furusawa, Y. Ikeda, M. Asadullah, K. Fujimoto, *Catal. Lett.* 76 (2001) 71-74.
- [127] K.W. La, J.C. Jung, H. Kim, S.H. Baeck, I.K. Song, *J. Mol. Catal. A: Chem.* 269 (2007) 41-45.
- [128] H.J. Lee, S. Park, I.K. Song, J.C. Jung, *Catal. Lett.* 141 (2011) 531-537.
- [129] D. Ballivet-Tkatchenko, J.H.Z. dos Santos, K. Philippot, S. Vasireddy, *C.R. Chim.* 14 (2010) 780-785.
- [130] S.P. Wang, L.F. Zhao, W. Wang, Y.J. Zhao, G.L. Xang, X.B. Ma, J.L. Gong, *Nanoscale* 5 (2013) 5582-5588.
- [131] (a) J. Bian, M. Xiao, S. Wang, Y. Lu, Y. Meng, *Catal. Commun.* 10 (2009) 1142- 1145.; (b) J. Bian, M. Xiao, S. Wang, X. Wang, Y. Lu, Y. Meng, *Chem. Eng. J.* 147 (2009) 287-296.; (c) J. Bian, M. Xiao, S.J. Wang, Y.X. Lu, Y.Z. Meng, *Catal. Commun.* 10 (2009) 1529-1533.; (d) J. Bian, M. Xiao, S.J. Wang, Y.X. Lu, Y.Z. Meng, *Appl. Surf. Sci.* 255 (2009) 7188-7196.; (e) Y. Zhou, S. Wang, M. Xiao, D. Han, Y. Lu, Y. Meng, *RSC Adv.*

- 2 (2012) 6831-6837.
- [132] Y. Zhou, M. Xiao, S. Wang, D. Han, Y. Lu, Y. Meng, *Chin. Chem. Lett.* 24 (2013) 307
- [133] X.J. Wang, M. Xiao, S.J. Wang, Y.X. Lu, Y. Z. Meng, *J. Mol. Catal. A: Chem.* 278 (2007) 92-96.
- [134] M. Honda, M. Tamura, Y. Nakagawa, S. Sonehara, K. Suzuki, K. Fujimoto, K. Tomishige, *ChemSusChem* 6 (2013) 1341-1344.
- [135] M. Arresta, A. Dibenedetto, C. Pastore, C.B. Corrado, A.B. Brunella, S. Cometta, E. De Giglio, *Catal. Today* 137 (2008) 125-131.
- [136] K. Almusaiter, *Catal. Commun.* 10 (2009) 1127-1131.
- [137] D. Aymes, D. Ballet-Tkatchenko, K. Jeyalakshmi, L. Saviot, S. Vasireddy, *Catal. Today* 147 (2009) 62-67.
- [138] D. Ballet-Tkatchenko, F. Bernard, F. Demoisson, L. Plasseraud, S.R. Sanapureddy, *ChemSusChem* 4 (2011) 1316-1322.
- [139] K. Tomishige, K. Kunimori, *Appl. Catal. A: Gen.* 237 (2002) 103-109.
- [140] M. Honda, A. Suzuki, B. Noorjahan, K. Fujimoto, K. Suzuki, K. Tomishige, *Chem. Commun.* (2009) 4596-4598.
- [141] V. Eta, P.M. Arvela, A.R. Leino, K. Kordás, T. Salmi, D.Y. Murzin, J.P. Mikkola, *Ind. Eng. Chem. Res.* 49 (2010) 9609-9617.
- [142] Z.F. Zhang, Z.W. Liu, J. Lu, Z.T. Liu, *Ind. Eng. Chem. Res.* 50 (2011) 1981-1988.
- [143] M. Honda, S. Kuno, S. Sonehara, K. Fujimoto, K. Suzuki, Y. Nakagawa, K. Tomishige, *ChemCatChem* 3 (2011) 365-370.
- [144] D.C. Stoian, E. Taboada, J. Llorca, E. Molins, F. Medina, A.M. Segarra, *Chem. Commun.* 49 (2013) 5489-5491.
- [145] <http://www.grandviewresearch.com/industry-analysis/catalyst-market/segmentation>
- [146] M.B. Gawande, R.K. Pandey, R.V. Jayaram, *Catal. Sci. Technol.* 2 (2012) 1113-1125.
- [147] F. Cavani, F. Trifird, A. Vaccari, *Catal. Today* 11 (1991) 173-301.
- [148] A. Corma, R.M.M. Aranda, *Appl. Catal. A: Gen.* 105 (1993) 271- 279.
- [149] S. Miyata, *Clays Clay Miner.* 31 (1983) 305-311.
- [150] X. Bi, H. Zhang, L. Dou, *Pharmaceutics* 6 (2014) 298-332.
- [151] T. Kasuga, M. Hiramatsu, A. Hoson, T. Sekino, K. Niihara, *Adv. Mater.* 11 (1999) 1307-1311.

- [152] X. Sun, Y. Li, Chem. Eur. J. 9 (2003) 2229-2238.
- [153] P. Roy, S. Berger, P. Schmuki, Angew. Chem. Int. Ed. 50 (2011) 2904 - 2939.
- [154] P.H.- Hipólito, M.G.- Castillejos, E.M.- Klimova, N.J.- Flores, A.G.- Cortés, T.E. Klimova, Catal. Today 220-222 (2014) 4-11.
- [155] X. Lei, L. Wang, Z. Cui, S. Xu, F. Zhang, Thin Solid Films 519 (2011) 3552-3556.
- [156] A. Clearfield, K. Demadis (Eds.), Metal Phosphonate Chemistry: From Synthesis to Applications, Royal Society of Chemistry, (2012).
- [157] J.D. Wang, A. Clearfield, Mater. Chem. Phys. 35 (1993) 208-216.
- [158] D.R. Mullins, Surf. Sci. Rep. 70 (2015) 42-85.
- [159] M. Yashima, Catal. Today 253 (2015) 1-13.
- [160] T. Sahu, S.S. Bisht, K.R. Das, S. Kerkar, Curr. Nanosci. 9 (2013) 1-5.
- [161] M. Melchionna, P. Fornasiero, Mater. Today 17 (2014) 349-357.
- [162] K.Reed, A. Kormack, A. Kulkarni, M. Mayton, D.Sayle, F. Klaessig, B. Stadler, Environ. Sci.: Nano 1 (2014) 390-405.

**Chapter - 2**  
**Experimental Methods and Characterization**  
**Techniques**



## 2.1. Introduction

This chapter describes the synthesis methodology of solid oxide catalysts investigated in this thesis. A concise narration of physicochemical characterization techniques used and the reaction procedure adopted for the synthesis of dimethyl carbonate (DMC) is provided. The solid catalysts used in the study are as follows:

- 1) Hydrotalcite (HT)-derived mixed oxide (for transesterification of cyclic ethylene and propylene carbonates (EC/PC) with methanol),
- 2) Sodium titanate nanotubes (NaTNT) (for transesterification of EC/PC with methanol),
- 3) Calcined zirconium phenyl phosphonate phosphite (ZrPP-C) (for direct synthesis of DMC from carbon dioxide (CO<sub>2</sub>) and methanol), and
- 4) Ceria (CeO<sub>2</sub>) of different morphologies (for direct synthesis of DMC from CO<sub>2</sub> and methanol).

The catalysts were characterized by powder X-ray diffraction (XRD), N<sub>2</sub>-physisorption, thermogravimetry (TG), scanning electron microscopy (SEM), high-resolution transmission electron microscopy (HRTEM), Fourier-transform infrared spectroscopy (FTIR), FT-Raman spectroscopy and <sup>27</sup>Al & <sup>31</sup>P magic-angle spinning nuclear magnetic resonance spectroscopy (MASNMR). The chemical composition of the catalysts was determined using inductively coupled plasma-optical emission spectroscopy (ICP-OES), micro elemental analysis and energy dispersive X-ray analysis (EDX). The acidic and basic properties of the catalysts were determined by temperature-programmed desorption techniques (TPD) using NH<sub>3</sub> and CO<sub>2</sub> as probe molecules, respectively. Catalytic activities of the above materials were tested for DMC synthesis by indirect (transesterification of EC and PC with methanol) and direct (reaction of CO<sub>2</sub> with methanol) means of utilization of CO<sub>2</sub>. Product analysis and quantification was done using <sup>1</sup>H NMR and gas chromatographic (GC) techniques.

## 2.2. Catalyst preparation

### 2.2.1. Hydrotalcites-derived mixed oxides

A hydrotalcite (HT) with Mg : Al molar ratio of 2:1 was prepared by a co-precipitation method [1,2]. In a typical synthesis, 8.2 g of Mg(NO<sub>3</sub>)<sub>2</sub>.6H<sub>2</sub>O (Merck, India) and 6 g of Al(NO<sub>3</sub>)<sub>3</sub>.9H<sub>2</sub>O (Merck, India) were dissolved in 75 ml of distilled water. In a separate beaker, 50 ml of distilled water was taken and the pH was adjusted to 10 using a solution containing NaOH and Na<sub>2</sub>CO<sub>3</sub> (3 M each; Thomas Baker). To it, the above-metal precursor solution was

added slowly while stirring continuously for 2 h while maintaining the pH of the contents at 10. The slurry obtained was transferred into a 250 ml Teflon-lined stainless steel autoclave and aged at 90 °C in an electric oven for 24 h. The solid (HT-as-syn) formed was separated by filtration and washed thoroughly with deionized water until the pH of the wash was 7. It was dried at 90 °C. The calcined form of HT-as-syn (600 °C for 6 h) was designated as HT-C.

Catalysts with varying amounts of La<sup>3+</sup> (2, 5, 8 and 10 mol% with respect to Al<sup>3+</sup>) and other rare-earth ions (8 mol% of Y<sup>3+</sup>, Ce<sup>3+</sup>, Pr<sup>3+</sup>, and Sm<sup>3+</sup> with respect to Al<sup>3+</sup>; Mg<sup>2+</sup> : (Al<sup>3+</sup> + Ln<sup>3+</sup>)= 2) modified HTs were prepared in a similar manner. Nitrate salts of rare-earth ions (Thomas Baker or Leonid Chemicals) were used as precursors. The modified catalysts, thus prepared, were designated as HT-X M, where M stands for rare-earth ion and X represents mol% of rare-earth ion incorporated. Calcined samples of these modified HT were designated as HT-X M-C.

For comparative study, MgO-La<sub>2</sub>O<sub>3</sub> (2:1 molar ratio) and "neat" MgO were also prepared adopting a similar procedure.

### **2.2.2. Sodium titanate nanotubes**

Sodium titanate nanotubes (NaTNT) were prepared by a hydrothermal synthesis method [3]. In a typical preparation, 10 g of anatase-TiO<sub>2</sub> powder (Merck India) was suspended in 200 ml of aqueous NaOH solution (10 M) and transferred into a 250 ml Teflon-lined stainless steel autoclave and placed in an electric oven maintained at 120 °C for 7 days. The solid formed was filtered, washed with deionized water until the pH of the water wash became 7 and dried at 110 °C for 12 h. The solid obtained was designated as NaTNT.

### **2.2.3. Calcined zirconium phenylphosphonate phosphite**

Zirconium phenylphosphonate phosphite samples were prepared in the presence (ZrPP-HF) and in the absence of HF (ZrPP-X; X stands for the molar ratio of phosphorous acid (H<sub>3</sub>PO<sub>3</sub>) to phenylphosphonic acid (C<sub>6</sub>H<sub>5</sub>PO<sub>3</sub>) used in the synthesis) [4,5].

#### **2.2.3.1. Synthesis of ZrPP-HF-C**

In a typical synthesis of ZrPP-HF, solution-A was prepared dissolving 4 g of ZrOCl<sub>2</sub>.8H<sub>2</sub>O (Loba chemie) in 20 ml of distilled water and 9 ml of concentrated HF (Thomas Baker) taken in a polyethylene beaker. Solution-B was prepared dissolving 1.06 g of phenylphosphonic acid (Spectrochem) and 26.8 g of phosphorous acid (Loba chemie) in 50 ml of distilled water taken in a polyethylene beaker. Solution-A was added to solution-B with

continuous stirring over 30 min. The beaker containing solution A was rinsed with 14 ml of water and the contents were added to the above reaction mixture which was then, heated at 70 °C for 34 h (placing in an temperature-controlled oil bath) till it got dried completely. The material (ZrPP-HF), thus formed, was washed with 2 l of distilled water and dried at 90 °C overnight. ZrPP-HF-C was prepared calcining ZrPP-HF at 550 °C for 2 h.

#### **2.2.3.2. Synthesis of ZrPP-1-C**

In the preparation of ZrPP-1, phenylphosphonic acid (1 g; 6.3 mmol) and phosphorous acid (0.52 g; 6.3 mmol) were dissolved in 20 ml of distilled water. To that, 2.04 g of  $\text{ZrOCl}_2 \cdot 8\text{H}_2\text{O}$  (6.3 mmol) dissolved in 5 ml of distilled water was added drop-wise during a period of 10 min. The mixture was heated to dryness at 90 °C for 3 h placing in a temperature-controlled oil bath. The solid was recovered, washed with 500 ml of distilled water and dried at 90 °C overnight. The solid obtained was designated as ZrPP-1. ZrPP-1-C was prepared by calcining ZrPP-1 at 550 °C for 2 h.

#### **2.2.3.3. Synthesis of ZrPP-2-C and ZrPP-3-C**

ZrPP-2 and ZrPP-3 were prepared in the same manner as described for ZrPP-1 but using phosphorous acid : phenylphosphonic acid molar ratios of 2:1 and 3:1, respectively. Calcination of those materials at 550 °C for 2 h yielded ZrPP-2-C and ZrPP-3-C, respectively.

#### **2.2.3.4. Zirconium pyrophosphate**

$\text{ZrP}_2\text{O}_7$  was prepared as per the known procedure [6]. In a typical synthesis, 50 g of  $\text{ZrOCl}_2 \cdot 8\text{H}_2\text{O}$  was dissolved in 100 ml of distilled water. To it, 20 ml of phosphoric acid ( $\text{H}_3\text{PO}_4$ ; 88% solution; Thomas Baker) was added drop-wise. The white precipitate obtained was separated by filtration and washed with distilled water until it was chloride free. The solid cake obtained was dried at 120 °C for 12 h and then, calcined at 500 °C for 5 h.

#### **2.2.4. $\text{CeO}_2$ of different morphologies**

$\text{CeO}_2$  samples of varying morphology were prepared by non-template, hydrothermal synthesis methods [7, 8].

##### **2.2.4.1. Spindles**

$\text{CeO}_2$  with spindle morphology was prepared as follows: 1.042 g of  $\text{Ce}(\text{NO}_3)_3 \cdot 6\text{H}_2\text{O}$  (Loba Chemie) and 0.384 g of urea (Merck, India) were dissolved in 80 ml of milli-Q water at room temperature. It was stirred for 15 min. The transparent solution obtained was transferred into a 100 ml Teflon-lined stainless steel autoclave. It was placed in a rotating hydrothermal

synthesizer (Hiro Co., Japan) and heated at 120 °C for 8 h (rotation speed = 30 rpm). The precipitate formed was separated, washed with 2.5% of ethanol in water (~ 500 ml). After drying at 80 °C for 24 h, the product was calcined at 600 °C for 5 h and was designated as Ce-S.

#### **2.2.4.2. Cubes**

CeO<sub>2</sub> with cube-shaped morphology was prepared as follows: 1.736 g of Ce(NO<sub>3</sub>)<sub>3</sub>.6H<sub>2</sub>O was dissolved in 10 ml of milli-Q water (solution-A). 19.2 g of NaOH (Thomas Baker) was dissolved in 70 ml of milli-Q water (solution-B). The latter was added to the former with continuous stirring at room temperature over 15 min to get a purple slurry, which was transferred into a 100 ml Teflon-lined stainless steel autoclave. It was placed in a rotating hydrothermal synthesizer (Hiro Co., Japan) and heated at 180 °C for 24 h (rotating speed = 30 rpm). The precipitate formed was separated, washed with 2.5% ethanol in water until the pH of the washings became 7. After drying at 80 °C for 24 h, the product was calcined at 600 °C for 5 h and was designated as Ce-C.

#### **2.2.4.3. Rods**

CeO<sub>2</sub> with rod-shape morphology was prepared by using same procedure adopted for the synthesis of Ce-C except that the synthesis temperature was 100 °C instead of 180 °C. The final sample obtained after calcination was designated as Ce-R.

#### **2.2.4.4. No-definite morphology**

For the comparative study, CeO<sub>2</sub> with no definite morphology was also prepared. In a typical synthesis, 6.31 g of Ce(NO<sub>3</sub>)<sub>3</sub>.6H<sub>2</sub>O was dissolved in 180 ml of distilled water and transferred into a triple-necked, glass, round-bottomed flask fitted with a water cooled condenser. Then, it was kept in an oil bath maintained at 80 °C. In the next step, aqueous NaOH solution (0.1 M) was added to it drop-wise for 1 h with constant stirring while maintaining the pH at about 10. Stirring was continued for another 3 h. It was cooled to room temperature. The precipitate formed was separated by filtration and washed several times with distilled water until the pH of washings was 7. The solid obtained was dried at 80 °C for 24 h and calcined at 600 °C for 5 h. It was designated as Ce-N.

### **2.3. Catalyst characterization techniques**

#### **2.3.1. X-ray powder diffraction**

XRD is an important characterization technique for phase identification and determination of the percentage of crystallinity and average crystallite size of a catalyst material.

Each crystalline solid has a unique XRD pattern which is a “fingerprint” for its identification. The interaction of monochromatic X-rays with the sample results in constructive interference of diffracted X-ray beams when the Bragg’s Law [9] given by Eq. (2.1) is satisfied.

$$n\lambda = 2d\sin\theta \quad (2.1)$$

Here,  $\lambda$  is the wave length of X-rays,  $d$  is the distance between two lattice planes,  $\theta$  is the angle of incidence with lattice plane (called Bragg's angle) and "n" is an integer that represents the order of reflection. Output of the diffraction measurement is a plot of intensity of diffracted X-rays versus incident angle. Analysis of the position, area and shape of diffraction peaks allows the identification of lattice parameters, type and composition of phase present, percentage crystallinity and crystallite size of the sample. Average crystallite size can be estimated using the Scherrer equation (Eq. 2.2),

$$\tau = K\lambda/\beta\cos\theta \quad (2.2)$$

where  $\tau$  is the mean size of the ordered (crystalline) domains (which may be smaller or equal to the grain size),  $K$  is a dimensionless shape factor, with a value close to unity, but varies with the actual shape of the crystallite,  $\lambda$  is the X-ray wavelength and  $\beta$  is the line width at half the maximum intensity (FWHM). Generally, heterogeneous catalysts exist as polycrystalline powders. Sharp diffraction pattern is observed only when the sample possesses a sufficiently long range order [9-12].

The XRD patterns of the catalyst samples in the present study were recorded on a Philips X'pert Pro diffractometer using Cu-K $\alpha$  radiation ( $\lambda = 0.15406$  nm) and a proportional counter detector. The diffraction patterns in the low-angle region ( $2\theta = 0.5 - 5^\circ$ ) were recorded at a scan rate of  $0.2^\circ/\text{min}$  and those in the high-angle region ( $2\theta = 5 - 90^\circ$ ) were recorded at a scan rate of  $4^\circ/\text{min}$ . The step size in the measurements was  $0.02^\circ$ .

### 2.3.2. *N<sub>2</sub>-physisorption*

Gas adsorption techniques are commonly employed for determining surface area and porosity of a catalyst sample [13]. Typically, dinitrogen at liquid nitrogen temperature ( $-196^\circ\text{C}$ ) is used as an adsorbate for determining the properties of adsorbent, although many other adsorbates have also been used. Determination of the adsorption isotherm is a preliminary step in the estimation of pore properties. An adsorption isotherm is attained by measuring the amount of

gas adsorbed across a wide range of relative pressures at a constant temperature. Contrarily, desorption isotherms are formed by measuring removed gas as pressure is reduced. The shape of isotherm depends on the porous structure of a solid. The hysteresis of adsorption isotherms gives an idea about the pore shape. Total pore volume, average pore size and pore size distribution are the important textural parameters. Its determination is based on the fact that the adsorbate gas condenses into a liquid on the capillary pores at lower pressure relative to the saturated vapor pressure of the adsorbate. Total pore volume is obtained from the amount of gas adsorbed at a relative pressure close to unity. At such a condition, it is assumed that pores are filled by the liquid adsorbate [13,14].

Brunner-Emmet-Teller (BET) model is the most accepted method for calculation of monolayer coverage of the adsorbate. The basic assumptions of BET model are the following: (1) The heat of adsorption of first layer is constant and lateral interactions are ignored. (2) Rate of adsorption of any layer is equal to the rate of desorption of the next layer lying above it. (3) The heat of adsorption of second and all the other layers is equal to the heat of liquefaction of gas [15]. For infinite number of layers, the adsorption is defined by Eq. (2.3),

$$\frac{1}{V\left[\left(\frac{P_0}{P}\right)-1\right]} = \frac{1}{V_m \cdot C} + \frac{C-1}{V_m \cdot C} \left(\frac{P}{P_0}\right) \quad (2.3)$$

where V is the volume of gas adsorbed at a pressure P,  $V_m$  is the volume of adsorbate as monolayer,  $P_0$  is the saturation vapor pressure of adsorbate,  $P/P_0$  is the relative vapor pressure and C is the BET constant related to heat of adsorption and liquefaction. This equation is of the linear form with an intercept  $1/V_m C$  and slope of  $(C-1)/V_m C$ . Substituting the value of  $V_m$ , the total surface area ( $S_t$ ) of a material can be determined using the following equation (Eq. (2.4)) [15,16],

$$S_t = \frac{V_m N \sigma}{V} \quad (2.4)$$

where N is Avogadro number,  $\sigma$  is cross sectional area of adsorbed molecule and V is molar volume of adsorbate gas. For nitrogen molecule, the generally accepted value of  $\sigma$  is  $0.162 \text{ nm}^2$ . Specific surface area is then determined from the total surface area. The volume of liquid nitrogen adsorbed on the pores is calculated using Eq. (2.5).

$$V_1 = \frac{P V_m V_a}{RT} \quad (2.5)$$

where  $P$  and  $T$  are the ambient pressure and temperature, respectively,  $V_a$  is the volume of nitrogen adsorbed,  $V_m$  is the molar volume of liquid adsorbate. The average pore size can be calculated using pore volume. The evaluation of pore size distribution of the material is carried out mostly on the basis of Barret, Joyner and Halenda model, where speculative emptying of the pores by a step-wise reduction of  $P/P_o$ , and allowance for the contraction of the multilayer in those pores already emptied by condensation are considered [17]. The pore size distribution is represented as a plot of  $\Delta V_p/\Delta r_p$  versus  $r_p$ , where  $V_p$  is the pore volume and  $r_p$  is the pore radius.

All these measurements in the present work were carried out using a Quadrasorb SI automated surface area and pore size analyzer (Quanta Chrome / NOVA 1200 equipment). Before the adsorption study, the sample was degassed at 200 °C for 3 h in vacuum (50 - 500 millitorr). After degassing, the sample was cooled to room temperature and the weight was recorded. The degassed sample was then analyzed in the relative pressure range of 0.01 to 0.99. The standard isotherm was measured with 40 data points. The specific surface area of the samples was determined by the BET method using the data points in the relative pressure ( $P/P_o$ ) region of 0.05 - 0.3. The total pore volume was determined from the uptake of adsorbate at a relative pressure ( $P/P_o$ ) of 0.99. A reference alumina sample (supplied by Quanta chrome, USA) was used to calibrate the instrument. The pore size distribution was determined using the desorption branch of the isotherms with the help of the BJH model.

### ***2.3.3. Inductively coupled plasma-optical emission spectroscopy***

ICP-OES is an emission spectrophotometric technique, where the component elements (atoms) are excited by the explosion of plasma energy. These excited electrons emit energy at a specified wavelength as they return to ground state. This emission is determined and the element present in the composition of the catalyst sample is detected from the position of the emission. The basic feature of this process is that each element emits energy at particular wavelength. The intensity of the energy emitted at a particular wavelength is proportional to the concentration of that element in the analyzed sample [18]. Accordingly, the elemental composition of the given sample can be estimated. A solution form of the sample is required to carry out ICP-OES analysis. Sample for the analysis can be made either by a combined acid attack (making use of HF, HNO<sub>3</sub> and HCl) or by a LiBO<sub>2</sub> flux-fusion technique. The acid digestion procedure results imperfect in the examination of obstinate elements such as Ti, Cr, and Zr because their host minerals are often difficult to dissolve. The flux-fusion approach is promising because of

numerous reasons: (1) HF is not involved, (2) it is a complete dissolution technique, permitting determination of all elements, including Si and the refractory elements and (3) the resultant solution is similar in composition of the catalyst [18].

In this thesis, the composition of ions in the oxide samples was determined using Spectro Arcos ICP-OES equipment. A known quantity (2-10 mg) of the catalyst was dissolved in a minimum amount of HNO<sub>3</sub> and made up to the required volume before using in the ICP-OES analysis.

#### **2.3.4. Fourier transform infrared spectroscopy**

FTIR spectroscopy measures the absorption of infrared radiation by the catalyst sample. When the applied infrared frequency is equal to the frequency of vibration of the molecule, absorption of IR radiation happens at that particular frequency. Only the vibrations associated with a change in dipole moment of the molecule result in an absorption band in IR spectroscopy. Solid samples can be examined by grinding a milligram of the sample with about 100 mg of KBr. The combination is then hard-pressed to create a transparent disk. In the reference beam path a disk of pure potassium bromide is placed [19, 20]. FTIR spectra of the samples used in this thesis were recorded on a Shimadzu 8201 spectrophotometer in the region of 400-4000 cm<sup>-1</sup>, with an accumulation of 100 scans at a spectral resolution of 4 cm<sup>-1</sup>.

#### **2.3.5. FT-Raman spectroscopy**

A monochromatic light, for example laser, incident on the molecule originates elastic and inelastic scattering of photons. Photon undergoing scattering without energy exchange is called elastic scattering, also known as Rayleigh scattering. Raman spectroscopy relies on the inelastic scattering of photons (scattering with energy change). The frequency of the reemitted photons is shifted up or down in comparison with original monochromatic frequency, which is called the Raman effect [21]. In Raman spectra, all the vibrations are not noticeable like in IR spectroscopy. The vibration which causes the change in polarizability of the molecule is Raman active. The laser beam can be considered as an oscillating electromagnetic wave with an electrical vector E, which induces electric dipole moment by the interaction with the sample, leads molecular deformation. Such a periodic deformation results in the vibration of molecule at a particular frequency. Consequently, the Raman shift provides information about the vibrational, rotational and other low frequency transitions in molecules [19, 22]. Raman spectroscopy is an important characterization tool for solid catalysts which includes



determination of the nature of molecular species and structure of non-crystalline phases, identification of active species formed during catalyst preparation and pretreatment, detection and quantification of defect sites. It is an important technique to examine oxidic catalysts [19]. FT-Raman spectra of the oxides were recorded on a Horiba JY Lab Raman HR 800 micro Raman spectrometer using 630 nm wavelength generated by a He-Ne laser operating at 20 mV. The samples were prepared as loosely pressed circular discs on a glass plate for analysis.

### **2.3.6. MAS NMR**

MAS NMR is a characterization technique used for solid samples to acquire high resolution NMR data. It was developed to overcome the line broadening observed in solid state, especially in powdered samples, due to their large anisotropic interactions such as dipolar coupling and chemical shift anisotropy, in contrast to liquid NMR. Powdered solid sample encompass several crystallites with random orientation and all those give different spectra, which makes the overall spectrum of a powdered sample complicated. In MASNMR, the sample is spun around an axis at magic angle ( $\theta_m = 54.74^\circ$ ) with respect to the stationary field. The sample is spun at higher rate than the anisotropy of the interaction. The anisotropic interactions are averaged and thereby, signal narrowing is observed [23-25].  $^{27}\text{Al}$  and  $^{31}\text{P}$  MASNMR spectra of hydroxalcalites and ZrPP were recorded on a Bruker AV300 NMR spectrometer using 4 mm sample rotors. Samples were spun at a speed of 8 kHz. A single pulse sequence was applied and the NMR measurements were performed at 25 °C.

### **2.3.7. Scanning electron microscopy/Energy dispersive X-ray analysis**

SEM is used for examine the morphological characteristics of materials. SEM scans over a sample surface with a probe of electrons (5- 50 eV) and detects the yield of either secondary or back-scattered electrons as a function of the position of the primary beam. Contrast is generally caused by the orientation of the sample towards detector. Parts of the surface facing the detector appear brighter than the surface pointing away from the detector. The interaction between the electron beam and the sample generates different kinds of signals providing detailed information about the surface structure and morphology of the sample [19]. When an electron from the beam encounters a nucleus in the sample, the resultant Coulombic attraction leads to a deflection in the electron's path, known as Rutherford elastic scattering. A fraction of these electrons will be completely backscattered, re-emerging from the incident surface of the sample. Since the scattering angle depends on the atomic number of the nucleus, the primary electrons arriving at a

given detector position can be used to produce images containing topological and compositional information [26]. SEM is also proficient for carrying out analysis of selected point regions on the sample, which is particularly important in qualitatively or semi-quantitatively determination of chemical composition by using EDX. The composition of the material is resolved by measuring the characteristic X-rays that are generated by the contact of the electrons with matter. SEM images of the catalyst samples in this work were recorded a Leica 440 instrument operating at 100 kV. The samples for the analysis were prepared by dispersing the catalyst (0.005 - 0.008 g) in isopropanol (5 ml) by ultrasonication (0.5 h) at room temperature and drop casting the solution (2 - 3 drops) on the holy carbon grid. It was dried at room temperature for 12 h and then used for analysis.

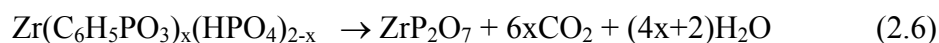
### **2.3.8. Transmission electron microscopy**

TEM is generally used for high resolution imaging of thin films of a solid sample for micro structural and compositional analysis. It reveals particle size distribution, metal dispersion, morphology and chemical composition of the supported metal particles. The technique involves: (i) irradiation of a very thin sample by a high-energy electron beam, which is diffracted by the lattices of a crystalline or semi-crystalline material and propagated along different directions, (ii) imaging and angular distribution analysis of the forward scattered electrons (unlike scanning electron microscopy where backscattered electrons are detected) and (iii) energy analysis of the emitted X rays [27]. In detail, a primary electron beam of high energy and high intensity passes through a condenser to produce parallel rays, which impinges on the sample. As the attenuation of the beam depends on the density and thickness, the transmitted electrons form a two-dimensional projection of the sample mass, which is subsequently magnified by the electron optics to produce the so-called bright field image. The dark field image is obtained from the diffracted electron beams, which are slightly off angle from the transmitted beam. Typical operating conditions of TEM instruments are 100-200 keV electrons,  $10^{-6}$  mbar vacuum, 5 nm resolution and magnification of about  $3 \times 10^5$  (or  $10^6$ ). For high resolution transmission electron microscopy (HRTEM), the operating conditions are: 100 - 300 keV electrons,  $10^{-6}$  vacuum, 0.5 nm resolution, and magnification of about  $3 \times 10^5$  (or  $10^6$ ). The topographic information obtained by TEM in the vicinity of atomic resolution can be utilized for structural characterization and identification of various phases [28]. TEM also provides real space image on the atomic distribution in the bulk and surface of a nano-crystal.

HRTEM images of the samples used in the thesis were collected on a FEI Technai-F30 instrument with a 300 kV (Cs = 0.6 mm, resolution 0.17 nm) field emission gun. The samples analysed by HRTEM were prepared by dispersing catalysts (0.001 - 0.005 g) in 5 ml of isopropanol and sonicated for 0.5 h at room temperature. The highly dispersed catalyst particles were single drop-casted on a copper grid (200 mesh, Icon Analytical) dried for 12 h at room temperature and then used for the analysis.

### 2.3.9. Thermogravimetric analysis

TG analysis measures the change in mass of a substance as a function of temperature or time in the scanning or isothermal mode under a controlled temperature programming in a controlled atmosphere. The change in mass associates with various thermal actions such as adsorption, desorption, oxidation, reduction, sublimation, vaporization and decomposition. The change in mass of a material relies on the experimental conditions adopted. It enables calculating the chemical composition of a material. For example, the chemical composition of zirconium phenylphosphonate phosphate (Eq. 2.6) is calculated as follows (Eq. 2.7) [4],



$$\% \text{ weight loss above } 400^\circ\text{C} = \frac{[92.22+158 x+96 (2-x)-266.2] \times 100}{\text{Formula weight of the complex}} \quad (2.7)$$

TG of the different samples was carried out under nitrogen (50 ml/min) atmosphere on a Perkin Elmer Diamond TG-DTA instrument in the temperature range 25 - 1000 °C with a ramp rate of 10 °C/min.

### 2.3.10. Temperature-programmed desorption

TPD technique is used for the quantitative determination of acid and basic sites present on the solid catalyst material. It quantifies the desorbed probe gas molecule which was evolved out from their adsorbed state from the catalyst surface, upon increasing temperature. Prior to measurement, the physically adsorbed species are removed by flushing the sample with an inert gas. In general, basic molecules like NH<sub>3</sub> and iso-propylamine are used as probe molecules for acidity measurements and an acidic gas CO<sub>2</sub> is used as a probe molecule for basicity measurements [10].

The acidity and basicity of different samples studied in this work were quantified using  $\text{NH}_3$  and  $\text{CO}_2$ , respectively, as probe molecules and using a Micromeritics AutoChem 2910 instrument. About 100 mg of the sample was placed in a U-shaped, flow-through, quartz sample tube. Before the TPD experiments, the catalyst was activated at a particular temperature under a flow of He. The sample was cooled to 50 °C and  $\text{NH}_3$  or  $\text{CO}_2$  (10% in He) was adsorbed for 30 min. Desorption of  $\text{NH}_3$  or  $\text{CO}_2$  was recorded followed by raising the temperature. A gold-plated filament thermal conductivity detector was used for detecting the amount of  $\text{NH}_3$  or  $\text{CO}_2$  molecules desorbed.

### **2.3.11. Titration method for ion-exchange capacity measurement**

The amount of exchangeable  $\text{H}^+$  ions or Brønsted acid sites can be determined by acid-base titration method. In a typical procedure, catalyst samples were weighed accurately (~ 50 mg) and dispersed in 10 ml of 0.01 M NaCl solution and allowed to equilibrate for a definite period of time (1 h). After that, the catalyst was separated out by filtration. The filtrate obtained was titrated against a 0.01 M NaOH solution using phenolphthalein as indicator. Volume of NaOH required to neutralize the  $\text{H}^+$  present in the liquid portion was calculated as follows:

$$\text{Amount of exchangeable } \text{H}^+ \text{ ion present in the catalyst} = \frac{V_{\text{NaOH}} \times M_{\text{NaOH}}}{W_C} \quad (2.8)$$

where  $V_{\text{NaOH}}$  is the volume of NaOH consumed,  $M_{\text{NaOH}}$  is the molarity of NaOH and  $W_C$  is the weight of catalyst, respectively [29].

## **2.4. Reaction procedure**

### **2.4.1. Transesterification of cyclic carbonate with methanol**

#### **2.4.1.1. Hydrotalcites-derived solid oxides**

Prior to the reaction, the catalyst was activated in air at 180 °C for 2 h. In a typical reaction, PC or EC (10 mmol; Spectrochem), methanol (100 mmol; Merck, India) and catalyst (5 wt% with reference to PC/EC) were taken in a Teflon-lined stainless-steel autoclave (100 ml) placed in a rotating hydrothermal reactor (Hiro Co., Japan; rotation speed = 50 rpm). Reactions were conducted at 40 - 100 °C and 80 - 190 °C (0.5 - 6 h) for EC and PC transesterifications, respectively. To determine the kinetic parameters (rate of reaction, equilibrium constant and activation energy), reactions were conducted at four different temperatures 40, 60, 80 and 100 °C (for EC-methanol) and 110, 130, 150 and 170 °C (for PC-methanol) over a period of 0 - 6 h using HT-8 La-C and HT-10 La-C catalysts. Initial rates were determined from the time versus

conversion plots collected at different temperatures. Activation energies were determined from the Arrhenius plots. Pseudo-first order kinetics was considered. Mass balance was > 98%.

*Catalyst recyclability study:* At the end of each run, the catalyst was separated, washed with methanol, dried at 200 °C for 4 h, and then subjected to recycle study. At the end of fourth recycle, the catalyst was separated, washed with methanol, activated at 600 °C for 6 h, and then used in the fifth recycle study.

#### **2.4.1.2. NaTNT**

Prior to the reactions, the catalyst was activated in air at 130 °C for 2 h. In a particular reaction, EC or PC (10 mmol), methanol (100 mmol) and catalyst (5 - 40 wt% of EC or PC) were taken in a glass, round-bottomed flask having a magnetic needle and placed on a magnetic stirrer. In some experiments the reactants were taken in a Teflon-lined stainless-steel autoclave (100 ml) placed in a rotating hydrothermal reactor (Hiro Co., Japan; rotation speed = 50 rpm). The reactions were conducted at 23 - 100 °C for 0 - 10 h. To determine the reaction rate and activation energy for EC transesterification, the reactions were conducted at three different temperatures (30, 40, 60 °C) over a period of 0 - 10 h. Initial rates were determined from the time versus conversion plots collected at different temperatures. Activation energies were estimated from the Arrhenius plots. Pseudo-first order kinetics was considered.

*Catalyst recycle study:* At the end of each run, the catalyst was separated by centrifugation, washed with methanol, dried at 80 °C for 8 h. Prior to recycling runs, the dried catalyst was activated at 130 °C for 4 h.

#### **2.4.2. Direct conversion of CO<sub>2</sub> into DMC**

##### **2.4.2.1. ZrPP**

Prior to reactions, the catalyst was activated at 170 °C for 2 h in air. All the reactions using ZrPP catalysts were conducted in a 100 ml stainless-steel Parr high pressure reactor (Parr Instrument Co., Parr 4871) equipped with a mechanical overhead stirrer, thermo-well, gas inlet and outlet, liquid sampling valve, safety rupture disk, transducer for digital pressure display and an automatic temperature controller system. Methanol (16.02 g; 500 mmol) and activated catalyst (0.1 - 0.4 g) were taken in the reactor which was then pressurized with CO<sub>2</sub> to 1 - 4 MPa. The temperature of the reactor was raised to 120 - 170 °C and the reactions were conducted while stirring at a speed of 600 rpm for 4 - 15 h. The effects of solvent (DMF, THF, 1,4-dioxane;

0 - 10 ml) and physical adsorbent - molecular sieve 3A (0 - 500 mg) were studied by charging them along with the reactants.

*Catalyst recycle study:* At the end of each recycle, the catalyst was recovered, washed with acetone, activated at 250 °C in air for 2 h and reused in the subsequent recycling experiment.

#### 2.4.2.2. $CeO_2$

Prior to reactions,  $CeO_2$  catalyst was activated at 200 °C for 2 h in air. All the reactions using  $CeO_2$  based catalysts were conducted in a 100 ml stainless-steel Parr high pressure reactor (Parr Instrument Co., Parr 4871). Methanol (3.2 g; 100 mmol), 2-cyano pyridine (2-CP, chemical water trapping agent; Aldrich Co.; 5.2 g, 50 mmol) and catalyst (0.1 g) were taken in the reactor which was then pressurized with  $CO_2$  to 5 MPa. The temperature of the reactor was raised to 120 - 160 °C and the reaction was conducted while stirring at a speed of 600 rpm for 1- 6 h.

### 2.5. Product analysis

#### 2.5.1. Transesterification of cyclic carbonate

##### 2.5.1.1. Gas chromatography

After the reaction, the autoclave was cooled to 25 °C and the catalyst was separated by centrifugation/filtration. The liquid product were analyzed by gas chromatography (GC, Varian 3800; CP-8907 column; 15 m × 0.25 mm × 0.25 μm or CP-SIL 5 CB column; 60 m × 0.32 mm × 0.25 μm) and identified by GC-MS [Varian CP 3800 GC and Saturn 2200 MS; coloumn HP-5 (30m x 0.25mm x 25 μm)] using a programme: 40 - 80 °C at 10 °C/min and 6 min hold at 80 °C, 80 - 270 °C at 20 °C/min and 8 min hold. For quantitative analysis of DMC, different known concentrations (0 - 100%) of standard analyte (reactants and possible products) mixtures were prepared, injected into GC and peak areas of each analyte were noted. A graph of peak area versus concentration of each analyte was drawn and response factor was calculated, which was then used in determining the exact concentration of the products formed in the reaction mixture. Conversion and selectivity were determined using the following equations:

$$\% \text{ Conversion} = \frac{(\text{Initial moles of cyclic carbonate} - \text{final moles of cyclic carbonate}) \times 100}{\text{Initial moles of cyclic carbonate}} \quad (2.9)$$

$$\% \text{ Product selectivity} = \frac{\text{Moles of product formed} \times 100}{\text{Moles of cyclic carbonate converted into products}} \quad (2.10)$$

2.5.1.2.  $^1\text{H}$  NMR.

$^1\text{H}$  NMR spectroscopy was used for the analysis and quantification of liquid products obtained from PC transesterification. Bruker Advance 200 MHz spectrometer with a sweep width of 4138.95 Hz, acquisition time of 7.9167 sec and  $\text{CDCl}_3$  as a solvent was used for this purpose. Signals due to methyl proton of PC (1.54; doublet), propylene glycol (PG) (1.14; doublet) and DMC (3.79; singlet) (Fig. 2.1) were integrated and the area of characteristic signals was determined. The following equation was used to estimate PC conversion and DMC selectivity from  $^1\text{H}$  NMR spectroscopy (Eqs. 2.11 and 2.12).

$$\text{PC conversion (mol\%)} = \left[ 1 - \frac{\text{area of CH}_3 \text{ signal of PC}}{\text{area of CH}_3 \text{ signal of PC+PG}} \right] \times 100 \quad (2.11)$$

$$\text{DMC selectivity (mol\%)} = \left( \frac{\text{area of CH}_3 \text{ signal of DMC}}{\text{area of CH}_3 \text{ Signal of PG}} \right) \times 100 \quad (2.12)$$

Catalytic activity data obtained from both GC and NMR techniques were comparable within the experimental error (2- 5 mol %).

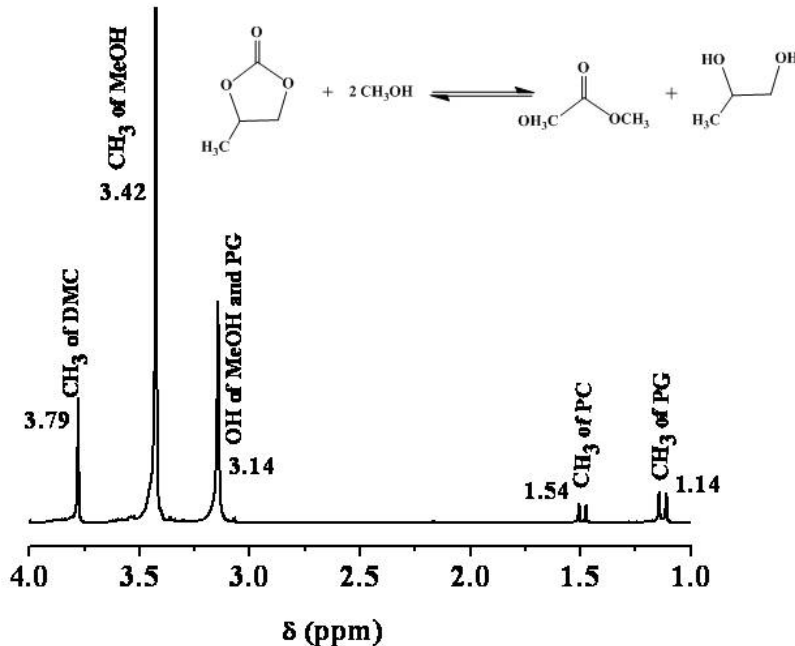


Fig. 2.1.  $^1\text{H}$ - NMR spectrum PC transesterification product

### 2.5.2. Direct conversion of CO<sub>2</sub> to DMC

The liquid products were analyzed and quantified with the help of a Varian 3400 gas chromatograph (GC) equipped with a flame ionization detector and CP-8907 (15 m × 0.25 mm × 0.25 μm) or CP-SIL 8CB column (30 m x 0.53 mm x 0.25 μm) or CP-SIL 5 CB (60 m × 0.25 mm × 0.25 μm) using a program: 40 - 80 °C at 10 °C/min and 6 min hold and 80 -270 °C at 20°C/min and 8 min hold. Nonane-1-ol was used as an internal standard for quantification of products by GC. For quantitative analysis, different known concentrations (0 - 100%) of standard analyte (reactants and possible products) mixtures were prepared and added to it a known amount (0.2020 g) of nonane-1-ol as an internal standard. The standard samples of the products - 2-picolinamide (2-PA), methyl carbamate (MC) and 2- methyl picolinate (2-MP) obtained from Aldrich Co., and DMC from Loba Chemie were used for calibration. Mixtures of different composition were injected into GC and peak areas of each analyte and internal standard were determined. A graph of ratio of peak area of particular analyte to internal standard versus ratio of exact concentration of analyte to internal standard was drawn and the response factor was determined, which was then used in determining the exact concentration of the products in the reaction mixture. DMC yield in mmol/g was determined by the amount of DMC formed divided by the amount of catalyst used. Conversion, selectivity, yield and mass balance were determined using the following equations (Eqs. 2.13. to 2.25).

$$\% \text{ DMC yield} = \frac{\text{mmol of DMC formed}}{(\text{mmol of MeOH taken}/2)} \times 100 \quad (2.13)$$

$$\% \text{ MeOH conversion} = \frac{\text{mmol of MeOH Consumed}}{\text{mmol MeOH taken}} \times 100 \quad (2.14)$$

$$\% \text{ 2 - CP conversion} = \frac{\text{mmol of 2-CP consumed}}{\text{mmol of 2-CP taken}} \times 100 \quad (2.15)$$

$$\% \text{ 2 - PA yield} = \frac{\text{mmol of 2-PA formed}}{\text{mmol of 2-CP taken}} \times 100 \quad (2.16)$$

$$\% \text{ MC yield} = \frac{\text{mmol of MC formed}}{\text{mmol of 2-CP taken}} \times 100 \quad (2.17)$$

$$\% \text{ 2 - MP yield} = \frac{\text{mmol of MC formed}}{\text{mmol of 2-CP taken}} \times 100 \quad (2.18)$$



$$\% \text{ DMC selectivity} = \frac{\text{mmol of DMC formed}}{(\text{mmol of MeOH consumed} / 2)} \times 100 \quad (2.19)$$

$$\% \text{ 2 - PA selectivity} = \frac{\text{mmol of 2-PA formed}}{\text{mmol of 2-CP consumed}} \times 100 \quad (2.20)$$

$$\% \text{ MC selectivity} = \frac{\text{mmol of MC formed}}{\text{mmol of MeOH consumed}} \times 100 \quad (2.21)$$

$$\% \text{ 2 - MP selectivity} = \frac{\text{mmol of 2-MP formed}}{\text{mmol of MeOH consumed}} \times 100 \quad (\text{based on MeOH}) \quad (2.22)$$

$$\% \text{ 2 - MP selectivity} = \frac{\text{mmol of 2-MP formed}}{\text{mmol of 2-CP consumed}} \times 100 \quad (\text{based on 2 - CP}) \quad (2.23)$$

$$\text{MeOH mass balance} = \frac{(\text{mmol of unreacted MeOH} + 2 \times \text{mmol of DMC formed} + \text{mmol of MC formed} + \text{mmol of 2-MP formed})}{\text{mmol of MeOH taken}} \times 100 \quad (2.24)$$

$$\text{2 - CP mass balance} = \frac{(\text{mmol of unreacted 2-CP} + \text{mmol of 2-PA formed} + \text{mmol of 2-MP formed})}{\text{mmol of 2-CP taken}} \times 100 \quad (2.25)$$

where MeOH = methanol, DMC = dimethyl carbonate, 2-CP = 2-cyano pyridine, 2-PA = 2-picolinamide, MC= methyl carbamate and 2-MP = 2-methyl picolinate).

## 2.6. Conclusions

In this chapter, the methods of preparation of catalyst samples (HT-derived mixed oxides, NaTNT, ZrPP and CeO<sub>2</sub>) used in the thesis were described. The basic principles of physicochemical techniques used for characterization of catalysts were presented. Reaction procedures for DMC synthesis by transesterification of cyclic carbonate with methanol and by direct synthesis from CO<sub>2</sub> as well as the methodology of product analysis were presented.

## 2.7. References

- [1] J. He, M. Wei, B. Li, Y. Kang, D.G. Evans, X. Duan, *Struct. Bond.* 119 (2006) 89-119.
- [2] E. Angelescu, O.D. Pavel, M. Che, R. Bîrjega, G. Constantin, *Catal. Commun.* 5 (2004) 647-651.
- [3] C.-Y. Hsu, T.-C. Chiu, M.-H. Shih, W.-J. Tsai, W.-Y. Chen, C.-H. Lin, *J. Phys. Chem. C*

- 114 (2010) 4502-4510.
- [4] A. Clearfield, J.D. Wang, Y. Tian, E. Stein, C. Bhardwaj, *J. Solid. State. Chem.* 117 (1995) 275-289.
- [5] J.D. Wang, A. Clearfield, G.-Z. Peng, *Mater. Chem. Phys.* 35 (1993) 208-216.
- [6] Ch. Srilakshmi, K. Ramesh, P. Nagaraju, N. Lingaiah, P.S. Sai Prasad, *Cat. Lett.* 106 (2006) 115-122.
- [7] S. Wang, L. Zhao, W. Wang, Y. Zhao, G. Zhang, X. Ma, J. Gong, *Nanoscale* 5 (2013) 5582-5588.
- [8] T. Fan, L.X. Zhang, H.F. Jiu, Y.X. Sun, G.D. Liu, Y.Y. Sun, Q.L. Su, *Micro&Nano. Lett.* 5 (2010) 230-233.
- [9] W.H. Bragg, W.L. Bragg, *The Crystalline state*, Vol.1 McMillan, Newyork (1949).
- [10] C.H. Bartholomew, R.J. Farrauto, *Fundamentals of Industrial Catalytic Process*, Second edn. Jhon Wiley& Sons, Inc. (2006).
- [11] G. Bergeret, in: *Handbook of Heterogeneous catalysis Vol. 2*, G. Ertl, H. Knozinger, J. Weitcamp (Eds.), Wiley- VCH, Weinheim (1997).
- [12] M. Che, J.C. Vedin (Eds.), *Characterisation of solid materials and heterogeneous catalysis from structure to surface reactivity*, Wiley-VCH VgmbH & CO. KGaA, weinheim (2012).
- [13] G. Leofantia, M. Padovanb, G. Tozzolac, B. Venturellia, *Catal. Today* 41 (1998) 207-219.
- [14] K.E. Gubbins, in: *Physical Adsorption: Experiment, Theory and Application*, J. Fraissard (ED.), Kluwer: Dordrecht (1997).
- [15] [www.quantachrom.com](http://www.quantachrom.com)
- [16] J.C. Santamarina, K.A. Klein, Y.H. Wang, E. Prencke, *Can. Geotech. J.* 39 (2002) 233-241.
- [17] E.P. Barret, L.G. Joyner, P.H. Halenda, *J. Amer. Chem. Soc.* 73 (1951) 373-380.
- [18] <http://www-odp.tamu.edu/publications/tnotes/tn29/technot8.htm>
- [19] J.W. Niemantsverdriet, *Spectroscopy in Catalysis*, WILEY-VCH Verlag GmbH & Co.KGaA, Weinheim, (2007).
- [20] [http://hiq.lindegas.com/analytical\\_method/infrared\\_spectroscopy.html](http://hiq.lindegas.com/analytical_method/infrared_spectroscopy.html)
- [21] C.V. Raman, R.S. Krishnan, *Nature* 121 (1928) 501-502.
- [22] [web.pdx.edu/raman\\_spectroscopy\\_basics\\_Princeton-in](http://web.pdx.edu/raman_spectroscopy_basics_Princeton-in)

- [23] F. Blanc, C. Cope'ret, A. Lesage, L. Emsley, *Chem. Soc. Rev.* 37 (2008) 518-526.
- [24] A. Alia, S. Ganapathy, H.J.M. de Groot, *Photosynth. Res.* 102 (2009) 415-425.
- [25] M.J. Duer, *Introduction to Solid-State NMR Spectroscopy*. Blackwell Publishing Ltd., Oxford (2004).
- [26] G. Lawes, *Scanning Electron Microscopy and X-Ray Microanalysis*, John Wiley and Sons Ltd., Chichester (1987).
- [27] J.M. Thomas, O. Terasaki, P.L. Gai, W. Zhou, J. Gonzalez-Calbet, *Acc. Chem.Res.* 34 (2001) 583-594.
- [28] D.B. William, C.B. Carter, *Transmission Electron Microscopy*, Plenum Press, New York (1996).
- [29] L. Saikia, J.K. Satyarthi, D. Srinivas, P. Ratnasamy, *J. Catal.* 252 (2007) 148-160.

**Chapter - 3**

**Transesterification of Ethylene and Propylene**

**Carbonate over Mixed Oxide Catalysts**

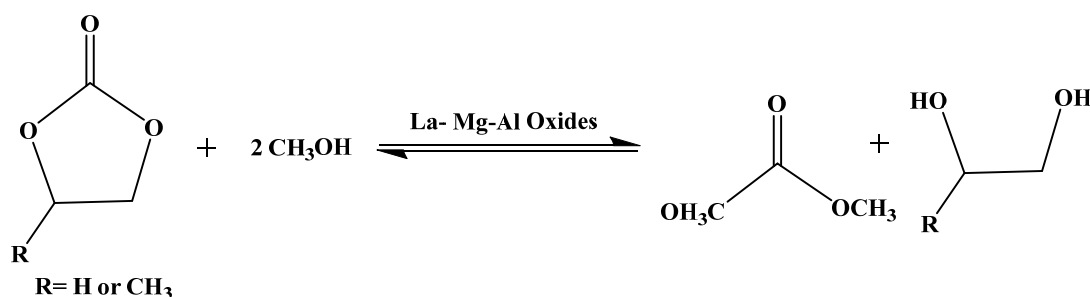
### 3.1. Introduction

Dimethyl carbonate (DMC) is an environmentally benign building block having a wide application in chemical industry [1,2]. It is used as a methylation and carbonylation agent alternative to toxic and corrosive methyl halide/dimethyl sulfate and phosgene, respectively. Furthermore, DMC can also be used as a fuel additive in place of toxic and less biodegradable methyl-*tert.*-butyl ether (MTBE) [2-6]. Its high dielectric constant enables its use as an electrolyte [7]. The traditional methods for DMC production such as phosgenation and oxidative carbonylation of methanol are unsafe [8]. The environmentally-friendly routes for DMC synthesis are the direct synthesis from methanol and CO<sub>2</sub> [9,10] and transesterification of cyclic carbonates with methanol [11-14]. The yield of DMC in the former route is low because of the thermodynamic limitation. Transesterification of cyclic carbonate with methanol is a promising route. Most of the hitherto known homogeneous or heterogeneous catalytic systems suffer from low catalytic activity, high reaction time/temperature and involvement of noble metals [15-19]. Sankar et al. [20] reported 80 mol% of DMC yield from transesterification of ethylene carbonate (EC) with methanol at ambient condition using an alkali and alkaline earth metal tungstate catalyst. Later, the same group [21] reported CaO-ZnO-based catalysts with varying Ca/Ca+Zn ratio for the synthesis of DMC with a yield up to 83 mol% at ambient conditions both in batch and continuous processes. However, this catalyst has limitation because of its low turnover number (TON) and metal oxide leaching into the product stream. Development of efficient, environmentally-friendly, stable, solid catalysts is, therefore, highly important. Both acid and base catalysts are used for this reaction. The latter are more efficient. Solid base catalysts have obtained greater attention, among which hydrotalcites (HTs) show unique catalytic activity.

HTs are layered double hydroxides (anionic clay) with a general formula  $[M_{(1-x)}^{2+}M_x^{3+}(\text{OH})_2]^{x+}(\text{A}^{n-}_{x/n})\cdot y\text{H}_2\text{O}$ . They have received much attention in recent years because of their eco-friendly nature and large variety of applications, including those in several base-catalyzed organic reactions, medicinal applications, etc [22-26]. Their structure resembles brucite, in which a part of the bivalent metal ion ( $M^{2+} = \text{Mg}^{2+}$ ) is isomorphously substituted with trivalent metal ions, resulting in the formation of a positive charge on the layers, which in turn is charge balanced by anions present in the interlayer. Water of crystallization is generally observed in the HT galleries. HTs can be used as additives in polymers and as precursors for magnetic materials [26,27]. Moreover, they are efficient solid base catalysts, which can replace the

homogeneous bases like NaOH, KOH, etc., for transesterification reactions. Watanabe and Tatsumi [12] & Murugan and Bajaj [28] have reported the catalytic use of Mg-Al HTs for the synthesis of DMC from ethylene and propylene carbonates (EC and PC). Wu et al. [29] reported the use of fluorine-modified Mg-Al mixed oxides for the preparation of propylene glycol methyl ether from methanol and propylene oxide. The main advantage of the HT catalysts is their controllable acid-base properties. HTs are decomposed to yield mixed oxides with strong Lewis base features [30].

In this chapter, Mg-Al HTs modified with rare-earth elements ( $\text{La}^{3+}$ ,  $\text{Ce}^{3+}$ ,  $\text{Y}^{3+}$ ,  $\text{Pr}^{3+}$  and  $\text{Sm}^{3+}$ , 8 mol% of Al) are investigated, for the first time. Their catalytic activity for transesterification of propylene carbonate/ethylene carbonate (PC/EC) with methanol producing DMC along with propylene glycol (PG)/ethylene glycol (EG) as a co-product is investigated (Scheme 3.1).



**Scheme 3.1.** Transesterification of EC/PC with methanol.

Different mol% of La containing Mg-Al HT catalysts were prepared by a co-precipitation method, calcination of which yielded ternary lanthanum-magnesium-aluminum oxides. These catalysts were characterized by chemical analysis, X-ray diffraction (XRD), N<sub>2</sub> adsorption and <sup>27</sup>Al magic-angle spinning nuclear magnetic resonance (<sup>27</sup>Al MAS NMR) and Fourier transform infrared (FTIR) spectroscopy. Basicity of the ternary oxides was determined by temperature-programmed desorption using CO<sub>2</sub> as a probe molecule (CO<sub>2</sub>-TPD). It should be noted here that HTs are the precursors of the catalysts. The ternary oxides formed on calcination of modified HTs are the actual catalysts in this study. The effects of preparation procedure (La content and calcination temperature) and reaction parameters on the transesterification activity were investigated. The products were identified and quantified by <sup>1</sup>H NMR and gas chromatographic (GC) methods.

## 3.2. Experimental

### 3.2.1. Catalyst preparation

Mg-Al hydrotalcites (Mg : Al = 2 : 1) and different rare-earth modified HTs were prepared by a co-precipitation technique as reported in Chapter 2 (Section 2.2.1). The materials obtained were labeled as follows: HT-as-syn and HT-X M, respectively, where M is the rare-earth element, X represents mol% of M and molar ratio of HT is  $Mg/(Al+M) = 2$ . They were then calcined at 600 °C for 6 h. The mixed oxides, thus, obtained were designated as HT-C and HT-X M-C, respectively.

### 3.2.2. Characterization techniques

The composition of  $Mg^{2+}$ ,  $Al^{3+}$  and  $La^{3+}$  ions in the ternary oxide samples were determined by inductively coupled plasma-optical emission spectroscopy (ICP-OES; Spectro Arcos). A known quantity of the catalyst (2 – 9 mg) was dissolved in a minimum amount of 2 N  $HNO_3$  and made up to the required volume (50 ml) before the ICP-OES analysis. X-ray diffraction (XRD) patterns of the powder samples were recorded on a Philips X'pert Pro diffractometer using  $Cu-K_{\alpha}$  radiation and a proportional counter detector. The diffractograms were recorded in the  $2\theta$  range of 5 to 80° with a scan rate of 2°/min and step size of 0.02°. Specific surface area ( $S_{BET}$ ) of the samples was determined from  $N_2$  adsorption measurements at -196 °C using a Nova 1200 Quanta Chrome equipment. FTIR spectra of the samples as KBr pellets were recorded on a Shimadzu 8201 spectrophotometer in 400-4000  $cm^{-1}$  region. Basicity of the catalysts was determined by temperature-programmed desorption of carbon dioxide ( $CO_2$ -TPD) technique. About 0.1 g of the catalyst was activated at 500 °C under He (30 ml/min). The sample was cooled to 50 °C and  $CO_2$  was adsorbed (40 ml/min) for 30 min. Desorption of  $CO_2$  was followed in the temperature range of 50 to 900 °C by rising the temperature at the ramp rate of 10 °C /min.

### 3.2.3. Reaction procedure

Details of the reaction procedure and methods used in the product identification and quantification are described in Chapter 2 (sections 2.4.1.1 and 2.5.1.1). Methanol (99%; Merck India) and PC & EC (Spectrochem, India) were procured and used in the reactions without any further purification. DMC, EG and PG were purchased from Loba Chem., India as standards for the identification and quantification of products.

### 3.3. Results and discussion

#### 3.3.1. Catalyst characterization

##### 3.3.1.1. XRD

XRD analysis was carried out to confirm the formation and structural changes occurred during calcination of HTs. Fig. 3.1(a) shows the powder XRD patterns of as-synthesized lanthanum (2-10 mol %) containing HTs. “Neat” HT-as-syn showed XRD pattern typical of a layered double hydroxide with sharp and symmetric peaks arising from (003), (006), (110) and (113) planes and broad asymmetric peaks arising from (012), (015) and (018) planes [30-36]. The XRD profile of HT-as-syn is consistent with the structure of  $[\text{Mg}_4\text{Al}_2(\text{OH})_{12}(\text{CO}_3)(\text{H}_2\text{O})_3]_{0.5}$  (hexagonal system, rhombo-centered lattice, space group R3m; JCPDS70-2151). The unit cell parameters (a and c) were calculated from the peak position of (110), (003) and (006) reflections by using the formulae:  $a = 2d(110)$  and  $c$  (basal spacing between the layers) =  $3/2[d(003) + 2d(006)]$ . Values of these parameters (Table 3.1) are in good agreement with those reported by others [30-36].

The XRD patterns of different mol% of La and 8 mol% of other rare-earth elements (Y, Ce, Pr, and Sm) incorporated HTs are shown in Fig. 3.1(a) and Fig. 3.2(a), respectively. Except for La and Pr modified HT, the rest of the samples showed XRD patterns typical of HT structure with observation of no additional peaks due to rare-earth oxide/hydroxide. In the case of La-containing HTs, the presence of a mixture of  $\text{La}(\text{OH})_3$  and  $\text{La}_2(\text{CO}_3)_2(\text{OH})_2$  (JCPDS 70-1774) phases was detected (Fig. 3.2(a)). The intensity of the XRD peaks corresponding to those phases increased with increasing La content. Lanthanum carbonate formation occurred in the early stages of co-precipitation because of the strong anionic character of La (lowest electronegativity as compared to other rare-earth elements). The La prefers to locate in the interlayer gallery of HT as separate hydroxide and hydroxy-carbonate phases due to its high ionic radius (0.103 nm). With an increase in lanthanum loading, the unit cell parameter, c, corresponding to interlayer separation, increased from 2.26 to 2.30 nm (Table 3.1). This indicates the decrease of electrostatic force of attraction between the layers and the interlayer anions. Calcination (at 600 °C for 6 h) of the trivalent rare-earth elements modified HTs led to mixed oxide-type materials. The XRD patterns of the calcined rare-earth modified HTs are shown in Fig. 3.1(b) and Fig. 3.2(b). All of these calcined materials showed reflections at 35.1, 43.4, and 62.6° corresponding to (111), (200), and (220) planes, respectively, of (Mg)Al oxide [37].



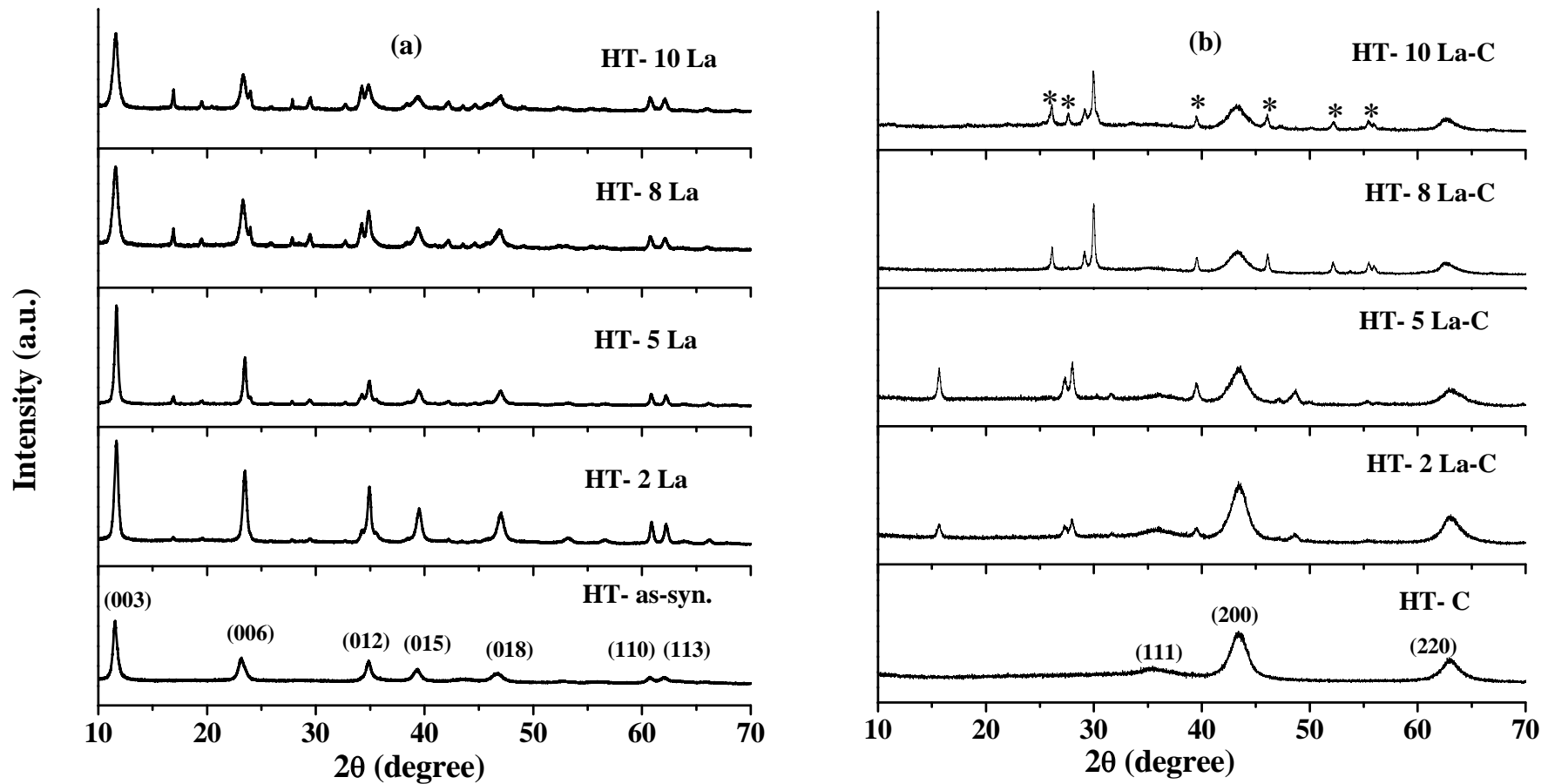


**Fig. 3.1.** Powder XRD patterns of “neat” and lanthanum incorporated HTs: (a) as-synthesized and (b) calcined samples. Peaks marked by an asterisk correspond to the  $\text{La}_2\text{O}_2\text{CO}_3$  phase.

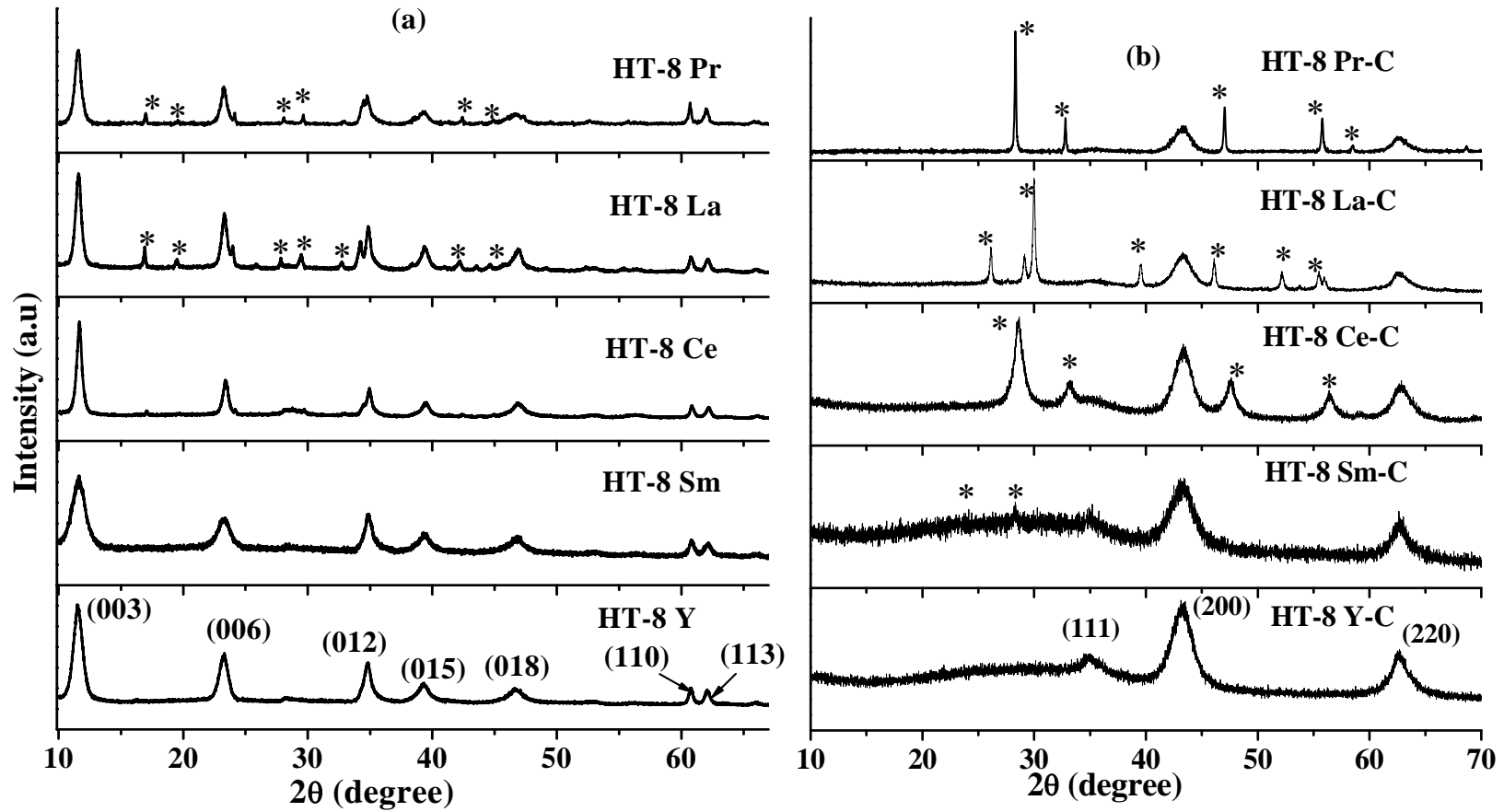


**Fig. 3.2.** Powder XRD of (a) as-synthesized and (b) calcined 8 mol% rare-earth ion incorporated HTs. Peaks marked by asterisks correspond to rare earth hydroxide/oxide and hydroxy carbonate/oxide carbonate phases.

Additionally, the formation of a segregated rare-earth oxide phase was also detected as revealed from the additional peaks. However, the intensity of these additional rare-earth oxide peaks were rather weak in the case of HT-8 Y-C and HT-8 Sm C (Fig. 3.2(b)). For HT La-C, the formation of  $\text{La}_2\text{O}_2\text{CO}_3$  phase (JCPDS 48-1113) due to re-adsorption of gaseous  $\text{CO}_2$  coming from HT decomposition or by the air contamination was also detected. The cell parameter (a) of (Mg)Al oxide calculated from the peak position of (200) plane is reported in Table 3.1.

### 3.3.1.2. ICP-OES

The chemical compositions of HTs were determined using ICP-OES technique (Table 3.1). The Mg:Al molar ratio of 1.9:1 for HT (as-syn & calcined) determined from ICP-OES is in good agreement with the nominal value of 2:1. The lanthanum content in HT-La catalysts has almost matched with the expected one. In HT-8 Y-C, the yttrium content is found to be 3 times lower than the expected value.

### 3.3.1.3. Surface area analysis

$\text{N}_2$ -physiorption analysis was carried out for determining the surface area of HTs and mixed oxides derived from them. The specific surface area ( $S_{\text{BET}}$ ) of the materials increased after calcination. The value of  $S_{\text{BET}}$  decreased with an increase in the lanthanum content in the materials. However,  $S_{\text{BET}}$  of the other rare-earth element containing oxides was found higher than La-Mg-Al oxides (Table 3.1).

### 3.3.1.4. FTIR

FT-IR spectra give information about interlayer species and structure of HTs. They also revealed the structural changes of HTs into oxides on calcination. FT-IR spectra of as-synthesized HT samples showed a broad, asymmetric band at  $3470\text{ cm}^{-1}$ , corresponding to the stretching vibrations of OH groups attached to Mg and Al in the brucite-like layer [31, 32, 36, 37]. The bending mode of water present in HT galleries was observed at  $1642\text{ cm}^{-1}$ . The various peaks corresponding to interlayer carbonate at  $1367$ ,  $867$  and  $659\text{ cm}^{-1}$  are designated as  $\nu_3$ ,  $\nu_2$ , and  $\nu_4$  modes, respectively. The bands corresponding to Al-O stretching modes were observed at  $943$  and  $762\text{ cm}^{-1}$ . The shoulder seen at  $1507\text{ cm}^{-1}$  is ascribed to  $\text{CO}_3^{2-}$  species. In calcined samples, the intensity of  $\nu_3$  mode decreased and the band corresponding to OH stretching had almost disappeared, consistent with the formation of a mixed oxide phase (Fig. 3.3).

**Table 3.1.** Elemental composition, structure, and textural properties of HTs

Sample	Elemental composition (ICP-OES) <sup>a</sup>	Unit cell parameters		S <sub>BET</sub> (m <sup>2</sup> /g)	Total basicity	
		(XRD, nm)			μmol/g	μmol/m <sup>2</sup>
		a	c			
HT-as-syn	Mg : Al = 1.9(2)	0.305	2.261	-	-	-
HT-2 La	Mg : (Al+La) = 1.8(2), Al : La = 64.8 (49)	0.304	2.264	64	-	-
HT-5 La	Mg : (Al+La) = 1.6(2), Al : La = 19.3(19)	0.304	2.270	61	-	-
HT-8 La	Mg : (Al+La) = 1.8(2), Al : La = 11.2(11.5)	0.304	2.276	60	-	-
HT-10 La	Mg : (Al+La) = 2(2), Al : La = 8.1(9)	0.304	2.301	53	-	-
HT-C	Mg : Al = 1.9(2)	0.416	-	121	422	3.5
HT-2 La-C	Mg : (Al+La) = 1.8(2), Al : La = 64.8 (49)	0.416	-	96	481	5.0
HT-5 La-C	Mg : (Al+La) = 1.6(2), Al : La = 19.3(19)	0.417	-	82	489	5.9
HT-8 La-C	Mg : (Al+La) = 1.8(2), Al : La = 11.2(11.5)	0.416	-	79	521	6.6
HT-10 La-C	Mg : (Al+La) = 2(2), Al : La = 8.1(9)	0.417	-	68	446	6.7
HT-8 Y- C	Mg : (Al+Y) = 1.9(2), Al : Y = 39.1 (11.5)	0.417	-	204	418	2.0
HT-8 Ce-C	Mg : (Al+Ce) = 2.2(2), Al : Ce = 10.2(11.5)	0.417	-	157	251	1.6
HT-8 Pr-C	Mg : (Al+Pr) = 2.2(2), Al : Pr = 16.1(11.5)	0.417	-	115	266	2.3
HT-8 Sm-C	Mg : (Al+Sm) = 2.1(2), Al: Sm = 11.2(11.5)	0.417	-	286	354	1.2

<sup>a</sup>Values in parentheses correspond to nominal values.

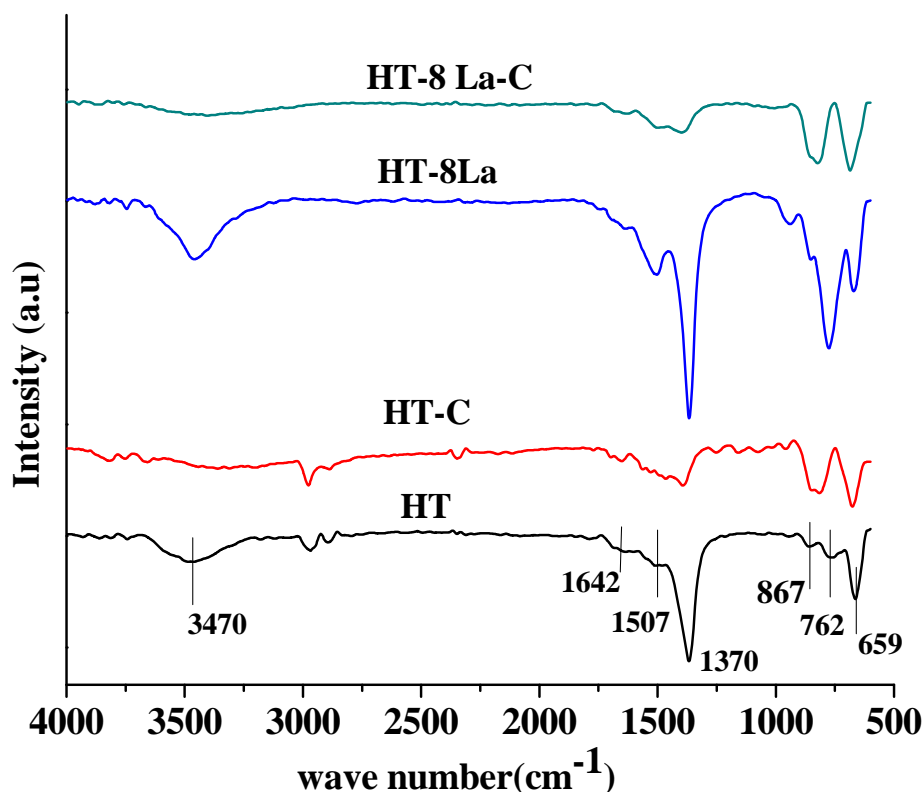
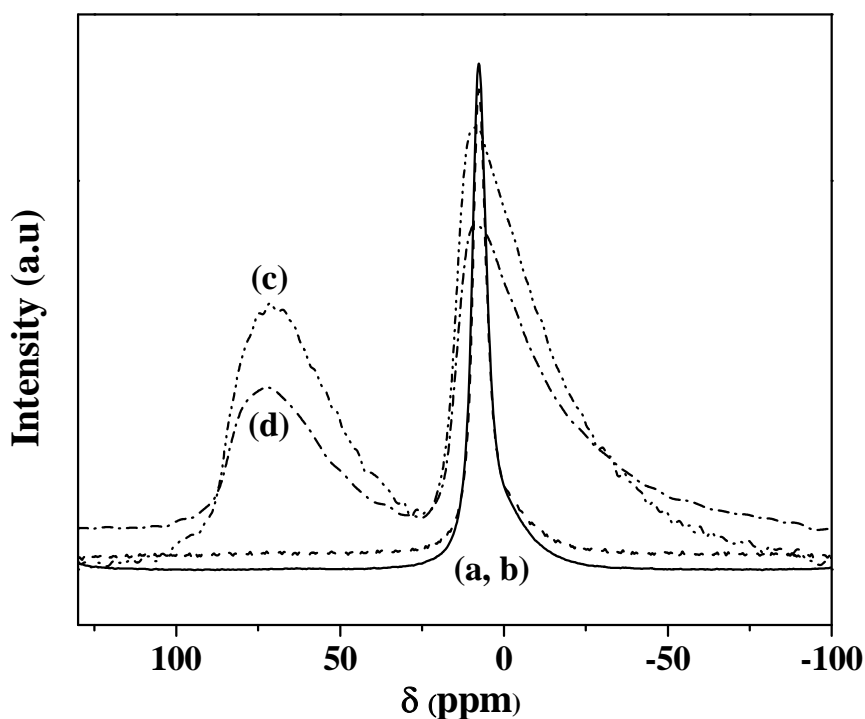


Fig. 3.3. FTIR spectra of as-synthesized and calcined HTs

### 3.3.1.5. $^{27}\text{Al}$ MAS NMR

$^{27}\text{Al}$  MAS NMR spectra of as-synthesized forms of HT and HT-8 La showed a sharp intense signal at 7.6 ppm corresponding to Al in an octahedral coordination (Fig. 3.4; curves a and b). HT-8 La-C showed two asymmetric broad signals at 72.2 and 8.7 ppm (Fig. 3.4, curve c). While the signal at 8.7 ppm is attributed to Al in octahedral coordination, that at 72.2 ppm is corresponded to Al in a tetrahedral coordination environment. The asymmetric nature of the NMR signal suggests non-zero quadrupolar coupling interactions. These signals for the calcined sample are consistent with the presence of Mg(Al) mixed oxides [38,39]. The spectrum of a spent HT-8 La-C (Fig. 3.4, curve d) is nearly the same as that of fresh HT-8 La-C, suggesting that the structure of the mixed oxide material is intact even after its use.



**Fig. 3.4.**  $^{27}\text{Al}$  MAS NMR spectra of (a) HT-as-syn, (b) HT-8 La, (c) HT-8 La-C and (d) spent HT-8 La-C.

### 3.3.1.6. $\text{CO}_2$ -TPD

The basicity of mixed oxides was determined using  $\text{CO}_2$ -TPD technique (Table 3.1). HT-C showed two  $\text{CO}_2$ -TPD peaks with maximum at 246 and 653 °C attributable to  $\text{CO}_2$  desorbed from weak and strong basic sites, respectively (Fig. 3.5). Rare-earth modified HTs showed four  $\text{CO}_2$  desorption peaks at 204, 349, 645 and 815 °C (for HT-8 La-C) consistent with the presence of four types of basic centers. Intensity of the 2<sup>nd</sup> and 4<sup>th</sup> peaks increased with increasing La content. Based on this observation, the 1<sup>st</sup> and 3<sup>rd</sup> peaks were attributed to those arising from (Mg)Al oxides while the 2<sup>nd</sup> and 4<sup>th</sup> peaks were assigned to a segregated rare-earth oxide phase. A change in peaks positions was noted with a change in the loading of rare-earth oxide (Fig. 3.5). With an increase in La loading, peaks corresponding to rare-earth oxide shifted to higher temperatures and an increase in the overall density of basic sites was noticed. This shift to higher temperatures could be a consequence of increase in the basic strength and particle size of dopent oxide. The overall basicity of different modified catalysts is reported in Table 3.1. It decreased in the order: HT-8 La-C (0.521 mmol/g) < HT-C (0.422 mmol/g) < HT-8 Y-C (0.418 mmol/g) <

HT-8 Sm-C (0.354 mmol/g) < HT-8 Pr-C (0.266 mmol/g) < HT-8 Ce-C (0.251 mmol/g). In other words, doping of Sm, Pr and Ce ions had adverse effects on the basicity of these oxides.

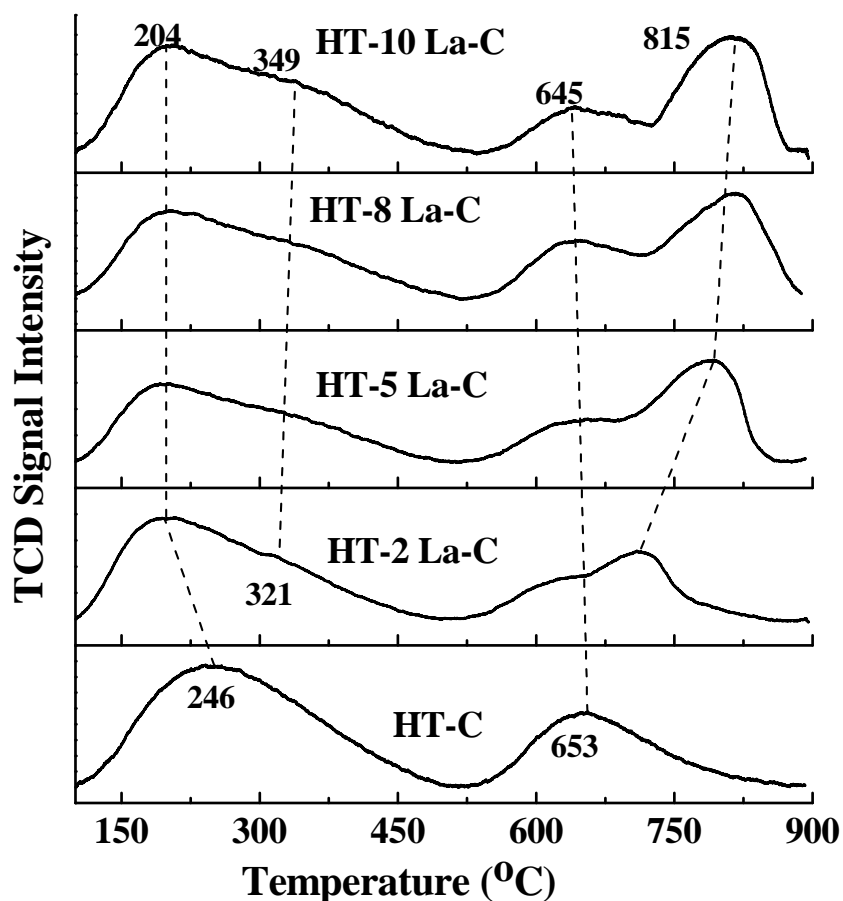


**Fig. 3.5.** CO<sub>2</sub>-TPD profiles of calcined HT and lanthanum modified HT catalysts.

### 3.3.2. Catalytic activity - transesterification of propylene carbonate

The catalytic activity data of calcined HT and La modified HTs for DMC synthesis by transesterification of PC with methanol are listed in [Table 3.2](#). One mole of PC on transesterification yields 1 mol of DMC and 1 mol of PG ([Scheme 1](#)). PC conversion and DMC selectivity were estimated by two independent techniques - <sup>1</sup>H NMR and GC. The data were found comparable within experimental error (2-5 mol %). This study shows that NMR is an alternative analytical tool to monitor and follow the reaction of PC with methanol producing DMC and PG. The methyl proton signals of DMC, PG, and PC were observed at 3.79 (singlet),

1.14 (doublet), and 1.54 ppm (doublet), respectively. The area of these signals was determined by integration. The equation used for calculation is explained in Chapter 2 (section 2.5.1.2).

**Table 3.2.** Catalytic activity data of rare earth modified HTs for transesterification of PC and methanol<sup>a</sup>

Catalyst	PC conversion (mol%)	DMC selectivity (mol%)	TON (mmol/g)
HT-C	7.2	68.0	10
HT-2 La-C	17.2	95.1	32
HT-5 La-C	26.1	94.7	49
HT-8 La-C	33.1	87.7	57
HT-10 La-C	33.8	77.3	51
HT-8 Y-C	9.1	78.5	14
HT-8 Ce-C	20.4	79.8	32
HT-8 Pr-C	34.1	91.8	61
HT-8 Sm-C	12.1	96.0	23

<sup>a</sup>Reaction conditions: PC = 1.02 g (10 mmol), methanol = 3.2 g (100 mmol), catalyst = 5 wt % of PC, reaction temperature = 150 °C, and reaction time = 1 h. <sup>b</sup>Turnover number (TON) = mmol of DMC formed per gram of catalyst

### 3.3.2.1. Effect of rare-earth element

Controlled experiments at our reaction conditions revealed that this reaction does not proceed in the absence of a catalyst. HT-C is weakly active (PC conversion = 7.2 mol% and DMC selectivity = 68 mol%). Incorporation of rare-earth ion enhanced the catalytic activity [turnover number (TON) = mmol of DMC formed per gram of catalyst] of HT catalysts (Table 3.2). This enhancement for different rare-earth ions increased in the order:  $Y^{3+} < Sm^{3+} < Ce^{3+} < La^{3+} < Pr^{3+}$ . DMC selectivity is higher on  $Sm^{3+}$ ,  $Pr^{3+}$  and  $La^{3+}$  than on  $Ce^{3+}$  and  $Y^{3+}$  modified HT catalysts. After 1 h of reaction, the catalyst was separated, and the reaction was continued for another 1 h. An increase in catalytic activity was observed in the case HT-8 Pr-C, indicating that  $Pr^{3+}$  ions got leached out from the solid catalyst. The reaction in this case had contributions from both homogeneous and heterogeneous phases of praseodymium oxide. Such leaching of metal ions was not noticed in the case of La incorporated HTs. Hence, all of the further studies were



conducted only on the La modified catalysts. PC conversion and DMC selectivity increased with La loading (Table 3.2). A near linear correlation between TON or PC conversion and surface density of basic sites was observed (Fig. 3.6). Thus, basicity of the catalyst plays an important role.

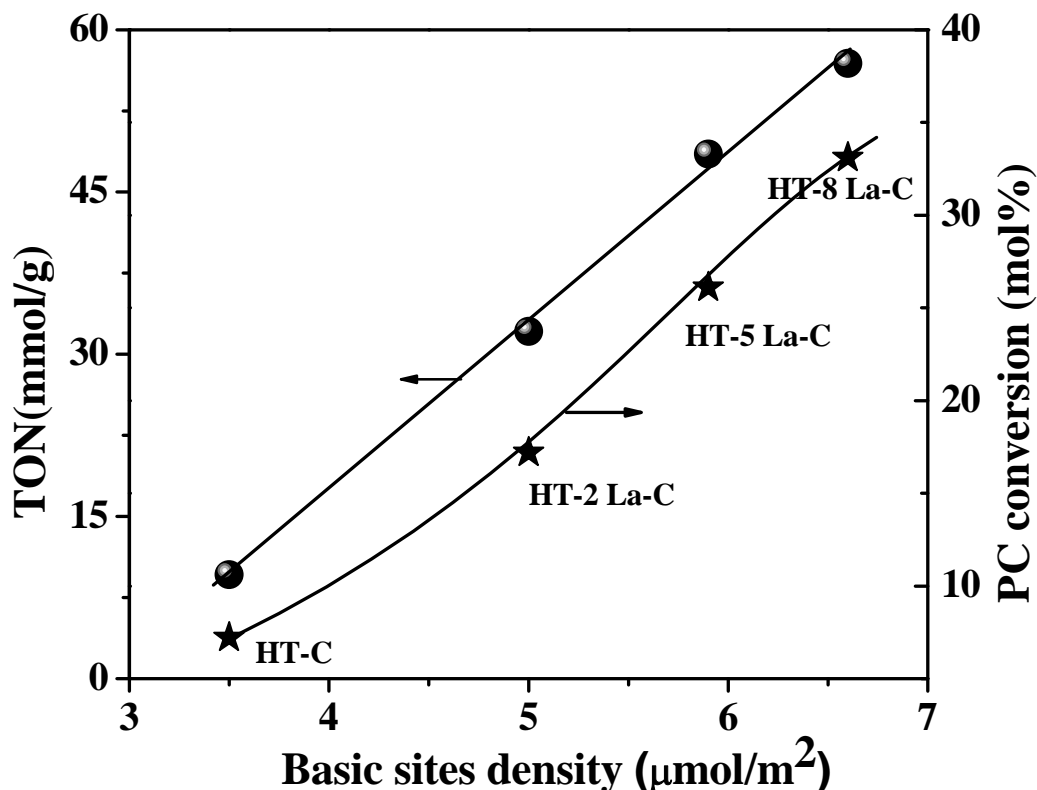


**Fig. 3.6.** Correlation between catalytic activity and density of basic sites on HT La-C catalysts. Reaction conditions: PC = 10 mmol, methanol = 100 mmol, catalyst = 5 wt % of PC, reaction temperature = 150 °C, and reaction time = 1 h. Turnover number (TON) = mmol of DMC formed per gram of catalyst.

Fig. 3.7 shows the progress of the reaction as a function of time over HT-8 La-C catalyst. The intensity of  $^1\text{H}$  NMR signals at 3.79 and 1.14 ppm due to the methyl protons of DMC and PG increased at the expense of the signals at 1.54 ppm due to the methyl protons of PC.

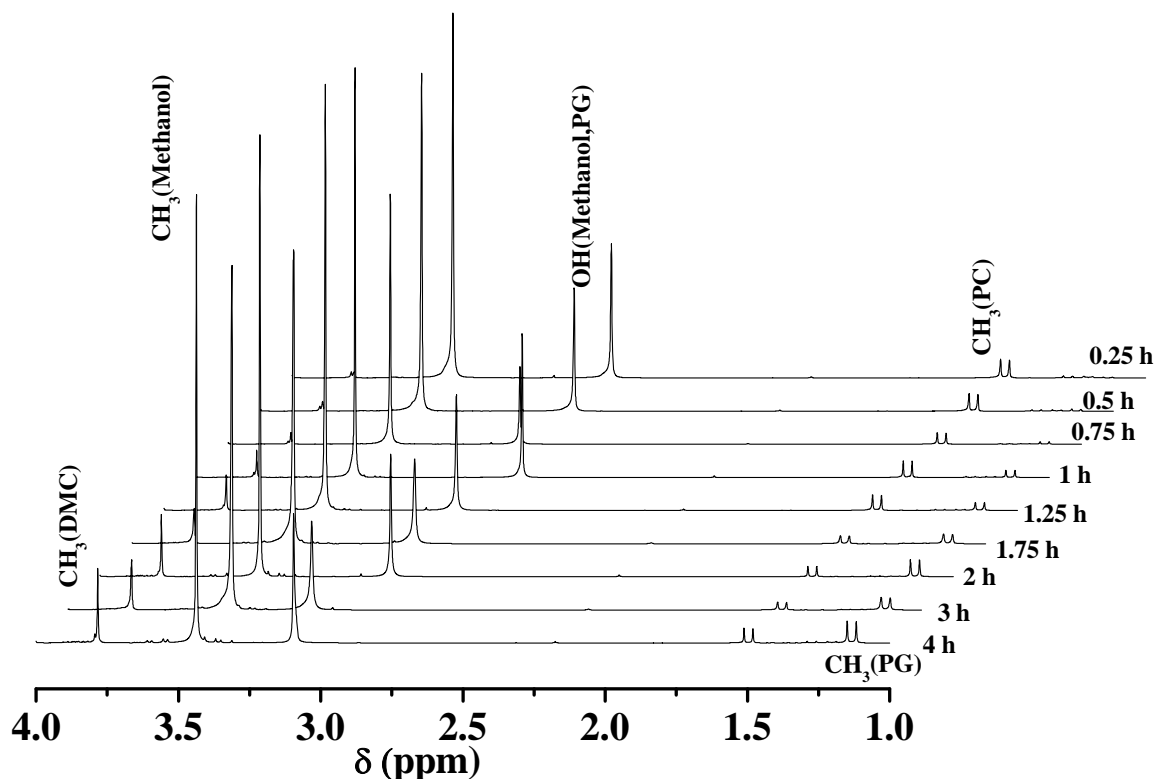


**Fig. 3.7.** Time profile of the  $^1\text{H}$  NMR spectra of the reaction mixture of transesterification of PC with methanol. Reaction conditions: PC = 10mmol, methanol = 100 mmol, catalyst (HT-8 La-C) = 5 wt % of PC and reaction temperature = 150 °C.

### 3.3.2.2. Effect of calcination temperature

Table 3.3 shows the effect calcination temperature on the catalytic activity of HT-8 La-C catalyst. Calcination enhanced the catalytic activity of the catalyst sample. The uncalcined sample was weakly active (PC conversion = 8.6 mol %; DMC selectivity = 98 mol %). Although some loss in DMC selectivity was observed, with increasing calcination temperature from 500 to 750 °C, an increase in PC conversion was observed. The overall DMC yield was found to be higher at a calcination temperature of 600 °C. Hence, in the remaining part of the study, only the catalyst calcined at 600 °C was investigated.

**Table 3.3.** Effect of calcination temperature of HT-8 La on the transesterification activity<sup>a</sup>

Catalyst calcination temperature (°C)	PC conversion (mol %)	DMC selectivity (mol %)
Uncalcined	8.6	98.0
500	29.2	97.4
600	33.1	87.7
750	34.4	82.4

<sup>a</sup>Reaction conditions: PC = 1.02 g (10 mmol), methanol = 3.2 g (100 mmol), catalyst = 5 wt % of PC, reaction temperature = 150 °C, and reaction time = 1 h.

### 3.3.2.3. Effect of reaction parameters

PC conversion increased sharply with increase in reaction temperature and reached a maximum value of 64.3 mol% at 190 °C for the reaction conducted for 1 h (Fig. 3.8). However, the DMC selectivity decreased as the temperature increased. At higher temperatures, part of DMC undergoes thermal decomposition and involves in methylation of methanol forming dimethyl ether (DME). The transesterification reaction is thermodynamically controlled. Higher temperatures facilitated higher PC conversions. The conversion of PC increased with increasing reaction time reaching a maximum after 3 h at 150 °C. Without much effect on DMC selectivity, the PC conversion increased with increasing amount of catalyst and reached a maximum at a catalyst loading of about 5 wt %. The methanol/PC molar ratio has a major effect on DMC yield. A ratio of 10 was found to yield higher amount of DMC.

### 3.3.2. 4. Catalysts recyclability

At the end of each run, the catalyst was separated, washed with methanol, dried at 200 °C for 4 h, and then subjected to recycle study. A loss in PC conversion by about 10 mol% and DMC selectivity by 5 mol% was detected at the end of fourth recycle (Fig. 3.9). At the end of fourth cycle, the catalyst was separated, washed with methanol, activated at 600 °C for 6 h, and then used in the fifth recycle study. As seen from Fig. 3.9, the original activity (PC conversion) of the catalyst was regained.

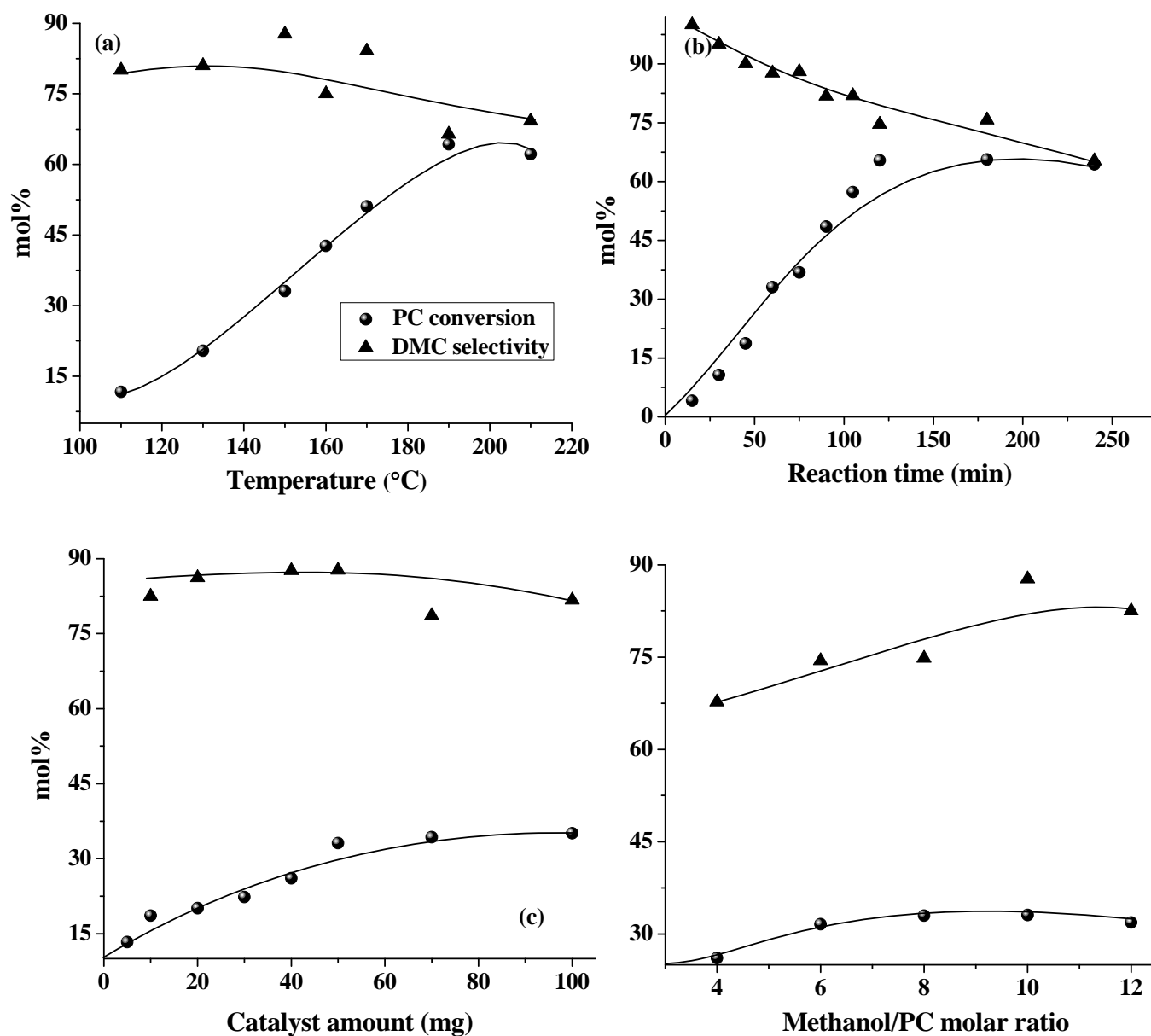


**Fig. 3.8.** Influence of reaction parameters on transesterification of PC with methanol over HT-8 La-C. Reaction conditions: (for a) PC = 10 mmol, methanol = 100 mmol, catalyst = 5 wt % of PC, reaction time = 1 h, and reaction temperature = 110-210 °C; (for b) conditions are the same as those of panel a except reaction temperature = 150 °C and reaction time = 0-4 h; (for c) conditions are the same as those of panel a except catalyst amount = 0-100 mg, reaction temperature = 150 °C, and reaction time = 1 h; (for d) conditions are the same as for panel a except that methanol/PC molar ratio = 0-12, reaction temperature = 150 °C, and reaction time = 1 h.

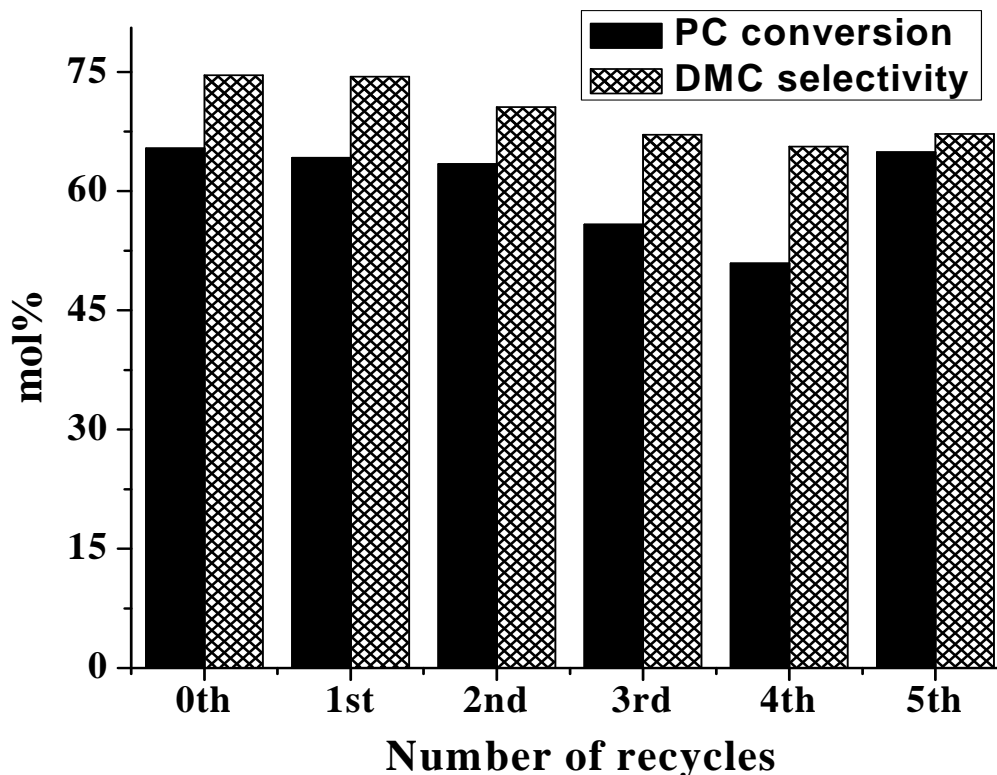


**Fig. 3.9.** Catalyst recyclability studies. Reaction conditions: PC = 10 mmol, methanol = 100 mmol, catalyst (HT-8 La-C) = 5 wt % of PC, reaction temperature = 150 °C and reaction time = 2 h.

The structure of the catalyst was not altered after its reuse as confirmed by XRD, FT-IR, and  $^{27}\text{Al}$  MAS NMR spectra (Figs. 3.4 and 3.10). The chemical compositions of fresh and reused (first and fourth cycle) catalysts were the same. The study thus reveals that La modified HT catalysts are stable and reusable

Table 3.4 compares the catalytic activity of HT-8 La-C with several known solid acid and base catalysts. The catalyst of the present study showed higher conversion of PC at lower reaction temperatures. On the whole, this section discussed the novel catalytic application of calcined rare earth ions modified HTs for producing DMC by transesterification of PC with methanol. The catalyst with 8 mol% of La loading (HT-8 La-C) showed higher catalytic activity than the hitherto known solid catalysts for this reaction. “Neat” lanthanum and aluminum oxides were weakly active, while the composite oxide prepared by calcination of La (8 mol%) loaded HT showed the best activity. The catalytic activity correlated with the surface density of basic sites.

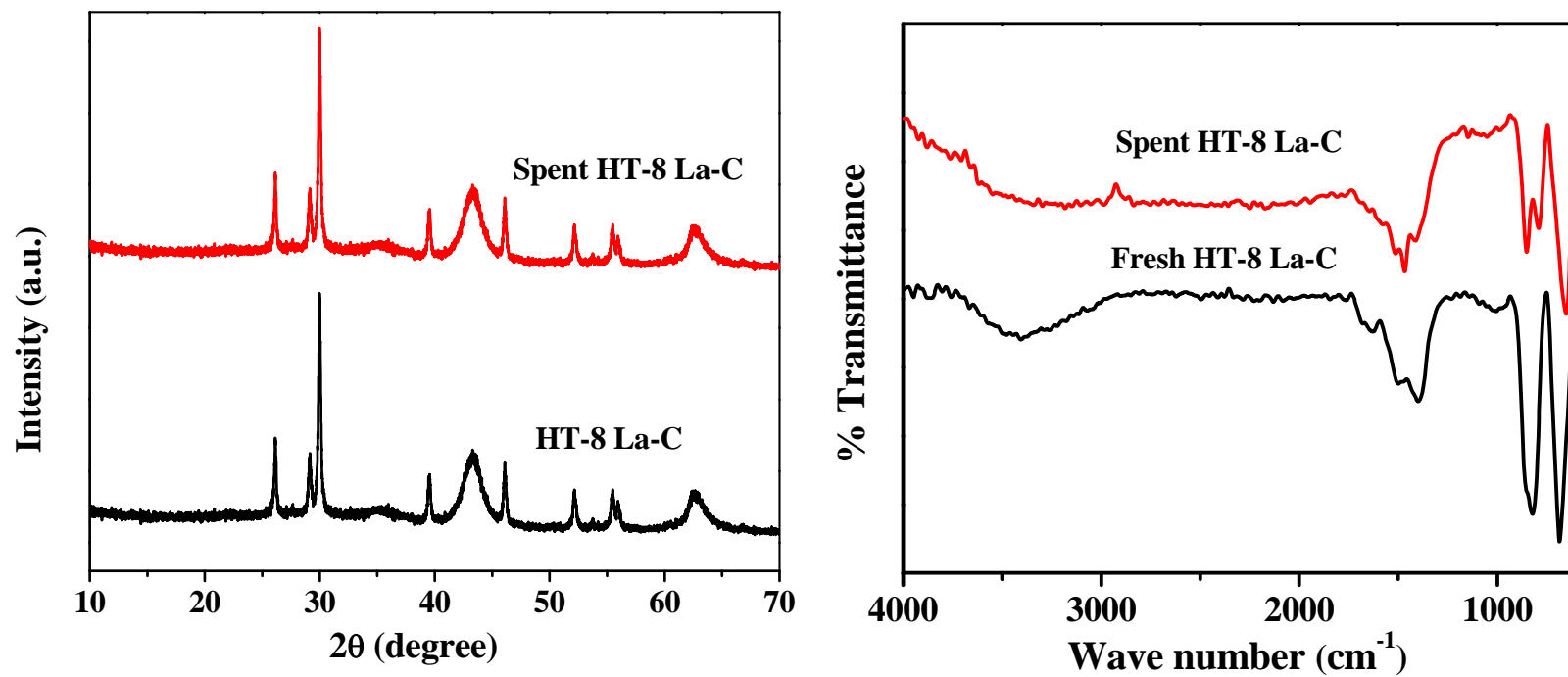


**Fig. 3.10.** Fresh and spent HT-8 La catalysts: (a) XRD and (b) FT-IR

**Table 3.4.** Comparative catalytic activities of different solid catalysts for transesterification of PC with methanol

Catalyst	Reaction temperature (°C)	Reaction time (h)	PC conversion (%)	TON <sup>a</sup>	Ref.
HT-8 La-C	150	2	65.4	96	<a href="#">This work</a>
Fe-Zn DMC	170	8	100	35	<a href="#">[15]</a>
Au/CeO <sub>2</sub>	140	6	63	30	<a href="#">[18]</a>
MgO	160	2	40	21	<a href="#">[23]</a>
MgO	150	4	28	14	<a href="#">[19]</a>
CaO	150	4	25.6	13	<a href="#">[19]</a>
CeO <sub>2</sub>	150	4	32.8	16	<a href="#">[19]</a>
ZrO <sub>2</sub>	150	4	11.8	6	<a href="#">[19]</a>
La <sub>2</sub> O <sub>3</sub>	150	4	7.1	4	<a href="#">[19]</a>
Al <sub>2</sub> O <sub>3</sub>	150	4	4.2	2	<a href="#">[19]</a>
K <sub>2</sub> CO <sub>3</sub>	150	4	61.6	20	<a href="#">[19]</a>

<sup>a</sup>Turnover number (TON) = mmoles of DMC formed per g of catalyst.

The La modified HT catalyst is heterogeneous and could be recovered and reused even after the fifth recycle with little loss of catalytic activity.

### 3.3.3. Catalytic activity - transesterification of ethylene carbonate

Transesterification of EC with methanol yielded equimolar amounts of DMC and ethylene glycol (EG). Controlled experiments revealed that this reaction doesn't occur in the absence of a catalyst. As-synthesized and calcined HTs without a rare-earth ion were weakly active ([Table 3.5, entry no. 1](#)).

#### 3.3.3.1. Effect of rare-earth elements

The calcined samples of Pr and La modified HT showed higher catalytic activity than HT-C and calcined Ce, Sm and Y modified HTs ([Table 3.5](#)). Catalytic activities of different ternary oxides used in this study increased in the following order: HT-C < HT-8 Sm-C < HT-8 Y-C < HT-8 Ce-C < HT-8 La-C < HT-8 Pr-C. However, Pr modified HT exhibited leaching as confirmed by hot filtration method. The higher activity of Pr modified HT compared to others was due to the homogeneous catalytic contribution. Lanthanum oxide and lanthanum oxy carbonate [La<sub>2</sub>O(CO<sub>3</sub>)<sub>2</sub>] phases are responsible for high catalytic activity of HT-8 La-C.

**Table 3.5.** Catalytic activity for transesterification of EC with methanol<sup>a</sup>

catalyst	EC conversion (mol %)	DMC selectivity (mol %)	TON (mmol/g)
HT-C	16.0	97.7	35
MgO-La <sub>2</sub> O <sub>3</sub>	19.2	99.0	42
MgO	27.5	99.5	61
HT-2 La-C	37.7	100	84
HT-5 La-C	52.9	100	118
HT-8 La-C	65.2	100	145
HT-10 La-C	73.8	100	164
HT-8 Y-C	19.0	100	42
HT-8 Ce-C	24.9	100	55
HT-8 Pr-C	70.2	100	156
HT-8 Sm-C	18.0	96.7	39

<sup>a</sup>Reaction conditions: EC = 0.88 g (10 mmol), methanol = 3.2 g (100 mmol), catalyst = 5 wt% of EC, reaction temperature = 60 °C, reaction time = 4 h. Turnover number (TON) = mmol of DMC formed per gram of catalyst.

EC conversion and turnover number (TON = mmol of DMC formed per gram of catalyst) increased with increasing La loading (2 - 10 mol%) on HT. These catalysts are active even at ambient temperature (40 °C) and EC conversion of 55.2 mol% with DMC selectivity of 100% was obtained using (HT-10 La-C). EC conversion was very low (3.2 mol%) with unsupported La<sub>2</sub>O<sub>3</sub> catalyst. Size reduction could be the possible cause for higher activity of supported lanthanum oxide phases. HT-10 La-C exhibiting superior activity was chosen for the detailed study. While there existed no correlation between catalytic activity (EC conversion/TON) and basicity in terms of per g catalyst, a linear correlation with the density of basic sites, was found (Fig. 3.11)



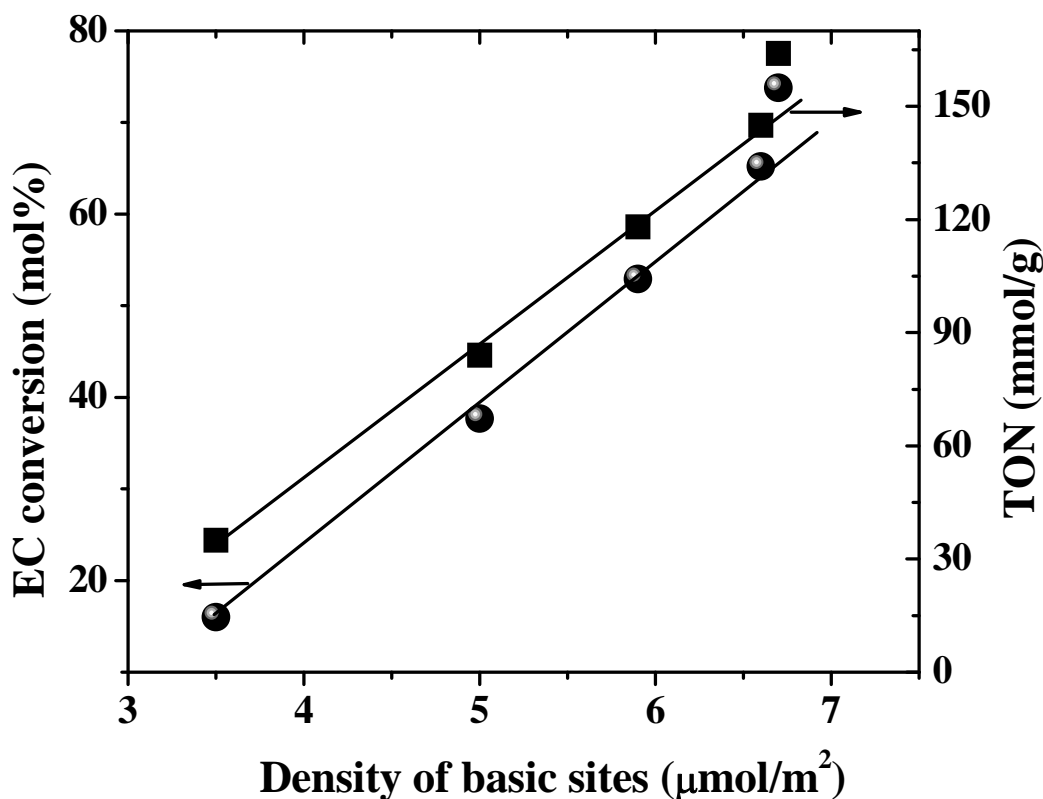


**Fig. 3.11.** Correlation between catalytic activity and density of basic sites on HT La-C catalysts. Reaction conditions: EC = 0.88 g (10 mmol), methanol = 3.2 g (100 mmol), catalyst = 5 wt% of EC, reaction temperature = 60 °C, reaction time = 4 h. Turnover number (TON) = mmol of DMC formed per gram of catalyst.

### 3.3.3.2. Effect of reaction parameters

EC conversion increased with increasing reaction time reaching a maximum of 90.6 mol% with DMC selectivity of 100 mol% at 100 °C in 4 h (Fig. 3.12. (a)). It increased also with reaction temperature without affecting the DMC selectivity (Fig. 3.12.(b)). EC conversion increased linearly with increasing amount of the catalyst indicating the role of basic sites in the reaction. This increase was marginal beyond 2 wt% of the catalyst (Fig. 3.12.(c)). It showed a non-linear conversion increase with the amount of catalyst. Two linear regimes could be seen in the figure (below and above 2 wt%). As the conversion was high above 2 wt% of catalyst, the products might inhibit transesterification.

### 3.3.3.3. Catalyst recyclability

HT-10 La-C was reusable in at least five recycling experiments with negligible loss in catalytic activity (EC conversion) and DMC selectivity (100 mol%; Fig. 3.13). At the end of

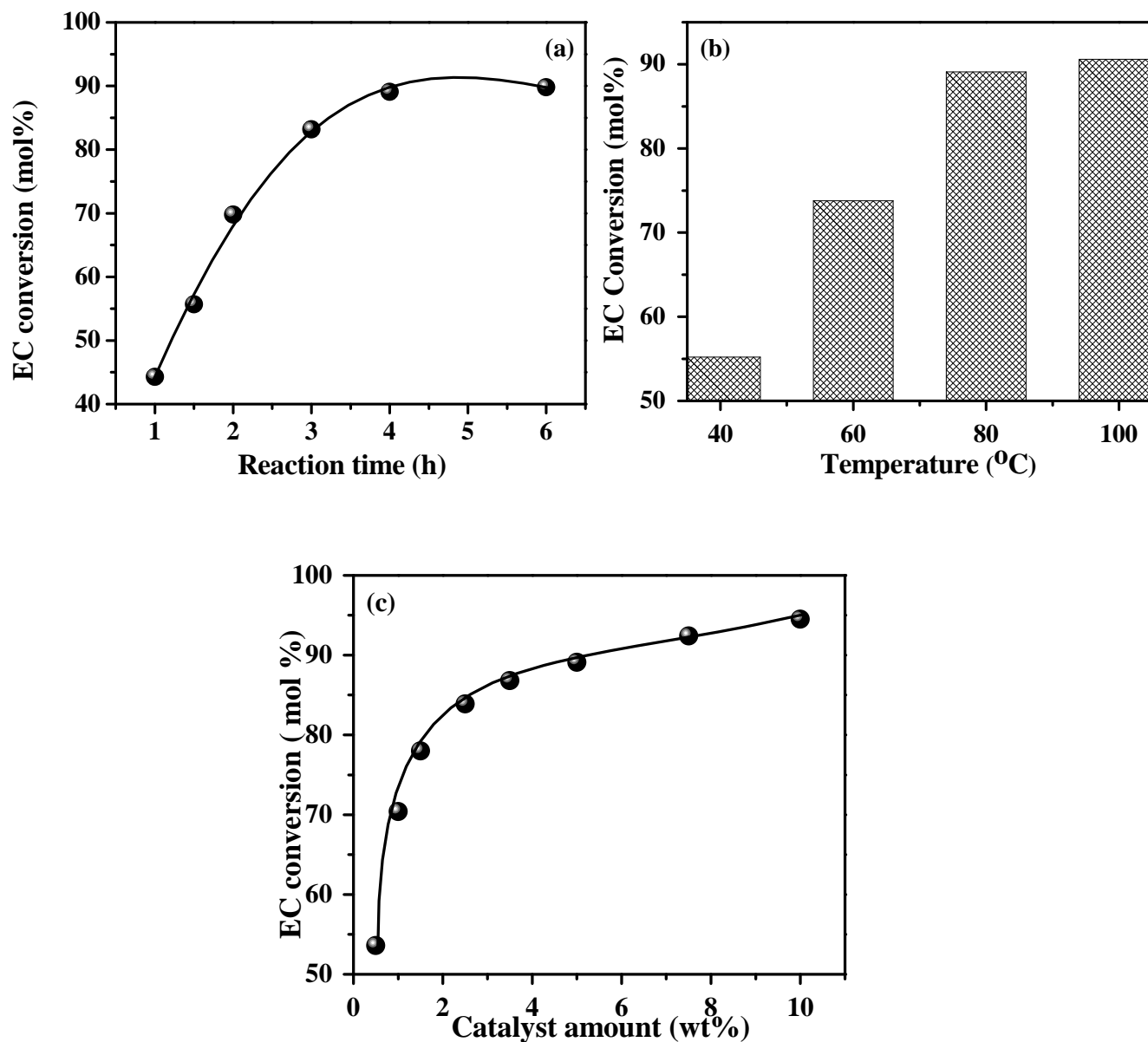


**Fig. 3.12.** Catalytic performance of HT-10 La-C in transesterification of ethylene carbonate (EC) with methanol. (a) Effect of reaction time. Reaction conditions: EC = 10 mmol, methanol = 100 mmol, catalyst = 5 wt% of EC and reaction temperature = 80 °C. (b) Effect reaction temperature. Reaction conditions: same as those for (a) except reaction time = 4 h and reaction temperature = 40 °C, 60 °C, 80 °C or 100 °C. (c) Effect of catalyst amount. Reaction conditions: same as those for (a) except reaction temperature = 80 °C and reaction time = 4 h.

each run, the catalyst was separated by filtration, washed with methanol, dried at 200 °C for 4 h and then, used in the successive recycle run. XRD and FTIR showed that the structure of the catalyst was intact even after its several reuses (Fig. 3.14). Chemical composition (ICP-OES) of fresh and spent (1<sup>st</sup> and 4<sup>th</sup> cycle) catalysts was almost the same. All these factors point out the absence of active sites leaching.

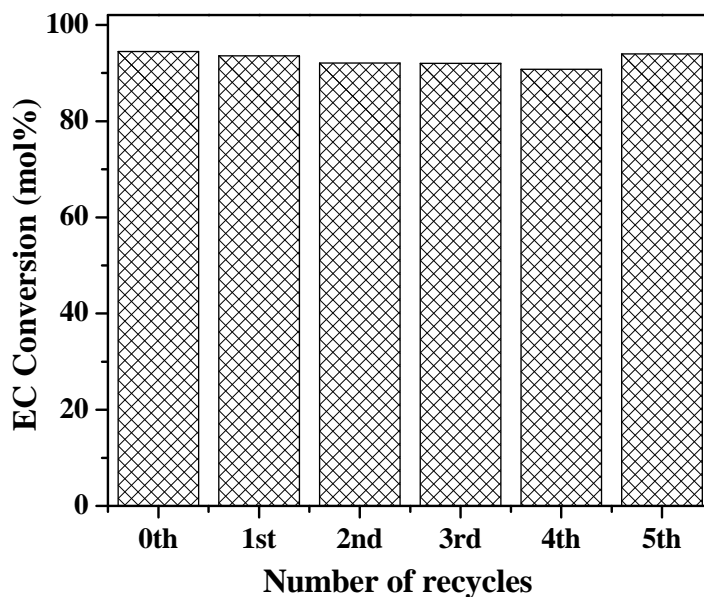


**Fig. 3.13.** Catalyst recyclability test. Reaction conditions: EC = 10 mmol, methanol = 100 mmol, catalyst (HT-10 La-C) = 10 wt% of EC, reaction temperature = 80 °C and reaction time = 4 h.

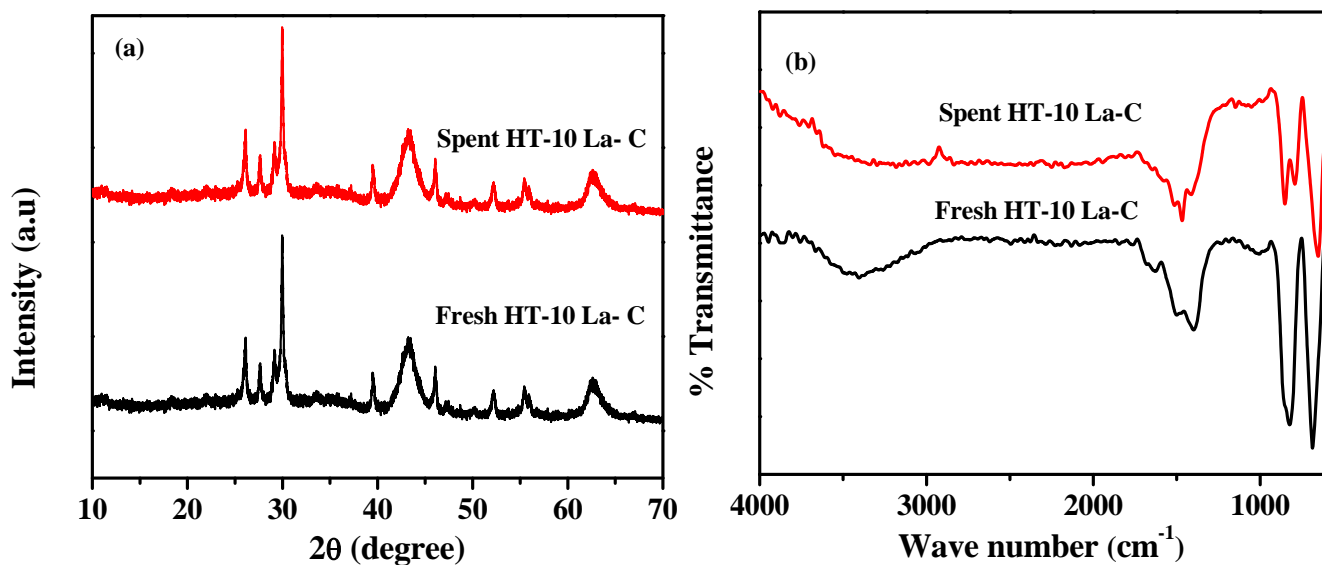


**Fig. 3.14.** (a) XRD and (b) FTIR spectra of fresh and spent HT-10 La-C catalyst.

**Table 3.6.** Comparison of activity of different catalysts for transesterification of ethylene carbonate (EC) with methanol

Entry no.	Catalyst	Reaction temperature (°C)	Reaction time (h)	EC conversion (%)	DMC yield (%)	TON (mmol/g <sub>cat</sub> )	ref.
1	Na <sub>2</sub> WO <sub>4</sub> .2H <sub>2</sub> O	150	5	82	71	36	[20]
2	CaO–ZnO (Ca/Ca+Zn =0.4)	27	4	-	83	166	[21]
3	ZnO	65	1	19	17	73	[42]
4	Y <sub>2</sub> O <sub>3</sub>	65	1	11	10	43	[42]
5	ZnO- Y <sub>2</sub> O <sub>3</sub> (3:1)	65	1	55	54	231	[42]
6	ZnO- Y <sub>2</sub> O <sub>3</sub> (3:1)	20	1	34	33	141	[42]
7	Na-Dawsonite-C	70	6	-	60	67	[43]
8	Mg-Al HT-C (Mg/Al=3)	70	6	-	35	39	[43]
9	MgO	70	6	-	20	22	[43]
10	MgO	150	4	82	60	30	[19]
11	Amberlyst A-21	120	14	88	85	-	[45]
12	Smectite-Mg-Na	150	4	70	78	43	[46]
13	Smectite-Mg-Na-K	150	4	75	88	49	[46]
14	polyvinylpyrrolidone	140	4	56	50	28	[17]
15	poly-4-vinyl pyridine	140	4	96	82	47	[17]
16	DABCO	70	6	95	84	449	[47]
17	[C <sub>4</sub> DABCO]OH	70	6	90	81	433	[47]
18	NaOH	70	6	91	73	405	[47]
19	K-TS-I	65	3	81	64	223	[44]
20	BuImBr-CS	160	6	81	74	93	[48]
21	BMImBr-AS	160	6	79	73	91	[49]
22	EMImCl	140	6	76	76	-	[40]
23	HT- 10 La-C	80	4	94.5	94	105	This work

Catalytic activity of HT-10 La-C was found superior to most of the known solid catalysts (Table 3.6). DMC in higher yields was synthesized at lower reaction temperature and in short duration. DABCO, [C<sub>4</sub>DABCO]OH and NaOH exhibited TON values higher (405 - 449) than of HT-10 La-C. But then, it should be noted that those catalysts are homogeneous and catalyst recycle poses an issue. Moreover, DMC selectivity over those catalysts was lower than that with HT-10 La-C. Among the reported solid catalysts, ZnO-Y<sub>2</sub>O<sub>3</sub> (entry no. 6), CaO-ZnO (entry no. 2) and K-TS-1 (entry no. 19) showed higher TON (166- 231) than HT-10 La-C (entry no. 23), but then, DMC selectivity was lower over those catalysts. A caution is, however, need at this point. The reaction conditions for different catalysts reported in Table 3.6 are different. As the temperature and loadings have bearing on selectivity and yield of DMC (*vide infra*), it is important to compare catalytic activity of different catalysts at similar reaction conditions.

#### 3.4. EC/PC transesterification with HT-X La-C - kinetic parameters and perspectives

Comparative catalytic performance of HT-8 La-C and HT-10 La-C in transesterification of EC and PC with methanol at similar conditions is reported in Table 3.7. At 100 °C, EC conversions of 80.2 and 90.6 mol% were obtained in 6 h over HT-8 La-C and HT-10 La-C, respectively. Under similar conditions PC conversions were 28.2 and 35.3 mol%, respectively. While the selectivity for DMC was 100 mol% with EC as reactant, it was lower when PC was used in place of EC. The other product included partially transesterified PC. At 150 °C and above, DMC decomposed through methylation of methanol and propylene glycol forming corresponding ethers. This led to reduction in the selectivity for DMC. This was also confirmed in separate experiments carried out at 170 °C (for 6 h) taking methanol + DMC + catalyst and propylene glycol + DMC + catalyst. Dimethyl ether formation in the former experiment was 6%. In the second experiment, dimethyl ether and methylpropylene glycol ethers formed along with large amount of propylene carbonate and methanol. Methanol alone too got converted into dimethyl ether over this catalyst. But this conversion was 2.9% at similar experimental conditions. By and large, the present study reveals that DMC synthesis through transesterification of EC is more advantageous than with PC. Lower conversion of PC to DMC than EC to DMC is attributed mainly to steric factors because of the chemical structures of the different alkylene carbonates [32].

Kinetic studies were carried out at four different temperature for EC (40, 60, 80 and 100 °C) and PC (110, 130, 150 and 170 °C) transesterifications. As the molar ratio of EC(PC)

**Table 3.7.** Catalytic activity as a function of reaction time for transesterification of cyclic carbonate with methanol over HT-8 La-C and HT-10 La-C.

Reaction time (h)	HT-8 La-C						HT-10 La-C					
	EC-methanol system			PC-methanol system			EC-methanol system			PC-methanol system		
	(mol%)			(mol%)			(mol%)			(mol%)		
	EC	DMC	DMC	PC	DMC	DMC	EC	DMC	DMC	PC	DMC	DMC
conv.	sel.	yield	conv.	sel.	yield	conv.	sel.	yield	conv.	sel.	yield	
0.5	33.8	100	33.8	4.6	62.3	2.8	29.1	100	29.1	5.1	64.0	3.2
1	47.7	100	47.7	7.8	68.8	5.3	50.1	100	50.1	7.8	70.1	5.4
1.5	57.5	100	57.5	11.8	77.7	9.1	62.3	100	62.3	14.2	76.7	10.8
2	68.5	100	68.5	13.9	81.2	11.2	76.4	100	76.4	21.6	80.2	17.3
3	79.0	100	79.0	16.6	84.2	13.9	85.4	100	85.4	26.4	84.6	22.3
4	79.8	100	79.8	21.4	87.1	18.6	90.6	100	90.6	31.8	86.9	27.6
6	80.2	100	80.2	28.2	89.0	25.1	90.6	100	90.6	35.3	89.1	31.4

Reaction conditions: cyclic carbonate = 10 mmol [0.88 g for ethylene carbonate (EC) and 1.02 g for propylene carbonate (PC)], methanol = 3.2 g (100 mmol), catalyst = HT-8 La-C or HT-10 La-C (5 wt% of EC or PC), reaction temperature = 100 °C.

to methanol was 1 : 10, pseudo-first order kinetics was considered. From the initial rates and Arrhenius plots, activation energy ( $E_a$ ) was calculated (Table 3.8).  $E_a$  values for EC-methanol and PC-methanol reactions with HT-10 La-C catalyst were 10.9 and 22.6 kJ/mol, respectively. The same with HT-8 La-C were 15.8 and 48.2 kJ/mol, respectively. Filippis et al [40] reported an  $E_a$  value of 29 kJ/mol for EC-methanol transesterification over  $\text{Na}_2\text{CO}_3$  and  $\text{Na}_3\text{PO}_4$ . Ju et al [41] found a value of 50.1 kJ/mol for the reaction catalyzed by ionic liquids. Lower  $E_a$  values observed for the catalyst of this study confirms its higher efficiency than the known catalyst systems. Equilibrium constant ( $K_{eq}$ ) for EC + methanol system is nearly two orders of magnitude higher than for PC + methanol (Table 3.8) indicating more facile nature of the former than the latter reaction.

**Table 3.8.** Kinetic parameters for transesterification of EC/PC with methanol over HT-8 La-C and HT-10 La-C.

Reactants	Equilibrium constant ( $K_c$ ) <sup>a</sup>	Reaction temperature (°C)	HT-8 La-C		HT-10 La-C	
			Rate constant (k)	$E_a$ (kJ/mol)	Rate constant (k)	$E_a$ (kJ/mol)
EC + CH <sub>3</sub> OH	1.15x10 <sup>2</sup>	40	8.10x10 <sup>-5</sup>	15.8	1.11x10 <sup>-4</sup>	10.9
		60	1.21x10 <sup>-4</sup>		1.42x10 <sup>-4</sup>	
		80	1.61x10 <sup>-4</sup>		1.78x10 <sup>-4</sup>	
		100	1.74x10 <sup>-4</sup>		2.01x10 <sup>-4</sup>	
		110	4.19x10 <sup>-5</sup>		7.23x10 <sup>-5</sup>	
PC + CH <sub>3</sub> OH	4.38	130	9.18x10 <sup>-5</sup>	48.2	1.08x10 <sup>-4</sup>	22.6
		150	1.78x10 <sup>-4</sup>		1.43x10 <sup>-4</sup>	
		170	2.07x10 <sup>-4</sup>		2.18x10 <sup>-4</sup>	

<sup>a</sup> $K_c$  value for EC + CH<sub>3</sub>OH at 100 °C and for PC + CH<sub>3</sub>OH at 170 °C.

### 3.5. Conclusions

A novel catalytic application of ternary oxides derived from rare-earth modified hydrotalcites for transesterification of propylene carbonate and ethylene carbonate with methanol

producing DMC was investigated. These catalysts were more efficient than the hitherto reported solid catalysts for this reaction. DMC was synthesized with high yield, selectivity and TON for both EC and PC with methanol. Basicity of the catalyst played an important role on the transesterification activity. A linear correlation between the density of basic sites and transesterification activity was found. The La modified HT catalyst is heterogeneous and could be recovered and reused even after fifth recycle with little loss of activity. DMC synthesis from EC-methanol than from PC-methanol reaction is more favorable.

### **3.6. References**

- [1] Y. Ono, *Appl. Catal. A: Gen.* 155 (1997) 133-166.
- [2] P. Tundo, *Pure Appl. Chem.* 73 (2001) 1117-1124.
- [3] S. Fujita, B.M. Bhanage, Y. Ikushima, M. Arai, *Green Chem.* 3 (2001) 87-91.
- [4] M.A. Pacheco, C.L. Marshall, *Energy Fuels* 11 (1997) 2-29.
- [5] Y. Ono, *Catal. Today* 35 (1997) 15-25.
- [6] Y. Sato, T. Yamamoto, Y. Souma, *Catal. Lett.* 65 (2000) 123-126.
- [7] T. Wei, M. Wang, W. Wei, Y. Sun, B. Zhong, *Green Chem.* 5 (2003) 343-346.
- [8] A.G. Shaikh, S. Sivaram, *Chem. Rev.* 96 (1996) 951-976.
- [9] H. Cui, T. Wang, F. Wang, C. Gu, P. Wang, Z. Dai, *Ind. Eng. Chem. Res.* 43 (2004) 7732-7739.
- [10] W. Li Dai, S. Luo, S.F. Yin, C. Tong Au, *C. Appl. Catal. A: Gen.* 366 (2009) 2-12.
- [11] J.F. Knifton, R.G. Duranleau, *J. Mol. Catal.* 67 (1991) 389-399.
- [12] Y. Watanabe, T. Tatsumi, *Micro. Meso. Mater.* 22 (1998) 399-407.
- [13] H. Wang, M. Wang, W. Zhang, N. Zhao, W. Wei, Y. Sun, *Catal. Today* 115 (2006) 107-110.
- [14] T. Wei, M. Wang, W. Wei, Y. Sun, B. Zhong, *Fuel Process. Technol.* 83 (2003) 175-182.
- [15] R. Srivastava, D. Srinivas, P. Ratnasamy, *J. Catal.* 241 (2006) 34-44.
- [16] S.G. Liu, J. Ma, L.X. Guan, J.P. Li, W. Wei, Y.H. Sun, *Micro. Meso. Mater.* 117 (2009) 466-471.
- [17] S.R. Jagtap, M.D. Bhor, B.M. Bhanage, *Catal. Commun.* 9 (2008) 1928-1931.
- [18] R. Juarez, A. Corma, H. Garcia, *Green Chem.* 11 (2009) 949-951.
- [19] B.M. Bhanage, S. Fujita, Y. Ikushima, M. Arai, *Appl. Catal. A: Gen.* 219 (2001) 259-266.



- [20] M. Sankar, C. Madhavan Nair, K.V.G.K. Murty, P. Manikandan, *Appl. Catal. A: Gen.* 312 (2006) 108-114.
- [21] M. Sankar, S. Satav, P. Manikandan, *ChemSusChem* 3 (2010) 575-578.
- [22] A. Corma, R.M.M. Aranda, *Appl. Catal. A: Gen.* 105 (1993) 271-279.
- [23] M.J. Climent, A. Corma, S. Iborra, J. Primo, *J. Catal.* 151 (1995) 60-66.
- [24] V.R.L. Constantino, T.J. Pinnavaia, *Catal. Lett.* 23 (1994) 361-367.
- [25] S. Miyata, *Clays Clay Miner.* 31(1983) 305-311.
- [26] D.G. Evans, X. Duan, *Chem. Commun.* 5 (2006) 485-496.
- [27] G. Centi, S. Perathoner, *Micro. Meso. Mater.* 107 (2008) 3-15.
- [28] C. Murugan, H.C. Bajaj, *Ind. J. Chem.* 49A (2010) 1182-1188.
- [29] G. Wu, X. Wang, W. Wei, Y. Sun, *Appl. Catal. A: Gen.* 377 (2010) 107-113.
- [30] J.I. DiCosimo, V.K. Díez, M. Xu, E. Iglesia, C.R. Apestegúa, *J. Catal.* 178 (1998) 499-510.
- [31] E. Angelescu, O.D. Pavel, M. Che, R. Birjega, G. Costentin, *Catal. Commun.* 5 (2004) 647-651.
- [32] D.P. Debecker, E.M. Gaigneaux, G. Busca, *Chem. Eur. J.* 15 (2009) 3920-3935.
- [33] F. Cavani, F. Trifirb, A. Vaccari, *Catal. Today* 11 (1991) 173-301.
- [34] T. Hibino, Y. Yamashita, K. Kosuge, A. Tsunashima, *Clays Clay Miner.* 43 (1995) 427-432.
- [35] M.A. Aramend, Y. Aviles, V. Borau, J.M. Luque, J.M. Marinas, J.R. Ruiz, F.J. Urbano, *J. Mater. Chem.* 9 (1999) 1603-1607.
- [36] J.C.A.A. Roelofs, J.A. van Bokhoven, A.J. van Dillen, J.W. Geus, K.P. de Jong, *Chem. Eur. J.* 8 (2002) 5571-5579.
- [37] R. Birjega, O.D. Pavel, G. Costentin, M. Che, E. Angelescu, *Appl. Catal. A: Gen.* 288 (2005) 185-193.
- [38] T.J. Park, S.S. Choi, Y. Kim, *Bull. Korean Chem. Soc.* 30 (2009) 149-152.
- [39] M.D. Romero, J.A. Calles, M.A. Ocana, J.M. Gomez, *Micro. Meso. Mater.* 111 (2008) 243-253.
- [40] H.Y. Ju, M.D. Manju, D.-W. Park, Y. Choe, S.-W. Park, *React. Kinet. Catal. Lett.* 90 (2007) 3-9.
- [41] P.D. Filippis, M. Scarsella, C. Borgianni, F. Pochetti, *Energy Fuels.* 20 (2006) 17-20.

- [42] L. Wang, Y. Wang, S. Liu, L. Lu, X. Ma, Y. Deng, *Catal. Comm.* 16 (2011) 45-49.
- [43] G. Stoica, S. Abello, J. Perez-Ramerez, *ChemSusChem* 2 (2009) 301-304.
- [44] T. Tatsumi, Y. Watanabe, K.A. Koyano, *Chem. Commun.* (1996) 2281-2282.
- [45] S. Dhuri, V.V. Mahajani, *J. Chem. Technol. Biotechnol.* 81 (2006) 62-69.
- [46] B.M. Bhanage, S. Fujita, Y. He, Y. Ikushima, M. Shirai, K. Torri, M. Arai, *Catal. Lett.* 83 (2002) 137-141.
- [47] Z.Z. Yang, L.N. He, X.Y. Dou, S. Chanfreau, *Tetrahedron Lett.* 51 (2010) 2931-2934.
- [48] K.H. Kim, D.W. Kim, C.W. Kim, J.C. Koh, D.-W. Park, *Kor. J. Chem. Eng.* 27 (2010) 1441-1445.
- [49] D.W. Kim, C.W. Kim, J.C. Koh, D.-W. Park, *J. Ind. Eng. Chem.* 16 (2010) 474-478.

**Chapter- 4**

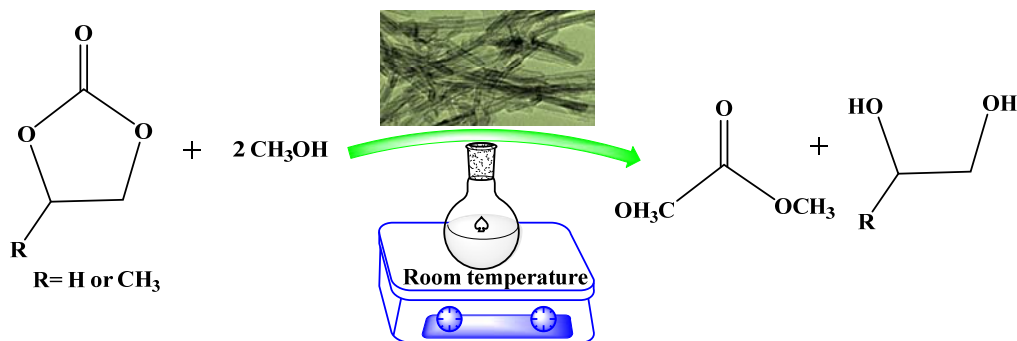
**Transesterification of Ethylene and Propylene  
Carbonate over NaTNT catalyst**

#### 4.1. Introduction

Development of a sustainable and eco-friendly alternative approach to the conventional hazardous routes (such as phosgenation and oxidative carbonylation of methanol) for making dimethyl carbonate (DMC) is highly essential. With such an outlook, the conversion of carbon dioxide (CO<sub>2</sub>) into DMC is most attractive. CO<sub>2</sub> can be converted into DMC either by a direct reaction with methanol or by an indirect two-step process [1-5]. Due to low yields, the direct synthesis of DMC from CO<sub>2</sub> and methanol is not promising as of now in the large scale production. Honda et al. [6] reported a high yielding DMC process using stoichiometric quantity of 2-cyanopyridine as a water trapping agent. But it is not a suitable reagent that meets the environmental and economic concerns. In the indirect conversion method of CO<sub>2</sub> via a two-step process, CO<sub>2</sub> is initially reacted with an epoxide preferably ethylene oxide to produce ethylene carbonate (EC) which in the second step is reacted with an excess of methanol resulting DMC and ethylene glycol (EG). This is a potential route for the commercial scale production of DMC [7]. Solid bases, especially basic oxides are more efficient than acid catalysts [8-12]. Watanabe and Tatsumi [13] reported EC conversion of 70% and DMC selectivity of 58% over Mg-Al hydrotalcites (HTs). Amine-functionalized MCM-41 provided DMC yield of 44 mol% in a continuous transesterification of EC with methanol [14]. According to Zhao et al. [15], quaternary ammonium salt functionalized chitosan gives DMC yield of 54% at a propylene carbonate (PC) conversion of 71%. Binary zinc-yttrium oxides were also tried for this reaction and a maximum EC conversion of 55% and DMC yield of 54% was obtained [8]. Polyvinyl pyridine (PVP) was found to be a highly efficient homogeneous recyclable catalyst for transesterification of EC with methanol [16]. PVP acted as a base catalyst through lone pair of electrons present on the nitrogen atom of the pyridine ring. Distillation or phase separation was adopted to isolate the catalyst from the reaction mixture. Tatsumi et al. [17] reported a study using K-TS-1 for this reaction. They obtained a DMC yield of 57%. Most of the hitherto known homogeneous or heterogeneous catalytic systems suffer from low catalytic activity, high reaction temperature and long reaction times. Among different solid base catalysts, CaO-ZnO (Ca/Ca+Zn = 0.4) was found to be the most efficient system for DMC synthesis (83 mol% DMC yield at 27 °C) through transesterification of EC. However, this catalyst has a limitation due to its disintegration into finer particles of Ca(OH)<sub>2</sub> which leach out during the reaction [12]. The known oxide-based catalysts used have low accessibility of active surface sites to the reactant

molecules. Development of active, solid base catalyst with high pore and surface accessibility is the key concern in DMC synthesis through the transesterification route.

Nano-structured solid base catalysts have received considerable attention [18]. Titanate nanotubes are attractive material due to their excellent physical and chemical properties. Kasuga et al. [19] proposed a new synthesis method for mesoporous sodium titanate nanotubes (NaTNT), in which titania is reacted with a concentrated NaOH solution under hydrothermal conditions (Scheme 4.1). NaTNT are promising catalysts and catalyst supports in heterogeneous catalytic reactions. In recent times, they were found to be highly efficient catalysts for several reactions which include biodiesel production [18,20-22]. This chapter discusses the catalytic application of sodium titanate nanotubes ( $\text{Na}_2\text{Ti}_3\text{O}_7$ ) in the synthesis of DMC through transesterification of cyclic carbonates (EC and PC) at ambient conditions.



**Scheme 4.1.** Benign route for DMC synthesis

## 4.2. Experimental

### 4.2.1. Catalyst Synthesis

NaTNT samples were prepared by mixing anatase titania ( $\text{TiO}_2$ ) with a highly concentrated NaOH solution followed by hydrothermal treatment (Chapter 2, section 2.2.2). It was activated at 130 °C for 4 h prior to use.

### 4.2.2. Characterization techniques

X-ray diffraction (XRD) patterns of the catalyst samples were recorded on a Philips X'pert Pro diffractometer using  $\text{Cu-K}_\alpha$  radiation and a proportional counter detector. The diffraction patterns were recorded in the  $2\theta$  range of 5-80° at a scan rate of 4°/min and step size of 0.02°. High-resolution transmission electron microscopic (HRTEM) images of the samples were collected on a FEI Technai F30 instrument equipped with a 300 kV field emission gun.

Scanning electron micrographs (SEM) and EDX data were collected on a Leica Stereoscan 440, LEO Microscopy instrument (Cambridge, UK). FTIR spectra of the samples as KBr pellets were recorded on a Shimadzu 8201 PC spectrophotometer in 400-4000  $\text{cm}^{-1}$  region. Specific surface area ( $S_{\text{BET}}$ ) of the samples was determined from nitrogen-adsorption measurements carried out at  $-196\text{ }^{\circ}\text{C}$  on a Quadrasorb SI automated surface area and pore size analyzer (Quanta Chrome Instrument). Before the adsorption study, the samples were evacuated at  $200\text{ }^{\circ}\text{C}$ .  $S_{\text{BET}}$  was determined from the linear portion of the adsorption isotherm ( $P/P_0 = 0.05\text{-}0.31$ ) using the BET equation. The pore size distribution was calculated employing Barrett-Joyner-Halenda (BJH) method. Basicity of the catalysts was determined by a temperature-programmed desorption technique using  $\text{CO}_2$  as a probe molecule (Micromeritics Auto Chem 2910 instrument). About 0.1 g of the catalyst was activated at  $250\text{ }^{\circ}\text{C}$  under He (30 ml/min). The sample was cooled to  $50\text{ }^{\circ}\text{C}$  and  $\text{CO}_2$  was adsorbed at a rate of 30 ml/min for 30 min. Then, the temperature was raised to  $100\text{ }^{\circ}\text{C}$  followed by purging with He gas to remove the physisorbed probe molecule. After the stabilization of base line, desorption of probe molecules was followed in the temperature range of  $100\text{ - }600\text{ }^{\circ}\text{C}$  (ramp rate =  $10\text{ }^{\circ}\text{C /min}$ ). The broad peak obtained was deconvoluted and the amounts of basic sites of different strength were determined.

#### **4.2.3. Reaction procedure**

EC/PC (10 mmol), methanol (100 mmol) and catalyst (5-40 wt% of EC) were taken in a glass round-bottom flask fitted with a magnetic stirrer or in a Teflon-lined stainless-steel autoclave placed in a rotating hydrothermal reactor (Hiro Co., Japan; rotation speed = 50 rpm). Reactions were conducted at  $23\text{-}100\text{ }^{\circ}\text{C}$  for 0-10 h. After the reaction, the autoclave was cooled to  $25\text{ }^{\circ}\text{C}$  and the catalyst was separated by centrifugation/filtration. The liquid product was analyzed and quantified by gas chromatography (GC, Varian 3800; CP-SIL 8CB column;  $60\text{ m} \times 0.32\text{ mm} \times 0.25\text{ }\mu\text{m}$ ). The identity of the product was further confirmed by  $^1\text{H}$  NMR spectroscopy (Bruker Avance 200 MHz). The influence of reaction parameters (reaction time, reaction temperature and catalyst amount) on the product yield was investigated.

### **4.3. Results and discussions**

#### **4.3.1. Catalyst characterization**

##### **4.3.1.1. Microscopic analysis**

Fig. 4.1 shows the SEM image of NaTNT catalyst. It reveals the presence of fibrous structures. Elemental analysis was done by EDX technique. The molar composition of Na, Ti,

and O (15.3, 24.4 and 60.4 mol%, respectively) revealed that NaTNT has a molecular formula of  $\text{Na}_2\text{Ti}_3\text{O}_7$ . The HRTEM images of NaTNT (Fig. 4.2) display tubular morphology. The nanotubes are of multiwalled nature with a outer diameter of 7 - 9 nm and an inner diameter of 3 - 5 nm.

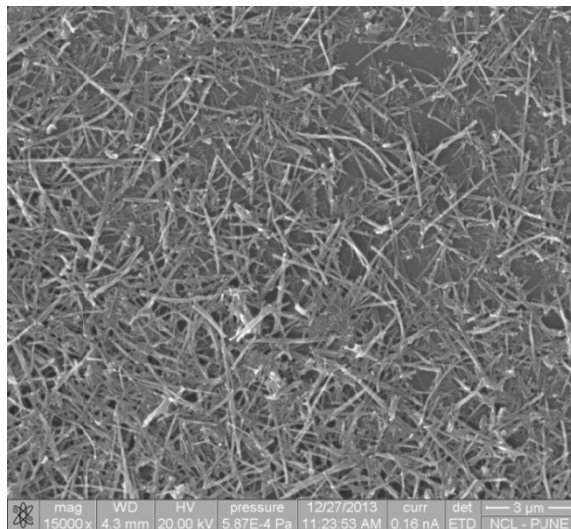


Fig. 4.1. SEM image of NaTNT.

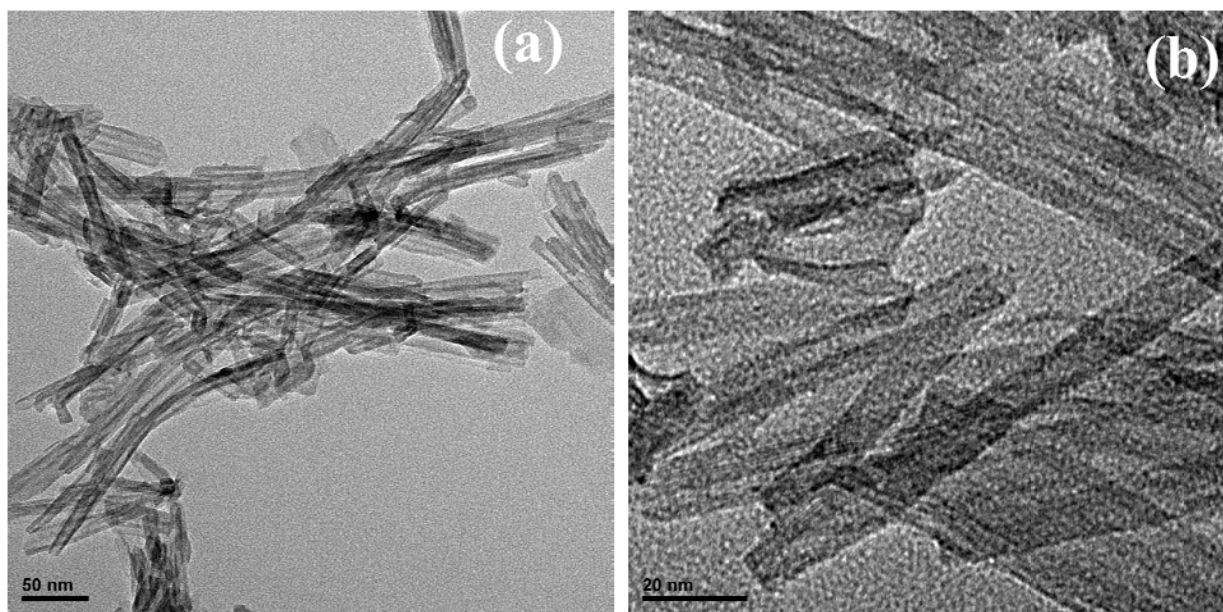
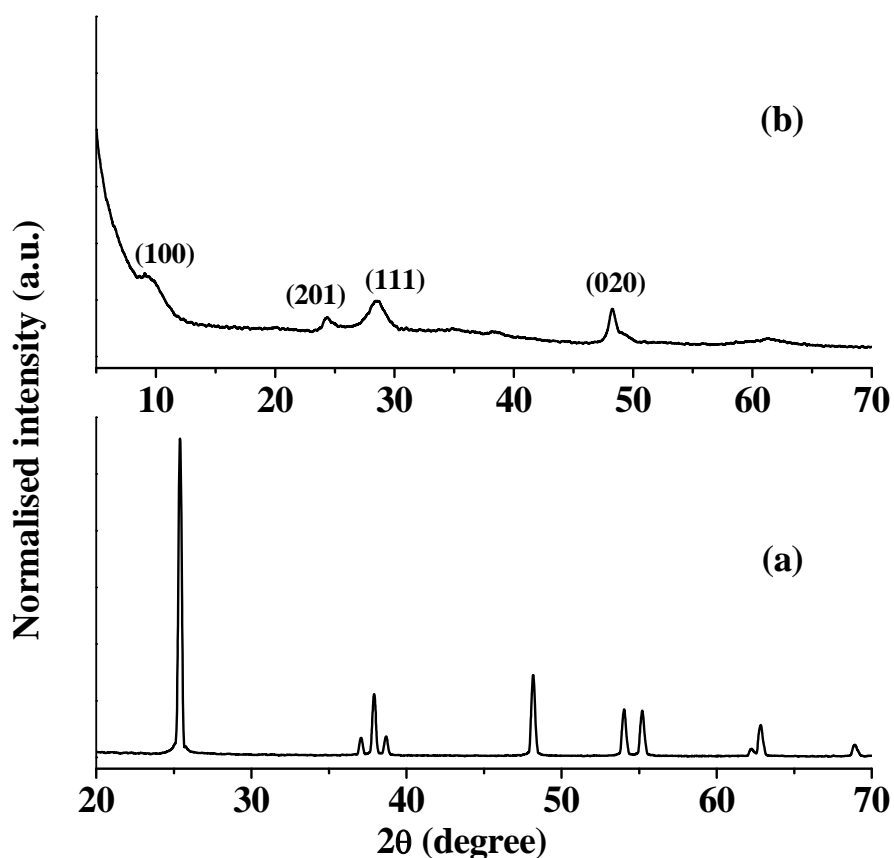


Fig. 4.2. HRTEM images of NaTNT.

#### 4.3.1.2. XRD

The XRD patterns of titania precursor and sodium titanate nanotubes are presented in Fig. 4.3. The diffraction pattern of titania (Fig. 4.3(a)) is consistent with the anatase phase (JCPDS

21-1272). NaTNT exhibited broad and diffused peaks at 9.6, 24.3, 28.4 and 48.1° (Fig. 4.3(b)). They are corresponded to (100), (201), (111) and (020) planes, respectively, of monoclinic NaTNT ( $\text{Na}_2\text{Ti}_3\text{O}_7$ ; JCPDS 31-1329). Absence of peaks corresponding to the precursor titania phase in the XRD pattern of NaTNT confirms the complete transformation of it into sodium trititanate nanotubes during the hydrothermal treatment. The characteristic band at 9.6° reveals an inter layer separation of 0.91 nm. The average crystallite size of NaTNT determined by Scherrer equation was found to be 8.5 nm. The broad and diffuse nature of peaks of NaTNT indicate their poor crystallinity [20].



**Fig. 4.3.** XRD patterns of (a) TiO<sub>2</sub> and (b) NaTNT.

#### 4.3.1.3. FTIR

FTIR spectra of anatase TiO<sub>2</sub> and NaTNT are depicted in Fig. 4.4. The sharp bands at 753 and 958  $\text{cm}^{-1}$  for anatase TiO<sub>2</sub> were attributed to Ti-O stretching vibrations. Shift in these band positions to 656 and 897  $\text{cm}^{-1}$  confirms the formation of NaTNT structure. Bands at 1634 and



3400  $\text{cm}^{-1}$  were corresponded to bending and stretching vibrations, respectively, of OH groups present in NaTNT [22].

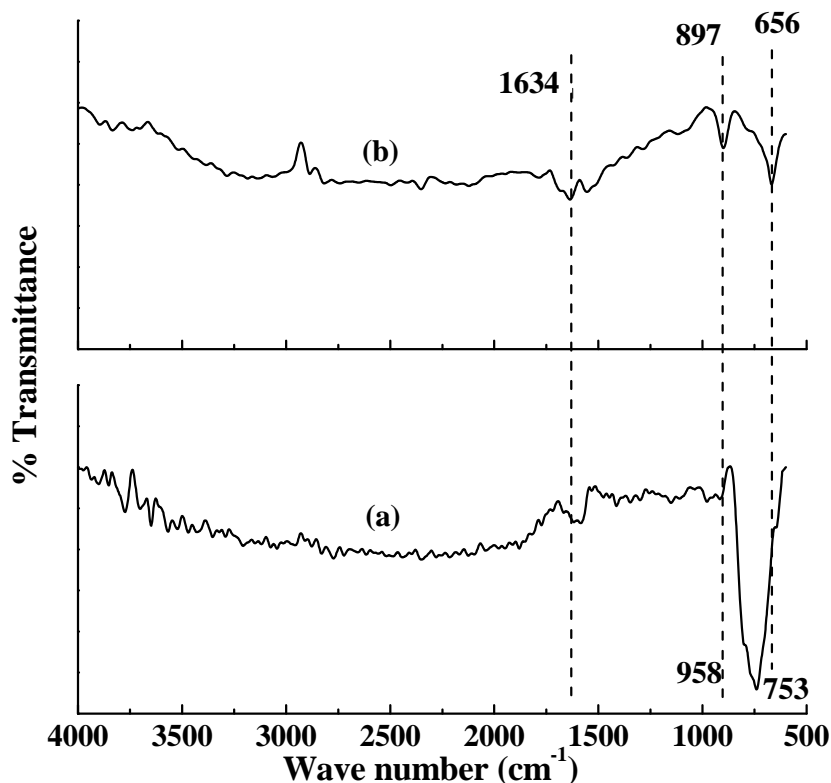


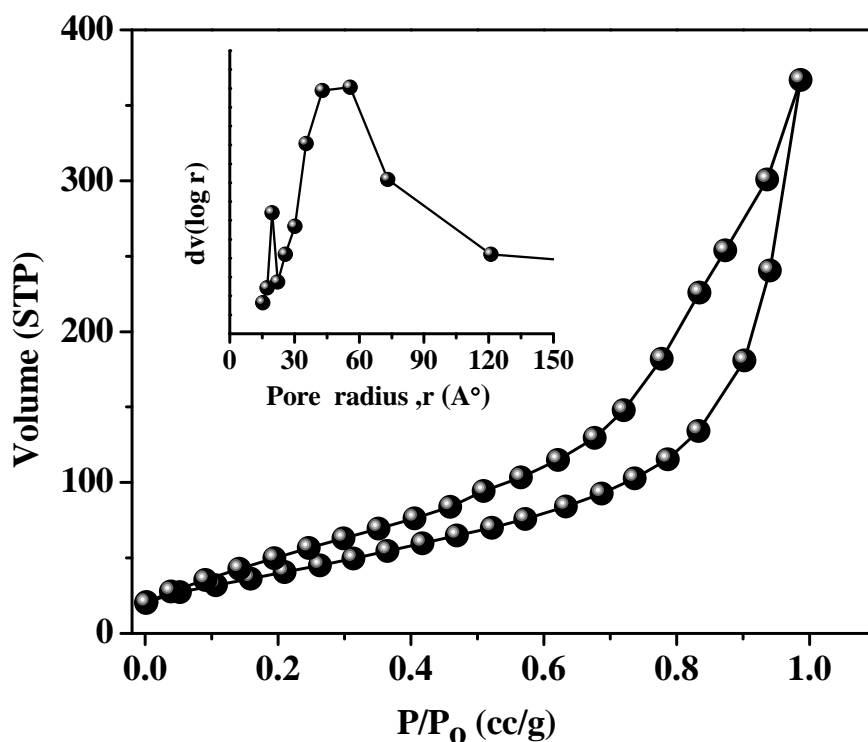
**Fig. 4.4.** FT-IR spectra of (a) anatase  $\text{TiO}_2$  and (b) NaTNT.

#### 4.3.1.4. $\text{N}_2$ -physisorption

Fig. 4.5 presents  $\text{N}_2$ -adsorption/desorption isotherms and the pore size distribution curve of NaTNT investigated in this study. The adsorption isotherm of NaTNT is of Type IV category. NaTNT has a specific surface area ( $S_{\text{BET}}$ ) of 143  $\text{m}^2/\text{g}$ , average pore radius of 7.9 nm and total pore volume of 0.567  $\text{cc}/\text{g}$  (Table 4.1). It has a bimodal pore distribution. The smaller pores are the internal pores of the tubes (pore diameter), while the larger ones are the interspace between the nanotube bundles. The broader distribution of the size of large pores indicates a random arrangement of nanotubes and nanotube bundles.

**Table 4.1.** Physicochemical properties of NaTNT.

$S_{\text{BET}}$ ( $\text{m}^2/\text{g}$ )	Average pore radius (nm)	Total pore volume ( $\text{cc}/\text{g}$ )	Basicity ( $\text{mmol}/\text{g}$ )			
			Weak (202 °C)	Medium (338 °C)	Strong (518 °C)	Total
143	7.9	0.567	0.106	0.081	0.043	0.231

**Fig. 4.5.**  $\text{N}_2$ -adsorption/desorption isotherms and pore size distribution (inset) of NaTNT.

#### 4.3.1.5. $\text{CO}_2$ -TPD

The  $\text{CO}_2$ -TPD profile of NaTNT is depicted in Fig. 4.6. The broad and diffused pattern indicates the presence of basic sites of different strength. The overall basicity of the sample was 0.231 mmol/g. Deconvolution of the desorption profile resulted into three well-defined peaks of desorption with maximum at 202, 338, and 518 °C corresponding to basic sites of weak,

moderate and strong strength, respectively. The density of weak sites was higher than those of medium and strong sites (Fig. 4.6 and Table 4.1).

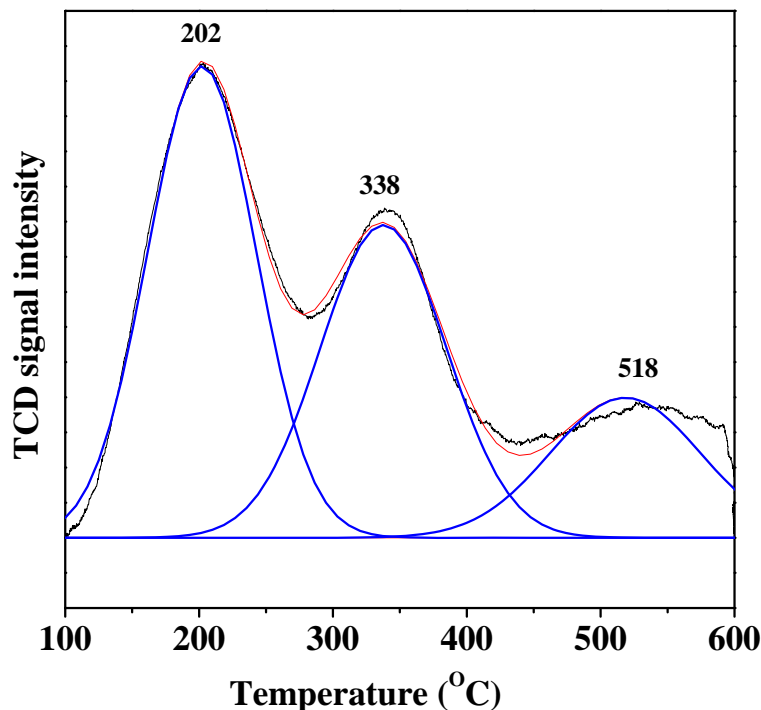


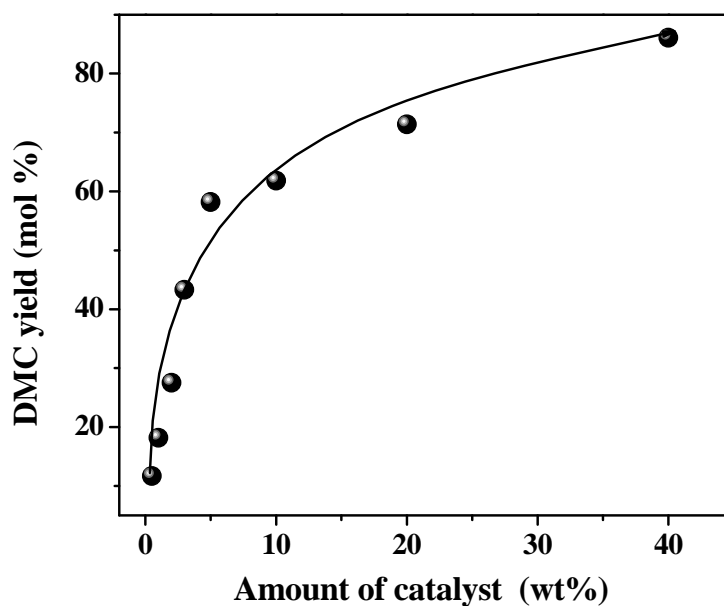
**Fig. 4.6.** CO<sub>2</sub>-TPD profile of NaTNT.

### 4.3.2. Catalytic activity

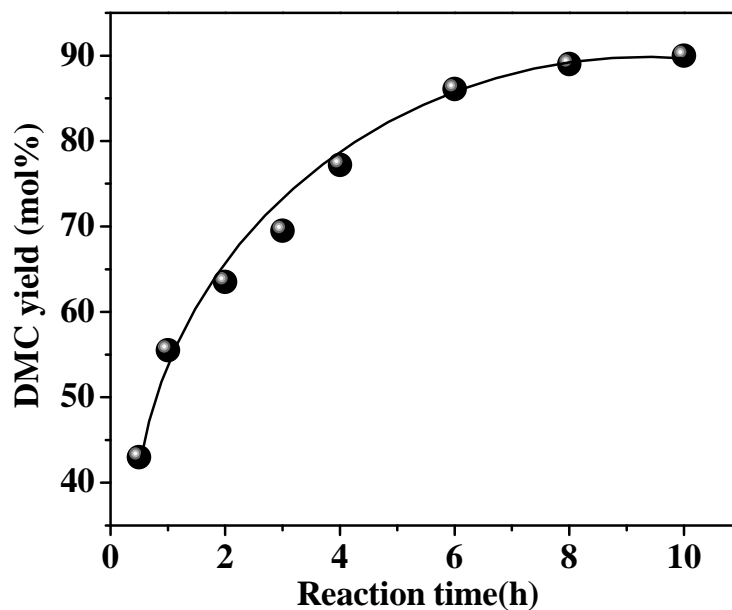
#### 4.3.2.1. Transesterification of ethylene carbonate

Controlled experiments revealed that the reaction of methanol with EC producing DMC doesn't take place in the absence of a catalyst. The anatase TiO<sub>2</sub> exhibited very low EC conversion (6%) with 100% DMC selectivity when 10 mmol of EC was reacted with 100 mmol of methanol in presence of 5 wt% of anatase TiO<sub>2</sub> at 25 °C for 6 h. Interestingly, NaTNT exhibited excellent catalytic activity at room temperature. It gave 58.2% EC conversion with 100% DMC selectivity at the above conditions. In order to determine the influence of the amount of catalyst on EC conversion, catalyst amount in the reaction medium was varied between 0.5 and 40 wt% (of EC). EC conversion increased sharply up to 5 wt% of the catalyst and beyond that amount, the increase was less indicating that the product might be inhibiting the transesterification. DMC yield as high as 86.1% was obtained with 40 wt% of catalyst in 6 h of reaction. DMC selectivity was 100% (Fig. 4.7). Fig. 4.8 shows the influence of reaction time on

the yield of DMC over NaTNT. An EC conversion of 43% (with DMC selectivity of 100%) was achieved in just 30 min and it touched 90% at 10 h of reaction.



**Fig. 4.7.** Influence of the amount of catalyst on transesterification of EC. Reaction conditions: EC = 10 mmol, MeOH = 100 mmol, reaction temperature = 25 °C, reaction time = 6 h.

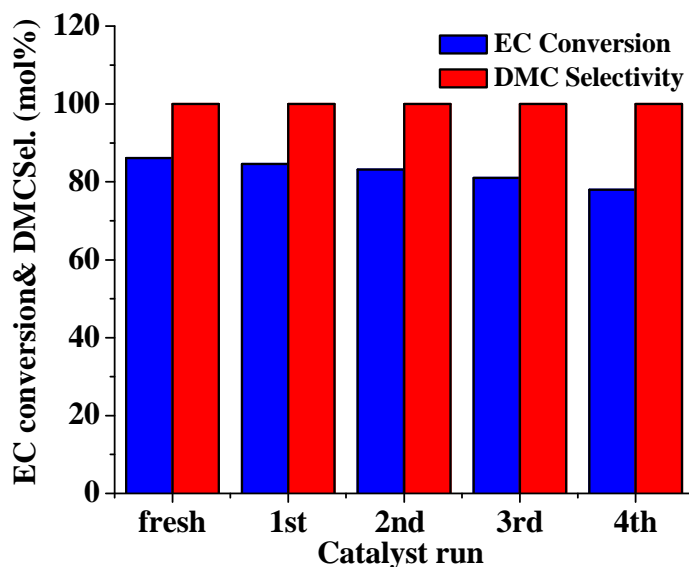


**Fig. 4.8.** Effect of reaction time on DMC yield. Reaction conditions: EC = 10 mmol, MeOH = 100 mmol, catalyst amount = 40 wt% of EC, reaction temperature = 25 °C.

**Table 4.2.** Kinetic parameters for transesterification of EC with methanol using NaTNT.

Reaction temperature (°C)	Rate constant (k)	E <sub>a</sub> (kJ.mol <sup>-1</sup> )
30	2.63 x 10 <sup>-4</sup>	9.67
40	2.96 x 10 <sup>-4</sup>	
60	3.74 x 10 <sup>-4</sup>	

The kinetic parameters for transesterification of EC using NaTNT catalyst were determined by carrying out the reaction at three different temperatures (30, 40, and 60 °C) wherein the molar ratio of EC : methanol was maintained at 1:10. The reaction follows a pseudo-first order kinetics. Initial rates were determined and the activation energy (E<sub>a</sub>) was determined from the Arrhenius plot (Table 4.2). It was found to be 9.67 kJ.mol<sup>-1</sup>. This value for La-modified Mg-Al hydrotalcites reported in Chapter 3 was 10.9 kJ.mol<sup>-1</sup>. In other words, NaTNT is catalytically more efficient than HT La-C catalysts discussed in Chapter 3.

**Fig. 4.9.** Catalyst recyclability test.

NaTNT catalyst was reusable in at least four recycling experiments. A small loss in EC conversion and 100% DMC selectivity was observed. The experiments were conducted at 25 °C for 6 h (Fig. 4.9). At the end of each run, the catalyst was separated by centrifugation, washed with methanol, dried at 80°C for 8 h. Prior to the successive run the dried catalyst was activated at 130 °C for 4 h. XRD and FTIR spectrum revealed that the structure of the catalyst was intact

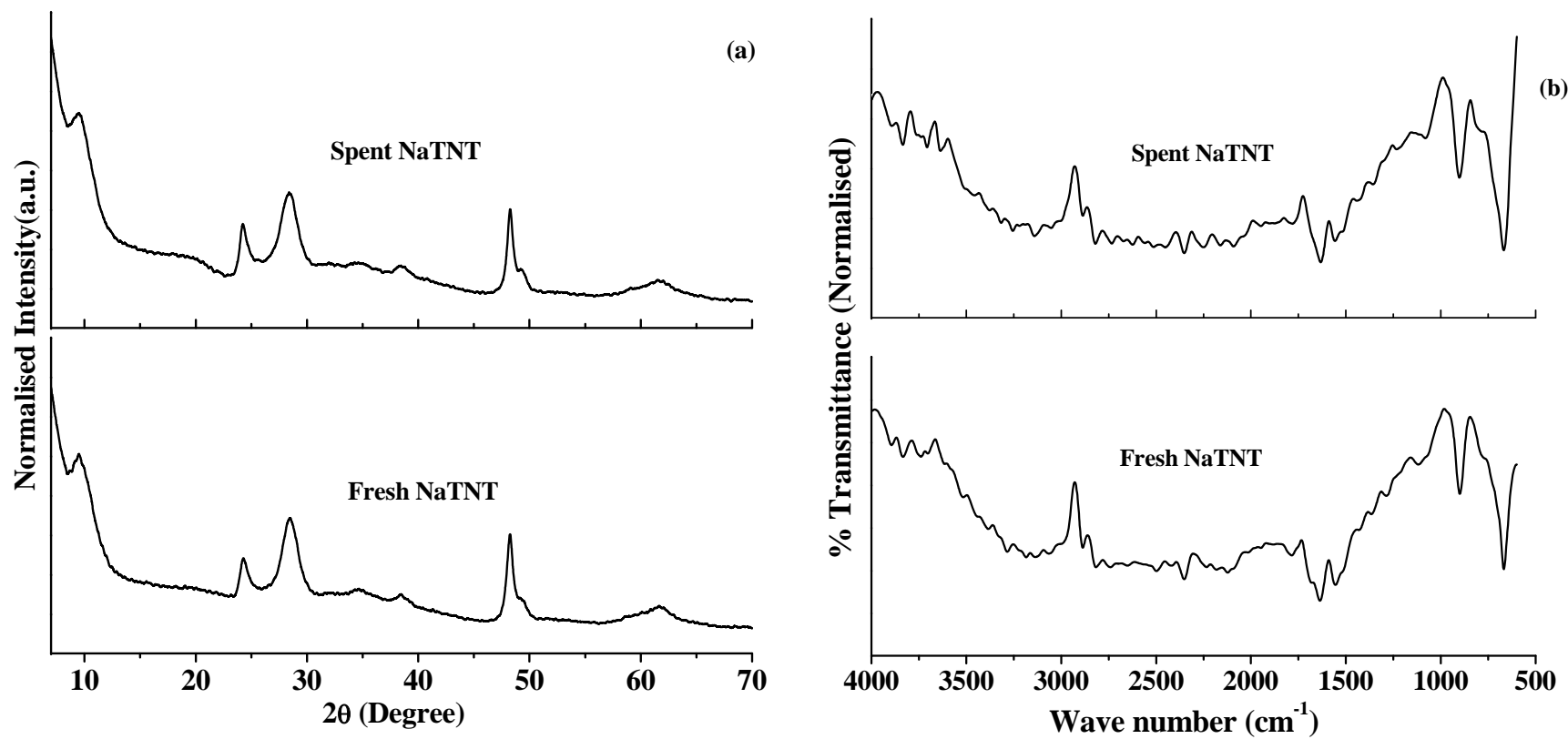


**Fig. 4.10.** (a) XRD and (b) FTIR of fresh and spent catalysts (after 4<sup>th</sup> recycle) of NaTNT.

even after four reuses (Fig. 4.10). Molar composition from EDX analysis of fresh and spent catalysts was almost the same.

#### 4.3.2.2. Transesterification of propylene carbonate

The application of NaTNT was extended to transesterify PC with methanol at 25 and 100 °C. Catalytic activity of NaTNT as function of reaction time is presented in Table 4.3. PC conversion increased with increasing reaction time and reached a value of 18.1 mol% in 10 h (with DMC selectivity of 93%) at 25 °C. Enhanced conversions were observed at higher temperature. At 100 °C, PC conversion of 72 mol% with 93.2 mol% of DMC selectivity was obtained. Higher accessibility of the active basic sites to reactant molecules is the possible cause for high catalytic activity of NaTNT compared to HTs and other solid base catalysts.

**Table 4.3.** Catalytic activity of NaTNT for transesterification of propylene carbonate with methanol.

Reaction time (h)	25 °C			100 °C		
	PC conv. (mol%)	DMC.sel. (mol%)	DMC yield (mol%)	PC conv. (mol%)	DMC sel. (mol%)	DMC yield (mol%)
0.5	5.9	84.0	4.9	16.4	88.6	14.5
1	6.9	84.1	5.8	21.2	91.0	19.3
2	8.0	84.2	6.7	36.3	95.9	34.8
4	10.6	84.4	8.9	50.1	98.7	49.4
5	10.9	88.6	9.7	53.6	93.7	50.2
6	12.9	89.8	11.6	64.3	95.5	61.4
8	14.6	89.0	13.0	69.9	93.4	65.2
10	18.1	93.0	16.8	72.0	93.2	66.2

Reaction conditions: PC = 10 mmol, methanol = 100 mmol, catalyst = 5 wt% of PC.

#### 4.4. Conclusions

A room temperature (25 °C) process for DMC synthesis by transesterification of cyclic carbonates (EC/PC) with methanol using sodium trititanate nanotubes catalyst is reported. The structural and textural properties of the catalyst were evaluated by XRD, EDX, FTIR, HRTEM, N<sub>2</sub>-physisorption and CO<sub>2</sub>-TPD techniques. Basicity of the catalyst with high surface accessibility played an important role on the catalytic activity. This catalyst was reusable with little loss of catalytic activity and selectivity.

#### 4.5. References

- [1] M. Pérez-Fortes, A. Bocin-Dumitriu, E. Tzimas, *Energy Procedia* 63 (2014) 7968-7975.
- [2] M. Honda, M. Tamura, Y. Nakagawa, K. Tomishige, *Catal. Sci. Technol.* 4 (2014) 2830-2845.
- [3] B. Schöffner, F. Schöffner, S.P. Vervikin, A. Börner, *Chem. Rev.* 110 (2010) 4554-4581.
- [4] D.B.- Tkatchenko, F. Bernard, F. Demoisson, L. Plasseraud, S.R. Sanapureddy, *ChemSusChem* 4 (2011) 1316-1322.
- [5] S. Huang, B. Yan, S. Wang, X. Ma, *Chem. Soc. Rev.* 44 (2015) 3079-3116.
- [6] M. Honda, M. Tamura, Y. Nakagawa, S. Sonehara, K. Suzuki, K. Fujimoto, K. Tomishige, *ChemSusChem* 6 (2013) 1341-1344.
- [7] L.F.S. Souza, P.R.R. Ferreira, J.L. de Medeiros, R.M.B. Alves, *ACS Sustainable Chem. Eng.* 2 (2014) 62-69.
- [8] L. Wang, Y. Wang, S. Lu, L. Lu, X. Ma, Y. Deng, *Catal. Commun.* 16 (2011) 45-49.
- [9] G. Stoica, S. Abello, J.- P. Ramirez, *ChemSusChem* 3 (2010) 575-578.
- [10] B.M. Bhanage, S. Fujita, Y. Ikushima, M. Arai, *Appl. Catal. A: Gen.* 219 (2001) 259-266.
- [11] R. Srivastava, D. Srinivas, P. Ratnasamy, *J. Catal.* 241 (2006) 34-44.
- [12] M. Sankar, S. Satav, P. Manikandan, *ChemSusChem* 3 (2010) 575-578.
- [13] Y. Watanabe, T. Tatsumi, *Micropor. Mesopor. Mater.* 22 (1998) 399-407.
- [14] X.J. Feng, X.B. Lu, R. He, *Appl. Catal. A, Gen.* 272 (2004) 347-352.
- [15] Y. Zhao, L.N. He, Y.Y. Zhuang, J.Q. Wang, *Chin. Chem. Lett.* 19 (2008) 286-290.
- [16] S. R. Jagtap, M. D. Bhor, B. M. Bhanage, *Catal. Comm.* 9 (2008) 1928-1931.
- [17] T. Tatsumi, Y. Watanabe, K.A. Koyano, *Chem. Commun.* (1996) 2281-2282.
- [18] P.H.- Hipólito, M.G.- Castillejos, E.M.- Klimova, N.J.- Flores, A.G.-Cortés, T.E. Klimova, *Catal. Today* 220-222 (2014) 4-11.
- [19] T. Kagusa, M. Hiramatsu, A. Hoson, T. Sekino, K. Niihara, *Adv. Mater.* 11 (1999) 1307-1311.
- [20] C.-Y. Hsu, T.-C. Chiu, M.-H. Shih, W.-J. Tsai, W.-Y. Chen, C.-H. Lin, *J. Phys. Chem. C.* 114 (2010) 4502-4510.
- [21] D. Nepak, D. Srinivas, *Catal. Commun.* 58 (2015) 149-153
- [22] Y.W.L. Lim, Y.Tamg, Y.H. Cheng, Z. Chen, *Nanoscale* 2 (2010) 2751-2757.



**Chapter - 5**

**Direct Synthesis of DMC from CO<sub>2</sub> and Methanol  
over ZrPP Catalysts**

## 5.1. Introduction

Conventional manufacturing processes for dimethyl carbonate (DMC) synthesis (phosgenation and oxidative carbonylation of methanol) are highly hazardous [1]. Among several eco-friendly routes, its direct synthesis from CO<sub>2</sub> and methanol is atom-efficient and attractive [1-4]. Further, CO<sub>2</sub> is a low-cost, renewable, non-toxic C1 building block associated with environmental benefits. Its utilization in the synthesis of fuels and value-added chemicals is an important challenge in the current century [5,6]. However, the direct synthesis of DMC is limited by thermodynamics ( $\Delta G = +26.21 \text{ kJ.mol}^{-1}$ ) [7]. Low yield is usually obtained. Catalyst deactivation in presence of by-product water is an issue with most of the known homogeneous and heterogeneous catalysts [8-13]. The development of a novel catalyst which overcomes the above limitation is desirable. From the previous reports it is evident that acid-base properties of a catalyst are an important factor to decide their catalytic activity. Hence, the development of a hydrophobic catalyst along with fine tuning of acid-base properties needs to be of special attention in catalyst designing for the direct synthesis of DMC from methanol and CO<sub>2</sub>. ZrO<sub>2</sub> based catalysts were identified as an active system for these reaction due to the amphoteric behavior of ZrO<sub>2</sub> [14,15]. Acidity of ZrO<sub>2</sub> enhanced by impregnation with phosphoric acid/tungstophosphoric acid which was in turn improved the catalytic activity [16,17].

In recent years layered metal organic hybrid materials showed great attention as heterogeneous catalysts. The preparation and characterization of a number of layered zirconium compounds containing inorganic phosphorus groups as well as organic phosphonate groups were reported in the literature. These hybrid materials have application in the field of ion exchange, adsorption, intercalation and heterogeneous catalysis. Zirconium phenyl phosphonate phosphites (ZrPP) are one of the interesting class having general formula,  $\text{Zr}(\text{C}_6\text{H}_5\text{PO}_3)_{2-x}(\text{HPO}_3)_x$ , where x varies according to phenyl phosphonic acid to phosphorous acid ratio, preparation method, synthesis conditions, etc. ZrPP belongs to the class of layered inorganic materials with novel proton conducting, hydrophobic and luminescent properties [18-22]. The application of calcined zirconium phenylphosphonate phosphite (ZrPP) as a highly efficient, reusable, solid catalyst for the direct synthesis of DMC in high selectivity and yield at moderate conditions is studied here for the first time. Controlled calcination results in the formation of zirconium pyrophosphate (ZrP<sub>2</sub>O<sub>7</sub>)-type interesting phosphor material. Surprisingly, the catalytic properties of calcined ZrPP have not been explored till date.

## 5.2. Experimental

### 5.2.1. Materials and catalyst preparation

Methanol (AR grade; Merck India),  $ZrOCl_2 \cdot 8H_2O$  and phosphorus acid (Loba Chemie), phenyl phosphonic acid (Spectrochem) and concentrated HF (48%) (Thomas Baker) were purchased and used as received. Carbon dioxide (purity = 98 vol%) was procured from De-luxe Industrial Gases, Pune. ZrPP-1-C, ZrPP-2-C and ZrPP-3-C were prepared by taking phosphorus acid : phenyl phosphonic acid in molar ratios of 1:1, 2:1 and 3:1, respectively (Chapter 2, sections 2.2.3.2 and 2.2.3.3). ZrPP-HF-C was prepared in presence of HF (Chapter 2, section 2.2.3.1).

### 5.2.2. Characterization techniques

X-ray powder diffraction (XRD) patterns of the samples were recorded on a Philips X'pert Pro diffractometer using  $Cu-K_{\alpha}$  radiation and a proportional counter detector. The diffraction patterns in the low-angle region ( $2\theta = 0.5- 10^{\circ}$ ) were recorded at a scan rate of  $0.2^{\circ}/min$  and those in the high-angle region ( $2\theta = 10- 90^{\circ}$ ) were recorded at a scan rate of  $4^{\circ}/min$ . The step size in the measurements was  $0.02^{\circ}$ . Fourier transform infrared (FTIR) spectra of the samples (as KBr pellets) were recorded on a Shimadzu 8201PC spectrophotometer in the region  $400 - 4000\text{ cm}^{-1}$ . Solid state  $^{31}P$  magic-angle spin nuclear magnetic resonance (MAS NMR) spectra were recorded at 121.49 MHz on a Bruker AV300 NMR spectrometer using 4 mm sample rotors. Samples were spun at a speed of 8 kHz. A single pulse sequence was applied and the NMR measurements were performed at  $25\text{ }^{\circ}C$ . Thermogravimetric analyses (TGA) of the samples was done under nitrogen (50 ml/min) on a Perkin Elmer Diamond TG-DTA instrument in the temperature range  $25 - 600\text{ }^{\circ}C$  and at a ramp rate of  $10\text{ }^{\circ}C/min$ . Specific surface area ( $S_{BET}$ ) of the samples was determined from nitrogen-adsorption measurements carried out at  $-196\text{ }^{\circ}C$  using a NOVA 1200 Quanta Chrome equipment. The percentage compositions of C and H in ZrPP-HF, ZrPP-1, ZrPP-2 and ZrPP-3 were determined using a Carlo-Erba 1106 elemental analyzer. Acidity of the calcined samples was quantified by temperature-programmed desorption of ammonia ( $NH_3$ -TPD) technique (Micromeritics AutoChem 2910). About 100 mg of the sample was placed in a U-shaped, flow-through, quartz sample tube. Before the TPD experiments, the catalyst was activated at  $500\text{ }^{\circ}C$  under a flow of He (30 ml/min). The sample was cooled to  $50\text{ }^{\circ}C$  and  $NH_3$  (10% in He; 30 ml/min) was adsorbed for 30 min. Desorption of  $NH_3$  was followed by raising the temperature from  $50$  to  $500\text{ }^{\circ}C$  at the ramp rate of  $10\text{ }^{\circ}C/min$ . Basicity of the samples was determined on the same instrument using  $CO_2$  (10% in He; 40 ml/min) as probe molecule.

### 5.2.3. Reaction procedure

All the reactions were conducted in a 100 ml stainless steel Parr high pressure reactor as reported in Chapter 2 (section 2.4.2.1). After the reaction, the reactor was cooled to 25 °C and gaseous products were vented out. The catalyst was separated out from the liquid products by centrifugation followed by filtration. The liquid products were analyzed and quantified with the help of a Varian 3400 gas chromatograph (GC) equipped with a flame ionization detector and CP-SIL8CB column (30 m long and 0.53 mm i.d.). Nonane-1-ol was used as an internal standard for quantification of the products by GC. The gas product was analyzed with the above GC but with thermal conductivity detector.

## 5.3. Results and discussions

### 5.3.1. Catalyst characterization

#### 5.3.1.1. XRD

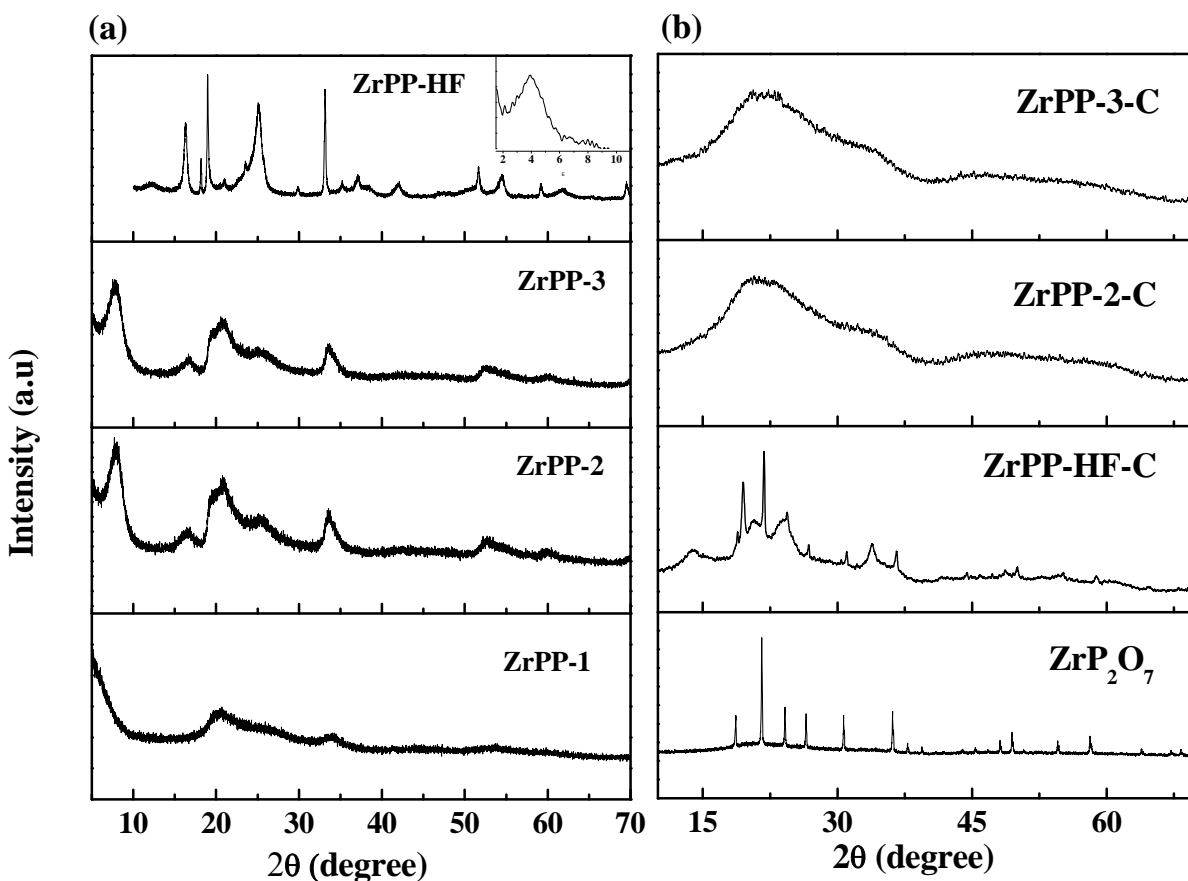


**Fig.5.1.** Powder XRD of (a) uncalcined and (b) calcined zirconium phenyl phosphonate phosphite catalysts and ZrP<sub>2</sub>O<sub>7</sub>

Uncalcined ZrPP-HF showed XRD pattern typical of a layered structure with a basal spacing of 22.6 Å (Fig. 5.1(a); inset shows the low-angle peak). The staged ZrPP reported by Alberti et al. [20] has a basal spacing of 21.1 Å. Clearfield et al [19,21] disclosed a material with 25.5 Å basal spacing. The difference in basal spacing was attributed to different amounts of water in the samples present in the phosphite interlayers. With increase in phosphorous acid to phenyl phosphonic acid molar ratio from 1:1 to 3:1 in uncalcined ZrPP-1 to ZrPP-3, a decrease in basal spacing from 15 to 11 Å was noted (Fig. 5.1(a)). XRD pattern of the calcined sample, ZrPP-HF-C was different from that of the uncalcined sample indicating change in molecular structure on calcination (Fig. 5.1(b)). Interestingly, the sharp peaks in the XRD resembled those of  $ZrP_2O_7$  [23]. Broad, background peaks indicate the presence of some amorphous structure. ZrPP-1/2/3-C showed only the broad and diffused peaks.

### 5.3.1.2. FTIR

FTIR spectroscopy provided further evidence for formation of  $ZrP_2O_7$  phase in the calcined samples showing intense peaks in the fingerprint region (750–1300  $cm^{-1}$ ) due to stretching modes of  $PO_2$  groups in the pyrophosphate (Fig. 5.2) [23].

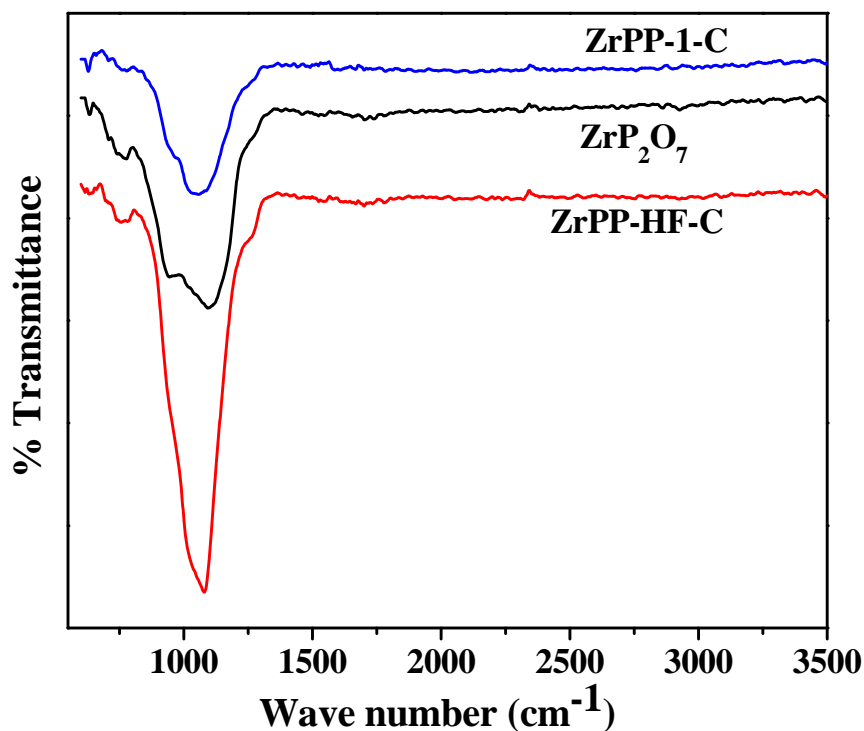
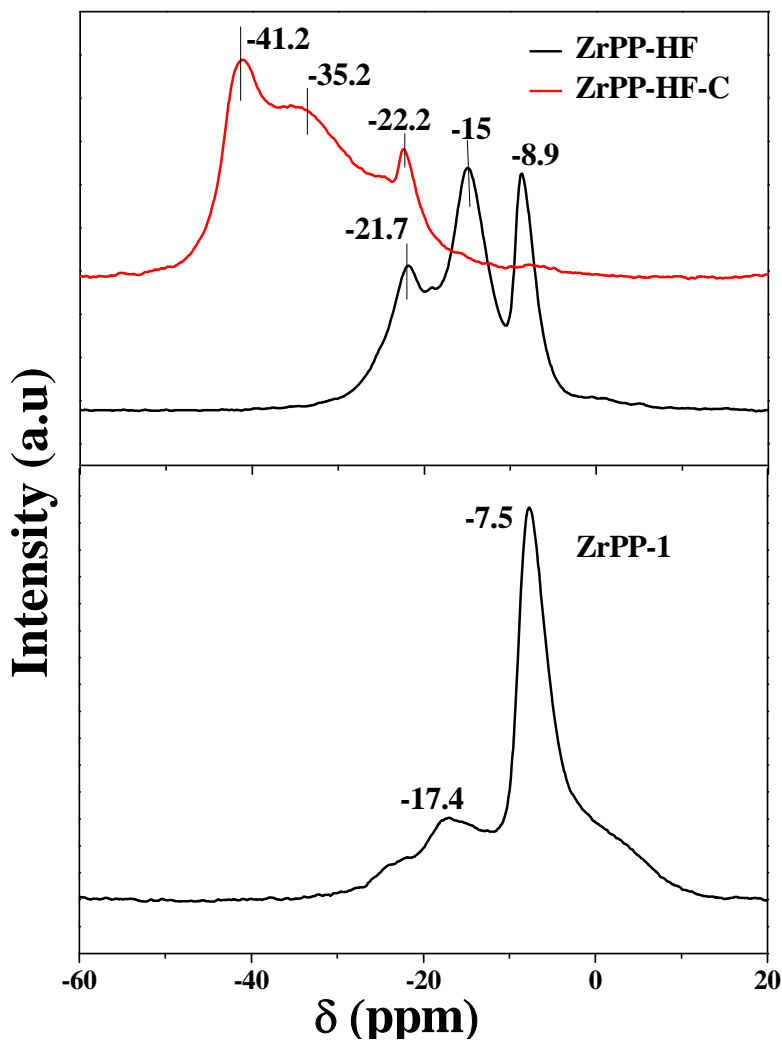


Fig. 5.2. FTIR spectra of calcined ZrPP catalysts and  $ZrP_2O_7$ .

### 5.3.1.3. $^{31}\text{P}$ MAS NMR

$^{31}\text{P}$  MAS NMR spectroscopy provided independent evidence for the presence of phosphorus groups in the uncalcined samples showing signals at  $\delta = -7.5$  to  $-9$  and  $-15$  to  $-18.3$  ppm due to phenyl phosphonate and P-H of phosphite groups, respectively. In the calcined samples these signals shifted to lower  $\delta$  values ( $-22$  to  $-42$  ppm) due to formation of the pyrophosphate structure (Fig. 5.3) [24].



**Fig. 5.3.**  $^{31}\text{P}$  MAS NMR spectra of uncalcined (ZrPP-1, ZrPP-HF) and calcined (ZrPP-HF-C) zirconium phenylphosphonate phosphites.

#### 5.3.1.4. Thermogravimetric analysis

In thermal analysis, the as-synthesized samples showed, in general, two stages of weight loss: (1) a minor loss in the temperature range 60 - 100 °C due to weakly bound water and (2) a major loss at 400 - 500 °C due to decomposition of phenyl phosphonate and conversion of  $\text{Zr}(\text{C}_6\text{H}_5\text{PO}_3)_x(\text{HPO}_3)_{2-x}$  to zirconium pyrophosphate ( $\text{ZrP}_2\text{O}_7$ ) having molecular weight of 265.2 (Fig. 5.4). Based on weight loss the structural formula was determined and the values were in good agreement with those determined from the elemental analysis (Table 5.1). As the weight loss due to water is very low and as it occurs at low temperature (< 100 °C) unlike that in the case of aluminosilicates (< 200 °C), the catalysts of this study can be designated as hydrophobic.

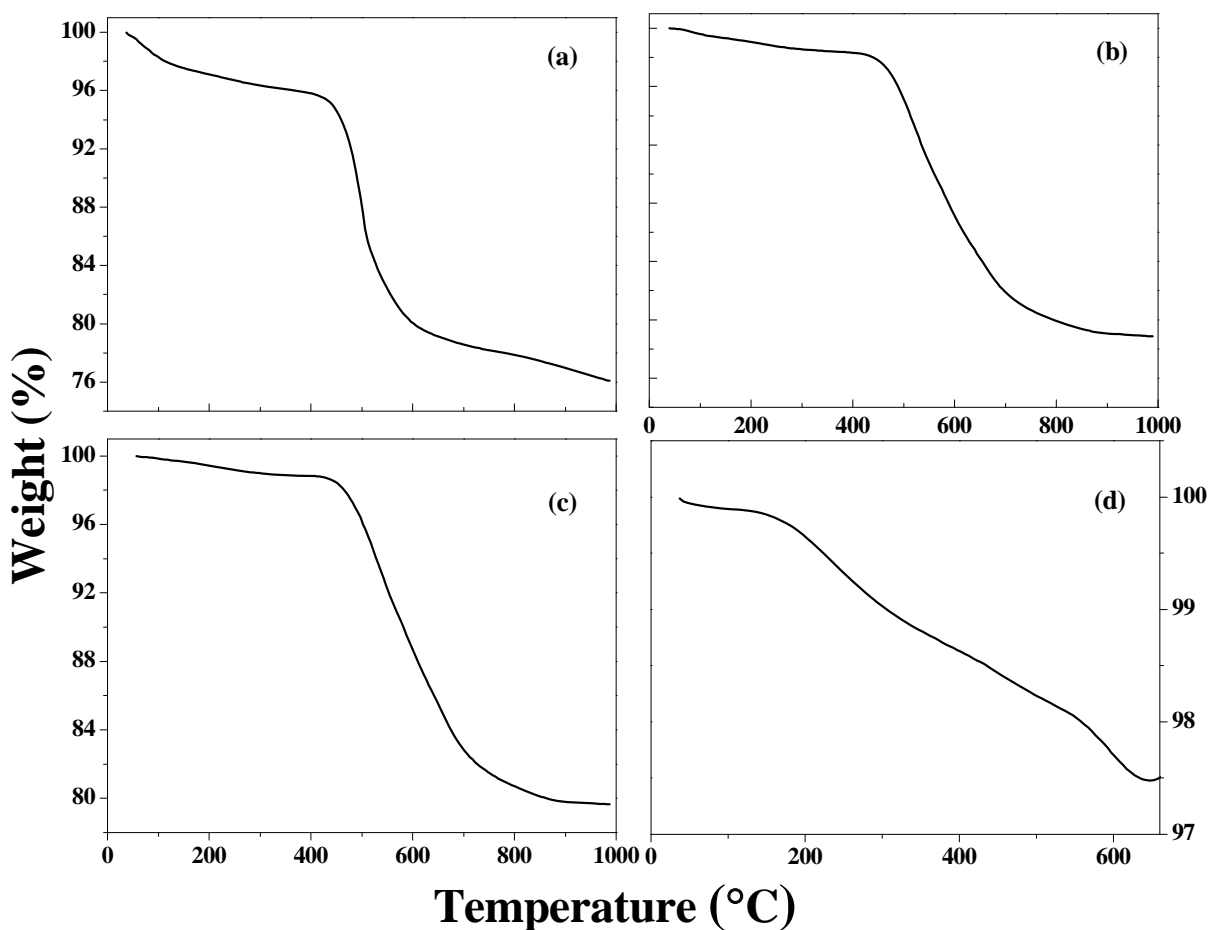


**Fig.5.4.** Thermogravimetric plots of (a) ZrPP-1, (b) ZrPP-2, (c) ZrPP-3, (d) ZrPP-HF.

**Table 5.1.** Structural and textural properties of ZrPP based catalysts.

Catalyst	S <sub>BET</sub> m <sup>2</sup> /g	Elemental composition (%)		d-spacing(A°)	Molecular formula
		C	H		
ZrPP-1	439	21.3(21.4)	1.9(2.0)	-	Zr(C <sub>6</sub> H <sub>5</sub> PO <sub>3</sub> ) <sub>0.99</sub> (HPO <sub>3</sub> ) <sub>1.01</sub> .0.4 H <sub>2</sub> O
ZrPP-2	260	21.3(21.3)	1.8(1.9)	11.3	Zr(C <sub>6</sub> H <sub>5</sub> PO <sub>3</sub> ) <sub>0.97</sub> (HPO <sub>3</sub> ) <sub>1.03</sub> .0.15 H <sub>2</sub> O
ZrPP-3	268	20.1(21.0)	1.6(1.8)	11.6	Zr(C <sub>6</sub> H <sub>5</sub> PO <sub>3</sub> ) <sub>0.95</sub> (HPO <sub>3</sub> ) <sub>1.05</sub> .0.1 H <sub>2</sub> O
ZrPP-HF	45	8.0 (7.8)	1.1(1.2)	22.6	Zr(C <sub>6</sub> H <sub>5</sub> PO <sub>3</sub> ) <sub>0.29</sub> (HPO <sub>3</sub> ) <sub>1.71</sub> .0.02 H <sub>2</sub> O
ZrPP-1-C	188	0.41	0.67	-	-
ZrPP-2-C	193	1.55	0.70	-	-
ZrPP-3-C	199	0.63	0.53	-	-
ZrPP-HF-C	26	1.05	0.20	-	-

Values in parenthesis correspond to the C and H% obtained from the formula.



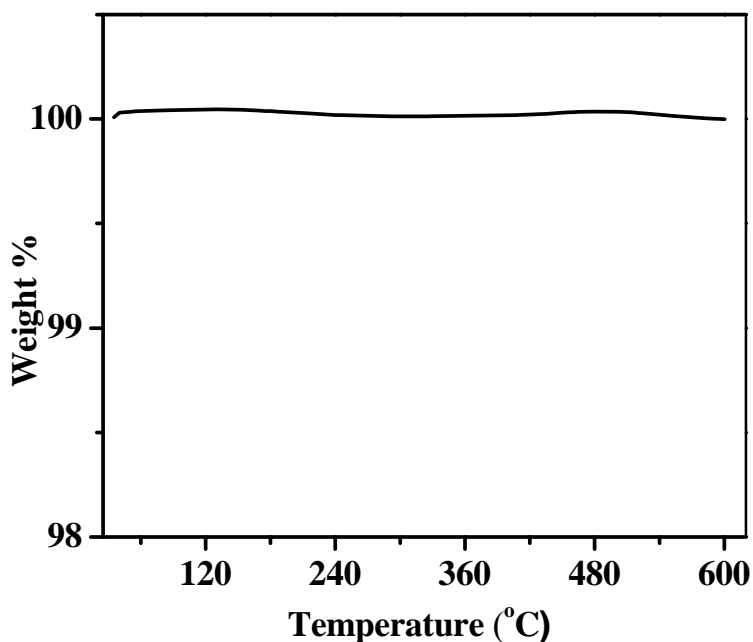


Fig. 5.5. Thermogravimetric plot of ZrPP-HF-C.

In spite of exposing to water vapors, the calcined samples showed no weight loss in thermal analysis in the temperature range 40–600 °C confirming hydrophobic nature of these calcined samples (Fig. 5.5).

#### 5.3.1.5. $N_2$ - physisorption analysis

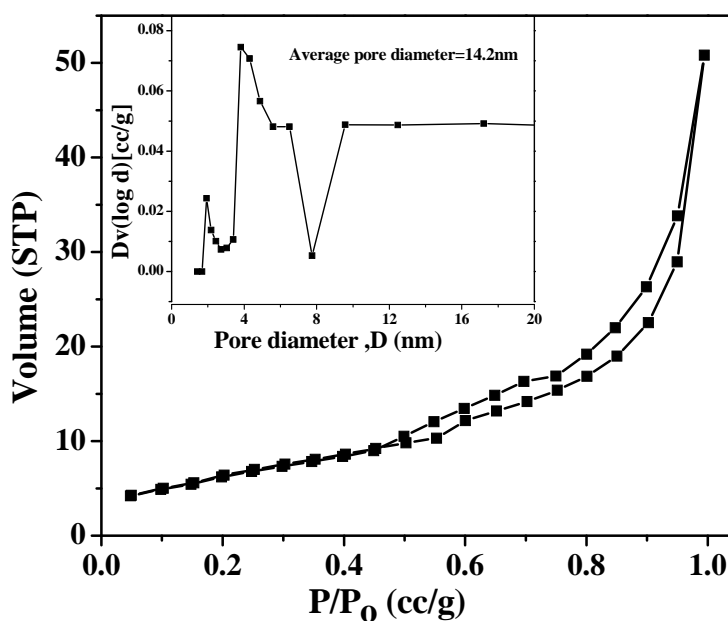
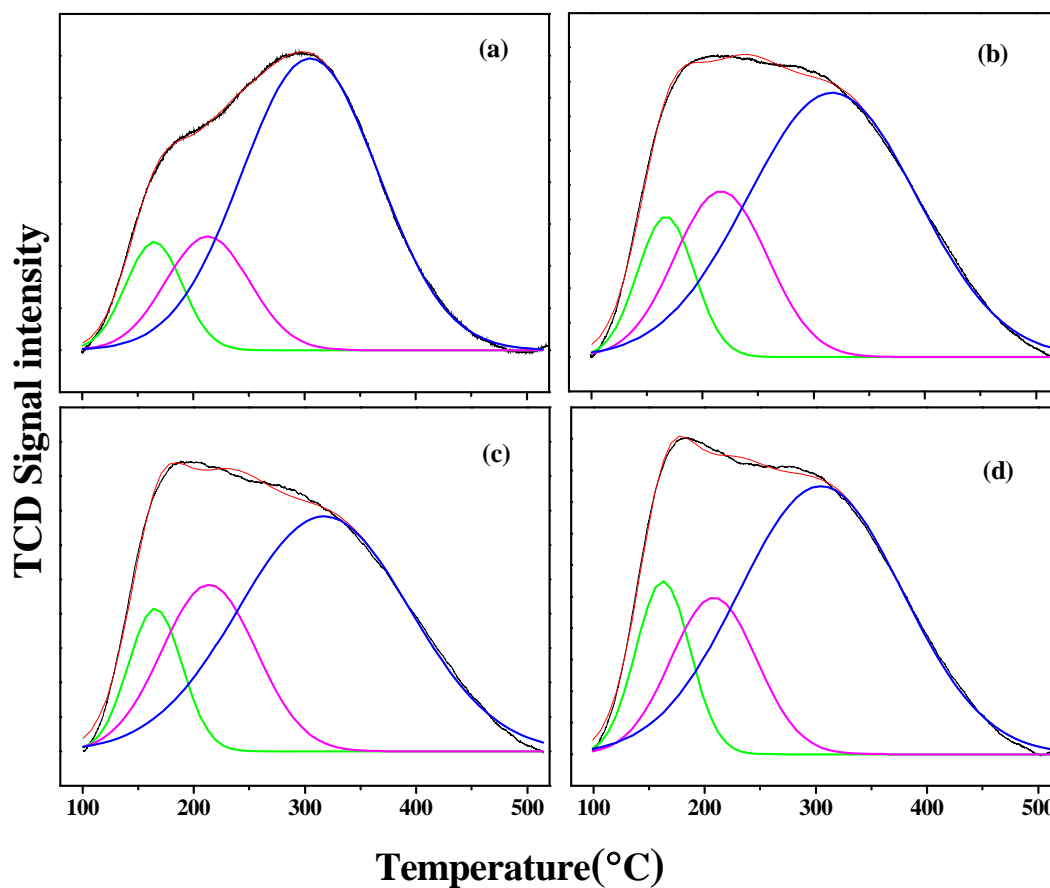


Fig. 5.6.  $N_2$  adsorption/desorption isotherms of calcined zirconium phenyl phosphonate phosphite.

Specific surface area ( $S_{\text{BET}}$ ), determined from  $\text{N}_2$  physisorption analysis, of the calcined samples prepared without using HF (ZrPP-1/2/3-C) is higher (188-199  $\text{m}^2/\text{g}$ ) than that of ZrPP-HF-C prepared using HF (26  $\text{m}^2/\text{g}$ ). This agrees well with the XRD results demonstrated wherein only broad peaks corresponding to amorphous nature were observed in the case of the former while sharp peaks indicating higher crystallinity was observed for the latter type calcined sample. ZrPP-HF-C was mesoporous having average pore diameter of 14.2 nm (Fig. 5.6).

### 5.3.1.6. Acidity-basicity measurement

Acid-base properties of the calcined samples were determined using  $\text{NH}_3$  and  $\text{CO}_2$  as probe molecules. Three overlapping  $\text{NH}_3$  desorption peaks with peak maximum at around 160, 210 and 300  $^\circ\text{C}$  were observed in the calcined ZrPP catalysts. While the first peak is corresponded to weak Lewis acid sites (surface OH groups), the second and third peaks are attributed to medium and strong acid ( $\text{Zr}^{4+}$ ) sites (Fig. 5.7).



**Fig. 5.7.**  $\text{NH}_3$ -TPD profiles of (a) ZrPP-HF-C, (b) ZrPP-1-C, (c) ZrPP-2-C, (d) ZrPP-3-C.

In CO<sub>2</sub>-TPD, two overlapping peaks were observed at 160 and 300 °C (Fig. 5.8), attributable to the presence of weak and strong basic sites (O<sup>-</sup>), respectively. The overall acid and base sites densities of ZrPP-HF-C are higher than those of ZrPP-1/2/3-C samples (Table 5.2). Ion-exchange capacity/m<sup>2</sup> of the catalyst was found higher for ZrPP-HF-C than for ZrPP-1/2/3-C (Table 5.2). This experiment in combination with NH<sub>3</sub>-TPD reveals that the calcined ZrPP catalysts have both Brønsted and Lewis acid sites.

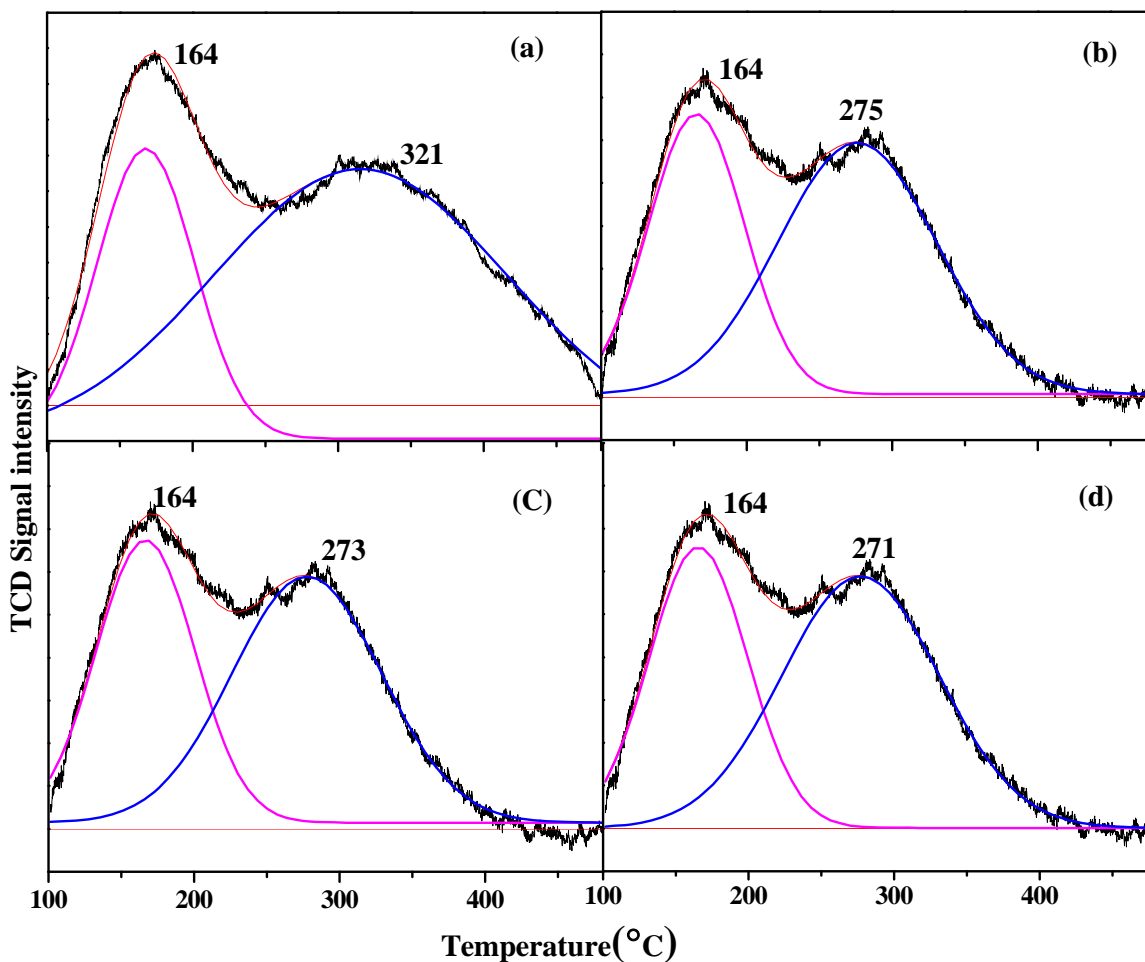


**Fig. 5.8.** CO<sub>2</sub>-TPD profiles of (a) ZrPP-HF-C, (b) ZrPP-1-C, (c) ZrPP-2-C and (d) ZrPP-3-C.

### 5.3.2. Catalytic activity

Controlled experiments revealed that the reaction of methanol with CO<sub>2</sub> producing DMC doesn't take place in the absence of a catalyst. While the uncalcined samples ZrPP-1, ZrPP-2 and ZrPP-3 were inactive, ZrPP-HF exhibited some activity (1.24 mmol/g. catalyst of DMC formed when 16.02 g of methanol was reacted with CO<sub>2</sub> (2 MPa) using 1 wt% of catalyst at 170 °C for 8

h). Interestingly, calcined ZrPP catalysts showed higher catalytic activity than the uncalcined samples (Table 5.2).

**Table 5.2.** Physicochemical and catalytic properties of calcined ZrPP.

Catalyst	S <sub>BET</sub> (m <sup>2</sup> /g) <sup>a</sup>	Acidity (μmol/m <sup>2</sup> ) <sup>b</sup>	Basicity (μmol/m <sup>2</sup> ) <sup>c</sup>	Ion exchange capacity (μeq/m <sup>2</sup> ) <sup>d</sup>	Catalytic activity (DMC yield; mmol/g. catalyst) <sup>e</sup>
ZrPP-1-C	188	5.4	0.95	3.65	0.597
ZrPP-2-C	193	4.8	0.83	3.24	0.505
ZrPP-3-C	199	4.6	0.70	3.14	0.486
ZrPP-HF-C	26	21.3	13.1	15.0	5.05

<sup>a</sup>N<sub>2</sub> physisorption. <sup>b</sup>NH<sub>3</sub>-TPD, <sup>c</sup>CO<sub>2</sub>-TPD, <sup>d</sup>50 mg of activated catalyst was suspended in 10 ml of 0.01 N NaCl solution at 25 °C for 30 min, then the solid was removed and the left out liquid was titrated against 0.01 N NaOH solution using phenolphthalein as indicator. <sup>e</sup>Reaction conditions: methanol = 16.02 g, CO<sub>2</sub> = 2 MPa, catalyst = 1 wt% of methanol, reaction temperature = 170 °C, reaction time = 8 h.

Among the calcined catalysts, the activity of ZrPP-HF-C was higher by 10 times than those of ZrPP-1-C, ZrPP-2-C and ZrPP-3-C. At the above-mentioned reaction conditions, ZrPP-HF-C provided DMC yield of 5.05 mmol/g. catalyst. These studies, thus, reveal that the method of preparation has a marked influence on the catalytic activity of zirconium phenyl phosphonates. Interestingly, DMC was the only product formed with 100% selectivity over these zirconium catalysts. Gaseous outlet at the end of reaction contained only unreacted CO<sub>2</sub>. Formation of side products like dimethyl ether and CO were not detected. The yield of DMC increased linearly with the density of both acid and base sites on ZrPP catalysts indicating their involvement in the reaction (Fig. 5.9).

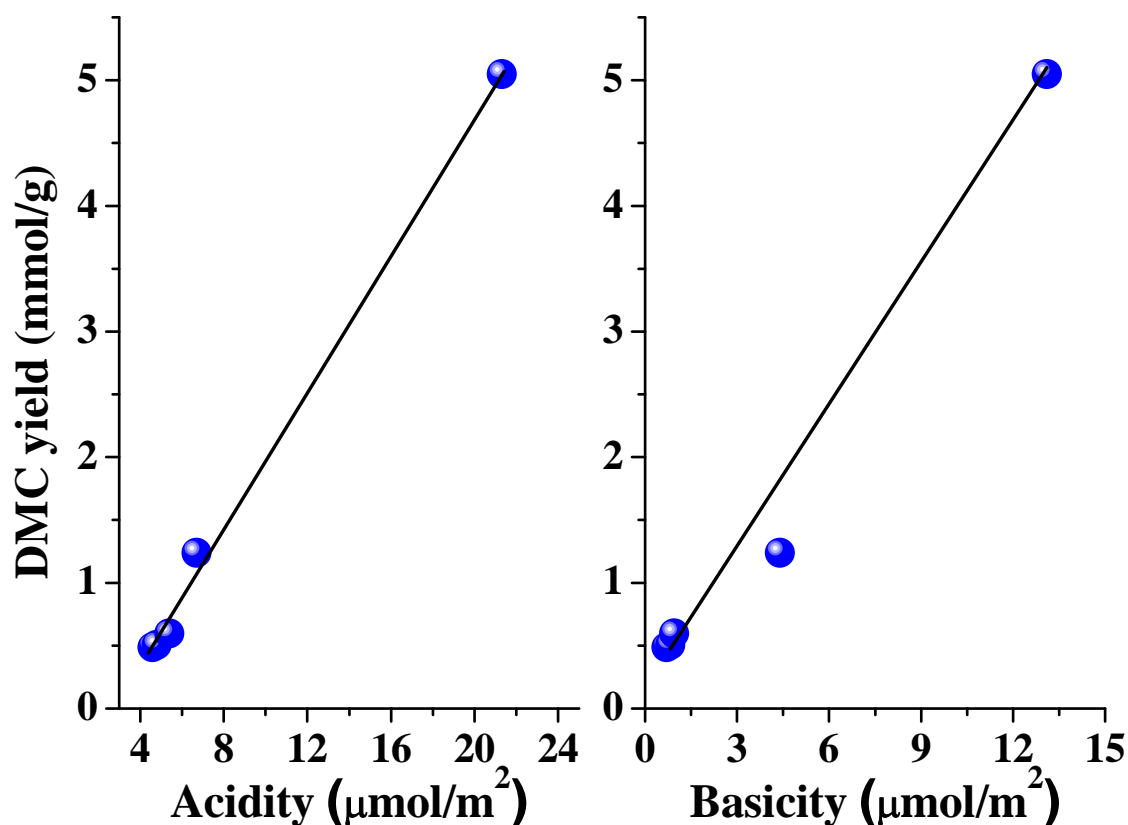


**Fig. 5.9.** Correlation of DMC yield with acidity and basicity of calcined ZrPP catalysts.

### 5.3.2.1. Effect of reaction parameters

Under the conditions of 16.02 g of methanol, 2 MPa of CO<sub>2</sub>, 1 wt% of ZrPP-HF-C catalyst and 170 °C, the yield of DMC increased with increasing reaction time and reached a maximum (5.78 mmol/g) beyond 12 h (Fig. 5.10(a)). The initial rate of the reaction over ZrPP-HF-C was found to be  $3.3 \times 10^{-4}$  mmol.sec<sup>-1</sup>. Also an increase in yield with raise in reaction temperature from 130 to 170 °C was noted (Fig. 5.10(b)). Actually this reaction is exothermic in nature ( $\Delta H = -27.90$  kJ.mol<sup>-1</sup>) [25]. Hence, higher temperatures are unfavorable to this reaction. However, in order to prevent adsorbed CO<sub>2</sub> and water molecules poisoning the surface active sites and to obtain necessary activation energy for CO<sub>2</sub> adsorption higher temperature is essential. ZrP<sub>2</sub>O<sub>7</sub> prepared by conventional methods was inactive for this reaction.

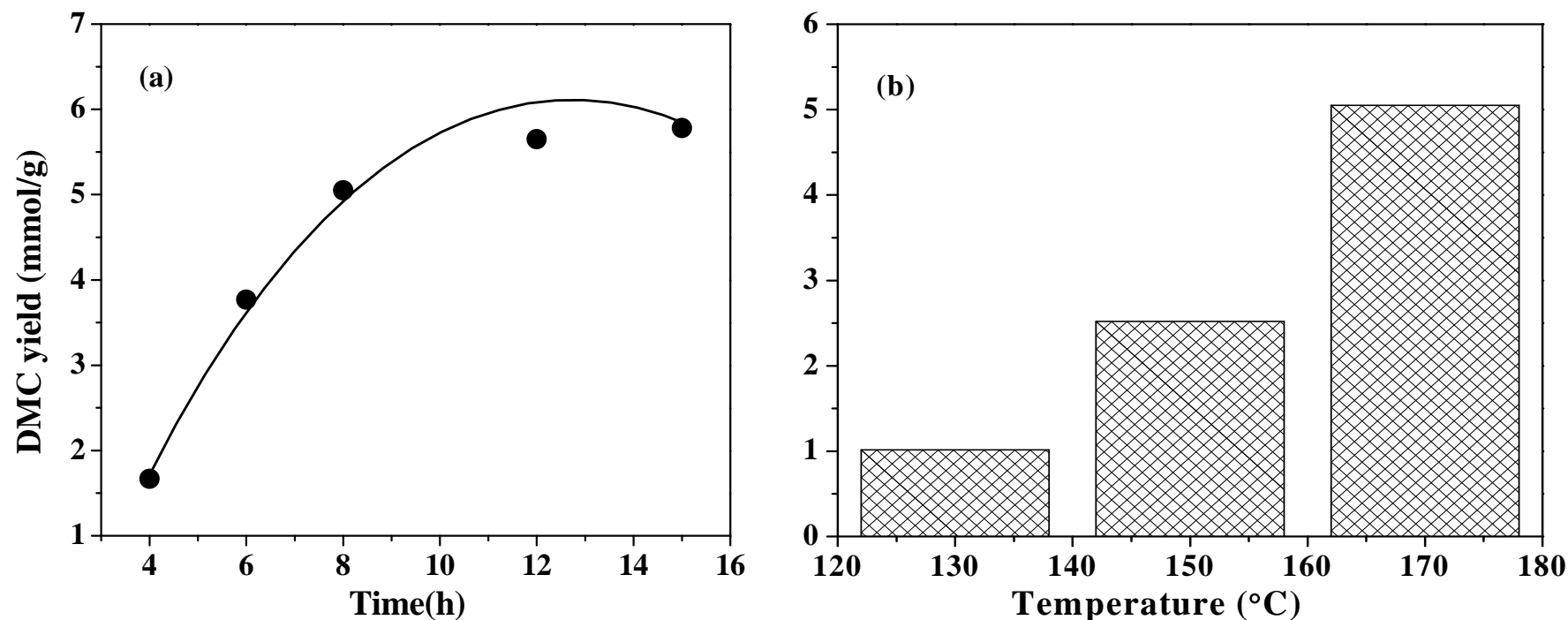


**Fig. 5.10.** Influence of (a) reaction time and (b) reaction temperature on the DMC yield. Reaction conditions: (a) methanol = 16.02 g (500 mmol), CO<sub>2</sub> pressure = 2 MPa, catalyst (ZrPP-HF-C) = 1 wt% of methanol, reaction temperature = 170 °C, reaction time = 4 -15 h; reaction conditions for (b) are same as of (a) except reaction time = 8 h and reaction temperature =130- 170 °C.

### 5.3.2.2. Effect of CO<sub>2</sub> pressure

CO<sub>2</sub> pressure has a marked effect on product yield. With increasing CO<sub>2</sub> from 1 to 3 MPa keeping the amount of methanol constant (16.02 g), a linear increase in DMC yield from 1.595 to 7.318 mmol/g.catalyst was noted at 170 °C in 8 h (Fig. 5.11).

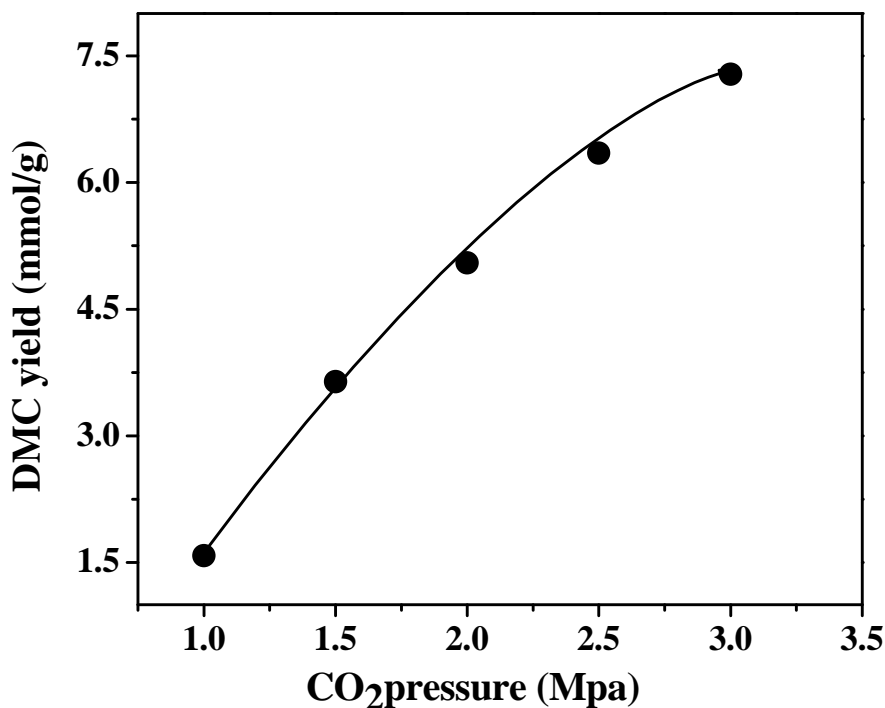


**Fig. 5.11.** Effect of CO<sub>2</sub> pressure on DMC synthesis in the absence of solvent using ZrPP-HF-C catalyst. Reaction conditions: methanol = 16.02 g (500 mmol), catalyst = 1 wt% of methanol, reaction time = 8 h and reaction temperature = 170 °C.

### 5.3.2.3. Effect of dehydrating agent and solvents

With a view to increase the amount of dissolved CO<sub>2</sub> in the liquid phase, reactions were conducted in presence of polar aprotic solvents [1,4-dioxane ( $pK_a = -2.92$ ), N,N-dimethylformamide (DMF;  $pK_a = -0.01$ ) and tetrahydrofuran (THF;  $pK_a = -2.92$ )]. DMC yield was higher in the presence of DMF (9.29 mmol/g. catalyst; Table 5.3, entry nos. 4 and 5). As water is the by-product of this condensation reaction, its removal from the system drives the equilibrium towards right side. This has been achieved by employing water trapping agents such as trimethyl orthoacetate, 2,2-dimethoxypropane, acetonitrile, cyanopyridine, epoxides and molecular sieves [25, 26]. Chemical dehydrating agents are more effective but generate their hydrated product which remains as contaminant increasing separation costs of DMC. Hence, 3A-molecular sieves

(0.5 g) were used in this study as water trapping agent. Yield of DMC increased from 8.03 to 10.14 mmol/g. catalyst without DMF and from 9.29 to 11.56 mmol/g. catalyst in presence of DMF (Table 5.3, entry nos. 1, 5, 6 and 7).

**Table 5.3.** Catalytic activity data of ZrPP-HF-C<sup>a</sup>.

Entry no.	Solvent <sup>b</sup>	CH <sub>3</sub> OH/CO <sub>2</sub> (molar ratio)	Molecular sieve-3A (g)	CO <sub>2</sub> pressure (MPa)	Catalyst (wt% CH <sub>3</sub> OH)	CH <sub>3</sub> OH conv. (mol%)	DMC yield (mmol/g)
1	-	4	-	3	1	3.2	8.03
2	1,4-dioxane	4	-	3	1	3.2	8.04
3	THF	4	-	3	1	3.2	8.09
4	DMF	4	-	3	1	3.6	8.95
5	DMF	4	-	3	1	3.7	9.29
6	-	4	0.5	3	1	4.1	10.14
7	DMF	4	0.5	3	1	4.6	11.56
8	DMF	1	0.5	3.5	3.5	19.9	14.30
9	DMF	1	0.5	4	1.9	31.8	26.05

<sup>a</sup>Methanol = 500 mmol (entry nos. 1-7), 144 mmol (entry no. 8) and 164 mmol (entry no. 9), reaction temperature = 170 °C, reaction time = 12 h, stirring speed = 600 rpm, 100 ml Paar autoclave. <sup>b</sup>Solvent = 5 ml (entry nos. 2, 3 and 4) and 10 ml (entry nos. 5 and 7-9).

Solvent alone could not catalyze this reaction. While maintaining the CO<sub>2</sub> pressure at 3 MPa, molar ratio of methanol/CO<sub>2</sub> was changed from 2 to 4; a marginal decrease in DMC yield from 12.64 to 11.56 mmol/g catalyst [170 °C, 3 MPa (CO<sub>2</sub>) and 12 h] was observed. All these findings point out that CO<sub>2</sub> activation is the crucial step in DMC synthesis. By changing CO<sub>2</sub> pressure to 4 MPa, we achieved DMC yield of 26.06 mmol/g. catalyst in presence of DMF (10 ml) and 3A-molecular sieves (0.5 g) (Table 5.3., entry no. 9). To the best of our knowledge, this is the highest DMC yield and methanol conversion (31.8 mol%) reported so far in a batch reactor over solid catalysts. The higher activity of ZrPP-HF-C is attributed to its hydrophobic nature which resists the backward reaction to occur.



#### 5.3.2.4. Catalyst recyclability

ZrPP-HF-C was reusable in at least four recycling experiments (Fig. 5.12). At the end of each recycle, the catalyst was recovered, washed with acetone, activated at 250 °C in air for 2 h and reused in the subsequent recycling experiment. No loss in DMC yield was detected. ICP analysis indicated no leaching of Zr or P elements into the liquid product. Further, the spent catalyst at the end of 4<sup>th</sup> recycle has the same XRD and FTIR characteristics as of fresh ZrPP-HF-C indicating structural and compositional stability of the catalyst (Fig. 5.13).

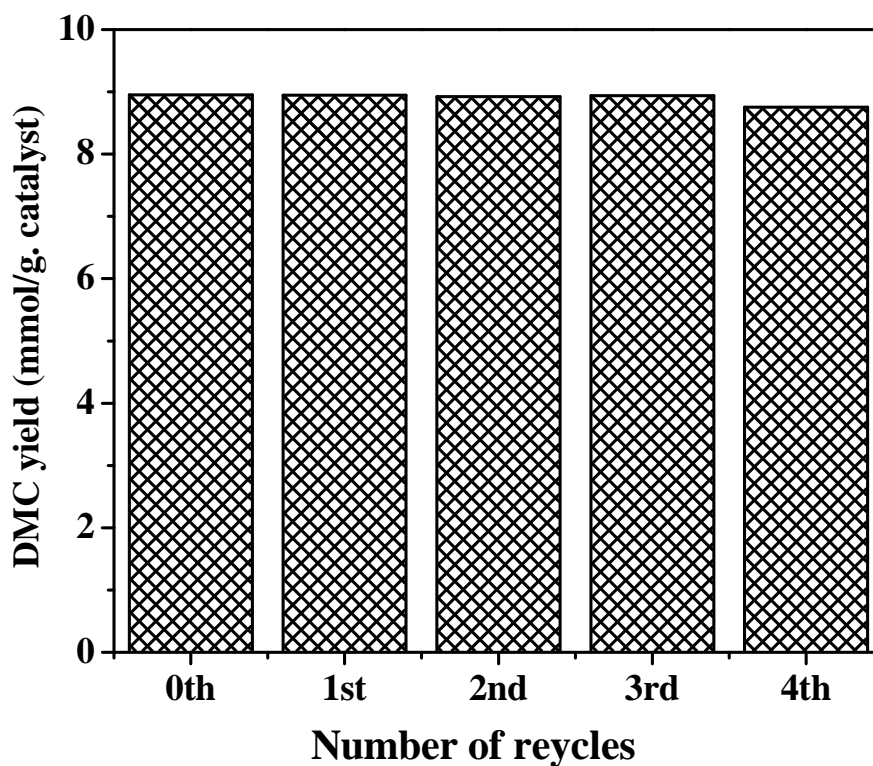


**Fig. 5.12.** Catalyst recyclability test. Reaction conditions: methanol = 16.02 g; CO<sub>2</sub> pressure = 3 MPa, solvent = DMF (5 ml), catalyst (ZrPP-HF-C) = 1 wt% of methanol, reaction temperature = 170 °C, reaction time = 12 h.

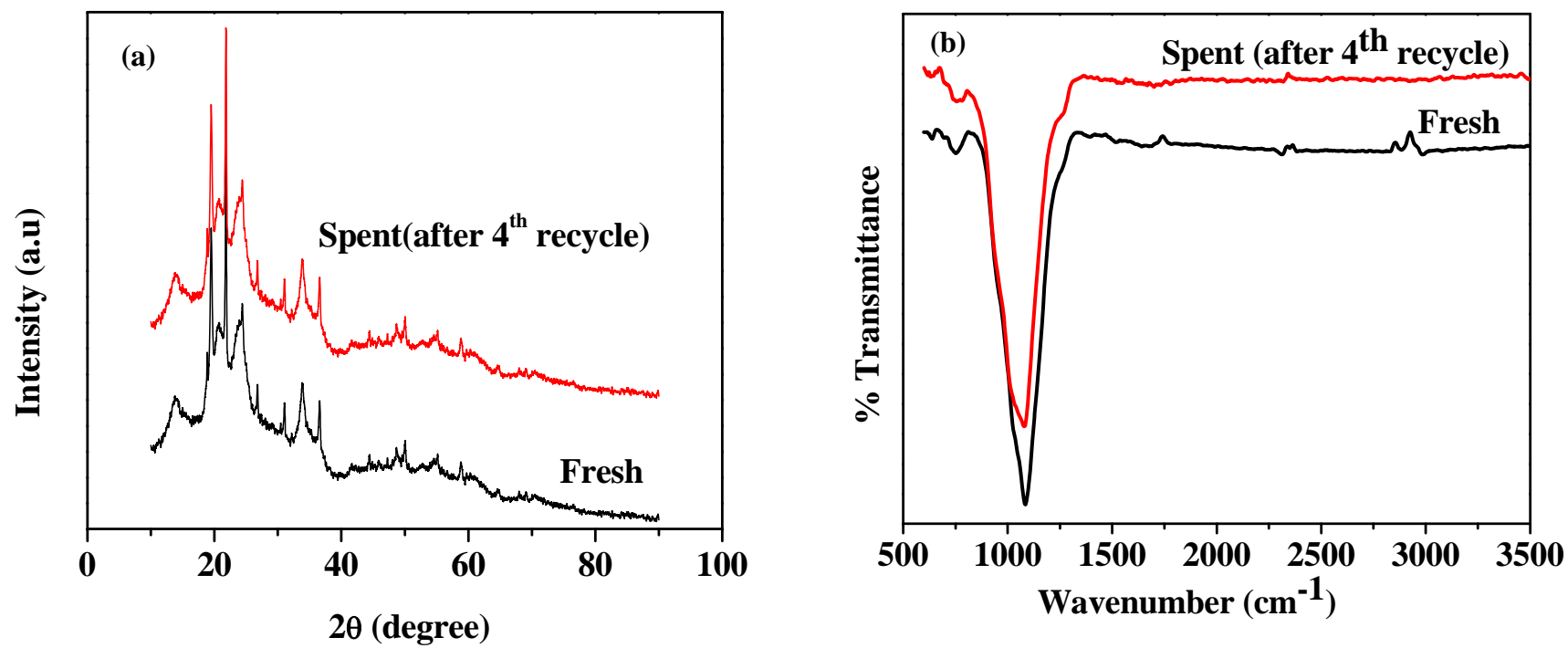
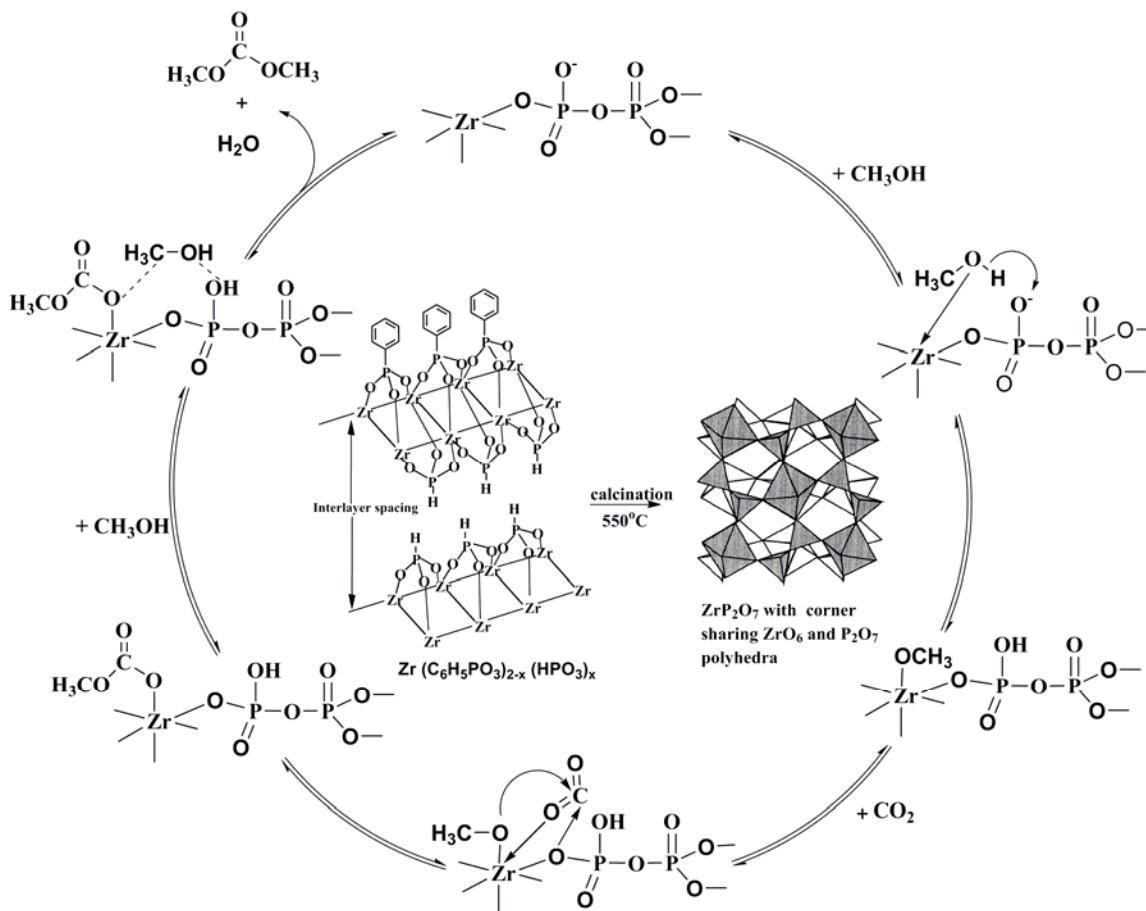


Fig. 5.13. (a) XRD and (b) FTIR of spent ZrPP-HF-C catalyst.

### 5.3.2.5. Tentative reaction mechanism

As seen from Fig. 5.14, O<sup>-</sup> ions are the possible basic sites that activate methanol and produce methoxide ion which in turn coordinates to Lewis acidic Zr<sup>4+</sup> sites. Thus, formed zirconium methoxide activates CO<sub>2</sub> leading to Zr(OCOOCH<sub>3</sub>) species. Reaction of methanol with this species assisted with adjacent acidic proton leads to DMC and water.



**Fig. 5.14.** Tentative reaction mechanism for direct DMC synthesis over ZrPP-HF-C.

## 5.4. Conclusions

In conclusion, a highly active, selective, reusable catalyst, ZrPP-HF-C for direct synthesis of DMC from methanol and CO<sub>2</sub> is reported in this chapter for the first time. Activity of this catalyst is superior to most of the hitherto known solid catalysts. Hydrophobicity and acid-base bifunctionality are the causes for the high activity of ZrPP-HF-C. Comparatively high yield of DMC is obtained even in the absence of solvents and dehydrating agent. The addition of solvent (DMF) and molecular sieve 3A results in further increase of DMC yield.

## 5.5. References

- [1] W. Peng, N. Zhao, F. Xiao, W. Wei, Y. Sun. *Pure Appl. Chem.* 84 (2012) 603-620.
- [2] P. Tundo, M. Selva, *Acc. Chem. Res.* 35 (2002) 706-716.
- [3] M.A. Pacheco, C.L. Marshall, *Energy Fuels* 11 (1997) 2-29.
- [4] T. Sakakura, K. Kohno, *Chem. Commun.* (2009) 1312-1330.
- [5] S.R. Loarie, P.B. Duffy, H. Hamilton, G.P. Asner, C.B. Field, D.D. Ack-erly, *Nature* 462 (2009) 1052–1055.
- [6] J. Davis, K. Caldeira, H.D. Matthews, *Science* 329 (2010) 1330-1333.
- [7] E. Leino, P. Maki-Arvela, V. Eta, D.Y. Murzin, T. Salmi, J.-P. Mikkola, *Appl. Catal. A: Gen.* 383 (2010) 1-13.
- [8] D.B. Tkatchenko, F. Bernard, F. Demoisson, L. Plasseraud, S.R. Sanapureddy, *ChemSusChem* 4 (2011) 1316-1322.
- [9] S. Fujita, B.M. Bhanage, Y. Ikushima, M. Arai, *Green Chem.* 3 (2001) 87-91.
- [10] K. Tomishige, Y. Ikeda, T. Sakaihoru, K. Fujimoto, *J. Catal.* 192 (2000) 355-362.
- [11] K.T. Jung, A.T. Bell, *Topics Catal.* 20 (2002) 97-105.
- [12] X.L. Wu, Y.Z. Meng, M. Xiao, Y.X. Lu, *J. Mol. Catal. A: Chem.* 249 (2006) 93-97.
- [13] M. Aresta, A. Dibenedetto, C. Pastore, A. Angelini, B. Aresta, I. Pápai, *J. Catal.* 269 (2010) 44-52.
- [14] K.T. Jung, A.T. Bell, *J. Catal.* 204 (2001) 339-347.
- [15] K. Tomishige, Y. Furusawa, Y. Ikeda, M. Asadullah, K. Fujimoto, *Catal. Lett.* 76 (2001) 71-74.
- [16] Y. Ikeda, M. Asadullah, K. Fujimoto, K. Tomishige, *J. Phys. Chem. B* 105 (2001) 10653-10658.
- [17] C.J. Jiang, Y.H. Guo, C.G. Wang, C.W. Hu, Y. Wu, E.B. Wang, *Appl. Catal. A: Gen.* 256 (2003) 203-209.
- [18] Z. Wang, J. M. Heising, A. Clearfield, *J. Am. Chem. Soc.* 125 (2003) 10375-10383.
- [19] A. Clearfield, J.D. Wang, Y. Tian, E. Stein, C. Bhardwaj, *J. Solid. State Chem.* 117 (1995) 275-289.
- [20] G. Alberti, U. Costantino, J. Kornyei, M.L.L. Giovagnotti, *React. Polym.* 4 (1985) 1-10.
- [21] J.D. Wang, A. Clearfield, G.-Z. Peng. *Mater. Chem. Phys.* 35 (1993) 208-216.
- [22] P. Varhadi, M. Kotwal, D. Srinivas, *Appl. Catal. A: Gen.* 462-463 (2013) 129-136.

- [23] Ch. Srilakshmi, K. Ramesh, P. Nagaraju, N. Lingaiah, P.S. Sai Prasad. *Catal. Lett.* 106 (2006) 115-122.
- [24] K. Segawa, Y. Nakajima, S. Nakata, S. Asaoka, H. Takahashi, *J. Catal.* 101 (1986) 81-89.
- [25] V. Eta, P. Maki-Arvela, A.- R. Leino, K. Kordas, T. Salmi, D.Y. Murzin, J.-P. Mikkola, *Ind. Eng. Chem. Res.* 49 (2010) 9609–9617.
- [26] M. Honda, M. Tamura, Y. Nakagawa, S. Sonehara, K. Suzuki, K.-I. Fujimoto, K. Tomishige, *ChemSusChem* 6 (2013) 1341-1344.

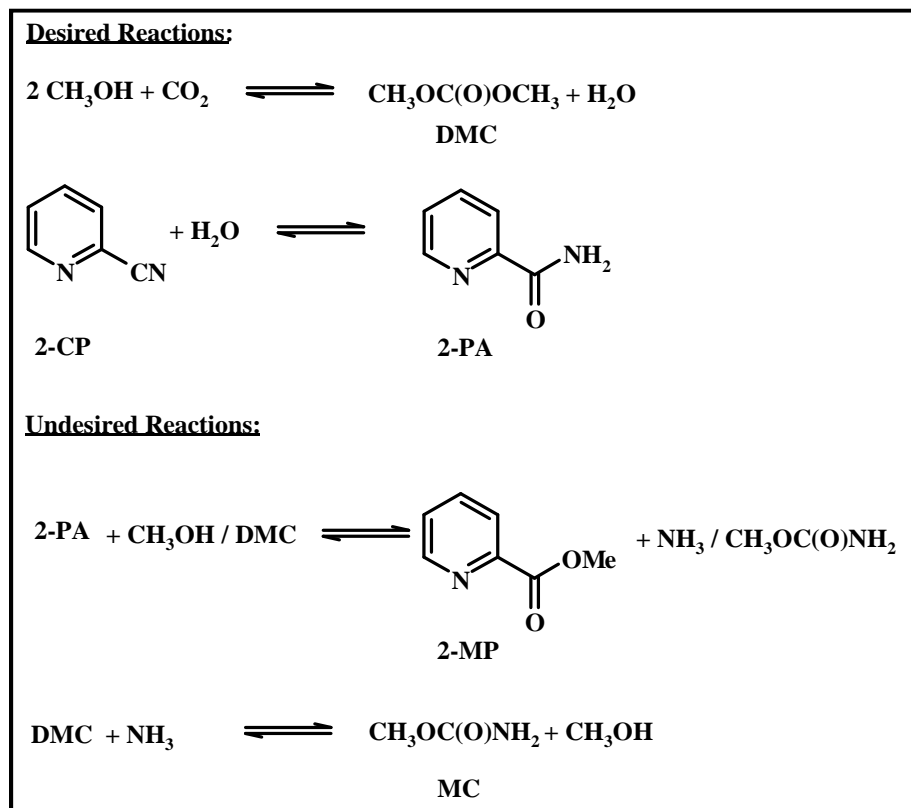
**Chapter - 6**

**Direct Synthesis of DMC from CO<sub>2</sub> and Methanol over  
CeO<sub>2</sub> Catalysts**

## 6.1. Introduction

Climate change due to increasing amount of CO<sub>2</sub> emissions into atmosphere has become a major hitch, for which much attention is being paid globally to control these emissions by way of converting CO<sub>2</sub> back into fuels or chemicals [1-3]. An efficient catalyst is needed for its activation and utilization because of its high thermodynamic stability and kinetic inertness. Conversion of CO<sub>2</sub> to dimethyl carbonate (DMC) has attracted interest as DMC is a green reagent/solvent, a raw material for manufacturing electrolytes used in lithium ion batteries, precursor for polycarbonates and a potential gasoline additive with an annual demand of about 30 million tons [4-6]. Direct synthesis of DMC from methanol and CO<sub>2</sub> is atom-efficient than other eco-friendly methods for its production [7,8]. Several homogeneous and heterogeneous catalysts were explored for this method, which include Sn-based catalysts, Cu-based catalysts, CeO<sub>2</sub> and ZrO<sub>2</sub>-based catalysts. Zirconia and ceria-based catalysts were most effective for the activation of methanol and CO<sub>2</sub> [4,9-13]. The acid-base property plays an essential role for their catalytic activity. However, the direct synthesis is low yielding and equilibrium limited. Removal of water co-generated in the reaction using traps is necessary to overcome those limitations. In recent times, research interest on the direct synthesis of DMC mainly focused on CeO<sub>2</sub>-based compounds because of their excellent activity as catalyst and catalyst support. Wang et al. [13] reported the influence of morphology of CeO<sub>2</sub> crystallites on DMC yield. They described a correlation between morphology, crystal planes, acidity / basicity and DMC yield. The spindle morphology showed the highest DMC yield among several. However, influence of morphology on methanol conversion and DMC selectivity was not addressed although it was highly important due to the azeotrope behavior of DMC with methanol. DMC forms an azeotrope with methanol at atmospheric pressure, which demands distinct separation steps through extractive distillation, liquid-liquid extraction, evaporation, etc. In order to overcome such problems, development of a catalyst system for complete conversion of methanol to DMC is desired. Honda et al. [14] reported, for the first time, that with ceria (CeO<sub>2</sub>) as a catalyst and 2-cyanopyridine (2-CP) as water trapping agent, methanol and CO<sub>2</sub> conversion could be quantitative with a DMC yield of 94% (Scheme 6.1). This study was quite attractive, however the role of defects, morphology and type and quantity of acid and base sites was not studied exclusively. Recently, Asahi Kasai Chemicals Corp. [15] declared construction of a validation plant for dialkyl carbonates to produce diphenyl carbonate using their proprietary catalyst. In

view of the industrial importance of DMC, it is of interest to know the factors governing the catalytic activity / selectivity of CeO<sub>2</sub> in the direct synthesis route using 2-cyanopyridine as dehydrating agent. In this study, it is reported that the morphology, defect site concentration and optimum medium type acid/base sites of CeO<sub>2</sub> significantly influence its catalytic activity / selectivity.



**Scheme 6.1.** Direct synthesis of DMC from CO<sub>2</sub> and methanol in presence of 2-CP.

## 6.2. Experimental

### 6.2.1. Catalyst preparation

Ceria samples of different morphology [cubes (Ce - C), rods (Ce - R), spindles (Ce - S) and no definite shape (Ce - N)] were prepared by non-template hydrothermal synthesis methods as reported in Chapter 2 (section 2.2.4) [13,16].

### 6.2.2. Characterization techniques

The X-ray powder diffraction (XRD) patterns of the catalyst samples were recorded on a Philips X'pert Pro diffractometer using Cu-K radiation and a proportional counter detector. The diffraction patterns were recorded in the 2θ range of 5- 90° at a scan rate of 4°/min. The step size



in the measurements was 0.02°. High resolution transmission electron micrograph (HRTEM) images of the samples were collected on a FEI Technai-F30 instrument with a 300 kV field emission gun. Scanning electron micrographs (SEM) were collected on a Leica STEREOSCAN 440, LEO Microscopy, Cambridge, UK instrument. FT-Raman spectra were recorded on a Horiba JY LabRaman HR 800 MicroRaman spectrometer using 630 nm wavelength generated by a He-Ne laser operating at 20 m. Specific surface area ( $S_{\text{BET}}$ ) of the samples was determined from the nitrogen-adsorption measurements carried out at -196 °C using Quadrasorb S automated surface area and pore size analyzer (Quanta Chrome Instrument). Before N<sub>2</sub> adsorption, the samples were evacuated at 200 °C.  $S_{\text{BET}}$  was determined from the linear part of the adsorption isotherm using the BET equation ( $p/p_0 = 0.05-0.31$ ). The pore size distribution was calculated with the Barrett-Joyner-Halenda (BJH) method. Acidity and basicity of the catalysts were determined by temperature-programmed desorption techniques using ammonia and carbon dioxide, respectively, as probe molecules (Micromeritics Auto Chem 2910 instrument). About 0.1 g of the catalyst was activated at 200 °C under He (40 ml/min). The sample was cooled to 50 °C and NH<sub>3</sub>/CO<sub>2</sub> was adsorbed at a rate of 40 ml/min for 30 min. Then the temperature was raised to 100 °C followed by purging with helium gas to remove the physisorbed probe molecule. After the stabilization of base line, desorption of probe molecules was followed between 100 and 900 °C at the ramp rate of 10 °C /min. The broad peak obtained was deconvoluted and the amounts of different kinds of acid basic sites were determined.

### 6.2.3. Reaction procedure

All the reactions were conducted in a 100 ml stainless steel Parr pressure autoclave as described in Chapter 2 (section 2.4.2.2). At the end, the reactor was cooled to 25 °C and unreacted CO<sub>2</sub> was vented out. Then, 30 ml of ethanol and 0.2 g of nonane-1-ol was added to the liquid portion as a solvent and internal standard, respectively, and stirred for 10 min to dissolve the solid product (2-picolinamide) completely into the liquid portion. The catalyst was then separated out from the liquid products by centrifugation followed by filtration. The liquid products were analyzed and quantified with the help of a Varian 3400 gas chromatograph (GC) equipped with a flame ionization detector and CP-SIL5CB column (60 m-long and 0.32 mm i.d.).

### 6.3. Results and discussions

#### 6.3.1. Catalyst characterization

##### 6.3.1.1. XRD

XRD patterns (Fig. 6.1) confirmed the formation of ceria in a cubic fluorite lattice (unit cell parameter:  $a = 0.540$  nm; space group = Fm-3m). The average crystallite size (determined from the full width at half maximum) and intensity of XRD peaks of different samples decreased in the order: Ce - C (23.7 nm) > Ce - S (17.6 nm) > Ce - N (12.0 nm) > Ce - R (11.2 nm) inferring that the ceria sample of cubic morphology (Ce-C) is more crystalline than that the spindle, no definite shape and rod-like morphologies.

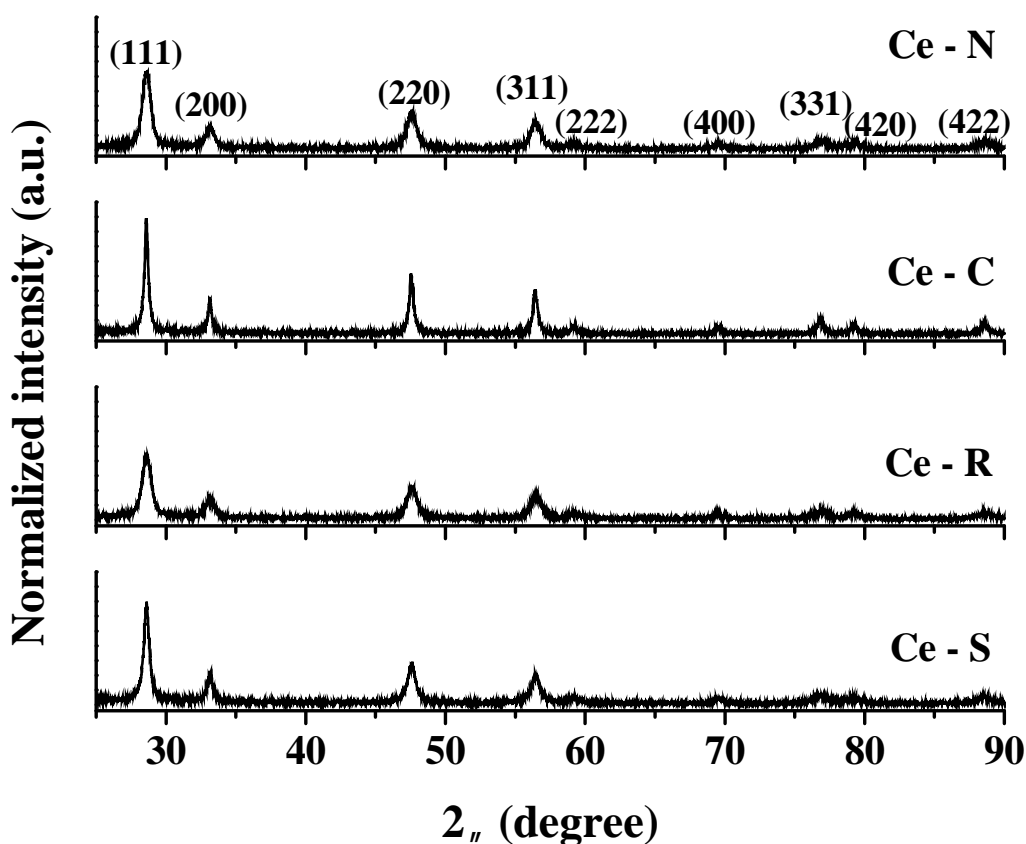
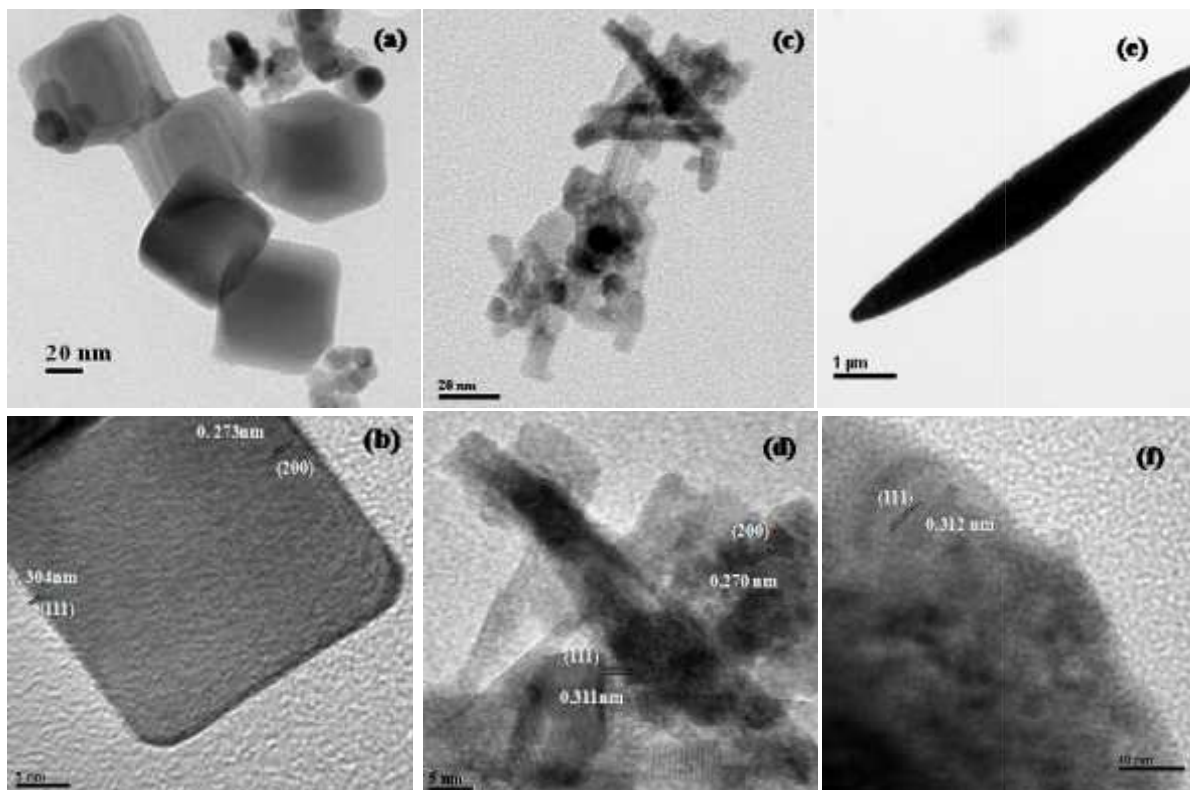


Fig.6.1. XRD patterns of ceria with different morphology.

##### 6.3.1.2. HRTEM

The sample with a cubic morphology had particles with size in the range of 20 - 140 nm (HRTEM; Fig.6.2(a)). Inter planar spacing (d-spacing) of 0.273 nm confirmed the exposed (100) planes in the cubic sample. A trace amount contained exposed (111) planes (Fig.6.2(b)). Ceria-

nano rods have a diameter of  $6.8 \pm 1$  nm and length of 50 - 100 nm (Fig.6.2(c)). They contained exposed (111) and (200) planes with a d-spacing of 0.311 and 0.270 nm, respectively (Fig.6.2(d)). Ceria-spindles had a length of 3 - 12  $\mu$ m and width of 0.8 - 2.5  $\mu$ m. The ends of the spindles were sharp and edges were curved indicating the existence of defect sites (Fig.6.2(e)). They had exposed (111) planes (Fig.6.2(f)). Ceria with no definite morphology (Ce - N) had a particle size in the range 10 - 16 nm (Fig. 6.3).



**Fig. 6.2.** HRTEM images of ceria samples: (a & b) Ce - C, (c & d) Ce - R and (e & f) Ce - S.

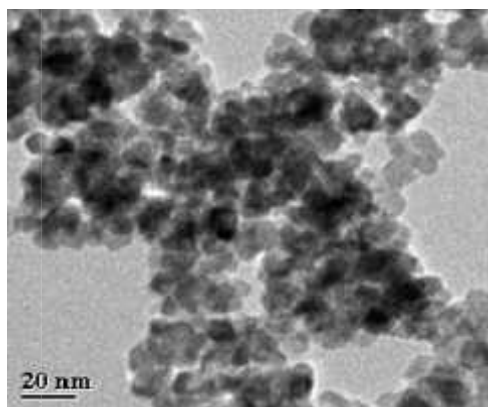


**Fig. 6.3.** TEM image of Ce-N.

### 6.3.1.3. Raman spectroscopy

FT-Raman spectrum showed an intense band at 463 cm<sup>-1</sup> attributable to the F<sub>2g</sub> mode of ceria fluorite phase (Fig. 6.4.). Weak bands centered at 250, 600 and 1179 cm<sup>-1</sup> were corresponded to second-order transverse acoustic mode (<sup>2</sup>T<sub>A</sub>), defect-induced mode and longitudinal optical mode, respectively [17,18]. The intensity of the defects peak (at 600 cm<sup>-1</sup>) was small due to its weaker sensitivity to visible Raman spectroscopy (Fig. 6.4). The concentration of the defect sites (ratio of the area of Raman band due to defect-induced mode to the band due to the F<sub>2g</sub> mode) was determined and found that ceria with a spindle morphology has higher amount of defect sites (1.1%) compared to the samples with no definite shape (0.8%), rod-like (0.5%) and cubic (0.2%) morphologies.

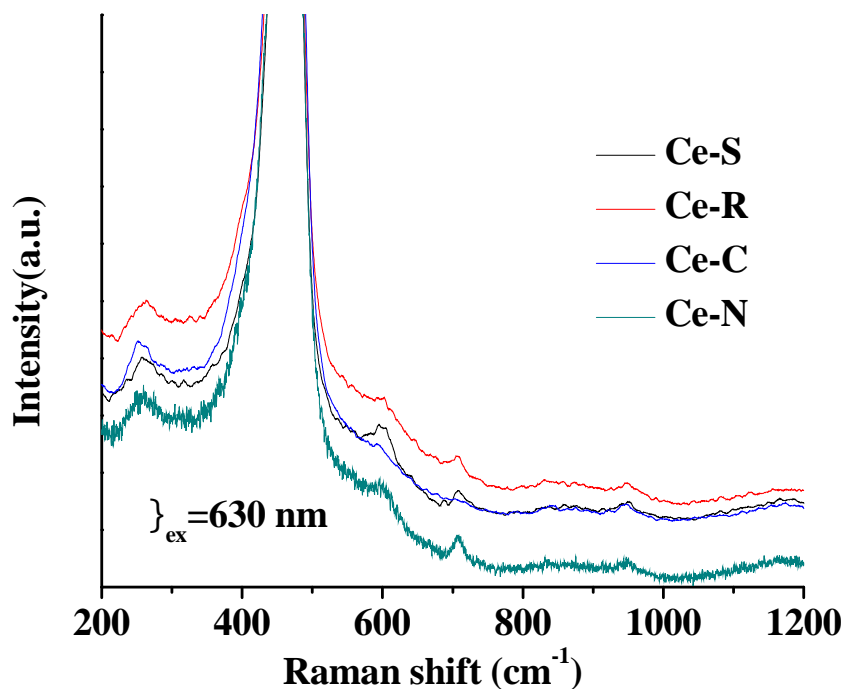


**Fig. 6.4.** FT-Raman spectra of ceria samples of different morphology.

### 6.3.1.4. Surface area analysis

The specific surface area ( $S_{\text{BET}}$ ) of ceria samples decreased in order: Ce - R (105 m<sup>2</sup>/g) > Ce - N (77 m<sup>2</sup>/g) > Ce - C (43 m<sup>2</sup>/g) > Ce - S (36 m<sup>2</sup>/g). This variation is in near agreement with that expected from their particle sizes (Table 6.1).

**Table 6.1.** Textural, acid-base and catalytic properties of ceria samples.

Sample	S <sub>BET</sub> (m <sup>2</sup> /g)	Average crystallite size (nm, XRD)	Particle size (μm; HRTEM)	Acidity (μmol/g; NH <sub>3</sub> -TPD) <sup>a</sup>			Basicity (μmol/g; CO <sub>2</sub> -TPD) <sup>a</sup>		
				Weak	Medium	Strong	Weak	Medium	Strong
Ce-N	77	12.0	0.01-0.016	106	240	77	16	51	23
Ce-C	43	23.7	0.02 - 0.14	85	128	241	12	25	28
Ce-R	105	11.2	0.05 - 0.1 x 0.007 ± 0.001	42	138	72	23	47	13
Ce-S	36	17.6	3 - 12 x 0.8 - 2.5	23	189	73	18	53	14

<sup>a</sup>Weak (< 200 °C), medium (200 - 400 °C) and strong (> 400 °C).

### 6.3.1.5. Acid and base properties

NH<sub>3</sub>-TPD showed three overlapping desorption peaks with peak maximum at 150 - 200 °C, 320 - 360 °C and 430- 570 °C, respectively (Fig. 6.5(a) to (d)). While the first peak is corresponded to weak Lewis acid sites, the second and third peaks are attributed to medium and strong acid sites. CO<sub>2</sub>-TPD also exhibited three overlapping peaks at 150 - 160 °C, 310 - 330 °C and 480 - 550 °C (Fig. 6.5(e) to (h)) attributable to weak, medium and strong basic sites, respectively. The total acidity of the catalysts decreased in the order: Ce - C (454 μmol/g) > Ce - N (423 μmol/g) > Ce - S (285 μmol/g) > Ce - R (252 μmol/g) and basicity in the order: Ce - N (90 μmol/g) > Ce - S (85 μmol/g) > Ce - R (83 μmol/g) > Ce - C (65 μmol/g) (Table 6.1). While Ce - C contained more amount of strong acid and base sites, the other samples contained a large amount of medium acid and base sites. The amount of strong acid sites was nearly the same for Ce - R, Ce - S and Ce - N. But the amount of strong basic sites was lower for Ce - R and Ce - S than for Ce - N and Ce - C. The concentration of medium acid and base sites decreased in the order: Ce - N > Ce - S > Ce - R > Ce - C. It should, however, be noted that the position of the desorption peak of medium and strong acid / base sites shifted to higher temperature as the morphology changed from cube to rod to no definite shape to spindle. Thus, ceria with spindle morphology contained medium and strong acid / base sites of higher strength than those of rods, cubes and no definite morphology (Fig. 6.5).

### 6.3.2. Catalytic Activity

Controlled experiments (at 150 °C for 2 h with a CO<sub>2</sub> pressure of 5 MPa) revealed that the reaction of methanol with CO<sub>2</sub> producing DMC (in presence of 2-CP as a dehydrating agent) doesn't occur without a catalyst. Morphology of ceria had a marked effect on its catalytic activity. The activity of ceria samples (methanol conversion) decreased in the order: Ce - S > Ce - N > Ce - R > Ce - C (Table 6.2). Conversions of methanol and 2-CP were 63 mol% over Ce - S catalyst and DMC and 2-picolinamide (2-PA) formed with 97 mol% selectivity (Table 6.2). With other catalysts, the yield of DMC was lower ( 35.4 mol%) and 2-methylpicolinate (2-MP) and methyl carbamate (MC) were detected in more amount 6.8 and 1.4 mol%, respectively. The mass balance was 100% with Ce - S, it was only 91% with Ce - R and Ce - C and 86% with Ce - N catalysts (Table 6.2). Conversion of 2-CP was higher than the conversion of methanol. This suggests that a part of 2-CP got decomposed. Such decomposition was minimal over Ce - S than on the other ceria catalysts.

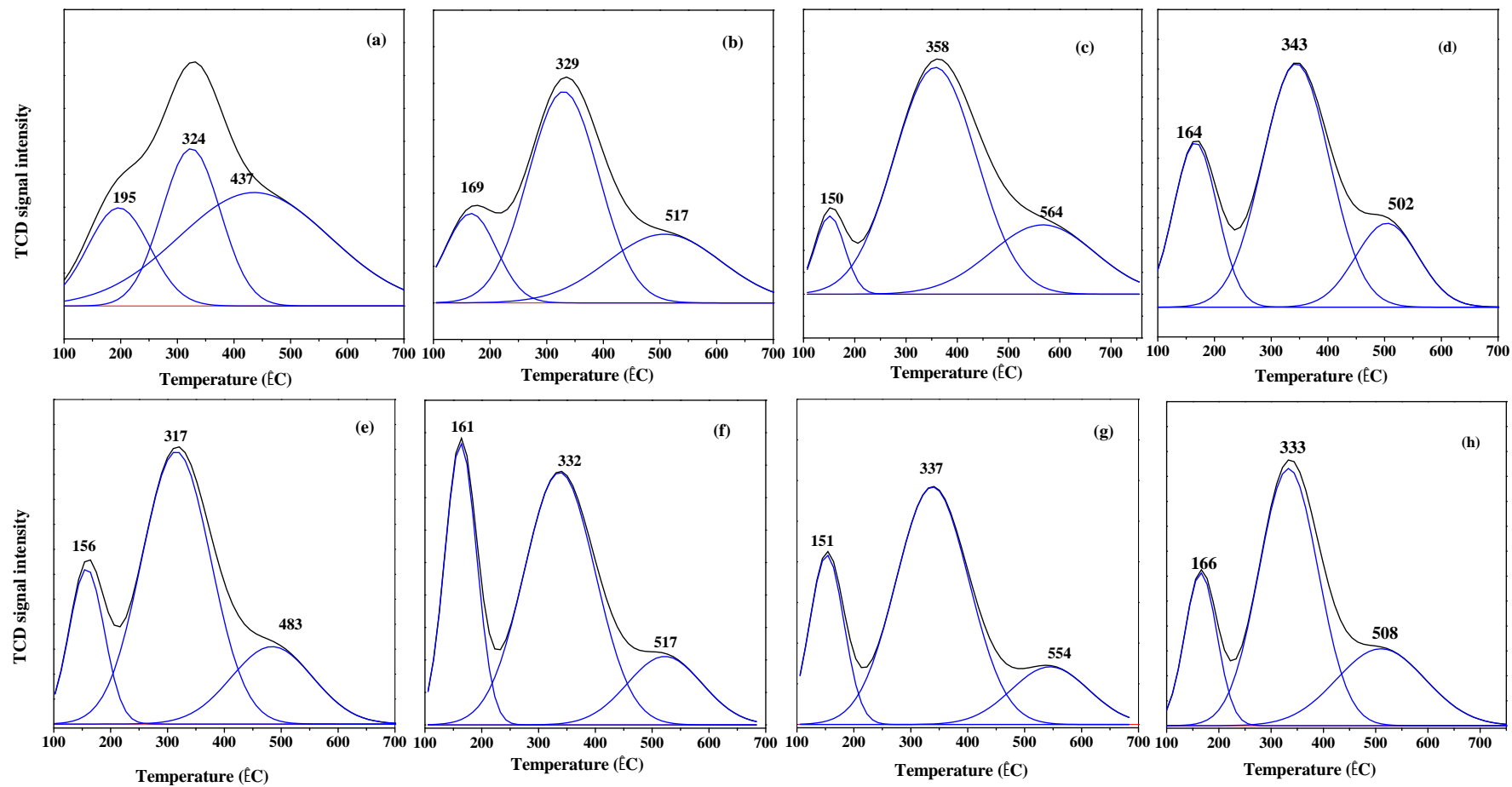


**Fig. 6.5.**  $NH_3$ -TPD (top) and  $CO_2$ -TPD (bottom) profiles of Ce - C (a & e), Ce - R (b & f), Ce - S (c & g) and Ce - N (d & h).

**Table 6.2.** Catalytic activity data of ceria for direct synthesis of DMC.

Catalyst	Conversion (mol%)		Yield (mol%)		Product selectivity (mol%; based on methanol)			Product selectivity (%; based on 2-CP)		Mass balance (%)	
	Methanol	2-CP	DMC	2-PA	DMC	MC	2-MP	2-PA	2-MP	Based on methanol	Based on 2-CP
Ce-N	51.2	64.6	31.6	44.0	61.7	2.1	6.8	68.1	10.8	85	86
Ce-C	37.3	49.6	31.4	33.2	84.2	1.4	9.4	66.9	14.1	98	91
Ce-R	50.0	61.8	35.4	45.4	70.8	2.2	7.0	73.5	11.3	90	91
Ce-S	63.0	63.0	61.0	60.8	97.0	1.2	2.9	96.5	5.4	100	101

Reaction conditions: methanol = 3.2 g (100 mmol), 2-cyanopyridine (2-CP) = 5.2 g (50 mmol), CO<sub>2</sub> pressure = 5 MPa, catalyst = 0.1 g, reaction temperature = 150 °C, reaction time = 2 h.



Gas analysis pointed out that a part of DMC decomposed into dimethyl ether over Ce - R, Ce - C and Ce - N. This was not the case with Ce - S. In other words, the present study reveals that ceria sample of spindle morphology is highly active and selective.

### 6.3.2.1. Effect of reaction parameters

Fig. 6.6 shows the influence of reaction temperature and reaction time on methanol conversion and DMC yield over Ce - S catalyst. Conversion of methanol increased with temperature and remained unaltered above 150 °C. The yield of DMC had also increased with temperature and decreased above 150°C. This behavior is due to self decomposition of DMC above 150 °C. Methanol conversion and DMC yield increased with reaction time and remained constant after 3 h. The initial rate of reaction over ceria spindles was found to be  $10.6 \times 10^{-3}$  mmol.sec<sup>-1</sup>. This reaction is exothermic in nature ( $\Delta H = -27.90$  kJ.mol<sup>-1</sup>) [19]. Hence, higher temperature is unfavourable. However, to prevent poisoning of the surface active sites with CO<sub>2</sub> and by-product water and also to activate CO<sub>2</sub> for the reaction to occur on the solid surface, a temperature of about 150 °C seems optimum.

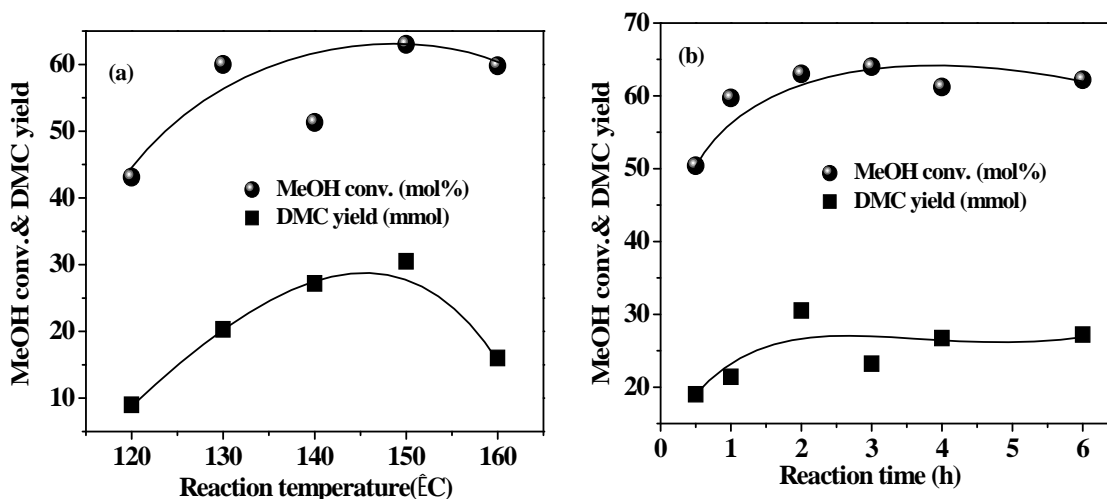


**Fig. 6.6.** Influence of (a) reaction temperature and (b) reaction time on DMC yield over Ce - S catalyst. Reaction conditions: methanol = 3.2 g, 2-CP = 5.2 g, CO<sub>2</sub> pressure = 5 MPa and catalyst = 0.1 g. (a) t = 2 h and (b) T = 150 °C.

### 6.3.2.2. Structure-activity correlations

Methanol conversion and DMC yield increased with increasing amount of medium type acid and base sites (Fig. 6.7). Any deviation from linearity could be due to difference in the

strength of acid/base sites of different ceria catalysts. The desorption occurred at higher temperature for Ce - S than for the other catalysts. While the medium type basic sites are responsible for formation of methoxide ions, the medium type acid sites assist generating CH<sub>3</sub><sup>+</sup> ions from methanol. A perfect tuning of the acid and base sites is crucial for achieving 100% DMC selectivity. Ce - S had a right balance of these active sites and thereby showed higher conversion and DMC selectivity. Methanol conversion (mol%) should be equal to 2-CP conversion. But, an excess amount of 2-CP got converted on Ce - N, Ce - R and Ce - C catalysts (Table 6.2). This is due to a large percentage of strong acid sites present on those catalysts that decompose a part of 2-CP taken in the reaction.

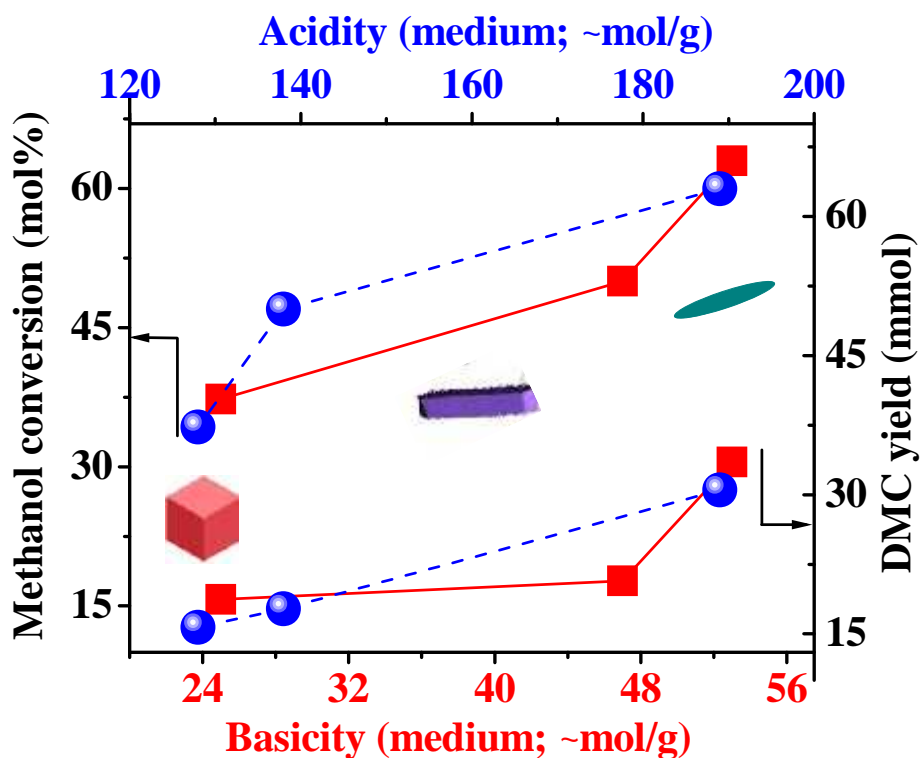


**Fig. 6.7.** Correlation between catalytic activity (methanol conversion and DMC yield) with acid / base sites of medium strength of ceria catalysts. Reaction conditions: methanol = 3.2 g (100 mmol), 2-cyanopyridine (2-CP) = 5.2 g (50 mmol), CO<sub>2</sub> pressure = 5 MPa, catalyst = 0.1 g, reaction temperature = 150 °C, reaction time = 2 h

DMC yield correlated with the defect sites concentration as well. The defect sites act as a source to activate CO<sub>2</sub>. The highly defected morphology (Ce - S in the present study) adsorbs more CO<sub>2</sub>, which is further activated by the base sites of medium strength present on the catalyst.

In addition to these, exposed facets may also play a role on catalytic activity. The most stable surface (111) is assumed to be the active surface for this reaction, which was exposed mainly in ceria with spindle morphology. Thus, acid-base sites of medium strength, defect sites, exposed facet and morphology control the catalytic activity and selectivity of ceria in the direct synthesis of DMC from methanol and CO<sub>2</sub>.

### 6.3.2.3. Tentative reaction mechanism

As seen from Fig. 6.8, surface OH group activate methanol and produce methoxide ion which in turn coordinates to Lewis acidic Ce<sup>4+</sup> sites. Thus, methoxide ion attached to Ce<sup>4+</sup> activates CO<sub>2</sub> adsorbed on the defect centers and further reaction of methanol with this species assisted with adjacent acidic proton leads to DMC and water.

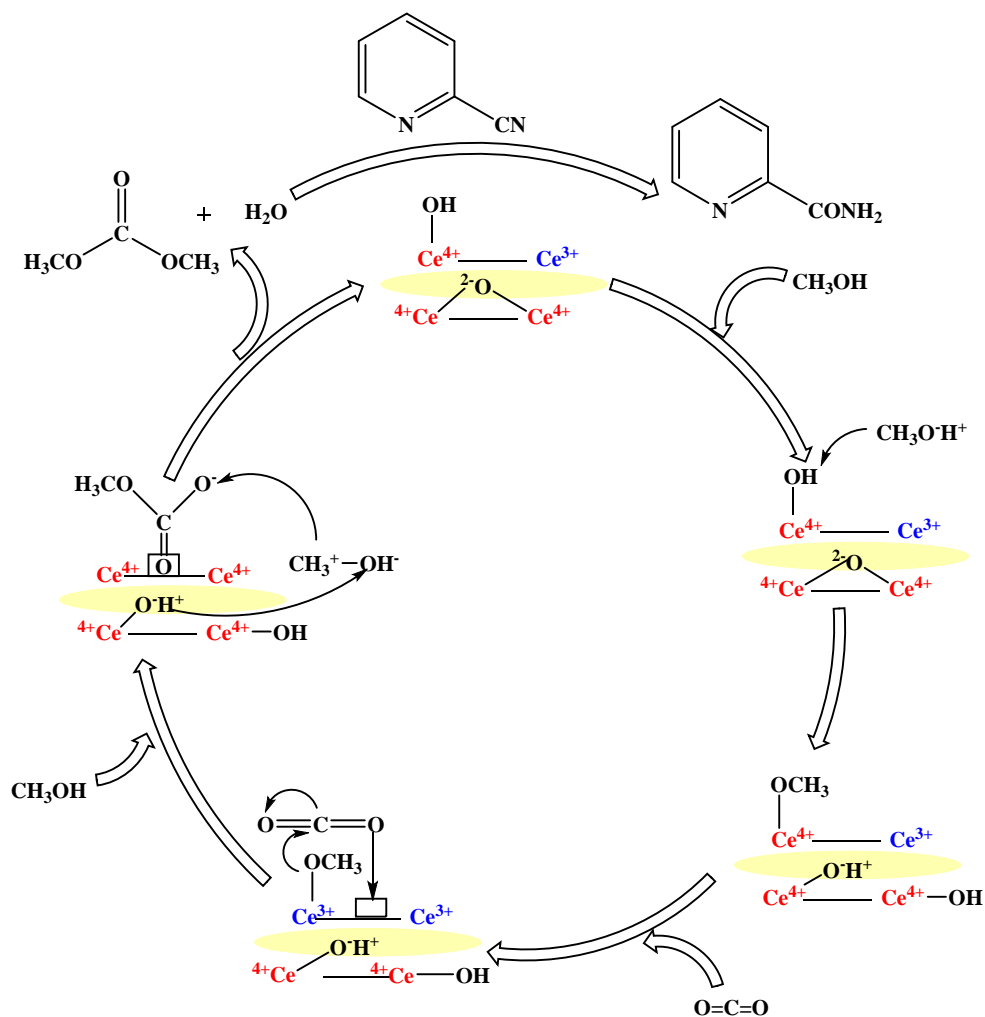


**Fig. 6.8.** Proposed mechanism for DMC synthesis from methanol and CO<sub>2</sub> over ceria catalysts.

#### 6.4. Conclusions

Ceria samples of different morphology were used as catalysts in the direct synthesis of DMC from methanol and CO<sub>2</sub> in presence of 2-CP, a dehydrating/water trapping agent. CeO<sub>2</sub> with spindle morphology was found superior. Quantitative conversion of methanol with nearly 100 mol% selectivity for DMC was obtained over Ce - S catalyst. Defect site concentration, medium type acid/base site ratio and exposed (111) surface of CeO<sub>2</sub> markedly influence its catalytic activity/selectivity which in turn was assisted by the morphology. Catalytic activity correlated with the amount of acid/base site of medium strength and defect sites. The highest catalytic activity of Ce - S was attributed to its spindle morphology having a right balance of medium acid-base sites and defect centers.

#### 6.5. References

- [1] M. Arresta (Ed.), Carbon Dioxide as a Chemical Feedstock, WILEY-VCH Verlag GmbH & Co., KGaA, Weinheim, (2010).
- [2] P. Unnikrishnan, D. Srinivas in: Industrial Catalysis and Separations: Innovations for Process Intensification, K.V. Raghavan, B. M. Reddy(Eds.), Apple Academic Press Inc., NJ, USA, (2015).
- [3] T. Sakakura, J.C. Choi, H. Yasuda, Chem. Rev. 107 (2007) 2365-2387.
- [4] M. Honda, M. Tamura, Y. Nakagawa, K. Tomishige, Catal. Sci. Technol. 4 (2014) 2830-2845.
- [5] P. Tundo, M. Selva, Acc. Chem. Res. 35 (2002) 706-716.
- [6] <http://www.icis.com/v2/chemicals/9076147/polycarbonate/process.html>
- [7] B.A.V. Santos, V.M.T.M. Silva, J.M. Loureiro, A.E. Rodrigues, ChemBioEng. Rev. 1 (2014) 214-229.
- [8] S. Huang, B. Yan, S. Wang, X. Ma, Chem. Soc. Rev. 44 (2015) 3079 - 316.
- [9] V. Eta, P. Mäki-Arvela, J. Wärnä, T. Salmi, J.P. Mikkola, D.Y. Murzin, Appl. Catal. A: Gen. 404 (2011) 39-46.
- [10] K. Tomishige, K. Kunimori, Appl. Catal. A: Gen 237 (2002) 103-109.
- [11] K.T. Jung, A.T. Bell, J. Catal. 204 (2001) 339-347.
- [12] Y. Ikeda, M. Asadullha, K. Fujimoto, K. Tomishige, J. Phys. Chem. B 105 (2001) 10653-10658.

- [13] S. Wang, L. Zhao, W. Wang, Y. Zhao, G. Zhang, X. Ma, J. Gong, *Nanoscale* 5 (2013) 5582-5588.
- [14] M. Honda, M. Tamura, Y. Nakagawa, S. Sonehara, K. Suzuki, K. Fujimoto, K. Tomishige, *ChemSusChem* 6 (2013) 1341-1344.
- [15] <http://www.asahi-kasei.co.jp/asahi/en/news/2014/e150119.html>.
- [16] T. Fan, L.X. Zhang, H.F. Jiu, Y.X. Sun, G.D. Liu, Y.Y. Sun, Q.L. Su, *Micro Nano Lett.* 5 (2010) 230-233.
- [17] A. Nakajima, A. Yoshihara, M. Ishigame, *Phys. Rev. B* 50 (1994) 297-307.
- [18] Z. Wu, M. Li, J. Howe, H.M. Meyer, S.H. Overbury, *Langmuir* 26 (2010) 16595-16606.
- [19] V. Eta, P. Maki-Arvela, A.R. Leino, K. Kordas, T. Salmi, D.Y. Murzin, J.P. Mikkola *Ind. Eng. Chem. Res.* 49 (2010) 9609-9617.

**Chapter - 7**  
**Summary and Conclusions**

Dimethyl carbonate (DMC) is an important chemical. Its synthesis has been widely investigated through phosgene and non-phosgene routes. Among several non-phosgene routes, transesterification of cyclic carbonates with methanol (indirect utilization of CO<sub>2</sub>) is one of the viable alternates for producing DMC. Hitherto known catalyst systems for this reaction are low productive or require high temperatures. Designing of stable and highly active solid base catalyst is most important for DMC synthesis by this route. On the other hand, the direct synthesis of DMC from CO<sub>2</sub> and methanol (direct utilization of CO<sub>2</sub>) is a greener and atom-efficient approach for DMC synthesis. However this reaction is restricted by low DMC yield due to thermodynamic and equilibrium limitations. In order to overcome such limitations development of highly efficient catalyst with suitable dehydrating systems is necessary.

This thesis work reported the application of basic and acid-base bifunctional solid oxide catalysts for making DMC through transesterification of cyclic carbonate with methanol and direct methanolysis of CO<sub>2</sub>. Catalytic activities of four set of catalysts viz., (i) rare-earth modified hydrotalcite-derived mixed oxides (Chapter 3), (ii) sodium titanate nanotubes (NaTNT; Chapter 4), (iii) calcined zirconium phenyl phosphonate phosphite (ZrPP; Chapter 5) and (iv) CeO<sub>2</sub> of different morphologies (Chapter 6) for DMC synthesis were examined. While catalysts (i) and (ii) were used for transesterification of cyclic ethylene and propylene carbonates (EC and PC) with methanol, (iii) and (iv) were used in the direct synthesis of DMC. The influence of reaction parameters on catalytic activity was probed. These catalysts were stable and reusable in recycling studies. Main conclusions from different chapters were provided below.

**Chapter 1** provided a general introduction to the significance and applications of DMC. It described the various methods for DMC synthesis and the relevance and advantages of CO<sub>2</sub> utilisation in DMC synthesis. The scope and objectives of the work were also presented.

**Chapter 2** revealed the synthesis and characterisation methodologies of different solid oxide catalysts used in this thesis which comprise rare-earth (La, Pr, Ce, Sm and Y)-modified Mg-Al hydrotalcites-derived mixed oxide (HT La-C), sodium trititanate nanotubes (NaTNT), calcined zirconium phenyl phosphonate phosphite (ZrPP-C), cerium oxide of cube, rod, spindle and no definite shape morphology. The general reaction procedures and product analysis were also discussed.

**Chapter 3** presented DMC synthesis through transesterification of EC and PC with methanol over rare-earth element (La<sup>3+</sup>, Ce<sup>3+</sup>, Y<sup>3+</sup>, Pr<sup>3+</sup> and Sm<sup>3+</sup>)-modified Mg-Al HTs-derived

ternary mixed oxide catalysts. The catalytic performance differed with the nature rare-earth ion modification. Among several mixed oxides, La(8 - 10 mol%)-modified HT showed the highest activity yielding 95 mol% of DMC from EC and 58 mol% from PC at moderate reaction conditions (80 °C and 4 h for EC-MeOH and 150 °C and 2 h for PC-MeOH). These catalysts were active than the hitherto known solid catalysts for this reaction. A linear correlation between catalytic activity and density of basic sites was found. The La-modified HT catalyst was recovered and reused in five recycle studies with little loss in catalytic activity.

**Chapter 4** reported the catalytic application of NaTNT for transesterification of EC and PC with methanol at ambient reaction conditions. Optimization study on reaction time and catalyst amount was conducted. NaTNT was highly active yielding 90% of DMC from EC at 25 °C and 66% of DMC from PC at 100 °C. The activation energy ( $E_a$ ) of this catalyst was lower than HT-10 La-C (studied in Chapter 3) and other known catalysts. The basicity with high surface accessibility to reactants is the possible cause for its efficient catalytic performance. This catalyst was recycled up to four times with little loss in activity.

**Chapter 5** presented DMC synthesis through the direct reaction of CO<sub>2</sub> with methanol with 100 mol% selectivity using a novel, reusable, hydrophobic, calcined zirconium phenyl phosphonate phosphite (ZrPP-C) catalyst. The method of preparation of the catalyst influenced surface acidity and catalytic activity. Among several, ZrPP-HF-C prepared using HF gave highest DMC yield. It was a hydrophobic, acid-base bi-functional catalyst and yielded DMC of 8.03 mmol/g catalyst at 170 °C over 12 h with the initial reaction rate being  $3.3 \times 10^{-4}$ . The activity/DMC yield was further enhanced up to 26.06 mmol/g catalyst using dimethyl formamide (DMF) (10 ml) and 3A-molecular sieves (0.5 g) as solvent and water scavenger, respectively. Activity of the catalyst correlated with acid-base site density. Detailed investigation of structure-function correlation, effect of CO<sub>2</sub> concentration and other reaction parameters were studied.

**Chapter 6** discussed the various causes that control the catalytic activity of CeO<sub>2</sub> for the direct synthesis of DMC. Stoichiometric quantity of 2-cyanopyridine (2-CP) was used as a dehydrating agent. Nano crystalline CeO<sub>2</sub> with cube, rod, spindle and no definite shape morphology were employed as catalysts. CeO<sub>2</sub> with spindle morphology (Ce-S) showed superior catalytic activity and DMC selectivity compared to other morphologies. Synergic effect of defect site concentration, exposed surface activity and medium type acid/base site ratio of CeO<sub>2</sub> influenced its catalytic activity/selectivity. The influence of reaction parameters on DMC yield



was investigated. Ce-S gave highest DMC yield of 305 mmol/g (61 mol%) at 150 °C and 2 h. The highest catalytic activity of Ce-S was attributed to its morphology, the right balance of moderate type acid-base sites and defect centres.

**Table 7.1** compares the catalytic activity of the best catalysts reported in this thesis (HT-8 La-C, HT-10 La-C and NaTNT) with the best-known catalysts ( $\text{Na}_2\text{WO}_4 \cdot 2\text{H}_2\text{O}$ , CaO-ZnO and Fe-Zn double metal cyanide) for the transesterification of EC/PC with methanol.  $\text{Na}_2\text{WO}_4 \cdot 2\text{H}_2\text{O}$  and CaO-ZnO are the best-known catalysts for the reaction of EC-methanol. They produced DMC yields of 80% and 83%, respectively at room temperature. However, they are limited due to the following reasons: turnover number (TON) for  $\text{Na}_2\text{WO}_4 \cdot 2\text{H}_2\text{O}$  was quite low. In case of CaO-ZnO, Ca leached into the product mixture. HT-10 La-C catalyst of this thesis gave a DMC yield of 95%. To best of our knowledge this is the highest DMC yield reported so far for EC transesterification. NaTNT gave a DMC yield of 58% even at 25 °C. DMC yield increased to 86% at 60 °C and 4 h. HT-8 La-C and NaTNT were superior in terms of TON to Fe-Zn double metal cyanide catalyst for transesterification of PC with methanol (**Table 7.1**).

**Table 7.1.** Comparative catalytic activity of solid oxide in transesterification of EC/PC with methanol.

Reaction	Catalyst	T (°C)	t (h)	DMC yield (mol%)	TON (mmol/g)
EC + Methanol	CaO-ZnO	25	4	83	166
	$\text{Na}_2\text{WO}_4 \cdot 2\text{H}_2\text{O}$	25	5	80	40
	HT-10 La-C	80	4	95	105
	NaTNT	25	4	58	116
PC + Methanol	Fe-Zn DMC	170	8	86	35
	HT-8 La-C	150	2	63	96
	NaTNT	100	8	66	130

**Table 7.2.** Direct synthesis of DMC from CO<sub>2</sub> and methanol.

Type of dehydrating agent	Catalyst	T (°C)	t (h)	P <sub>CO<sub>2</sub></sub> (MPa)	Water trap	DMC yield (mmol/g)
With out /with an inorganic adsorbent	H <sub>3</sub> PW <sub>12</sub> O <sub>40</sub> /Ce <sub>0.1</sub> Ti <sub>0.9</sub> O <sub>2</sub>	170	12	5	-	10.0
	ZrPP-HF-C	170	12	3	-	8.1
	ZrPP-HF-C <sup>a</sup>	170	12	4	Molecular sieve 3A	26.1
Reactive dehydrating agent	CeO <sub>2</sub> (Daiichi)	150	48	0.5	Acetonitrile	52.6
		150	86	1	Benzonitrile	138.2
		120	12	5	2-CP	138.2
		150	2	5	2-CP	305.0

<sup>a</sup>10 ml DMF was used as a solvent.

A comparison of catalytic activity of ZrPP-HF-C and Ce-S with the best known systems in the direct synthesis of DMC from CO<sub>2</sub> and methanol is presented in [Table 7.2](#). H<sub>3</sub>PW<sub>12</sub>O<sub>40</sub>/Ce<sub>0.1</sub>Ti<sub>0.9</sub>O<sub>2</sub> gave a DMC yield of 10 mmol /g. catalyst only. In the absence of a dehydrating agent, ZrPP-HF-C (catalyst of this work) gave a DMC yield of 8.1 mmol/g. catalyst. However, the yield improved to 26 mmol/g. catalyst when DMF as solvent and molecular sieves-3A as water trapping agent were used. Ceria with spindle morphology resulted the highest DMC yield of 305 mmol/g catalyst while using 2-CP as a chemical dehydrating agent ([Table 7.2](#)). In other words, catalysts reported in this study are more active and selective in DMC synthesis by indirect and direct utilization of carbon dioxide. By and large, the work reported in this thesis contributes green and sustainable catalytic process for making DMC in high yields utilizing CO<sub>2</sub> as a renewable raw material.

## List of Publications

1. Calcined, rare-earth modified hydrotalcite as a solid, reusable catalyst for dimethyl carbonate synthesis  
**P. Unnikrishnan** and D. Srinivas  
Ind. Eng. Chem. Res. 51 (2012) 6356-6363.
2. Efficient, direct synthesis of dimethyl carbonate from CO<sub>2</sub> using a solid, calcined zirconium phenylphosphonate phosphite catalyst  
**P. Unnikrishnan**, P. Varhadi and D. Srinivas  
RSC Adv. 3 (2013) 23993-23996.
3. Catalytic conversion of CO<sub>2</sub> into fuels and chemicals: a green CCU option  
**P. Unnikrishnan** and D. Srinivas  
Industrial Catalysis and Separations: Innovations for Process Intensification. K.V. Raghavan & B.M. Reddy (Eds.), Apple Academic Press Inc, NJ, USA and distributed by CRC Press, A Taylor and Francis Group (2015), Ch. 5, pp. 155-218.
4. Highly active and reusable ternary oxide catalyst for dialkyl carbonates synthesis  
**P. Unnikrishnan** and D. Srinivas  
J. Mol. Catal. A: Chem. 398 (2015) 42-49.
5. Heterogeneous Catalysis  
**P. Unnikrishnan** and D. Srinivas  
Industrial Catalytic Processes for Fine and Specialty Chemicals. V.V. Ranade and S.S. Joshi (Eds.), Elsevier (2016).

## List of Patents

1. Process for Making Dimethyl Carbonate  
D Srinivas and **P. Unnikrishnan**  
US 9073849, WO 2013175510, EP 2852568
2. An Improved Process for Preparing Dimethyl Carbonate  
D Srinivas and **P. Unnikrishnan**  
India and PCT (2014-INV-0110; 2734/DEL/2014; CSIR No. 2014-NF-0252) filed on September 24, 2015.